



HAL
open science

Study of Fission Products (Cs, Ba, Mo, Ru) behaviour in irradiated and simulated Nuclear Fuels during Severe Accidents using X-ray Absorption Spectroscopy, SIMS and EPMA

Ernesto Geiger

► **To cite this version:**

Ernesto Geiger. Study of Fission Products (Cs, Ba, Mo, Ru) behaviour in irradiated and simulated Nuclear Fuels during Severe Accidents using X-ray Absorption Spectroscopy, SIMS and EPMA. Material chemistry. Université Paris Saclay (COmUE), 2016. English. NNT : 2016SACLS064 . tel-01309027

HAL Id: tel-01309027

<https://theses.hal.science/tel-01309027>

Submitted on 28 Apr 2016

HAL is a multi-disciplinary open access archive for the deposit and dissemination of scientific research documents, whether they are published or not. The documents may come from teaching and research institutions in France or abroad, or from public or private research centers.

L'archive ouverte pluridisciplinaire **HAL**, est destinée au dépôt et à la diffusion de documents scientifiques de niveau recherche, publiés ou non, émanant des établissements d'enseignement et de recherche français ou étrangers, des laboratoires publics ou privés.

NNT : 2016SACLS064

THESE DE DOCTORAT
DE
L'UNIVERSITE PARIS-SACLAY
PREPAREE A
L'UNIVERSITE PARIS-SUD
ET AU COMMISSARIAT A L'ENERGIE ATOMIQUE ET AUX ENERGIES
ALTERNATIVES

ECOLE DOCTORALE N° 576

Particules hadrons énergie et noyau : instrumentation, image, cosmos et simulation

Spécialité de doctorat : Energie nucléaire

Par

M. Ernesto Geiger

Study of Fission Products (Ba, Cs, Mo, Ru) behaviour in irradiated and simulated
Nuclear Fuels during Severe Accidents using X-ray Absorption Spectroscopy,
SIMS and EPMA

Thèse présentée et soutenue à Saclay, le 14 janvier 2016

Composition du Jury :

Pr. Giorgio, Suzanne	Professeure Université Aix-Marseille	Présidente
Dr. Hazemann, Jean-Louis	Directeur de Recherche, CNRS	Rapporteur
Dr. Herranz, Luis Enrique	Directeur de Recherche, CIEMAT	Rapporteur
Dr. Bonin, Bernard	Expert International, CEA	Examineur
Dr. Wiss, Thierry	Ingénieur Chercheur, ITU	Examineur
Dr. Journeau, Christophe	Expert International, CEA	Directeur de thèse
Dr. Martin, Philippe	Expert Senior, CEA	Encadrant CEA
Dr. Pontillon, Yves	Expert Senior, CEA	Encadrant CEA
Dr. Ducros, Gérard	Directeur de Recherche, CEA	Invité

Acknowledgements

Je tiens à remercier dans un premier temps Jean-Louis Hazemann et Luis Enrique-Herranz, rapporteurs de cette thèse, pour leurs corrections et conseils. Je remercie aussi Bernard Bonin, Suzanne Giorgio et Thierry Wiss d'avoir accepté d'être examinateurs de cette thèse.

Ce manuscrit est le résultat de trois ans de travail au Commissariat à l'Energie Atomique et aux Energies Alternatives de Cadarache. Bien sûr, je n'ai pas travaillé seul et je voudrais exprimer ma plus grande gratitude aux personnes qui ont rendu ce travail à la fois possible et agréable.

Tout d'abord, je tiens à remercier mon directeur de thèse, Christophe Journeau et particulièrement mes encadrants : Yves Pontillon, du LAMIR, qui m'a tant appris, pas seulement sur le plan technique mais aussi humain (nos prises de tête me manqueront !) et Philippe Martin, du LLCC, avec qui j'ai partagé des heures et des heures de manip sur synchrotron. Merci pour ce que tu m'as enseigné sur la Spectroscopie d'Absorption des rayons X. Je garderai aussi en mémoire (toutes) les bières que nous avons partagées ! Je tiens à remercier également Gérard Ducros, pour avoir accepté l'invitation à participer au jury ainsi que pour tous ses conseils avisés. Merci d'avoir mis ton expérience au service de ma thèse avec tant de simplicité. J'espère que la version finale de la thèse ne comportera pas «plus de 100 coquilles».

Je tiens aussi à remercier Corine Farnaud, la meilleure secrétaire au monde. Tu as toujours été disponible pour répondre à mes innombrables petites questions et m'as énormément aidé à affronter la bureaucratie française. Je veux remercier également au « jefe » du SA3C, Olivier Dugne, pour nos longues discussions, les blagues, ses conseils et sa bonne disposition.

Je remercie aussi Eric Hanus, chef du LAMIR et tous les membres du labo, particulièrement Guillaume Volle et Marina Pontillon pour leur aide lors des traitements thermiques sur les SIMFUELS. Merci aussi à Sébastien Bernard, Hélène Capdevila, Hélène Desmonts-Giacalo, Hélène Juhan, Frank Fiorito, Bernard Gleizes, Pierre-Philippe Malgouyres, Jean-Christophe Richaud, Sidonie Clément, Annelise Gallais-During, Guillaume Brindelle, Manon Vadon, Vincent Marty, Benoit Petitprez, Julien Piquemal et Gilles Cecilia, tous trois du LEGEND. Merci pour votre bonne humeur et l'ambiance lors des repas du labo, cafés, pique-niques, etc. J'ai passé, grâce à vous, trois années très agréables au sein du LAMIR.

Un grand merci aussi aux secrétaires Maria Lento qui a fait partie du LAMIR et qui m'a beaucoup aidé quand j'ai commencé ma thèse, à Priscilla Rey du LAMIR et à Myriam Ablon du LEGEND.

Je remercie Chantal Riglet-Martial, du LLCC, pour son aide à l'utilisation du logiciel FactSage ainsi que pour la réalisation des calculs thermodynamiques, une partie importante de cette thèse. Merci à Catherine Tanguy, aussi du LLCC, pour sa grande aide sur toute la partie expérimentale sur les SIMFUELS, les caractérisations au laboratoire LBF, et l'organisation des transports de matière nucléaire, particulièrement complexe.

Je remercie aussi tous les membres du LEMCI pour leur aide sur la partie des combustibles irradiés, et plus particulièrement:

- Laurent Fayette, Stéphane Réboul et Nicolas Robert pour la préparation des échantillons et les métallographies,
- Jérôme Lamontagne et Thierry Blay pour les acquisitions à la μ -sonde et l'interprétation des résultats,
- Isabelle Zacharie-Aubrun et Pierre Delion pour les acquisitions MEB,
- Jean Noirot pour son aide sur l'analyse des images et plein, plein d'autres choses,

- Karine Hanifi et Laurent Brunaud pour son aide pour l'acquisition et le traitement des diffractogrammes X,
- Philippe Bienvenu et Ingrid Roure pour les acquisitions SIMS sur les combustibles irradiés mais aussi sur les SIMFUELS.

Je tiens aussi à remercier l'ensemble des membres du LCU, et particulièrement Nicolas Tarisien pour son aide pour les acquisitions MEB sur les SIMFUELS, Hélène Rouquette pour les acquisitions DRX et Joseph Sanchez pour son aide au quotidien au LBF.

À tout le personnel de la ligne de lumière MARS, Synchrotron SOLEIL, où j'ai fait toutes mes expériences XAS, merci. Particulièrement, je remercie Pier-Lorenzo Solari, Sandrine Schlutig et Herbé Hermange. Je tiens à remercier aussi René Bès pour son aide lors des premières acquisitions et le traitement des données XAS.

A tous les thésards, intérim, stagiaires, apprentis et CDD qui m'ont accompagné depuis le début de ma thèse, nous avons passé trois supers années à Cadarache et à Aix-en-Provence lors des randonnées, soirées, etc. Particulièrement, je tiens à remercier

- Giannina Dottavio, qui est devenue une grande amie et qui m'a dit que faire une thèse en France c'était top : elle avait raison (gracias Gigi! 😊);
- Pierre Mallebay qui était mon coloc de bureau tout au début et qui m'a beaucoup aidé avec le français ;
- chica Claire Le Gall, ma deuxième coloc de bureau qui a mis une ambiance géniale;
- chica Marion Ledieu pour son soutien, les corrections et plein d'autres choses;
- señor Jean-Éric Mathonnet qui est devenu un grand ami et avec qui on a fait partie l'Asthec et voyagé au Japon ;
- mais aussi Simon, Gaëlle, Lise, Marcelle, Emerson, Micka, Marion, Nathan, Vanessa, Clément, Vincent, Arno, enfin tous...

Por último, quiero agradecer a mis padres Laura y Francisco por el apoyo de siempre y por haber insistido en que aceptara la tesis, que no fue una decisión fácil, y a mis hermanos Federico y Carla. Gracias también a los amigos que están siempre, aun en la distancia.

General Index

Glossary.....	7
General Introduction.....	9
1. Chapter One: Context of the Study	13
1.1. Introduction	13
1.2. Scientific Background.....	14
1.3. Remaining questions on FP behaviour and thesis objective	39
1.4. Hypothetical Release Mechanism.....	40
2. Chapter 2: Irradiated Fuels.....	53
2.1. Introduction	53
2.2. Samples description	54
2.3. Experimental characterization of irradiated fuel samples.....	60
2.4. Discussion: Results vs. mechanism	80
2.5. Conclusion.....	85
3. Chapter 3: Model Materials	89
3.1. Introduction	89
3.2. Samples and annealing tests description.....	92
3.3. Thermodynamic Analysis	94
3.4. FP Behaviour	96
3.5. Discussion.....	130
3.6. Conclusions	135
4. Chapter 4: Discussion.....	141
4.1. Introduction	141
4.2. Summary of samples and characterizations performed.....	141
4.3. Experimental results comparison	144
4.4. Comparison between experimental results and the release mechanism	147
4.5. Summary of validated and refuted chemical phases.....	149
4.6. Modified release mechanism.....	149
5. Conclusion and Perspectives	161
5.1. Conclusion.....	161
5.2. Perspectives	161
6. Appendices.....	167
6.1. Appendix I: The INES scale	167
6.2. Appendix II: Experimental Research Programs on Fission Products release	169

6.3.	Appendix III: SIMFUEL samples preparation.....	181
6.4.	Appendix IV: Thermodynamic estimations.....	183
6.5.	Appendix V: Experimental loops.....	184
6.6.	Appendix VI: Characterization methods	189
6.7.	Appendix VII: Résumé en Francais.....	195
	References.....	201
	Figures List.....	208
	Tables List.....	212

Glossary

ATR	Advanced Test Reactor
BSE	Back Scattered Electrons
BWR	Boiling Water Reactor
CEA	<i>Commissariat à l'Énergie Atomique et aux Énergies Alternatives</i>
CRL	Chalk River Laboratories
ECD	Equivalent Circle Diameter
EDF	<i>Electricité de France</i>
EDS	Electron Dispersive X-ray Spectroscopy
EPMA	Electron Probe Micro Analysis
EXAFS	Extended X-ray Absorption Fine-structure Spectroscopy
FP	Fission Product
FR	Fast Reactor
HBS	High Burn-up Structure
INES	International Nuclear and radiological Events Scale
IRSN	<i>Institut de Radioprotection et Sécurité Nucléaire</i>
JAEA	Japan Atomic Energy Agency
JRR	Japan Research Reactor
LOCA	Loss Of Coolant Accident
LWR	Light Water Reactor
MFPR	Module for Fission Products Release
MOX	Mixed Oxide Fuels
NPP	Nuclear Power Plant
NSRR	Nuclear Safety Research Reactor
OM	Optical Microscope
OP	Oxide Precipitate
ORNL	Oak Ridge National Laboratory
PWR	Pressurized Water Reactor
RBMK	Reaktor Bolshoy Moshchnosti Kanalnyi (High Power Channel-type Reactor)

RE	Rare Earth
RIA	Reactivity Injection Accident
SA	Severe Accident
SBO	Station Black-Out
SE	Secondary Electrons
SEM	Scanning Electron Microscope
SET	Separate-Effect Tests
SIMS	Secondary Ion Mass Spectrometry
SPS	Spark Plasma Sintering
TMI	Three Mile Island
WI	White Inclusion
XANES	X-ray Absorption Near Edge Structure
XAS	X-ray Absorption Spectroscopy
XPS	X-ray Photoelectron Spectroscopy
XRD	X-Ray Diffraction

The energy produced by the fission of uranium atoms is exploited in Nuclear Power Plants (NPP) for producing electricity. Particularly in France, around 77% of the total generated electricity is produced in NPP. As the uranium atoms fission takes place, lighter atoms, also called Fission Products (FP) are created. These FP are mostly radioactive and accumulate in the nuclear fuel during the life of the nuclear fuel. The more the nuclear fuel remains in a reactor, the more its burn-up increases (the amount of energy generated per ton of U) and so the concentration of FP increases.

Despite the safety level, accidents may occur in nuclear reactors due to devices malfunction, human errors or external factors such as natural disasters. These accidents may have different consequences, but when an important release of FP into the atmosphere is among them, then it is called a severe accident. Examples of such accidents are the Chernobyl accident in 1986, Ukraine, and the Fukushima Dai-Ichi accident in 2011, Japan. The total amount and characteristics of the radioactive species released into the atmosphere is called the Source Term, which today are estimated using scenario codes. In order to improve these estimations, the behaviour of FP during severe accident must be better understood. Several research programs have been carried out in different countries in order to study the behaviour of FP in these conditions, though many uncertainties still remain.

Among the many FP, barium, caesium, molybdenum and ruthenium present a particular interest, since they may interact among them but also with other FP or even materials present in the reactor, and thus affect their release. Understanding the behaviour of these four FP is the main objective of this work. To this end, two experimental work axes were set up, aiming at reproducing conditions representative of nuclear severe accidents, using both high burn-up irradiated fuel samples and model materials. These model materials are called SIMFUELS and consist in natural UO_2 doped with stable isotopes of FP in concentrations that match a targeted Burn-up. Therefore, SIMFUELS are representative of irradiated nuclear fuels but without their radioactivity. The importance of this kind of materials lies in the possibility of using powerful characterization techniques, such as X-ray Absorption Spectroscopy, which today are unavailable for large samples of irradiated nuclear fuels.

This manuscript is structured in four chapters:

Chapter 1 is dedicated to present the context of this work. The three main Severe Accidents in history are recalled, followed by a bibliographical overview of the main research programs carried out to study the behaviour of FP during nuclear severe accidents. A release mechanism for barium, caesium, molybdenum and ruthenium has been proposed in literature and is also presented. This mechanism, which is based on the results obtained from the different research programs and on thermodynamic estimation, constitutes the main hypothesis of this work. The experimental approach implemented to validate this release mechanism is lastly presented.

Chapter 2 is dedicated to the Irradiated Fuels work axis. The studied samples were representative to an initial state (i.e. normal operation conditions in a Pressurized Water Reactor), to an intermediate state and to an advanced state (i.e. imminent fuel melting) of a nuclear severe accident. The performed annealing tests, characterizations and the obtained results are presented.

Chapter 3 is dedicated to the Model Materials work axis. The SIMFUEL samples studied in this axis, the annealing tests to which they were submitted, both under reducing and oxidizing conditions, the performed characterizations and obtained results are presented.

Chapter 4 is dedicated to the comparison of results obtained in irradiated fuels and SIMFUEL samples, as well as to the comparison of experimental results to the release mechanism proposed in literature. As a consequence, a new release mechanism is proposed, which contemplates both reducing and oxidizing conditions.

Finally, conclusions on barium, caesium and ruthenium behaviour are presented, along with the perspectives which would allow answering the remaining questions of this work. A French summary of this work is available in **Appendix VII**.

Chapter 1: Context of the study

1.1. Introduction.....	13
1.2. Scientific Background.....	14
1.2.1. Severe accidents	14
1.2.2. Research Programs and their results.....	17
1.2.3. Fission products behaviour.....	35
1.3. Remaining questions on FP behaviour and thesis objective	39
1.4. Hypothetical Release Mechanism.....	40
1.4.1. Experimental bases of the hypothetical evolution.....	45
1.4.2. Methodology	49

1.1. Introduction

The fission reaction of heavy atoms such as ^{235}U and ^{239}Pu is very exothermic, capable of releasing huge amounts of energy. This phenomenon is exploited in Nuclear Power Plants (NPP) for electricity generation, and it is much extended in countries such as France, where around 77% of the electricity is generated by NPP. In France, all operating reactors are currently Pressurized Water Reactors (PWR), a subtype of Thermal Reactor. As a result of the fission of uranium and plutonium atoms lighter elements are produced, which are called Fission Products (FP).

The energy generated by a nuclear reactor is linked to the burn-up, which units are commonly expressed in Giga Watt day per ton of fuel (GWd.t^{-1}). As the burn-up of the fuel increases, so does the amount of FP.

Despite the high degree of control and safety in NPP, they are not exempt from device malfunction, human errors or even natural disasters, which may lead to nuclear incidents or even accidents. When consequences involve a high degradation of the reactor core (melting), associated with the release of FP and other radioactive materials from the reactor core, it is classified as a Severe Accident. These released FP may be transported by air masses or water and thus cover extensive areas. FP affect all living beings due to their radiological effect and may as well act as poisons.

The amount and isotopic composition of the released radioactive material released from the core is called Source Term, and its quantification has been the main objective of several international research programs for more than thirty years. These research programs, summarized in **Section 1.2**, are classified into two groups, according to their approach: Integral programs studying the response of a whole nuclear core during a severe accident, in a reduced scale; on the other hand, Analytical programs studying the behaviour of FP when submitted to accidental conditions, by means of Separate-Effect Tests (SET). Examples of these are the VERCORS and VERDON programs, conducted by the CEA. As result from all the research programs an extensive database on FP behaviour has been generated. There are, though, remaining uncertainties regarding the behaviour of major FP such as caesium, molybdenum, barium and ruthenium. It has been observed that these FP present a very different behaviour depending on the studied conditions and that they affect the behaviour of other FP and structural materials as well. These uncertainties are presented in **Section 1.3**, along with the thesis objective.

A mechanism describing the behaviour of the mentioned FP, presented in **Section 1.4**, has been proposed in (Nicaise, 2004a). This mechanism, which proposes intermediary compounds that are created and destroyed during the accidental sequence, is based on observations done mainly during the VERCORS series program and on thermodynamic calculations. Nevertheless, the proposed intermediate compounds have not been observed experimentally. In order to validate or refute the proposed mechanism, two work axes have been set up. These axes consist in performing annealing treatments in conditions representative of those of a severe accident. Thermodynamic calculations have also been performed for each axis, for a better interpretation of experimental results.

1.2. Scientific Background

This section presents the specific context in which the thesis was developed and summarises the experimental work that has been done on nuclear severe accidents research programs. In **Section 1.2.1**, the INES scale for nuclear events classification, the phenomenology of a typical LOCA type accident (Loss Of Coolant Accident), and the main three nuclear accidents in history are presented (TMI-2, Chernobyl and Fukushima). In **Section 1.2.2**, Integral and Analytical programs are presented, describing the range of variables studied and the results obtained. The discussion of these results and conclusions on FP behaviour is given in **Section 1.2.3**.

1.2.1. Severe accidents

1.2.1.1. Classification

Nuclear events are classified according to the INES scale (International Nuclear and radiological Event Scale) (AIEA, 2001). This scale categorizes nuclear events in 8 levels, from 0 to 7, in relation to their consequences. Events of **Level 0** are simple deviations from operation conditions, which do not have any importance from a security point of view. **Levels 1 to 3** correspond to nuclear incidents, with limited consequences such as contamination or operators exposure to radiation. **Levels 4 to 7** correspond to nuclear accidents which involve the release of radioactive materials.

Three factors are considered in order to classify the different nuclear events:

- Impact over population and environment, where the radiation doses on the population surrounding the place where the event takes place and the unexpected release of materials on a big scale are considered.
- Impact on barriers and radiological controls, which concerns events happening inside facilities and which do not have a direct impact over the population or the environment. The unexpected presence of intense radiation sources and the release of important quantities of radioactive substances inside facilities are taken into account.
- Impact on the in-depth defence for events without a direct impact on the population or the environment, but for which the different measures aiming to prevent the accident did not work as expected.

A further description of the INES scale is available in **Appendix I**.

1.2.1.2. Progression of a Severe Accident

Usually, severe accidents in PWR start by the more or less progressive loss of the primary fluid, as was the case of TMI-2 and Fukushima accidents. This situation may be triggered by a combination of factors such as natural events, equipment malfunction, human errors, etc. The loss of the primary coolant fluid for a long period of time leads to the heat up of the uncovered fuel rods, due to the decay heat of radioactive species.

Three phases may be distinguished during a Severe Accident triggered by the loss of coolant: the **Early in-vessel phase**, the **Late in-vessel phase** and a potential **Ex-vessel phase** (Sehgal, 2012a, 2012b, 2012c). The phenomena taking place during the first two phases are:

Early In-Vessel Phase

- Core uncover
- Metals oxidation
- Cladding deformation and failure
- Release and transport of FP
- Liquefaction and melting of core materials - Loss of core geometry
- Reflooding of the damaged core

Late In-Vessel Phase

- Massive melt formation
- Melt discharge to the lower head
- Extension of the degradation to the bottom of the vessel (as in TMI-2) leading potentially to the lower head rupture

These phenomena do not occur in an ordinate way, but instead they may take place simultaneously in different parts of the reactor vessel. The atmosphere in the vessel and the fuel rods temperature are affected by these phenomena and, with them, the chemical state of the FP residing in the fuel. As it will be demonstrated further in this section, the chemical state affects the rate and the total fraction that may be released out of the fuel during an accident.

In this thesis, we are interested in the early in-vessel phase, since it is when the main release of FP takes place, depending on the atmosphere and temperature conditions. How these two variables are modified by the In-vessel phase phenomena is briefly explained below.

Core uncover: When the primary fluid is partially lost or any other cooling system stops working, the fuel rods overheat and the remaining fluid starts boiling. The steam produced generates an oxidizing atmosphere.

Metals oxidation: Due to the increased temperature and the oxidizing atmosphere, the zirconium, iron, and other metals present in the cladding and structural materials are oxidized. Oxidation reactions are exothermic and so they induce local increments of temperature. The zirconium oxidation is an auto-catalytic reaction, meaning that once it starts oxidizing, the reaction is accelerated. The oxidation of metals generates H₂, and thus the atmosphere becomes reducing. Hydrogen tends to accumulate in the higher parts of the vessel or containment, where it may achieve concentrations high enough as to surpass the ignition threshold, leading to possible explosions. These hydrogen explosions are one of the main risks during severe accidents.

Cladding deformation and failure: The many phenomena taking place in different sections of the cladding (heating, oxidation, local hot spots, etc.) and the stresses associated lead to ballooning and rupture. This allows material slumping, sudden release of the FP located in the fuel-cladding gap and the beginning of FP release from the fuel.

Release and transport of FP: Some FP are released as soon as the cladding fails. Initially, the FP trapped in the cladding-fuel gap and the most volatile ones are released. As the accident progresses and temperature keeps increasing, other FP may be released as well. The kinetics and released fractions depend on conditions such as temperature, oxygen potential (which depends on the atmosphere), Burn-up and type of fuel, etc. Once released, FP are transported into the primary circuit and even further into the containment depending on the evolution of the accident. The behaviour of FP in the primary circuit as well as in the containment is very complex due to the many possible reactions that may occur with structural materials.

Liquefaction and melting of core materials - Loss of core geometry: The UO_2 -Zr interaction is of great importance since it affects the mechanical characteristics and consequently the integrity of the fuel rods. UO_2 may form a liquid solution with Zr from the cladding, leading to rods melting at temperatures significantly below the normal fusion temperature of the UO_2 ceramic, which is 3138 K. Dissolution of UO_2 by solid Zr takes place between 1470 and 2030 K, though the process is very slow and requires a good fuel - cladding contact. Melted materials are capable of dissolving other structural materials (such as the components of control rods), resulting in a very complex liquid solution denominated corium. The corium is continuously oxidised, with production of H_2 and grows bigger as it continues to dissolve materials.

Reflooding of a damaged core: The objective of reflooding is to stop the degradation of the core and corium formation. If the degradation is not stopped, the corium may lead to the failure of the reactor vessel, which would have major consequences such as fission products release into the containment and the possibility of Molten Core-Concrete interactions. Despite being a necessity, reflooding a damaged core has some serious risks, such as:

- Enhancement of the oxidation: as soon as metal get in contact with water they are oxidised, producing a temperature escalation and a large peak of H_2 production;
- Additional core damage: debris bed formation due to thermal shock and collapse of upper fuel rods above the core molten pool;
- Large steam production and heat transfer to upper structures;
- Large FP release due to fuel shattering.

1.2.1.3. Main Severe accidents in history

To this date, there have been three main accidents related to light water reactors: The Three Mile Island accident, which occurred in 1979 in the USA and was classified as Level 5 in the INES scale; The Chernobyl accident in 1986 in Ukraine, classified as level 7 and more recently the Fukushima Daiichi accident in 2011 in Japan, also classified as Level 7.

TMI station consisted on two 900 MW Pressure Water Reactors (PWR), the reactor number two (TMI-2) being the one involved in the accident. This event was triggered by a simple operation incident: a failure in the water supply system of the steam generators. Operators' mistakes and security devices malfunction led to a LOCA type accident. Even though radioactive volatile FP were released into the facility, most of them were retained in the containment so there was a reduced impact on the environment. Six years after the accident it was found that about 45% of the reactor core had melted.

The Chernobyl Plant, named Lenin Nuclear Power Station, consisted of 4 operating RBMK (graphite moderated-Boiling Water Reactors) with a power of 1000 MW each, and two other similar reactors which were under construction by the time of the accident. Ironically, the accident occurred during a test aimed at verifying the response of the reactor to an accident scenario. This test was performed without following the procedures, which led to making wrong decisions. Due to the specific characteristics of the RBMK design, a Reactivity Induced Accident (RIA) took place, in which the power of the reactor rose up to 100 times the nominal value causing the disintegration of the fuel, followed by a steam explosion which blew the top of the reactor, instantaneously releasing to the environment huge amounts of radioactive materials. The Chernobyl accident has been the most severe accident in terms of environmental damage.

The Fukushima Dai-ichi plant was among the 15 biggest nuclear plants in the world, with a total capacity of 4.7 GW distributed in 6 BWR (Boiling Water Reactors). Units 1 (460 MW), 2 and 3 were running at full power at the moment of the accident, while units 4, 5 (these last four with a capacity of 784 MW) and 6 (1100 MW) were out of service for maintenance. The main cause of the accident was a natural disaster: a magnitude 9 (Richter scale) earthquake cut the off-site power system, triggering the safety emergency shutdown of the reactors and emergency power generators. Almost one hour later, a tsunami produced by the earthquake hits the plant, destroying nearly all the power generation emergency systems and producing a Station BlackOut (SBO, a situation in which there is no power at all). As a consequence, the reactor core of units 1, 2 and 3 was gradually exposed due to the loss of coolant. The environmental consequences were quite important: the release of fission gases into the environment was superior to that of Chernobyl, nearly all the initial inventory of xenon from reactors 1 to 3 was released into the atmosphere. Besides fission gases, significant amounts of volatile FP (such as iodine and caesium), representing around 10% of Chernobyl releases in this category, as well as less volatile ones (such as molybdenum and barium) were released into the atmosphere and also directly to the sea through contaminated water discharges.

These severe accidents, particularly the TMI-2 accident, have promoted many research programs in different countries, all aiming at understanding the response of nuclear reactors and nuclear facilities to severe accidents conditions and to allow an assessment of the Source Term. These research programs and their results are presented and discussed below.

1.2.2. Research Programs and their results

The TMI-2 accident made obvious the need of understanding the behaviour of the large variety of components of a nuclear reactor during severe accidents. This need was reinforced later with the Chernobyl and more recently with the Fukushima accident. Many international research programs were initiated across the world in order to determine how these structural materials and FP behave during such critical conditions, by means of numerous in-pile (integral programs) and out-of-pile (analytical programs) tests. The main objectives of these programs have been to understand the core degradation as a result of interactions between core materials and fuel liquefaction; the relocation behaviour of the core with melt formation leading to partial core blockage, fuel debris beds and molten pools; the hydrogen production by steam-oxidation of core materials with relocation; the influence of core degradation on the release, transport and deposition of FP and aerosols and finally the fragmentation of the degraded core due to cooldown and/or quenching.

Integrals tests include: the Source Term Experiments Project (STEP), the Annular Core Research Reactor (ACRR) Source Term (ST) tests, the Power Burst Facility (PBF) Severe Fuel Damage (SFD) tests, the Full-Length High Temperature (FLHT) tests, the Loss-Of-Fluid Test facility (LOFT) Fission Product (FP) test, and the PHEBUS Fission Product (FP). Regarding Analytical tests, the most representative tests have been the HI (Horizontal Induction) and VI (Vertical Induction) tests conducted at the Oak Ridge National Laboratories (ORNL); the Chalk River Laboratories (CRL) analytical tests; the verification experiments of radionuclides gas/aerosol release (VEGA) program at the Japan Atomic Energy Agency (JAEA); and the HEVA, VERCORS series and VERDON programs carried out at the *Commissariat à l'Énergie Atomique et aux Énergies Alternatives* (CEA). The main characteristics of the tests performed in each program, including experimental condition studied and sample characteristics, are summarized in **Table 1**, adapted from (Lewis et al., 2008).

Integral tests recreated whole nuclear reactors at reduced scale, employing different types and sizes of bundles, from four rods to up to 100 rods with rod lengths between 0.15 and 4 m. Nuclear fuels of different burn-up were employed in these tests, from 0 (un-irradiated) up to 47 GWd.t⁻¹. The effect of system pressure from 0.2 to 8 MPa on bundle degradation was also studied. Steam flows spanned from steam-limited to steam-rich conditions, to determine how such flows affect the oxidation of fuel rods and structural materials, as well as the hydrogen generation. The main heating method employed for these integral tests was fission heating. Structural materials (i.e., Inconel and Zircaloy spacer grids) and absorber materials (i.e., Ag--In--Cd or B₄C control rods within stainless steel tubes or blades) were also used in the in-pile experiments to investigate their effect on the core meltdown progression and aerosol production. In-pile tests provided data on core melt progression and FP release. Examples of these programs are:

- The STEP (Baker et al., 1988) experiments, which focused on FP and aerosol chemistry,
- The ST tests, which were devoted to study FP and aerosol release from highly irradiated fuel under reducing atmosphere (hydrogen-inert gas mixture),
- The SFD tests, which studied the fuel bundle behaviour, hydrogen generation, and the release, transport and deposition of FP,
- The FLHT tests, which studied oxidation and hydrogen generation in full-length rods,
- The LOFT FP-2 test (Pena et al., 1992), a relatively large experiment aiming at determining FP transport and the effect of steam supply and reflooding on a severely damaged core assembly,
- The PHEBUS FP tests (Schwarz et al., 1999a; Von der Hardt and Tattegrain, 1992), which simulated the core, cooling system and containment response to a severe accident, including FP release, transport and long term behaviour within the containment.

Regarding Analytical tests, the ORNL program (HI and VI tests) (Lorenz and Osborne, 1995) and CEA (HEVA and VERCORS tests) (Ducros et al., 2013; Leveque et al., 1991), were principally designed to investigate FP release from spent fuel under various atmospheric conditions (i.e., hydrogen, steam and air). The VERCORS program investigated also FP release from MOX fuels and debris bed configurations, as well as FP transport in the primary circuit. In addition, the VEGA annealing tests at JAERI investigated oxidation, dissolution and FP release behaviour on PWR, BWR and Mixed Oxide (MOX) fuels at high temperatures, in helium and helium/steam mixtures at pressures of 0.1 and 1.0 MPa (Hidaka, 2011). The VERDON program (Ferroud-Plattet et al., 2009; Gallais-During et al., 2014), a follow up of the VERCORS one, started at the CEA Cadarache in 2011, and the only ongoing experimental program in the world related to FP behaviour from genuine irradiated fuel.

	Test or accident	Burn-up (GWd.t ⁻¹)	Control materials	Max Temp. (K)	Steam input (g.s ⁻¹)	Atmosphere	N° rods/length (m)	Heating method	Pressure (MPa)	Reference
Integral tests	STEP-1-4	31-36	None	2200-2900	Limited	Steam	4/1.0	Fission	0,16-8	(Baker et al., 1988)
	ACRR ST-1, ST-2	47	None	2450	None	Argon/H ₂	4/0.15	Fission	0,16-1,9	(Allen et al., 1988)
	PBF SFD-ST	trace	None	2800	Excess (16)	Steam	32/0.9	Fission	6,9	(Knipe et al., 1986)
	PBF SFD 1-1	trace	None	2800	Limited (0,7-1,0)	Steam	32/0.9	Fission	6,8	(Martinson et al., 1986)
	PBF SFD 1-3	35-42	None	2800	Limited (0,6-2,4)	Steam	28/1.0	Fission	6,85 and 4,7	(Martinson et al., 1989)
	PBF SFD 1-4	29-42	Ag-In-Cd	2800	Limited (0,6-1,3)	Steam	28/1.0	Fission	6,95	(Petti et al., 1991)
	FLHT-1	trace	None		Excess	Steam	12/4.0	Fission	1.38	(Rausch et al., 1986)
	FLHT-2	trace	None		Limited (1,4)	Steam	12/4.0	Fission	1.38	(Lombardo et al., 1988)
	FLHT-4, 5	trace to 28	None	2500	Limited (1,26)	Steam	12/4.0	Fission	1.38	(Lanning et al., 1988a, 1988b)
	BTF 104-105A,B-107	trace to 28	None	2200-2770	Limited (1,23)	Steam	3-1/4.0	Anneal		(Dickson and Dickson, 1998)
	LOFT FP-2	0,45	Ag-In-Cd + H ₃ BO ₃	2800	Excess (180)	Steam	100/1.7	Decay	1,1	(Carboneau et al., 1989)
	TMI-2	3	Ag-In-Cd + H ₃ BO ₃	2800	Excess	Steam	36816/4	Decay	5-15	(Broughton et al., 1989)
	FPT-0	trace	Ag-In-Cd	2870	Limited (0,5-3,0)	Steam	20/1.5	Fission	0,2	(Hanniet and Repetto, 1999)
	FPT-1	23,4	Ag-In-Cd	2500	Limited (0,5-2,2)	Steam	20/1.5	Fission	0,2	(Bonnin et al., 1997)
	FPT-2	23,4	Ag-In-Cd			Steam	20/1.5	Fission	0,2	(Clément and Zeyen, 2013)
	FPT-3	23,4	B ₄ C			Steam	20/1.5	Fission	0,2	(Clément and Zeyen, 2013)
CORA	None	Ag-In-Cd/B ₄ C	≤2200-2700	Variable (2-12)	Steam	25-57/1.0	Electric	0,2-1,0	(Hofmann et al., 1997)	
Analytical tests	HI 1-6	oct-40	None	1675-2275	(8-500)x10 ⁻⁶	Steam	1/0.15-0.20	Anneal	0.1	(Lorenz and Osborne, 1995)
	VI 1-7	40-47	None	200-2700	0-0,021	Steam/H ₂ /air	1/0.15-0.20	Anneal	0.1	(Lorenz and Osborne, 1995)
	HEVA 1-8	19,37	None	1900-2370	0-0,10	Steam/H ₂	1/0.08	Anneal	0.1	(Leveque et al., 1991)
	VERCORS 1-6	38-55	None	2130-2620	0-0,025	Steam/H ₂	1/0.08-0.087	Anneal	0.1	(Ducros et al., 2013)
	VERDON 1-4	60 (MOX) 72 (UO ₂)	None	2600-2880	Variable	Steam/H ₂	1/0.06	Anneal	0.1	(Gallais-During et al., 2014) (Bernard and Gallais-During, 2013)
	HT 1-3, RT 1-8	39-70	None/Ag-In-Cd/B ₂ O ₃	2970-fuel melting	Variable	Steam/H ₂ /air	1/0.08	Anneal	0.1	(Pontillon and Ducros, 2010a)
	VEGA 1-8, M1, M2	43-56	None	2770-3120	Variable	Helium/Steam	1/0.020	Anneal	0.1 or 1	(Kudo et al., 2006)

Table 1: Main characteristics of Integral and Analytical tests and the TMI-2 accident

1.2.2.1. Integral tests

STEP

The STEP (Source Term Experiments Project) (Baker et al., 1988) was carried out in the TREAT reactor at the Argonne National Laboratory (ANL), USA. Four tests were carried out under steam atmosphere, simulating accidental sequences in PWR and BWR (the total duration of the sequences varied from 20 to 30 min). The test bundle consisted in 4 UO₂ fuel rods, 1 m long, pre-irradiated in the BR3 reactor up to 30-35 GWd.t⁻¹. An additional control rod made of Ag-In-Cd was included only in the STEP-4 test. The maximal temperatures attained were 2900, 2600, 2200 and 2200 K for tests STEP-1 to 4, respectively. The results of this program, regarding FP behaviour, were obtained from chemical analyses and/or SEM observations and were mainly qualitative, though they were relatively consistent regarding the present knowledge on FP volatility.

ACRR

This program was carried out at the Annular Core Research Reactor, Sandia National Laboratory, USA, with the objective to complete the database generated through the HI/VI analytic program (Royle et al., 1987). Two ST (Source Term) tests were carried out between 1987 and 1988, on fuel bundles consisting of four 15 cm fuel elements, pre-irradiated in the BR3 reactor up to 47 GWd.t⁻¹. The temperature attained in both tests was 2450 K, maintained for 20 min under a reducing atmosphere (hydrogen and argon). The tests pressure was 0.16 MPa for ST1 and 1.9 MPa for ST2. The released FP were collected in TGTs (Thermal Gradient Tubes) and filters. Releases measured for I and Cs attained 70% and 80%, respectively, which is in good agreement to other programs. On the other hand, a very small released fraction of Te was observed, less than 1%, and a surprisingly high release of Eu, between 15 and 20%. The releases of Ba and Sr were probably equivalent to that of Eu, since similar released fractions were collected for these three FP (Ba, Sr and Eu) in downstream filters. The unusual released fractions may be due to the test conditions, where the cladding was not previously oxidized, leading to a fuel-cladding interaction. The small released fraction of Te may be due to the retention in the corium of a non-volatile chemical form. The elevated released fractions of Sr, Ba and Eu are the result of a strong reducing atmosphere: the molten Zr from the cladding would have penetrated into the fuel, thus reducing these FP oxides.

PBF-SFD

The PBF-SFD (Power Burst Facility - Severe Fuel Damage) program was carried out at the Idaho National Laboratory (INEL), USA, from 1982 to 1985 (Petti et al., 1989). Four transient tests were carried out under steam atmosphere, up to 2800 K with (for tests SFD-ST and SFD 1-1) and without (for tests SFD 1-3 and SFD 1-4) a reflooding stage. The test bundle consisted in 32 UO₂ fuel rods of 1 m long and Inconel grids. Rods were un-irradiated for the first two tests, and pre-irradiated for the other two (from 29 to 42 GWd.t⁻¹). The last test included four control rods made of Ag-In-Cd. The melted fraction attained 15 to 18% in each of the four tests. Only fission gases and volatile FP such as I, Cs and sometimes Te were quantified, their significant releases were consistent to the degree of core melting.

FLHT

The FLHT (Full-Length High Temperature Tests) was carried out in the NRU reactor at the Chalk River Laboratory (CRL), Canada, supervised by the US Pacific North-west Laboratory (PNL) (Lanning et al., 1988a,

1988b; Lombardo et al., 1988; Rausch et al., 1986). Four tests were carried out, with bundles consisting in 3.7 m long PWR UO₂ fuel rods. For the first two tests, FLHT-1 and 2, the bundle consisted in 12 un-irradiated fuel rods, while for the two following tests, FLHT 4 and 5, it consisted in 10 un-irradiated and 1 pre-irradiated rods, the latter up to 28 GWd.t⁻¹. The main findings in this program were related to core degradation phenomena. Nevertheless, some information on FP behaviour was obtained. Particularly for the FLHT-5 test, where the maximum fuel temperature attained was 2500-2600 K, 50% of fission gases were released and volatile FP deposits were found and quantified at the upper part of the fuel rods: 0.7 to 0.9% of iodine and caesium and 0.02% of tellurium.

BTF

The BTF program (Blowdown Tests Facility) was also carried out in the NRU reactor at the Chalk River Laboratory, Canada, using CANDU fuel bundles, some of which had been pre-irradiated up to 5 GWd.t⁻¹. This facility, rather similar to PHEBUS FP described below, had for objective the study of core degradation phenomena as well as FP release and transport up to a tank which simulated the containment. Many γ -spectrometry detectors and FP sampling systems were installed to that end. Four tests were carried out between 1990 and 1997. In the first of them, BTF-107, a bundle consisting in 3 fuel elements attained a maximal temperature of 2770 K (DeVaal et al., 1992; MacDonald et al., 1991). A flow blockage developed during the test due to the relocation of U--Zr--O alloy and the high temperature transient was terminated with a cold water quench. The other three experiments in the BTF program, BTF-104, BTF-105A and BTF-105B, were conducted with single CANDU-sized fuel elements at maximum temperatures of 1800-2200 K in a steam-rich environment (5 g.s⁻¹ steam flow). The BTF-104 experiment provided data on fuel behaviour, and volatile FP release and transport (Kr, Xe, I, Cs, Te and Ba) from a pre-irradiated fuel element at a fuel temperature of about 1800 K (Dickson et al., 1995a, 1995b; Dickson and Dickson, 1998). The primary objectives of the BTF-105A experiment were to obtain data for validation of transient fuel performance codes and to test instrumentation for the BTF-105B experiment (DeVaal et al., 1997; Valliant et al., 1999). The BTF-105B experiment had thermal hydraulic boundary conditions which were better quantified and was performed to investigate FP release and transport from a pre-irradiated fuel element at a fuel temperature of 2100 K (Irish et al., 1999, 1998).

LOFT-FP

The LOFT-FP (Loss Of Fluid Test Facility-Fission Products) program was carried out at the Idaho National Laboratory (INEL), USA. This facility reproduced a PWR reactor in a 1:50 scale; the main loop included a steam generator, a pressurizer, two primary pumps in parallel configuration. A second loop, connected to a reservoir, allowed the simulation of breaches. Two integral tests were carried out in this facility, aiming to study FP release in complete accident scenarios: The LP-FP1 test, carried out in 1984 simulated a LOCA and LP-FP2 test, carried out in 1985, simulated an accident similar to that of TMI-2, including a late core reflooding stage. For test LP-FP2, the bundle placed in the LOFT reactor consisted of 100 UO₂ fuel rods, 1.7 m long, irradiated up to 0.45 GWd.t⁻¹ and 11 control rods made of Ag-In-Cd. The bundle reflooding was initiated at temperatures between 2100 and 2400 K attaining maximum temperatures between 2800 and 3100 K. The LP-FP2 test, the largest scale test simulating a severe accident performed to this day besides the TMI-2 and Fukushima accidents, provided important results: cladding oxidation and failure, partial melting of the core (15%), debris bed formation, pressure increase and steam and hydrogen generation during reflooding. Regarding FP release, the information obtained was limited due to measuring problems.

Small released fractions were expected for volatile FP, but instead important ones were observed: 16% for I and Cs, 12% for Kr, 3% for Te and 9% for Ba. Around 80% of Ba release would have taken place during the reflooding stage, probably due to a temperature increase at the beginning of this stage (exothermic reaction of cladding oxidation) and to the fuel fracturing, leading to a debris bed formation. Finally, post-test examinations demonstrated that iodine had been essentially transported as AgI and caesium as CsOH.

PHEBUS FP

The PHEBUS Fission Product (PHEBUS FP) program objectives were to investigate severe accident phenomena, FP release from the core, FP transport in the primary circuit and FP transport in the containment. This program consisted in five in-pile tests, described in **Table 2**, in which the phase behaviour of in-vessel core melt degradation was studied over various atmospheric conditions (i.e., oxidizing and reducing) in a temperature range up to 2800 K (Von der Hardt and Tattegrain, 1992). The first two PHEBUS FP experiments were designed to provide information on the differences between the degradation of fresh (FPT-0) and irradiated (FPT-1) fuel rods for a low-pressure transient (0.2 MPa) (Bonnin et al., 1997; Hanniet and Repetto, 1999). Tests FPT-2 and FPT-3, with similar fuel samples and test conditions, were designed in order to provide information on FP interaction with the control rod (Ag-In-Cd for FPT-2 and B₄C for FPT-3) and pH effect on iodine chemical forms in the containment. The FPT-4 test was performed to investigate semi-volatile FP and actinide release from a UO₂/ZrO₂ debris bed. Except for FPT-4, each of these tests employed 20 PWR fuel rods, 0.8 m long.

These experiments provided information on core melt progression and materials oxidation with hydrogen production; release of volatile FP from overheated/liquefied fuel and their interaction with structural material aerosols; aerosol depletion in the primary circuit and containment (including iodine re-volatilization phenomena in the containment); and the influence of condensation, pool boiling and containment sprays on the source term (Von der Hardt and Tattegrain, 1992). The data obtained from this program, as well as the VERCORS program, have been extensively used for verification of codes for source term analyses (Dubourg et al., 2005; Herranz et al., 2007; Veshchunov et al., 2007, 2006).

Test	Fuel type	Fuel degradation	Primary circuit	Containment	Date
FPT-0	Fresh Fuel Pre-irradiated Ag-In-Cd rod	Melt Progression and FP release in steam atmosphere	FP chemistry and deposits in non-condensing steam generator	Aerosol deposition. Iodine radiochemistry at pH5	December 1993
FPT-1	23 GWd.t ⁻¹ Re-irradiated Ag-In-Cd rod	As FPT-0	As FPT-0	As FPT-0	July 1996
FPT-2	As FPT-1	As FPT-1 under poor steam conditions	As FPT-1 with effect of boric acid	pH9 evaporating sump	October 2000
FPT-3	As FPT-1 B ₄ C rod	As FPT-2	As FPT-0	pH5 evaporating sump re-combiner coupons	November 2004
FPT-4	No re-irradiated debris bed 38 GWd.t ⁻¹	Low volatile FP and actinide release from UO ₂ -ZrO ₂ debris bed up to melting	Integral filters in test device. Post-test analyses on samples		July 1999

Table 2: PHEBUS program test grid.

The PHEBUS program made some key findings in the behaviour of FP and structural materials during an accidental sequence:

- It highlighted the interactions of the fuel with other materials such as the cladding and control rods, as it was observed that the system would start melting at temperatures below UO₂ or ZrO₂ melting points (Hofmann, 1999);
- Regarding FP transport, it was observed that the chemical compounds (of Cs and Mo, for example) found in the Reactor Cooling System were different to those assumed.
- It helped improve the ICARE code (Chatelard et al., 2006) used by IRSN for cladding oxidation, leading to more accurate estimations of hydrogen production rates for various accidental conditions;

The program also made important contributions to the understanding of gas phase reactions, including the interactions of gaseous iodine with painted surfaces and air-radiolysis products that can be, in many cases, predominant over classical liquid phase reactions. Detailed information on the PHEBUS experimental program may be found in **Appendix II**.

1.2.2.2. *Analytical tests*

As mentioned before, many out-of-pile tests have been conducted at the ORNL (USA), at the CEA (France), at the JAEA (Japan), and at the CRL (Canada). These tests were designed to investigate the release behaviour of FP in high temperature accidents with variable atmospheric conditions. Detailed information on the analytical programs experimental facilities may be found in **Appendix II**.

ORNL experiments

Program description

The HI and VI programs, detailed in **Table 3** and **Table 4** respectively, have been carried out at the Oak Ridge National Laboratory, USA (Lorenz and Osborne, 1995). In these tests, UO₂ fuel samples 15-20 cm long (100-200g) in their Zircaloy cladding and irradiated to typical LWR burn-up were used. Fuel samples were heated under atmospheric pressure up to 1700-2700K using induction furnaces, where the time at maximum temperature varied from 2 to 60 min.

The major differences between the VI and HI tests were:

- (a) VI tests were oriented vertically while the HI tests were horizontal;
- (b) Fuel burn-up in most VI tests were higher than those used in the HI tests;
- (c) VI tests temperatures (2300-2700 K) were higher than those of the HI tests (1675-2275 K).

The VI-3, VI-5 and VI-6 tests were performed at maximum test temperatures of approximately 2700 K; the test atmosphere (steam in VI-3, hydrogen in VI-5, hydrogen followed by steam in VI-6, and air and steam in VI-7) was varied so that the influence of the atmosphere on the FP release could be studied.

There were limited on-line measurements of FP release rates (only ¹³⁷Cs and ⁸⁵Kr, because fuel samples were not re-irradiated prior to tests). Since a segmented furnace tube was used in the tests to allow a rapid heating, the containment of the test environment was not good and there is evidence of oxidation of the graphite susceptor in some tests (Lewis et al., 1995). Generally, samples were maintained at the test temperature for short periods of time (about 20 min), which may not have been long enough to see the releases in oxidizing conditions, especially at lower temperatures.

Program results

These tests showed similar release rates for noble gases, Cs and I; however, a difference in transport behaviour was noted for Cs in steam relative to hydrogen. Reactive gaseous forms of Cs predominate in hydrogen conditions, while transportable aerosols were observed in steam conditions. The releases of Te and Sb appear to occur from the UO₂ at release rates similar to those for the volatile FP, but these elements are retained by metallic Zircaloy so their release is delayed until cladding oxidation is nearly complete. Both Eu and Sb showed sensitivity to the oxygen potential at high temperature (Lorenz and Osborne, 1995). Sb release rates were observed to increase in steam conditions relative to hydrogen at higher temperatures while hydrogen-rich conditions caused higher releases of Eu compared with steam environments (Lorenz and Osborne, 1995).

Conditions	HI Tests					
	HI-1	HI-2	HI-3	HI-4	HI-5	HI-6
Mass ^a (g)	168	166	167	306	133	170
Length (mm)	203	203	203	203	152	152
Burn-up (GWd.t ⁻¹)	28.1	28.1	25.2	25.2	38.3	40.3
Max temperature (K)	1675	2000	2275	2200	2025	2100
Time maintained (min)	33	20	22	20	23	9
Steam flow (g/min)	0.81	0.76	0.31 ^b	0.29 ^b	0.30 ^b	1.07
Element	Released fraction (%)					
⁸⁵ Kr	2.83	51.5	59	21.1	15.8	29.6
¹²⁵ Sb	<0.02	1.55	>0.001	>0.009	>0.33	0.068
¹²⁹ I	2.48	65.6	43.2	30.1	27.3	30.1
¹³⁴ Cs	1.75	50.5	58.8	31.7	20.3	33.1
¹⁵⁴ Eu				<0.6	0.021	
Sr ^c	<0.002			<0.005		
Mo ^c		5.9				
^{110m} Ag ^c	0.3	2.9	>0.015	<0.094	18	6
Te ^c	0.25	0.5	0.3	<0.4		
Ba ^c	0.01			<0.04	0.08	
La ^c	0.02		<0.0002			
U ^c	<0.00002			<0.00004		

Table 3: HI series test grid

^afuel + cladding; ^bincomplete oxidation of the cladding, fuel prematurely delocalised by dissolution;

^capproximate values.

Conditions	VI Tests						
	VI-1	VI-2	VI-3	VI-4	VI-5	VI-6	VI-7
Mass ^a (g)	140.4	103.3	102.3	99.3	102	103	178.7
Length (mm)	152	152	152	152	152	152	152
Burn-up (GWd.t ⁻¹)	40	44	44	47	42	42	40
Temperature (K)	2020, 2300 ^b	2300	2000, 2700 ^b	2440	2000, 2720 ^b	2310	2025, 2300 ^b
Time at T (min)	20, 20	60	20, 20	20	20, 20	60	20, 20
Atmosphere	Steam	Steam	Steam	H ₂	H ₂	H ₂ + Steam	Air + steam
Element	Released fraction (%)						
⁸⁵ Kr	46		99.5	94.4	100	75.3	69
¹⁰⁶ Ru			5.01	0	0		<2.8
¹²⁵ Sb	33.2	68.1	99.2	6.4	17.9	63.5	52
¹²⁹ I	45.3	40	79	86.8	70.2	76.7	42
¹³⁴ Cs	63.2	67.2	99.9	95.9	99.9	80.2	71.4
¹⁴⁴ Ce			< 0.2		2		
¹⁵⁴ Eu			< 0.01	18.6	57.4	13.7	0.05
Sr ^c			2.7		33.7	5.8	1.2
Mo ^c	43.0	85.6	77	6.9	2.3	12.6	5.3
Te ^c			98.8		81.5	63.4	
Ba ^c		18.9	29.7	26.8	75.7	32.4	4.1
U ^c	0.01	0.03	1.3		0.015	0.001	
Pu ^c		0.003	0.005	0.1			

Table 4: VI series test grid

^afuel + cladding; ^btest with two phases; ^capproximate values.

CEA experiments

Programs description

FP and structural material releases from PWR fuel samples have been studied in out-of-pile experiments at the CEA (Ducros et al., 2001; Iglesias et al., 1999; Leveque et al., 1991; Lewis et al., 1995; Pontillon et al., 2005b). The HEVA program was conducted between 1983 and 1989, and consisted of 8 tests carried out in a 1900-2370 K temperature range. An induction furnace was used to heat Zircaloy-cladded PWR fuel samples, and gamma spectrometry was used to measure the FP releases from the fuel and transport to different locations in the experimental loop. Aerosols were collected in a heated cascade impactor during each test. The temperature of the impactor varied in the HEVA tests (but not in the VERCORS tests series). Control rod materials were used in the last two tests (HEVA-7 with Ag--In--Cd and fresh fuel and HEVA-8 with Ag-In-Cd and irradiated fuel). Mixtures of steam/H₂ and pure H₂ have been used as the environments for the HEVA tests. **Table 5** details the HEVA test conditions and FP release results.

The VERCORS program (Pontillon et al., 2010) was an extension of the HEVA tests from 1989 to 1994 using a modified experimental loop and better instrumentation. The fuel sample consisted of three spent PWR pellets with two half pellets of depleted uranium placed at both sides, which were held in place by crimping the cladding so that the fuel specimens were not fully sealed. In most of the more recent tests the fuel specimens were re-irradiated in SILOE or OSIRIS research reactors after a short period of decay following the discharge from the power reactor, in order to recreate the inventory of short-lived FP such as I, Te, Mo, Ba and La. Six tests were carried out in the VERCORS program to study volatile and semi-volatile FP behaviour up to a maximum temperature of 2620 K. Extensive post-test gamma scanning (including gamma tomography) were performed after each test. Test conditions and results from the VERCORS test series are detailed in **Table 6**.

From 1996 to 2002, the VERCORS HT (High Temperature) and RT (Release of Transuranians) programs, described in **Table 7** and **Table 8**, were carried out to improve the database and to study the release of FP and actinides during the late phase of an accident, with fuel liquefaction (Ducros et al., 2013; Pontillon et al., 2010; Pontillon and Ducros, 2010a, 2010b).

The VERDON program, started in 2011 at the Cadarache centre, has an experimental loop similar to that of the VERCORS HT series, including extensive instrumentation (Ducros et al., 2009; Ferroud-Plattet et al., 2009). Samples consist in two re-irradiated fuel pellets together in their original cladding, along with a half depleted UO₂ pellet at each side.

Four tests were performed in the framework of the ISTP (International Source Term Program). The VERDON 1 test (Pontillon and Gallais-During, 2012), was carried out in September 2011. A 72 GWd.t⁻¹ burn-up UO₂ fuel sample was submitted to an annealing sequence similar to the VERCORS RT6 test, with a final stage under reducing atmosphere. The VERDON 2 test (Gleizes and Morin, 2012) was carried out in June 2012. A 59 GWd.t⁻¹ burn-up MOX fuel sample was submitted to very oxidizing conditions, simulating an air-ingress scenario. The VERDON 3 test (Bernard and Gallais-During, 2013) was carried out in April 2013. A MOX fuel sample, irradiated up to around 60 GWd.t⁻¹ was submitted to oxidizing conditions (steam + He) during this test. Regarding VERDON 4, performed in October 2014, a MOX fuel identical to the one used for VERDON 3 has been submitted to reducing conditions.

Programs results

Post-test gamma scanning enabled a complete FP mass balance in the VERCORS programs. Nearly total release of volatile species such as Cs, I, Te and Sb was confirmed for tests performed up to around 2600 K, with release kinetics very sensitive to the oxygen potential. However, Te and Sb were observed to be trapped in the unoxidized cladding although the total released fraction from the fuel sample eventually reached that of the other volatile species. Furthermore, their release kinetics were also sensitive to fuel type (UO₂, MOX) and burn-up. The so-called semi-volatile FP such as Mo, Pd, Tc, Rh and Ba, which chemical forms limit their release to nearly half of that of volatiles, were also sensitive to the atmospheric conditions. Interactions between these FP as well as the sample burn-up affect the release of some of these species. Ba can be trapped by the Zr in the cladding and Mo can react with Cs reducing its volatility. The Mo release was observed to increase in oxidizing conditions (e.g., 92% release in VERCORS 5 versus only 47% in VERCORS 4) while, in contrast, Ba and Rh releases increased in reducing conditions (e.g., 45% and 80% of Rh and Ba, respectively, in VERCORS 4 as compared with only 20% and 55% in VERCORS 5). The so-called low-volatile FP species consisted of Ru, Nb, Sr, Y, La, Ce and Eu, with releases generally between a few and 10%. An increase in sample burn-up was shown to enhance the release of some elements of this group, particularly for Ru and Nd (Pontillon and Ducros, 2010a). Ru releases are also known to be significantly enhanced in air (Cox et al., 1991; Pontillon and Ducros, 2010a, 2010b). There were no significant releases of Zr, Nd and Pr under the temperature range studied in the VERCORS 1-6 experiments, and so they were classified as non-volatile FP. In the VERCORS 6 test performed with high burn-up fuel, although early fuel collapse and partial liquid corium was observed, there was no significant enhancement in release, where the liquid phase retained a fraction of semi and low-volatile FP.

The RT and HT programs also provided information on the release behaviour of FP: fuel nature influence (UO₂ vs. MOX), effect of the fuel morphology (intact pellets vs. debris fragments), effect of fuel burn-up, impact of absorber materials (Ag, In, Cd and boric oxide) and influence of the environmental sequence of the accident (oxidizing or reducing conditions). In the more severe VERCORS HT and RT test, Nb and La have been observed to be released more readily from the fuel. These tests also provided information on the temperature of fuel collapse, which occurred over a temperature range of 2400-2600K for fuel burn-ups of 47-70 GWd.t⁻¹; which is about 500 K below the UO₂ melting temperature. The observed differences may be explained by the stoichiometric change of the fuel samples during the tests and maybe the presence of FP within the fuel matrix (Pontillon et al., 2005b).

Summarizing, the VERCORS series tests have shown that the release kinetics of the volatile species are sensitive to the environment oxygen potential, burn-up and fuel type. The VERDON tests performed so far have confirmed the behaviour observed for FP in terms of volatility and conditions effect. They have also confirmed the MOX fuel effect on FP behaviour, already observed in the VEGA tests, which tends to accelerate the release of volatile FP.

Conditions	HEVA Tests							
	HEVA 1	HEVA 2	HEVA 3	HEVA 4	HEVA 5	HEVA 6	HEVA 7	HEVA 8
Burn-up (GWd.t ⁻¹)	19.4	19.4	27.7	36.7	36.7	36.7		36.7
Temperature (K)	1900	2140	2070	2270	2070	1570, 2370	2070	2070
Time at T (min)	15	15	30	7	96	60, 30	30	12
Steam flow (g.min ⁻¹)	6	1.8	2.2	1.8	1.5	0	1.5	1.5
H ₂ flow (g.min ⁻¹)	0	0	0.03	0.03	0.03	0.012	0.03	0.03
Element	Released fraction (%)							
Mo				21	55	~4		<DL
Ru		<DL	<2			0		
Sb	1	41	20	18				<DL
Te				52	54	11		<DL
I				43	62	30		12
Xe				~42	~65	30		
Cs	~2	69	38	44	66	30		15
Ba				5.6		27		<DL
Ce		<DL	<3			0		
Eu		~15	<3			~5		
Ag ^a							10	10
In ^a							95	100
Cd ^a							100	100

Table 5: HEVA test grid

^aelements from neutron absorbers. DL= Detection Limit.

Conditions	VERCORS Test					
	VERCORS 1	VERCORS 2	VERCORS 3	VERCORS 4	VERCORS 5	VERCORS 6
Burn-up (GWd.t ⁻¹)	42.9	38.3	38.3	38.3	38.3	60
Temperature (K)	2130	2150	2570	2570	2570	2620
Time at T (min)	17	13	15	30	30	30
Atmosphere ^a	H ₂ O+H ₂	H ₂ O+H ₂	H ₂ O+H ₂	H ₂	H ₂ O	H ₂ O+H ₂
Steam flow (g.min ⁻¹)	0.15	1.5	1.5	1.5-0	1.5	1.5
H ₂ flow (g.min ⁻¹)	0.003	0.027	0.03	0.012	0	0.03
Element	Released fraction (%)					
Sr				<6	<6	<6
Y			17			
Zr				<3	<4	<4
Nb						0.3
Mo		15	42	47	92	79
Ru			0.36	6	6	0.6
Rh			0.52	45	20	
Sb	2	7	69	97	98	96
Te	4	18	76	100	98	97
I	30	23	70	87	93	97
Xe	33	23	77	86	87	~100
Cs	42	30	70	93	93	97
Ba	4	4	13	80	55	29
La			<4	<3	<3	<3
Ce				3	<3	0.2
Eu			<6	<5	<3	<4
Np	0.006	0.016	0.4	6	<4	0.3
U ^b				~2	~2	
Pu ^b				~0.2	~0.2	

Table 6: VERCORS test grid

^aAtmosphere at the end of the test; ^bapproximate values.

Conditions	VERCORS RT Tests						
	RT1	RT2	RT3	RT4	RT6	RT7	RT8
Fuel type	UO ₂	MOX	Debris	Debris	UO ₂	MOX	UO ₂
Burn-up (GWd.t ⁻¹)	47.3	45.6	39	37.6	71.8	43	70
Temperature (K)	2570	2440	2520	2970	2890	2470	2650
Atmosphere ^a	H ₂ O + H ₂	H ₂ O + H ₂	Reducing	Oxidizing	H ₂ O + H ₂	H ₂	He + 10% air
Steam flow (g.min ⁻¹)	1.5	1.5	0.075	0.876	1.5	1.5-0	
H ₂ flow (g.min ⁻¹)	0.027	0.027	0.075	0.024	0.027	0.012	
Air flow (g.min ⁻¹)							0.048
Element	Released fraction (%)						
Kr	~100	~100	~100	>90	~100	~100	~100
Sr							
Y							
Zr			<2		<2	<2	<2
Nb			40.3		30.4	3	10.9
Mo			33.2		100	7	100
Ru	9	5.4	1.5	7.7	28.1	2	17
Rh							
Ag	>90	>97		~100	~100		~100
Sb	95	77	60-95	89	90	86	84
Te			100		99.5	99	100
I			100		100	99	100
Xe			100		100	~100	100
Cs	100	100	99.8	96	100	98	100
Ba			93.9		57.7	64	67.2
La			12.5		7	3	10.6
Ce	3.2	<3		2.5	16	14	18
Eu	1.2	0.3	3.5	0.8	1.7	10	2.6
N			1.4		10.3	4	2.7
U	7.8	3.8-4.9	2.3	9.9			
Pu	0.3	0.1		<0.1			

Table 7: VERCORS RT test grid

^aAtmosphere at the end of the test

Conditions	VERCORS HT Tests		
	HT1	HT2	HT3
Burn-up (GWd.t ⁻¹)	49.4	47.7	49.3
Max temperature (K)	2900	2420	2690
Atmosphere ^a	H ₂	Steam	H ₂
Steam flow (g.min ⁻¹)	1.5-0	1.5	1.5-0
H ₂ flow (g.min ⁻¹)	0.012	0	0.012
Element	Released fraction (%)		
Kr	~100	~100	~100
Sr	<5		
Y	-	-	-
Zr	<3	<2	<2
Nb	9	9.7	18
Mo	49	100	33
Ru	8	65	6
Rh	-	-	-
Ag	-	-	-
Sb	100	71	98
Te	100	100	98
I	100	100	100
Xe	~100	100	100
Cs	100	100	100
Ba	49	38.5	85
La	8	5.5	13
Ce	5	1	0.8
Eu	9	1	10.5
Np	7	<2	5

Table 8: VERCORS HT test grid

^aAtmosphere at the end of the test

JAEA experiments

Program description

Ten tests have been performed in the VEGA experimental facility from 1999 to 2004, conducted at the JAEA (Japan Atomic Energy Agency) (Hidaka, 2011). In these tests, the impact of temperature, atmosphere, pressure and fuel type on FP release was investigated. The main characteristic of this program was the possibility of performing annealing test at high pressure (up to 1 MPa) and high temperature (up to 3120 K). A model for FP release under pressure effect was developed from these results (Hidaka, 2011). Samples were sections of PWR, BWR (both UO₂) and ATR (MOX) fuel about 60 mm long with a mass between 40 and 100 g, most of them without cladding. Some samples were re-irradiated during 8 h (VEGA 5) to 26 days (VEGA 6 and 7). Tests conditions and results from the VEGA test series are detailed in **Table 9**.

Program results

These tests showed that the release of caesium at 1.0 MPa was reduced by about 30% for temperatures below 2773 K, compared with tests at 0.1 MPa. Consequently, caesium releases in high pressure scenarios may be lower than that predicted by current models. Low-volatile species such as Eu, Ru and Ce were deposited close to the sample location but Cs was transported downstream, where it deposited in the TGT (Thermal Gradient Tube) at about 800 K. During the high temperature tests, enhanced Cs release rates observed for temperatures above 2800 K were attributed to fuel frothing and melting (Hidaka et al., 2002a).

The releases from MOX fuels were studied in the VEGA-M1 and M2 tests (Hidaka et al., 2002a, 2002b; Kudo et al., 2001). Significant Cs releases were observed at around 1000 K while similar releases were only evident at 1623 K in the UO₂ tests. The variation in Cs release at low temperature is explained by the difference in irradiation history. Despite this difference in the kinetic behaviour, the total Cs releases for both fuel types were similar. In particular, enhanced Cs release rates for temperatures higher than 2800 K observed in UO₂ samples were also evident during the MOX tests. Similar results were also observed for U, Pu, Sr and Mo for UO₂ and MOX fuels. Results of the VEGA tests under flowing steam are consistent with those from other programs (Hidaka, 2011; Kudo et al., 2006). Here an increased deviation in UO_{2+x} stoichiometry resulted in an enhanced release of volatile FP. In the case of Zircaloy-cladded samples, this effect is absent at temperatures above 2030 K, which was attributed to the competing process of UO₂ reduction by molten Zircaloy. Dissolution rates of UO₂ by molten Zircaloy were estimated to be about 1000 times lower in steam than in hydrogen environments.

Conditions	JAEA Tests									
	VEGA-1	VEGA-2	VEGA-3	VEGA-4	VEGA-5	VEGA-M1	VEGA-6	VEGA-M2	VEGA-7	VEGA-8
Burn-up (GWd.t ⁻¹)	47	47	47	47	47	43	56	43	56	56
Cladding	NO	NO	NO	YES	NO	NO	YES	NO	YES	NO
Reirradiation	NO	NO	NO	NO	NSRR	NO	JRR-3	NO	JRR-3	NO
Max T (K)	2773	2773	3123	2773	2900	3123	2773	3123	2773	3123
Atmosphere	He	He	He	Steam	He	He	Steam	He	Steam	He
Pressure (MPa)	0.1	1.0	0.1	0.1	1.0	0.1	0.1	1.0	1.0	0.1
Element	Released fraction (%)									
¹³⁷ Cs	86	61	100	93	84	97	93	98	98	97
¹²⁵ Sb	89	68	95		67	95	-	96	83	-
¹³¹ I	-	-	-	-	-	-	97	-	96	-
¹³² Te	-	-	-	-	-	-	98	-	98	-
¹⁴⁰ Ba	-	-	-	-	7	-	49	-	34	-
¹⁰³ Ru	5	0	0	22	0	6	14	3	6	0
¹⁴⁰ La	-	-	-	-	-	-	3	-	4	-
Mo	-	-	-	-	-	0.6	-	-	-	0.3
Sr	-	-	-	-	-	2	-	-	-	11
U	-	-	-	-	-	0.4	-	-	-	0.1
Pu	-	-	-	-	-	2.8	-	-	-	2.1

Table 9: VEGA program test grid and results

AECL-CRL experiments

Program description

In this program, conducted at AECL Chalk River Laboratories (Canada) from 1983 to 1992, more than 300 annealing tests were carried out. Fuel specimens with and without cladding of 0.2-1.5 g each, extracted from irradiated fuel elements were submitted to temperatures between 800 to 2350 K in Ar/H₂, steam and air atmospheres (D. S. Cox et al., 1992; Cox et al., 1991; Hunt et al., 1986; Liu et al., 1994). Test conditions and FP released fractions of some tests are presented in **Table 10**.

One of the main features of the AECL program was the possibility of on-line measurement of the oxygen potential in the gas stream, enabling the calculation of the fuel oxidation kinetics (D. S. Cox et al., 1992). These tests also provided information on FP release from bare UO₂ without any Zircaloy barrier. The role of Zircaloy on FP release has been investigated using fragments of UO₂ enclosed in Zircaloy foil bags, and short segments of Zircaloy-clad fuel elements with end caps fitted at the tops to exclude the surrounding atmosphere from direct contact with the UO₂.

Program results

It has been shown that the presence of a Zircaloy sheath can either inhibit or delay the release of volatile FP, compared to tests under the same conditions using unclad UO₂ samples. The delay is primarily associated with the time required to oxidize the Zircaloy cladding, after which the UO₂ oxidation begins, causing enhanced release rates. The release rates of volatile FP from clad fuel samples after complete cladding oxidation are almost independent of temperature in the range 1670--2140 K (Liu et al., 1994). It has also been demonstrated that releases of volatile FP (Kr, Xe, I, Cs and Te) are relatively low in inert or reducing atmospheres but increase significantly after the cladding oxidation, in oxidizing atmospheres.

In some of the high temperature tests on unclad fuel samples, large fractions of the UO₂ fuel was volatilized in highly oxidizing environments, leading to the release of low-volatile FP (e.g., Zr, La, Ba, Ce, Pr, Eu) via a "matrix stripping" process, where these products are normally soluble in the UO₂ (Liu et al., 1994). An improved release of low volatile FP, such as Eu and Ba, was observed in hydrogen-rich atmospheres, while steam atmospheres favoured the release of Mo, Ru, Nb, etc.

The major contribution of these tests concerns the influence of the oxygen potential in the release of low-volatile FP, such as ruthenium. For example, as it is observed in **Table 10**, in the MCE1-6 test in reducing conditions at 2273 K, Ru release was quite low while during the MCE 1-1 test under air atmosphere at 1973 K, Ru was completely released 13 minutes after the air injection. This effect was such that the release of Ru was faster and greater than that of the volatile FP, Cs and I (Iglesias, 1989; Iglesias et al., 1999). These tests also made possible to develop models for steam and air oxidation of UO₂ (Cox et al., 1990; Lewis et al., 1995).

Sample	Test							
	MCE1-1	MCE1-6	MCE1-7	MCE2-13	HCE2-BM3	MCE2-19	HCE2-CM4	UCE12-8
Type	Fragment ^a	Fragment	Fragment	Fragment	Fragment	Segment ^c	Segment	Segment
Burn-up (GWd.t ⁻¹)	25.7	25.7	25.7	45.7	45.7	54.4	45.7	37.0
Conditions								
Temperature (K)	1973	2273	2350	2080	2300	1775	1625	1675
Time at T (min)	13	37	17	17	10	110	140	200
Heating rate (K.s ⁻¹)	0.2	0.2	0.2	0.2	0.2	0.1	0.1	0.9
Atmosphere	Air	Ar + 2% H ₂	Air	Steam	Steam	Steam	Air	Steam
	Release fraction (%)							
¹³⁷ Cs	80	80	100	92	100	75	75	96
¹³¹ I	80	80	100	NA	NA	NA	NA	NA
⁹⁵ Nb	0	10	45	25	47	<2	3	<1
⁹⁵ Zr	0	0	30	<2	<2	<2	<1	<1
¹⁰³ Ru	100	1	100	NA	NA	NA	NA	NA
¹⁰⁶ Ru	NA ^b	NA	NA	80	80	<2	20	<1
¹⁴⁰ Ba	0	40	90	NA	NA	NA	NA	NA
¹⁴⁰ La	0	0	35	NA	NA	NA	NA	NA
¹⁴⁴ Ce	NA	NA	NA	20	20	<2	<2	<2

Table 10: Conditions and results of some CRL tests

^aBare fragment of UO₂; ^bIsotope was not present at the time of the test; ^cFuel element with zircaloy cladding (2-5 cm long)

1.2.3. Fission products behaviour

FP behaviour in severe accident conditions has been widely studied through analytical research programs such as the French HEVA, VERCORS series and VERDON programs, the Japanese VEGA program, the Canadian AECL-CRL program and the ORNL program from the USA; as well as in integral research programs such as the PHEBUS FP, STEP, ACRR, LOFT and FLHT programs. These programs recreated the conditions of severe accidents in terms of atmosphere and temperatures. Analytical tests were dedicated to single-effects analysis on FP behaviour (such as burn-up or oxygen potential effect on the release rates), while the more complex Integral tests were dedicated to the study of reduced-scale nuclear facilities response to accidental sequences. Some integral and analytical programs experimental results, along with those from the TMI-2 accident are summarized in **Table 11**, extracted from (Lewis et al., 2008).

Conditions	PBF			PHEBUS		TMI-2	ORNL		VERCORS	
	SFD-ST	SFD 1-1	SFD 1-4	FPT-0	FTP-1		VI-3	VI-5	VERCORS-4	VERCORS-5
Max. Temperature (K)	2800	2800	2800	2870	2500	2800	2700	2720	2570	2570
Atmosphere	H ₂ O	H ₂ O	H ₂ O	H ₂ O/H ₂	H ₂ O/H ₂	H ₂ O/H ₂	H ₂ O	H ₂	H ₂	H ₂ O
Test environment	Steam rich	Steam starved	Steam starved	Steam rich	Steam rich	Steam rich	Steam rich	Steam starved	Steam starved	Steam rich
Fuel Burn-up (GWd.t ⁻¹)	Trace	Trace	29-42	Fresh	23	3	44	47	47	38
Zr oxidized (%)	75	28	38	85	68	45				
Fuel melted (%)	15	16	18	50	20	45				
Element	Released Fractions (%)									
Kr, Xe	50	2.6-9.3	23-52	96	77	54	100	100	86	87
I	51	12	24	91	87	55	79	70	87	93
Cs	32	9	39-51	66	84	55	100	100	93	93
Te	40	1	3	92	83	6	99	82	100	>98
Ba	1.1	0,6	0.8	1	1		30	76	80	55
Sr	0.002		0.88			0.1				
Sb			0.13	62	31	1.6	99	18	97	98
Ru	0.03	0.02	0.007	4	1	0.5	5	0	7	6
Ce	0.002	0.009	0.013			0.01				
Eu			0.08			<0.1				
Zr/Nb					<1					
Mo				No data	56		77	2	47	92
Actinides			<0.001		<1					

Table 11: Representative results from PBF, PHEBUS FP, ORNL and VERCORS tests and TMI-2 accident

The results presented above have allowed classifying FP into four categories, according to their volatility:

- Volatile FP, which include fission gases (Xe and Kr) as well as I, Cs, Te and Sb;
- Semi-volatile FP, including Mo, Ba, Rh, Pd and Tc;
- Low-volatile FP including Ru, Ce, Nb, La, Y, Sr and Eu; and finally
- Non-volatile FP: Zr, Nd and Pr.

This classification is rather indicative, since some FP may present a characteristic behaviour corresponding to another category depending on the thermodynamic conditions (temperature, atmosphere) as it will be explained below.

Volatile FP exhibited very high releases both in integral and analytical tests. Indeed, as shown in **Table 11**, iodine, caesium and noble gases presented a similar behaviour, with releases generally up to 90%. These results are also consistent with the releases observed in the Fukushima accident, where most releases correspond to fission gases and volatile species of Cs and I. Regarding caesium and iodine, it has been observed that their global release is rather equivalent (Pontillon and Ducros, 2010b). Indeed, these FP (like other volatile FP) may be completely released from the fuel if a high enough temperature is reached. Though certain conditions such as atmosphere and fuel burn-up affect their release kinetics, the final released fraction is independent of these variables. Nevertheless, in some analytical tests such as VERCORS 6 and RT 7 (Pontillon and Ducros, 2010b), integral tests such as PBF SFD and in the TMI-2 accident (Hobbins et al., 1993), small but significant quantities of caesium (3-10%) remained in the fuel, possibly due to retention in the form of Cs_2UO_4 or Cs_2ZrO_3 or even of Cs_2MoO_4 , as proposed in (Ducros, 1996). The comparable tests, PBF SFD 1-1 and 1-4, indicate that the release is enhanced in high burn-up fuel compared to trace-irradiated fuel possibly due to the presence of grain boundary tunnels that serve as pathways for gaseous release. Enhanced release rates (due to fuel morphology) occur primarily during the initial heat up, while this difference is reduced afterwards (above 2200 K), where releases are then dominated by the dissolution of the fuel by the molten Zircaloy cladding (Hobbins et al., 1993). Te releases, between 1% and 83%, seemed to be dependent on the Zircaloy oxidation degree, where large releases occurred when the Zircaloy cladding was nearly completely oxidized. Although tellurium is released from the fuel during heat-up, it will chemically react with the Zircaloy cladding and become trapped (De Boer and Cordfunke, 1997, 1995; Johnson and Johnson, 1988). During complete oxidation, there is a production of elemental tellurium and zirconium oxide from $ZrTe_2$ reaction with oxygen. Te would then react with Sn (also present in the cladding) leading to the release of tellurium. Indeed, a SnTe compound has in fact been observed under accident conditions (Collins et al., 1987). Only at high oxygen partial pressures, which are above the equilibrium value of Sn/SnO₂, tellurium can be released in its elemental form. This delayed release behaviour for tellurium has been observed in numerous analytical tests (André et al., 1996; Hobbins et al., 1993; Iglesias et al., 1999; Osborne and Lorenz, 1992). Although Sb like Te is readily released from the fuel during heat up in a severe accident, a lower release is observed since Sb is mostly retained in metallic melts (as it alloys with other metals such as Ni and Ag) (Hobbins et al., 1993).

Regarding Semi-Volatile FP, barium presented generally low releases of a few percent but could be extensively released, up to 80% in hydrogen atmosphere. In a similar way, molybdenum presented generally released fractions of about 50%, but which increased up to 90% in oxidizing atmospheres. This highlighted the important role that the oxygen potential, dictated by the atmosphere, plays in the release

of semi-volatile FP. Indeed, only small releases of Ba were observed in the steam experiments of **Table 11**, as the atmosphere typically hindered the formation of the more volatile metallic species, favouring instead low volatility oxides and hydroxides (Lewis et al., 1998); in fact, releases for these species occurred in the PHEBUS FPT-0 test during the temperature escalation phase when hydrogen generation was at a maximum (Hanniet and Repetto, 1999). This observation is consistent with the integral ACRR ST tests, where higher releases of Ba were observed in reducing environments which would promote higher-volatile metallic forms of these species (Allen et al., 1988). These results are also supported by the analytical VI, HEVA and VERCORS annealing tests (André et al., 1996; Iglesias et al., 1999; Osborne and Lorenz, 1992). However, there is a remarkable difference for Ba release between PHEBUS FPT-0 and FPT-1 experiment (1%) and the ORNL and VERCORS tests (>40%) (Dubourg and Taylor, 2001). This difference may be due to the presence of a significant amount of ZrO_2 in the fuel melt (about 47 mol %) as well as small amounts of Fe oxides which can reduce the volatility of Ba (Dubourg and Taylor, 2001). Indeed, it has been demonstrated that barium may interact with the zirconium present in the cladding, leading to the formation of $BaZrO_3$. A gamma emission tomography was performed on the fuel rod sample used in the VERCORS 5 tests, presented in **Figure 1** (Ducros, 1994a). This tomography (where colour red indicates regions of high Ba γ -emission and therefore high concentration) shows that there was no more Ba in the fuel peripheral area and that 15% of its initial inventory was retained in the cladding (represented by the white circles in this figure).

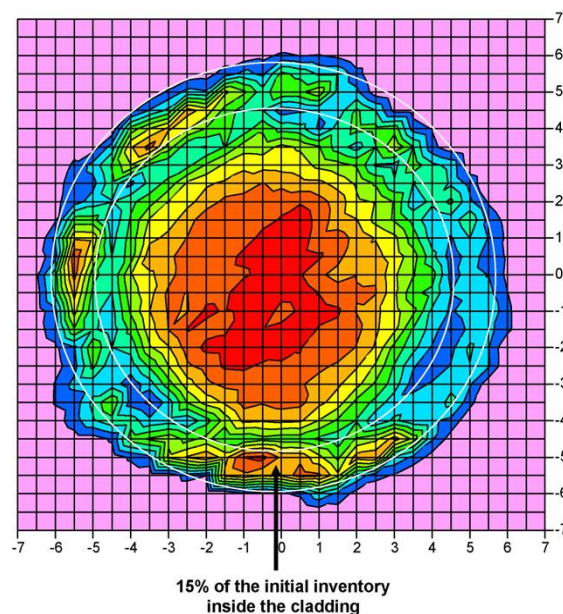


Figure 1: γ -emission tomography of the fuel rod extracted from VERCORS 5.

This interaction would also explain the behaviour observed for Ba during analytical tests where un-cladded fuel samples were employed, such as the RT3 test: Barium began to release at low temperatures (about 1700 K) reaching 40% at 2570 K.

Molybdenum also exhibits a strong dependence on the oxygen potential. Indeed, in the VI-3 test under a steam atmosphere the released fraction was around 77% while for the VI-5 test (similar fuel and final temperature) under hydrogen atmosphere the released fraction was around 2%. This tendency was also confirmed through the HEVA and VERCORS series tests. In all the tests of the VERCORS RT and HT where the fuel was melted, the residual distribution of Mo in the corium was always associated with the Ru residual distribution and sometimes located in metallic precipitates, immiscible with the oxide phase of the

corium (Pontillon and Ducros, 2010b). Molybdenum may also be associated with caesium, as it has been often observed that a fraction of these two elements precipitated together in areas of the loop close to the emission point of FP in the VERCORS tests (Pontillon and Ducros, 2010b). Rhodium, palladium and technetium showed a similar behaviour to that of barium or molybdenum: Rh releases were greater in reducing conditions while Pd and Tc releases were greater in oxidizing conditions, though their release seems lower under all conditions studied (Pontillon and Ducros, 2010a).

Low-volatile FP releases were generally very low, from 10% to 20% (Pontillon and Ducros, 2010a). Nevertheless, the oxygen potential was also a determining factor. Indeed, releases around 40% of Nb have been observed in very oxidizing conditions and un-cladded fuel, which would imply an interaction of this element with the components of the cladding, and releases of 60% of Eu in very reducing conditions such as in the VI-5 test (Osborne, 1991). Ruthenium's behaviour is also very dependent on the oxygen potential conditions. Though the released fractions of the tests in **Table 11** were very low, it has been reported that in very oxidizing conditions ruthenium may form volatile species. Indeed, released fractions of 28% and 65% were observed in VERCORS RT6 and HT2 tests, under steam atmospheres (Pontillon and Ducros, 2010a, 2010b) and up to 100% under air atmosphere in the CRL MCE 1-1 and MCE 1-7 tests (Iglesias et al., 1999).

Lastly, Non-volatile FP always exhibited very low releases (below 1%) independently of the oxidizing conditions.

The FP release behaviour observed in analytical and integral tests has been compared and examined, as well as that determined in the TMI-2 core examination. Consistent release behaviour of the volatile (Xe, Kr, I, Cs, Te and Sb), semi-volatile (Mo, Rh, Pd, Tc), low volatile (Ru, Ce, Nb, La, Y, Sr and Eu) and non-volatile (Zr, Pr, and Nd) FP was observed in the analytical experiments at the ORNL, CEA, JAEA and CRL and the various integrals tests. It was observed that the prevailing local atmospheric conditions (i.e., oxygen potential) particularly influence the release characteristics of the semi-volatile and low-volatile FP, in terms of final released fraction, and that of volatile FP, in terms of release kinetics. Moreover, the complex nature of melt progression tends to mask individual release mechanisms as identified in the out-of-pile experiments. A significant enhancement of release due to fuel liquefaction is not typically observed in the separate-effects experiments.

1.3. Remaining questions on FP behaviour and thesis objective

The behaviour observed for Cs, Mo, Ba and Ru still presents some peculiar characteristics, yet to be explained. Firstly, caesium release kinetics observed in the VERCORS series exhibits a two-step release: an initial release around the beginning of the oxidation plateau (at 1573 K) which practically stops during this plateau but then continues at the beginning of the high-temperature ramp. This behaviour indicates that the release mechanism is not only diffusive but instead chemical reactions may be involved. Indeed, it has been observed that caesium and molybdenum tend to precipitate together in some regions of the experimental circuit (Pontillon and Ducros, 2010b) though the chemical species remain unknown. A better understanding of caesium behaviour would also help understand the behaviour of iodine, tellurium and molybdenum among other FP, by explaining the co-precipitation observed during the VERCORS program.

Regarding molybdenum, the main uncertainty lies on its chemical behaviour during the accidental sequence since it may react with other FP (i.e. caesium (Lewis et al., 2012)) and also act as an oxygen potential buffer (Kleykamp, 1985; Lewis et al., 2012), and thus affect the oxidation state of the other FP. In both cases, molybdenum would have an important impact on other FP behaviour and volatility.

The behaviour of barium was not consistent through the integral and analytical tests, contrary to the other FP. A reduced volatility was observed in the integral experiments compared to analytical ones. As stated above, it may be attributed to the presence of iron and zirconium oxides which would react with barium giving non-volatile species such as BaZrO_3 (Ducros, 1994a; Lewis et al., 2012). Understanding the release mechanism of barium would improve its release assessment in real accidents which is of major importance, since barium is responsible of up to 25% of the decay heat of the core few days after an accident, due to the $^{140}\text{Ba}/^{140}\text{La}$ couple (Baichi, 2001).

Finally, ruthenium was classified as a low-volatile FP since generally releases were in the order of a few percent. Nevertheless, it has been observed that in very oxidizing conditions, such as air ingress scenarios, its release is comparable to that of volatile FP, and that the Ru volatile chemical species could remain in the atmosphere of the containment for a long time.

Understanding the mechanisms and the intermediate phases involved in the release of these FP would improve the source term estimation. This would be important from a health and environmental points of view due to the radiological and direct health damage of these FP, particularly of Ba and Ru which act as poisons (Bair, 1970; Johnson and VanTassell, 1991).

Summarizing, there are remaining questions regarding the behaviour of Cs, Ba, Mo and Ru in accidental conditions and further research is required on these FP, in order to improve the accuracy in the source term assessment and the associated impact. **The objective of the thesis is, then, to understand the mechanism involved in the release of Ba, Cs, Mo and Ru.** A release mechanism has already been proposed in bibliography, based mainly on thermodynamic calculations and some experimental observations. This mechanism, presented below, is the central hypothesis of the thesis.

1.4. Hypothetical Release Mechanism

As described above, the release mechanism proposed by (Nicaise, 2004a) is the main hypothesis of this work and is described first in this section, followed by the experimental and theoretical bases. Lastly, the methodology implemented in order to validate or refute the release mechanism is presented.

The mechanism presented here has been proposed in bibliography (Nicaise, 2004a) to describe the release of the mentioned FP: Cs, Mo, Ba and Ru. This mechanism is based on the behaviour observed (in terms of release kinetics and global released fraction) in VERCORS tests, particularly VERCORS 4 and 5. Moderate burn-up irradiated fuel samples (40 GWd.t^{-1}) were employed for these tests. The temperature sequence for both tests may be separated into 3 stages: the first one consisting on a temperature ramp up to 673 K followed by a temperature plateau under inert atmosphere; a second one consisting on a ramp up to 1573 K followed by an oxidation plateau under a steam/ H_2 (oxidizing) atmosphere and a final temperature ramp followed by a 30 minutes plateau at 2573 K. The atmosphere of the final ramp varied from one test to another, being pure H_2 in VERCORS 4 and pure steam for VERCORS 5.

A special feature of this mechanism is that it considers a different approach for caesium release, taking into account possible reactions with other FP, contrary to the previously accepted mechanisms which considered intra-granular diffusion as the only limiting phenomena. The assumed localization of the considered FP is first presented, taking into consideration the bibliography on chemical state of FP, followed by the interpretation of the results obtained during VERCORS 4 and 5 and finally the proposed mechanism is summarized.

The mechanism proposed by (Nicaise, 2004a) is presented in **Figures 2 to 6**. These figures represent the initial state and 4 different stages considered for the annealing sequence followed generally in the VERCORS tests.

These stages are:

- During the second temperature ramp (around 1273 K);
- The first release of Cs at the oxidation plateau (at 1573 K);
- The second release of Cs, along with the beginning of release of Mo and Ba during the third temperature ramp; and finally
- The release of Ru at the high-temperature plateau (around 2573 K).

Stage 1: Simplified chemical state of the considered FP and their locations in the fuel at the initial temperature (T_0) of the accident

The considered phases are:

■ Cs_2UO_4 : Precipitates at the grain boundaries, along with CsI.

■ MoO_2 : Intra-granular precipitates of small size.

■ Ru: Present in the white inclusions, along with different ruthenium oxides (RuO_x , ■)

■ BaO: Present in the Perovskite phase along with many other FP. Barium is present in many chemical forms, of which the primary oxide is the simplest one.

■ Zr: Only the zirconium present in the Zircaloy cladding is considered.

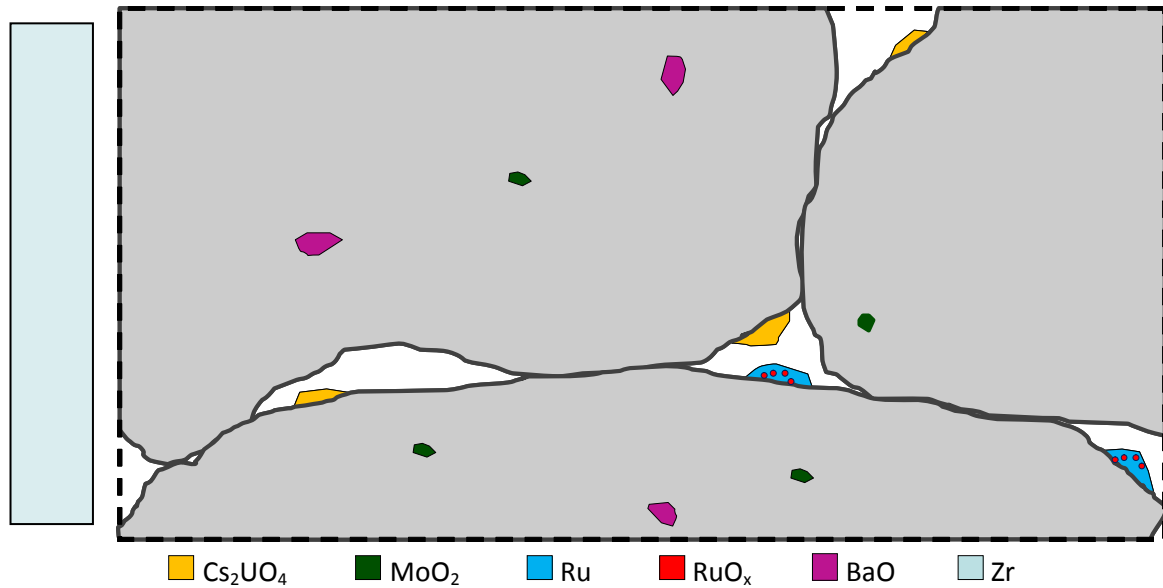


Figure 2: Proposed mechanism - Initial state

Stage 2: At about 1273 K MoO_2 precipitates migrate towards the grain boundaries, vaporise and condensate since the temperature is lower in the intergranular porosity than in the fuel. MoO_2 would react with most Cs of the Cs_2UO_4 , according to **Reaction 1.1**. Intergranular porosities grow bigger as pressure increases due to fission gases migration and higher temperature.

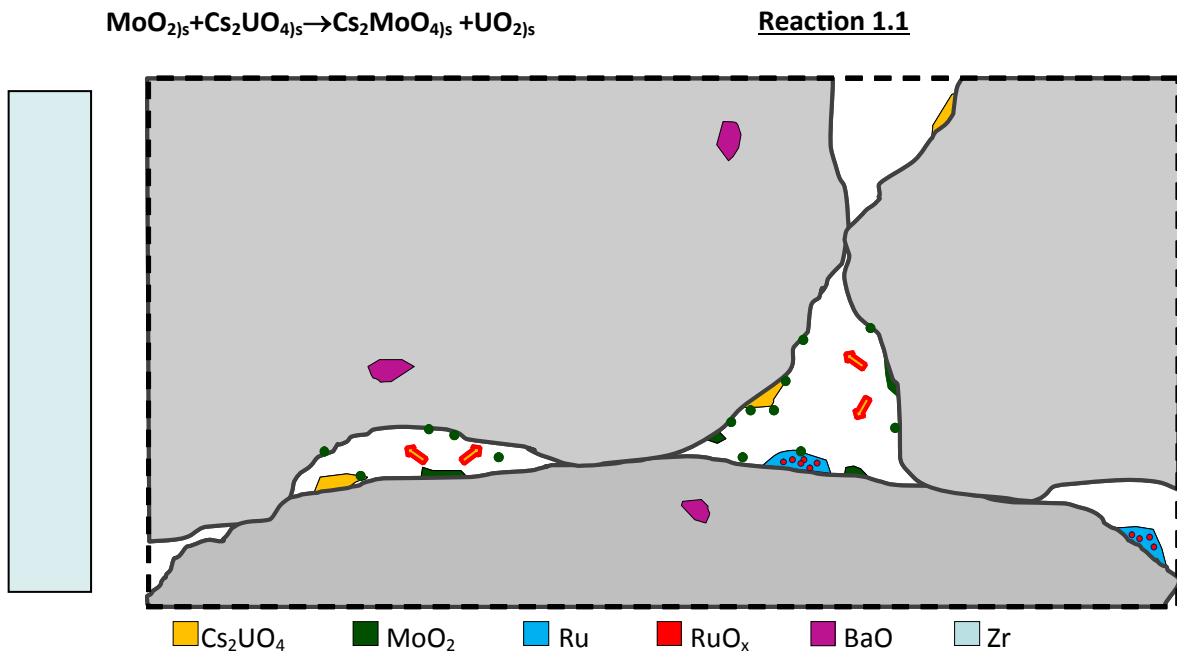


Figure 3: Proposed mechanism - Stage 2: 1273 K

Stage 3: During the oxidation plateau the Cs_2UO_4 phase would be destroyed, according to **Reaction 1.2**. The pressure in the intergranular porosity is high enough as to generate a first interconnection of the pores, leading to the first release of caesium as $\text{Cs}_{(g)}$. The remaining caesium is found as Cs_2MoO_4 . The zirconium present in the cladding starts to oxidize, and ZrO_2 is produced.



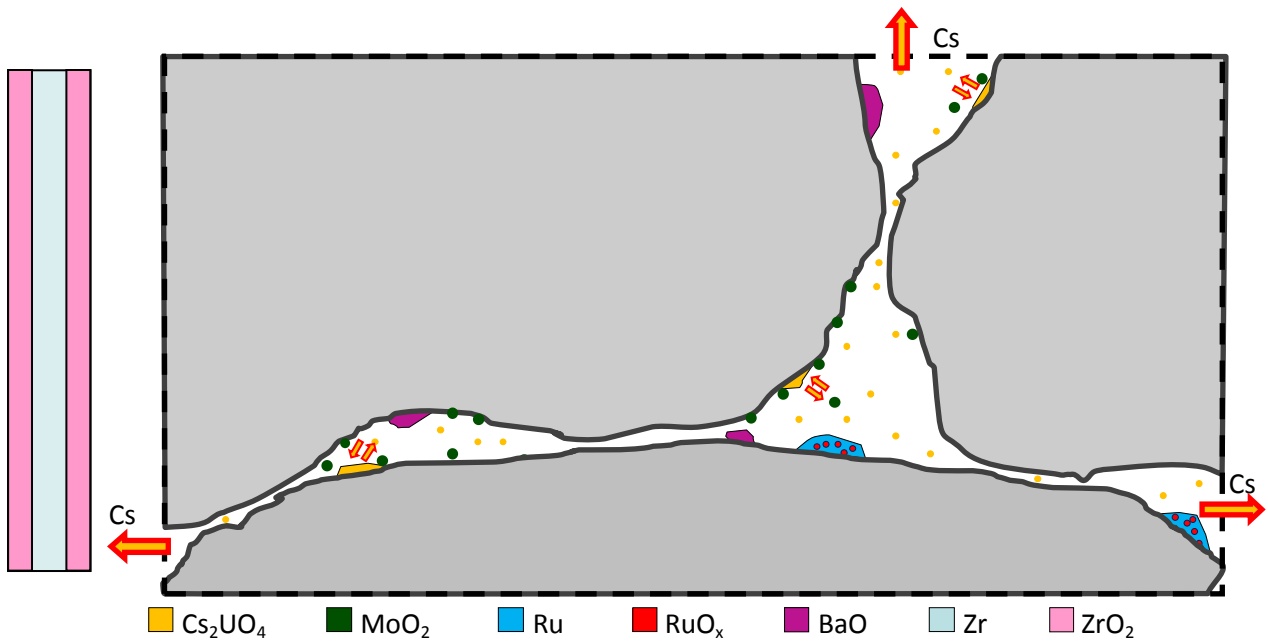


Figure 4: Proposed mechanism - Stage 3: second half of temperature ramp, beginning of the oxidation plateau

Stage 4: During the high temperature ramp, there is simultaneous release of Ba (as $\text{BaO}_{(g)}$), Cs and Mo (as $\text{Cs}_2\text{MoO}_{4(g)}$, $\text{Cs}_{(g)}$ and $\text{MoO}_{2(g)}$) according to **Reactions 1.3 and 1.4**. BaO is partially retained due to reaction with the oxidised cladding, according to **Reaction 1.3**. The atmosphere of the tests has a major impact on the chemical equilibrium of the phase destruction reactions. Indeed, MoO_2 would be reduced and partially retained as metallic Mo, according to **Reaction 1.5**.

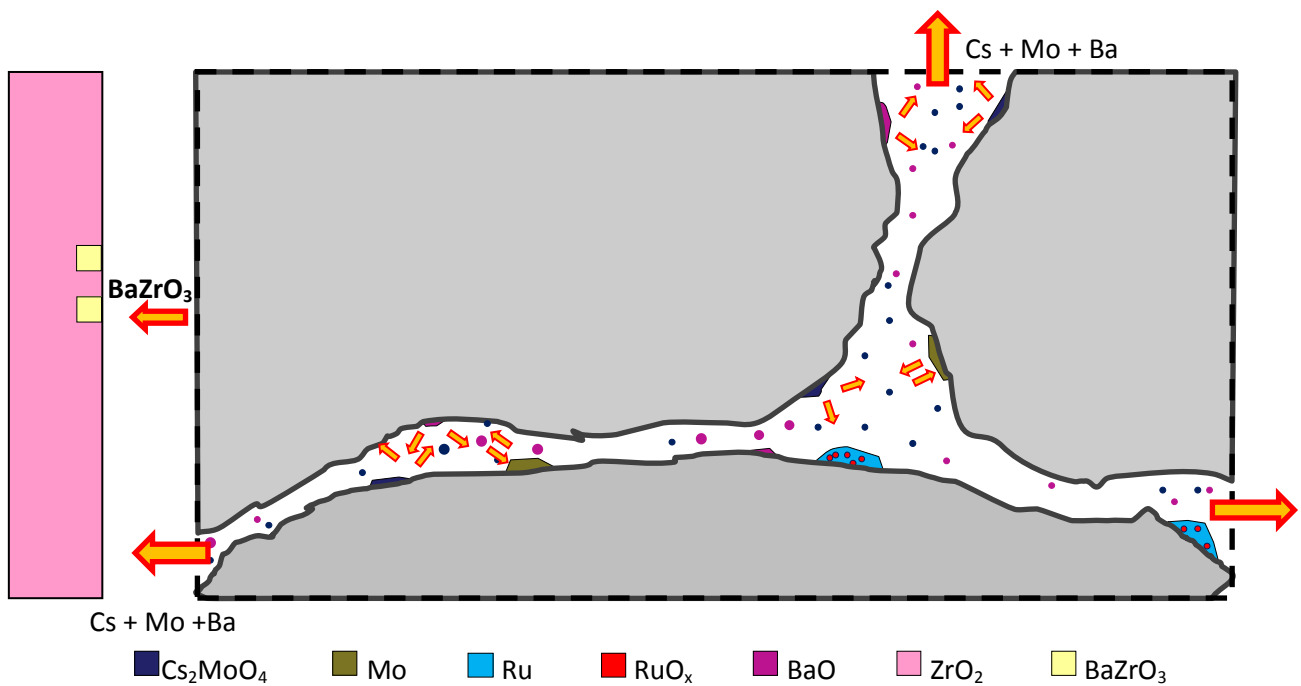
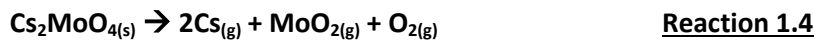


Figure 5: Proposed Mechanism - Stage 4: Ramp to high temperature plateau.

Stage 5: At the high temperature plateau there is simultaneous release of barium, through decomposition of BaZrO₃ and of ruthenium, due to vaporisation of the oxides (Reactions 1.6 and 1.7).

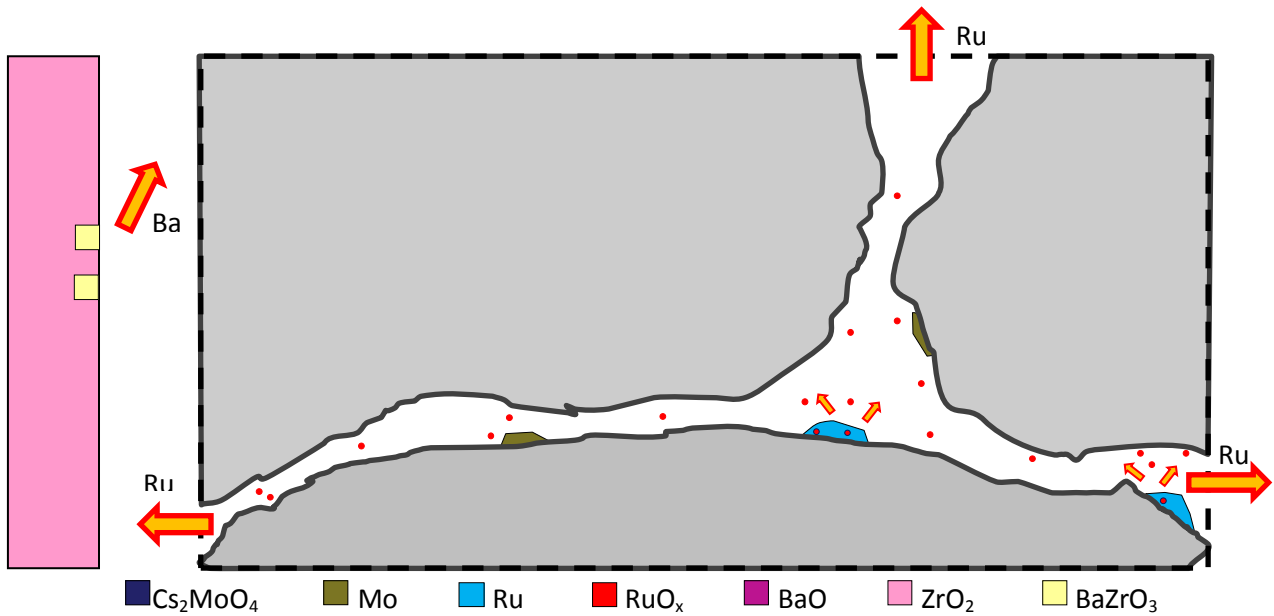
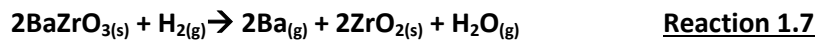


Figure 6: Proposed Mechanism - Stage 5: At the high temperature plateau.

A summary of the stages described in the mechanism is presented in Figure 7.

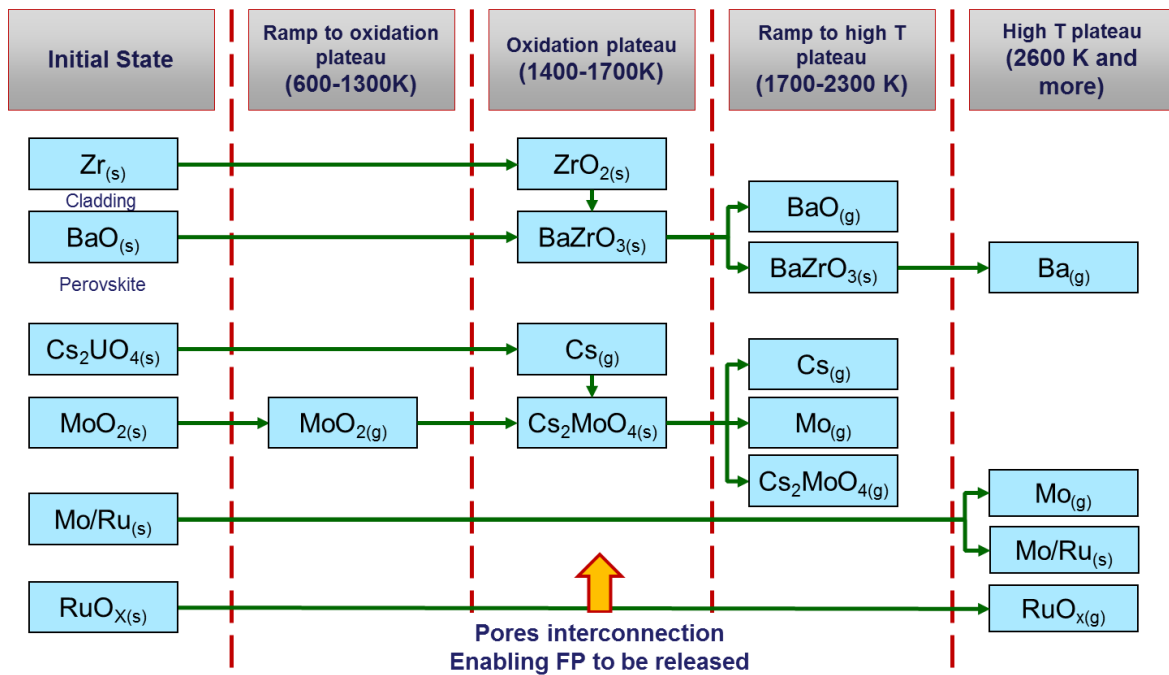


Figure 7: Simplified release mechanism for Ba, Cs, Mo and Ru

1.4.1. Experimental bases of the hypothetical evolution

As explained at the beginning of this section, the mechanism presented above is mainly based on thermodynamic estimations and some experimental observations done on irradiated fuels and during the VERCORS program. The bases of the mechanism are presented below.

1.4.1.1. *FP initial localization*

Caesium is a very volatile and reactive element which has a very low solubility in the UO_2 matrix (Kleykamp, 1993). Characterization by axial gamma-scanning suggests that caesium tends to migrate from the fuel matrix towards the surface, where high concentrations of this element have been detected. The presence of some compounds (i.e., CsI) in the gap is well supported by experimental evidence (Gittus et al., 1989). Indeed, thermodynamic calculations show that, independently of the oxygen potential, the most stable compound for Cs is always CsI in the [Cs-I-U-Mo-O] system (Kleykamp, 1985). Nevertheless, caesium concentration in the irradiated fuel is about 15 times higher than that of iodine. The remaining caesium is assumed to precipitate under uranate forms, the simplest one being Cs_2UO_4 (Duriez et al., 2008; Kleykamp, 1993). Another caesium ternary oxide, Cs_2MoO_4 , may be found in equilibrium with Mo in the ternary Cs-Mo-O system (Ugajin et al., 1996; Walle et al., 2005), but it is believed to be formed at temperatures higher than the normal operation temperature of a LWR, as it was observed only in Fast Reactors fuel pins (Tourasse et al., 1992). To simplify the mechanism, it is considered that all caesium is found in the uranate form and located at the fuel grains boundary.

Barium also presents a very limited solubility in the fuel matrix (Kleykamp, 1993) and is assumed to form a separate phase with perovskite structure along with many other FP, called "grey phase". This phase may be represented as $(\text{Ba,Sr,Cs})(\text{Zr,U,Pu,Mo,RE})\text{O}_3$ (Kleykamp, 1985) though no barium precipitates have been observed in a 50 GWd.t^{-1} UO_2 fuel (Thomas et al., 1992). This may indicate that barium precipitates in high burn-up fuels or in fuels submitted to temperatures higher than the normal operation temperature of a LWR. In the mechanism, it is assumed that barium is present in grey phase intra-granular precipitates, as BaO.

Molybdenum is easily oxidised to MoO_2 according to the Ellingham diagram, forming nanometric precipitates within the fuel (Kleykamp, 1985). Kleykamp also observed that molybdenum is equally present in metallic inclusions along with ruthenium, technetium, rhodium and palladium (called white inclusions, with a size from 10 to 100 nm) at the grain boundaries and inner surface of the intra-granular gas bubbles. Molybdenum has also been observed in the perovskite phase (Tourasse et al., 1992), but given the very low concentration it will not be taken into consideration further in the mechanism. Therefore, it is assumed that molybdenum is present as MoO_2 precipitates, located within the grains, and as metallic Mo in the white inclusions, located at the grain boundaries.

Ruthenium, as mentioned before, is also found in the white inclusions of which it is the main component (more than 50 at.% of ruthenium) (Kleykamp, 1985). Contrary to molybdenum, strong oxidizing conditions are required in order to oxidize ruthenium (stronger oxidizing conditions than those achieved in most tests). It is then assumed that some Ru oxides are created during irradiation and are located along with the white inclusions.

1.4.1.2. Interpretation of FP release

The tests grids of tests VERCORS 4 and 5 are presented in **Table 12** and the release kinetics of the considered FP in **Figure 8** and **Figure 9** (Pontillon and Ducros, 2010a, 2010b). As explained above, four different stages of the annealing tests were considered in this mechanism, where different reactions of phases destruction/formation are presumed to take place.

Conditions	Test	
	VERCORS 4	VERCORS 5
T max (K)	2570	2570
Atmosphere	H ₂	H ₂ O
FP released fraction (%)		
Cs	93	93
Ba	80	55
Ru	6	6
Mo	47	92
Fuel Burn-up (GWd.t ⁻¹)	38	38

Table 12: VERCORS 4 and 5 tests conditions and results

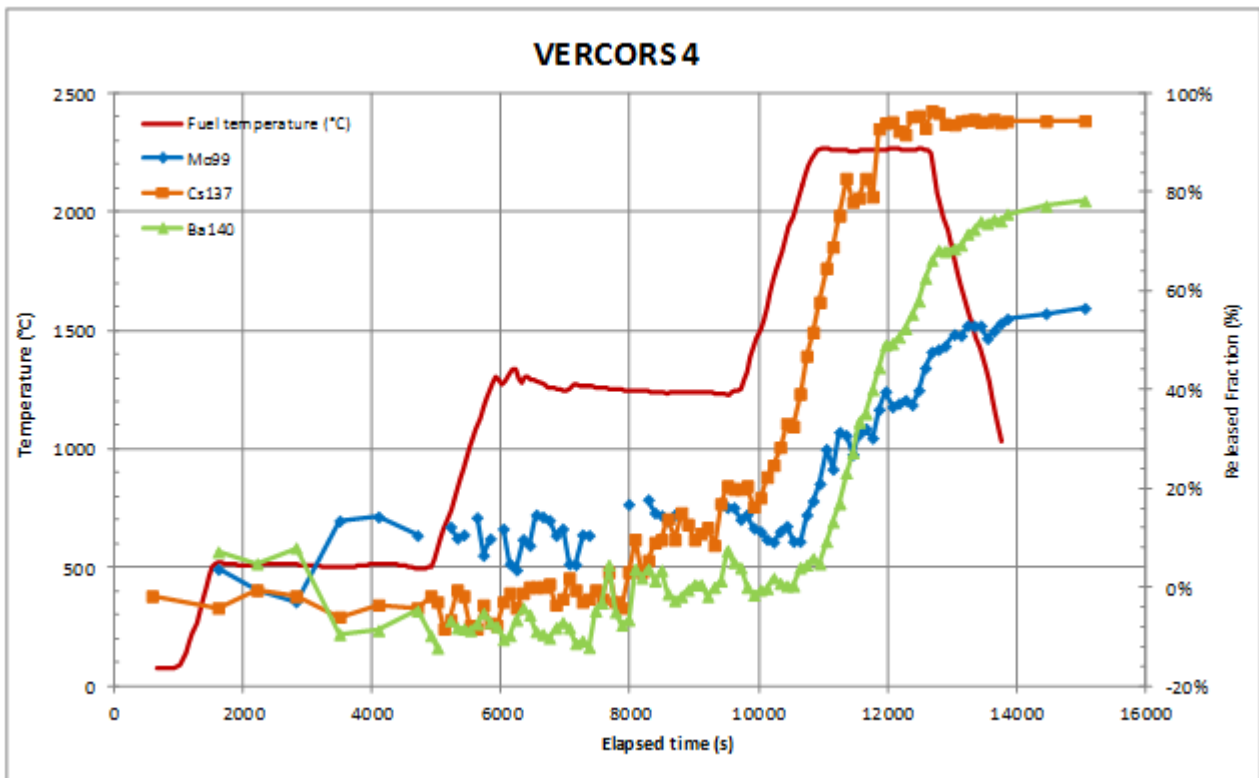


Figure 8: VERCORS 4 Released Fractions

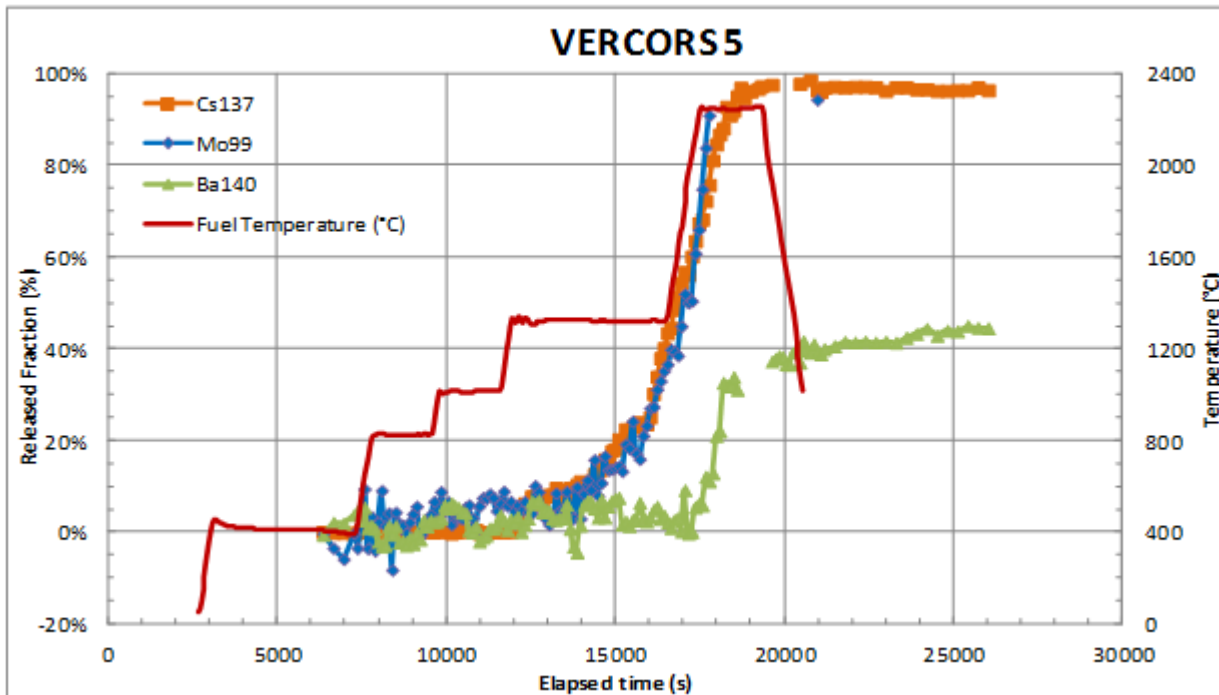
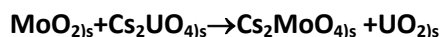


Figure 9: VERCORS 5 released fractions

Second temperature ramp (1273K)

It has been reported that MoO_2 has singular vaporization properties (Giacchetti and Sari, 1976; Nicoll et al., 1997; Tourasse et al., 1992): as a pure solid, thermodynamic data predict that the vaporization at 1 atm should occur at 2800 K, but when present in a nuclear fuel this temperature is drastically reduced to about 1273K. From the analysis of the VERCORS 5 loop components (Pontillon and Ducros, 2010b) it may be deduced that molybdenum is released in two different chemical forms. A first species which condensates quickly, found in the high temperature part of the loop, and a second species which represents about 50% of the total molybdenum, that was fully collected in the impactor of the experimental loop (a multistage collector for trapping aerosols). It is assumed then, that all the MoO_2 would be vaporised in the intergranular porosities around 1273 K and transported through the partially inter-connected porosity (generated by gases migration towards these pores as temperature rises and consequent pressure increase). Some MoO_2 would then react with caesium precipitates located at the grain boundaries, according to **Reaction 1.1**. A similar mechanism of vaporization/reaction was observed in the Phenix reactor pins (Tourasse et al., 1992), where no Mo was found in the centre of the pellets and caesium molybdates were found at the periphery. In this case MoO_2 is supposed to vaporize from the hot parts of the fuel and then condensate in colder ones, reacting in solid phase with caesium uranates.



Reaction 1.1

Beginning of release of Cs:

During the cladding oxidation phase as hydrogen is produced in the fuel-to-cladding gap, the oxygen potential ($\Delta G_{\text{O}_2} = RT \ln(\text{PO}_2)$) decreases and with it the stability of the caesium uranate (Cs_2UO_4). Considering that the inter-connection of the pores continued, forming channels and allowing FP to be released, the first release of caesium would be explained according to **Reaction 1.2**.



Reaction 1.2

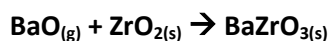
This phase destruction reaction would explain the differences in caesium release kinetics observed in the different tests, where the redox conditions have an important impact. The remaining, unreleased caesium is assumed to be present as Cs_2MoO_4 .

Second release of Cs, beginning of Mo and Ba release

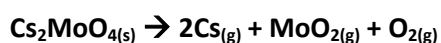
During the last temperature ramp the behaviour of these FP changes from VERCORS 4 to VERCORS 5, due to the different atmospheres:

For VERCORS 5, under pure steam, Cs_2MoO_4 is vaporized at about 2200 K leading to some Cs and Mo release. BaO is vaporized at about 2500 K and some of it is released, though half of barium is retained by reaction with the ZrO_2 of the oxidised cladding, giving BaZrO_3 according to **Reaction 1.3**.

For VERCORS 4, under pure H_2 , Cs_2MoO_4 is affected by the low oxygen potential coming from fuel reduction; leading to the decomposition of this phase and giving Cs and some Mo release, though some of this released Mo is partially reduced and returns to the metallic phase, according to **Reactions 1.4** and **1.5**. Also, according to the analysis of the experimental loop components it may be deduced that a small part of Cs_2MoO_4 may be vaporized and released. There would be then, a competition between the molybdate destruction and its vaporization. In fact, for VERCORS 4, 10% of Mo was collected in the impactor (instead of 50% for VERCORS 5) coming from Cs_2MoO_4 vaporization. Some BaO would also be retained by the Zr from the cladding, but given the reducing atmosphere it is possible that the cladding is partially reduced and thus limiting the retention, or even that the BaZrO_3 phase is partially destroyed.



Reaction 1.3



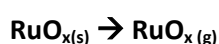
Reaction 1.4



Reaction 1.5

Ruthenium release

Ruthenium release takes place at the high temperature plateau, around 2573 K. The involved reaction is assumed to be the vaporization of the existing ruthenium oxides, according to **Reaction 1.6**. Release of barium continues due to the destruction of the zirconate, as indicated by **Reaction 1.7**. Since this reaction would take place in reducing conditions, Ba would be released as $\text{Ba}\text{(g)}$.



Reaction 1.6



Reaction 1.7

Though the proposed reactions and the localization of the selected FP are based on thermodynamic calculations and some experimental observations, most of the chemical species have not been detected in irradiated nuclear fuel. Such is the case of Cs_2UO_4 which has never been observed in PWR or in FR fuels (in the latter due probably to the higher operation temperature at which this compound becomes unstable). Cs_2MoO_4 has not been observed in PWR fuels either, though it has been detected in FR pins. Post-tests examinations of the VERCORS series experimental loop components indicate, though, a co-precipitation of

Mo and Cs. Regarding barium, the behaviour observed through the analytical and integral tests would be explained by interactions with the cladding. Indeed, the tomography presented in **Figure 1** would indicate so. Nevertheless, the involved intermediary compound, BaZrO_3 , has not been observed yet. Finally, the behaviour of ruthenium in strong oxidizing conditions is attributed to the volatilisation of Ru oxides. The main uncertainty on this element lies in the important released fractions obtained during test such as VERCORS RT 6 and HT 2, where the oxygen potential conditions generated by a steam atmosphere were not as strong as to allow the formation of higher oxides. This would imply that some ruthenium is already in a RuO_x form at an early state.

These phases remain hypothetical so, in order to validate or refute this mechanism, which is the objective of this doctoral research, experimental observation have to be performed both at the initial state and at different intermediate stages. To this end, two experimental work axes have been adopted. These axes, presented below, share the same objective which is the identification of the chemical phases produced during irradiation and their evolution in severe accident conditions, but have a different approach.

1.4.2. Methodology

As indicated in the previous section, there are remaining uncertainties regarding the initial localization of the four studied FP (Ba oxide precipitates, Mo and Ru together in metallic inclusions as well as their oxides and Cs_2UO_4) in the nuclear fuel and their evolution (temperatures at which the initial phases are destroyed and other are created) during an accidental sequence. These uncertainties may be overcome by experimental observations.

Two work axes were proposed for the thesis, in an attempt to validate or refute the proposed mechanism. The difference between these two axes lies in the type of samples used and the characterization techniques: irradiated fuel samples for the first one, while model materials representative of irradiated fuels, called SIMFUELS, for the second. The model materials axis is complementary to the first one, and was implemented in order to answer remaining question on FP behaviour, that were impossible to answer using irradiated fuels.

On one hand, the use of irradiated fuels is a must since there are two main phenomena, which are a consequence of the irradiation process, which have a major impact on FP behaviour and cannot be reproduced in model materials. These phenomena are:

- The distribution of FP, which is not completely homogeneous from the centre to the periphery of samples. Indeed, since the periphery of the sample is more affected by irradiation, the fission of U atoms is more important in this region than in the rest of the fuel section. This leads a higher FP concentration in the periphery of the sample. Besides, there is a radial temperature gradient in the fuel pellets, which also affects the FP distribution.
- The microstructure of the fuel, which is highly affected by irradiation. Indeed, as explained above, the periphery of the pellet is more affected by irradiation, leading to a higher local burn-up. After many irradiation cycles, a region called High Burn-up Structure is observed in the periphery. This region presents a higher concentration of FP, more and bigger pores than in the rest of the sample and reduced UO_2 grain size.

On the other hand and despite their limitations, model materials present some important advantages:

- The possibility of decoupling thermodynamics from irradiation. Indeed, model materials allow to study the FP chemistry at an "early state", since their state is purely dictated by thermodynamic stability without the impact of irradiation.
- The use of powerful characterization techniques, such as X-ray Absorption Spectroscopy (XAS) using synchrotron radiation, which allows determining accurately FP oxidation state, their local environment and the chemical phase structure.

Intermediate stages of a severe accident were recreated in the two axes, by means of annealing tests under representative conditions, in a similar way to the tests carried out in the VERCORS program. Samples were characterized before and after tests using the available techniques at the LECA-STAR facility and, particularly for model materials, by X-ray Absorption Spectroscopy. A diagram describing how these two axes are articulated is presented in **Figure 10**.

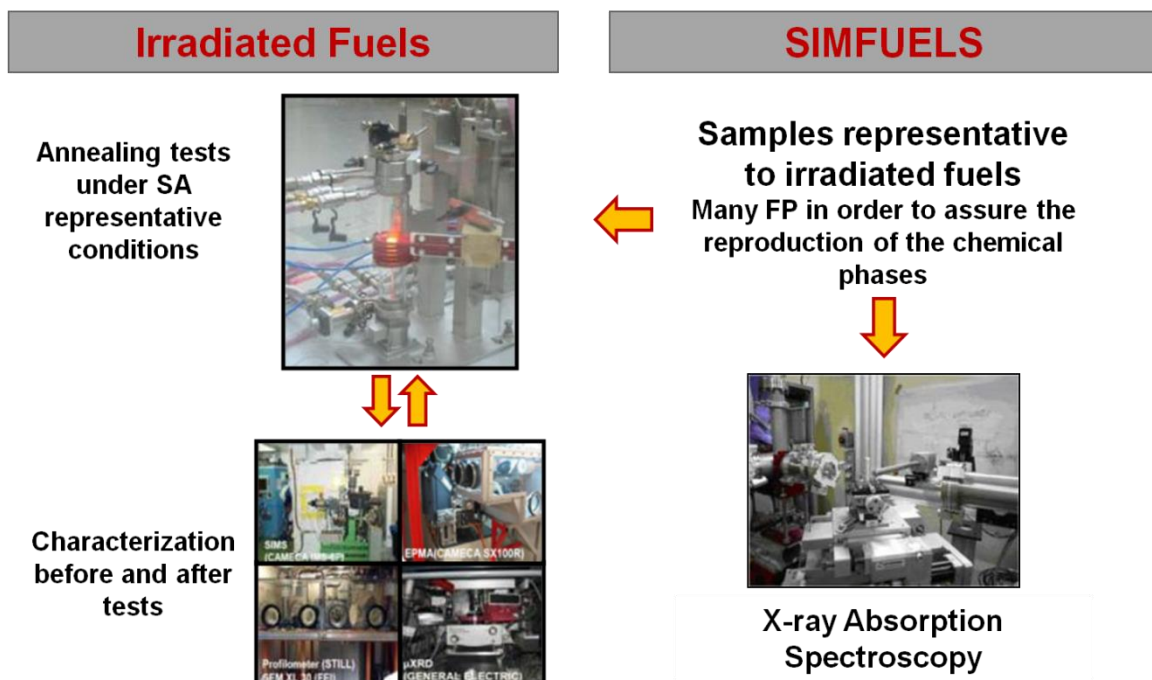


Figure 10: Representation of work axes

Another important aspect of the thesis are thermodynamic estimations, performed mainly for model materials considering the different annealing tests conditions, in order to facilitate experimental identification of phases. These estimations were done using the FactSageTM software with the SGPS database, provided with the software. Detailed descriptions of the software and of the experimental loops are presented in **Appendix IV** and **Appendix V**, respectively.

Chapter 2: Irradiated Fuels

2.1. Introduction	53
2.2. Samples description	54
2.2.1. FX0GAC-E04	54
2.2.2. T ₀ -IF Sample	56
2.2.3. IF1500 Sample.....	56
2.2.4. VERDON 1	57
2.3. Experimental characterization of irradiated fuel samples.....	60
2.3.1. T ₀ -IF Sample: Initial state	60
2.3.2. Caesium	62
2.3.3. IF1500 Sample: Intermediate state of a severe accident	63
2.3.4. VERDON 1 Sample: Advanced state of a severe accident	67
2.4. Discussion: Results vs mechanism	80
2.4.1. Fuel micro-structure evolution.....	80
2.4.2. Barium.....	81
2.4.3. Caesium	84
2.4.4. Molybdenum and Ruthenium.....	84
2.5. Conclusion.....	85

Chapter 2: Irradiated Fuels

2.1. Introduction

As described in the first chapter, the irradiated fuels work axis is the main experimental axis of this doctoral research. The results on Ba, Cs, Mo and Ru behaviour in severe accident conditions are presented in this chapter. Three different samples were studied, corresponding to three stages of a severe accident: an initial state (T_0 -IF sample), that correspond to the normal operation conditions before the accident starts; an intermediate state (IF1500 sample) under reducing atmosphere; and an advanced state of an accident (VERDON-1 sample), where the fuel sample collapse was imminent.

Regarding the release mechanism presented in the first chapter (Nicaise, 2004a), several hypotheses corresponding to three different stages will be studied in this chapter, as indicated in **Figure 11**. These hypotheses are:

- The existence of BaO precipitates (perovskite phase);
- The existence of Mo/Ru precipitates (white inclusions);
- The existence of Cs_2UO_4 precipitates in a high burn-up irradiated fuel under normal reactor operation conditions;
- The pores interconnection and Ba-Zr interaction around 1673 K; and finally
- The chemical state of the remaining FP of interest in the fuel, in an advanced stage of a severe accident.

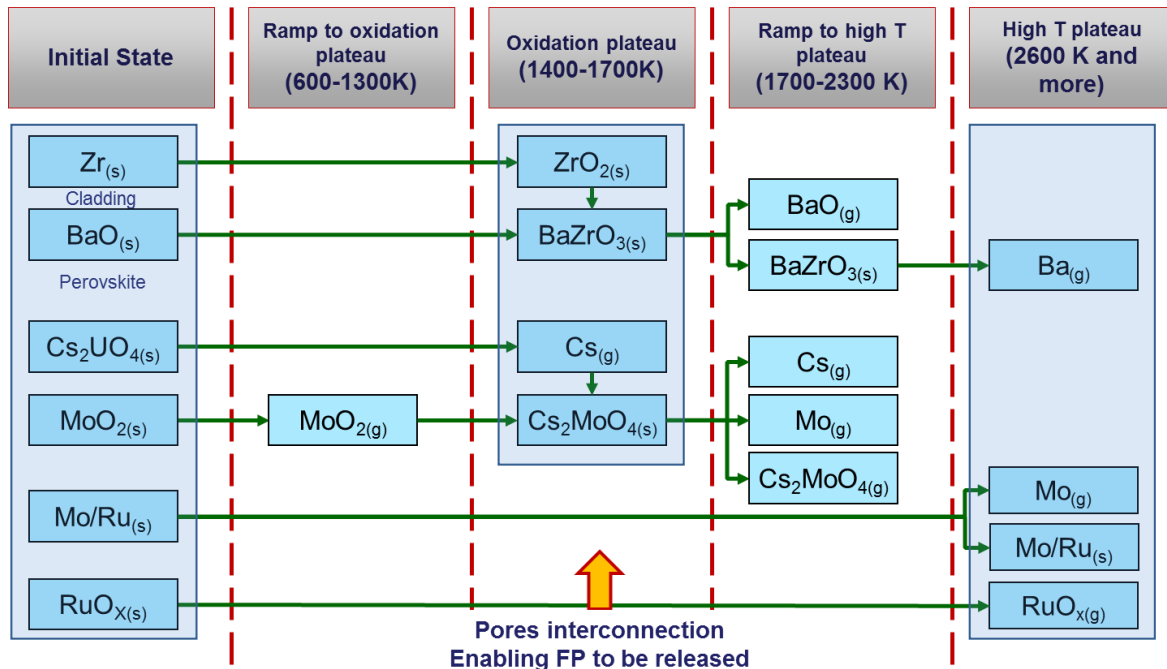


Figure 11: Hypothetical phases to be verified in this axis

The three irradiated samples considered in this study were prepared from the same father fuel, FX0GAC-E04, which is described first and is followed by the results obtained during the characterization of

the three samples. All samples were characterized at the LECA-STAR facility, CEA Cadarache. A brief description of the different characterization techniques used is presented in **Appendix VI**.

2.2. Samples description

As explained above, three irradiated fuel samples were studied in this work axis, representative of different stages of a severe accident: T₀-IF sample, which is representative of an initial state before the accident starts; IF1500 sample, annealed up to 1773 K under reducing atmosphere and representative of an intermediate stage; and finally the VERDON 1 sample, representative of an advanced stage of a severe accident. These samples, the test conditions to which they were submitted and the characterizations performed are summarized in **Table 13**, followed by a detailed description of the samples. Firstly the father rod from which all samples were prepared is described, followed by the T₀-IF, IF1500 and VERDON 1 samples.

Sample	Max temperature (K)	Atmosphere	Characterization
T ₀ -IF	PWR operation Temperature	-	SEM, EPMA, SIMS
IF1500	1773	Ar+ 4% H ₂ (reducing)	EPMA
VERDON 1	2873	H ₂ /H ₂ O (oxidizing, then reducing)	OM, SEM, EPMA, XRD

Table 13: Summary of samples studied in the Irradiated Fuels work axis

2.2.1. FX0GAC-E04

The father fuel from which the three samples studied were prepared was irradiated during six cycles in the Gravelines-5 Nuclear Power Plant operated by EDF. Though the mean burn-up of the rod was calculated to be 67.535 GWd.t⁻¹, the samples were taken from a segment with a local burn-up of 72 GWd.t⁻¹. The fabrication characteristics of the father rod are presented in **Table 14**, extracted from (Decanis, 2003; Martella et al., 2002).

Rod number	4034
Position in assembly FX0GAC	E04
Cladding material	M5
Rod length (mm)	3851.8
Outer diameter of clad (mm)	9.50
Inner diameter of clad (mm)	8.25
Fuel type	UO ₂
Enrichment (²³⁵ U %wt)	4.4943
Mean pellet height (mm)	13.65
Mean pellet diameter (mm)	8.086
Number of pellets*	267

Table 14: VERDON 1 Father Rod characteristics

*Estimated value, based on the nominal fabrication length

Many characterisation analyses were performed on the fuel rod, such as metallographic analyses, SEM, EPMA and SIMS, at the LECA-STAR facility, CEA Cadarache. An optical microscope image from the periphery of a FXOGAC-E04 sample, where the High Burn-up Structure (HBS) region is clearly observed, is presented in **Figure 12**. As described in chapter one, the HBS is produced at the periphery of high burn-up fuels due to irradiation. The main characteristics of this region are a higher concentration of FP and heavy elements produced by neutron capture of uranium atoms, an elevated porosity and smaller UO_2 grains. Particularly for the E04 fuel, the HBS extends up to 60 μm from the periphery.

Some important characteristics of FXOGAC-E04 that must be mentioned are: the existence of an internal ZrO_2 layer between the cladding and the fuel; and the increased Pu concentration at the periphery (HBS). These two can be observed in the SEM-BSE image and Pu X-ray map in **Figure 13**, and in the Pu and Nd concentration profile obtained by EPMA analysis, presented in **Figure 14**. Since elements such as Nd and Pu do not migrate at all in the fuel matrix, their concentration depends directly on the irradiation process, allowing estimating a local burn-up. Regarding the FXOGAC-E04 fuel, a local burn-up equal to 150 GWd.t^{-1} was estimated in the HBS zone.

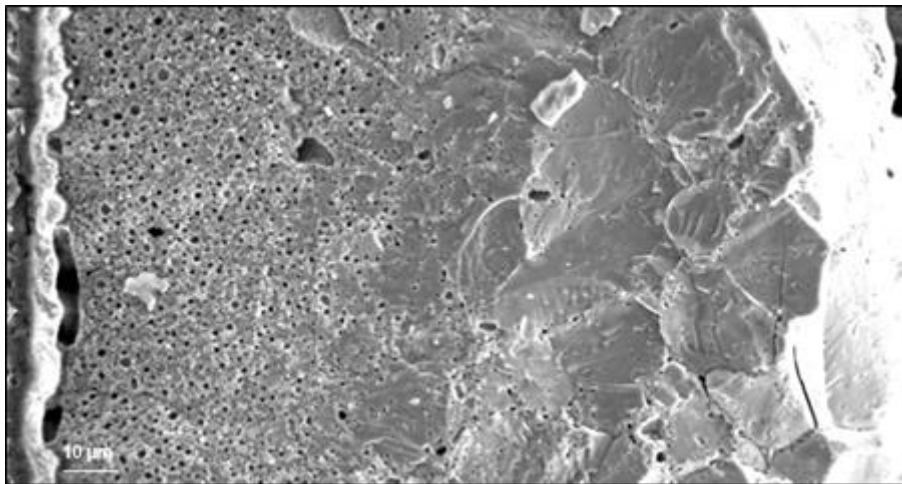


Figure 12: Fractography of the E04 periphery

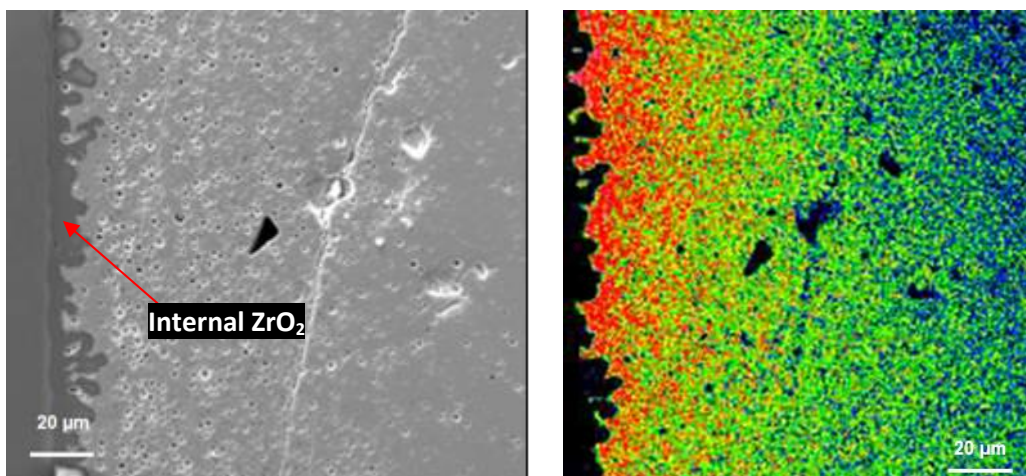


Figure 13: SEM-BSE image (left) of the periphery of a FXOGAC-E04 sample and Pu X-ray map (right)

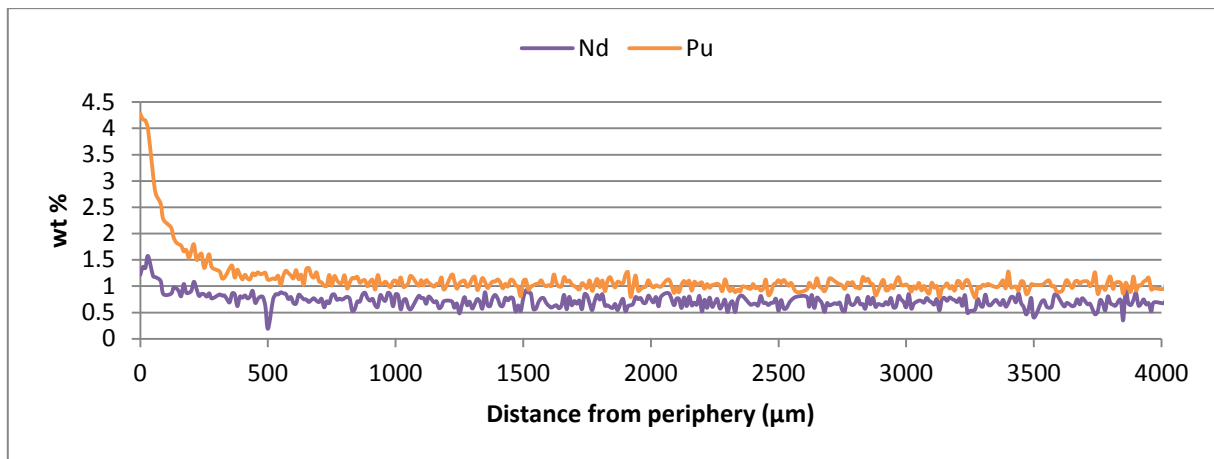


Figure 14: Pu and Nd quantitative profiles, sample FX0GAC-E04

2.2.2. T₀-IF Sample

This sample is representative of the normal operation conditions of a high burn-up fuel, before the accident starts. An Optical Microscope (OM) image of the sample is presented in **Figure 15**. Characterization analyses performed on this sample include SIMS, SEM and EPMA.

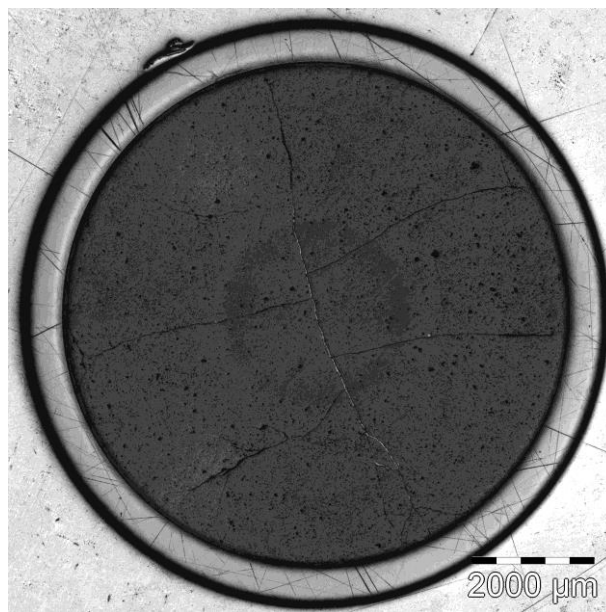


Figure 15: T₀-IF sample SEM-SE image

2.2.3. IF1500 Sample

This sample, also taken from a FX0GAC-E04 pellet, was submitted to an annealing test consisting in three temperature plateaus, at 573, 1473 and 1773 K, in reducing atmosphere (Ar + 4% H₂). The last temperature plateau was maintained for 35 min, in order to achieve a final Cs released fraction of about 47%. The annealing test was carried out in the MERARG experimental loop (Pontillon et al., 2005a), described in **Appendix V**. This sample allowed studying FP behaviour at an intermediate stage of an accident. The annealing sequence and Cs release kinetics are presented in **Figure 16**. After the annealing test, this sample was embedded in an epoxy resin and polished down to half its diameter. An image of the sample after the

preparation process is presented in **Figure 17**. IF1500 sample was characterized by EPMA at the LECA-STAR facility.

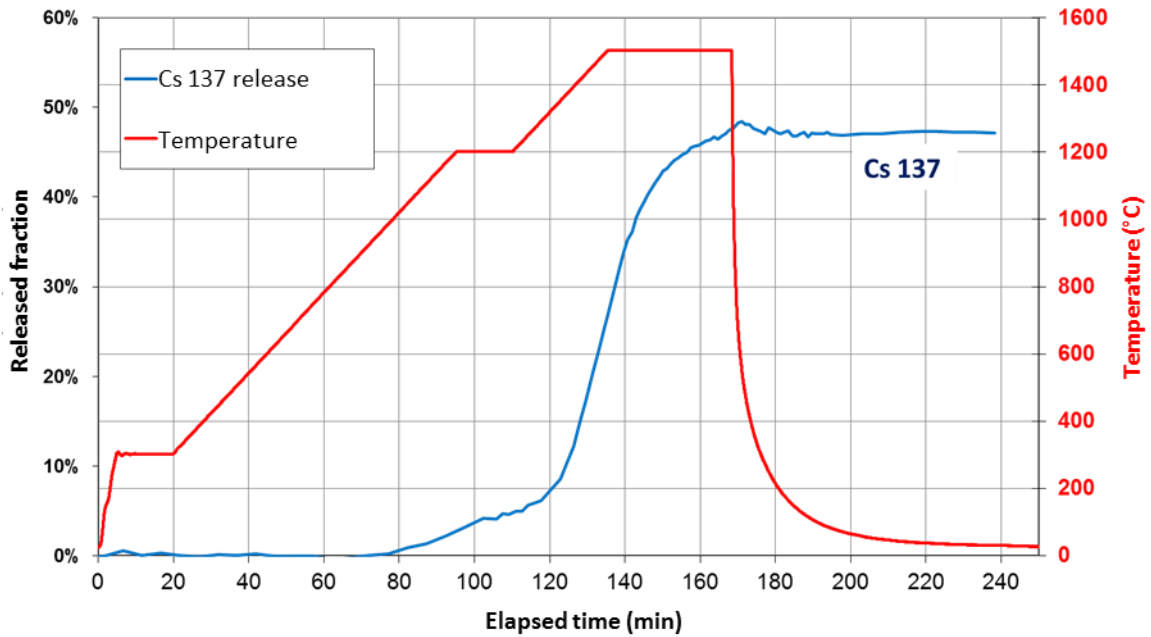


Figure 16: Annealing sequence followed by the IF1500 sample and Cs release

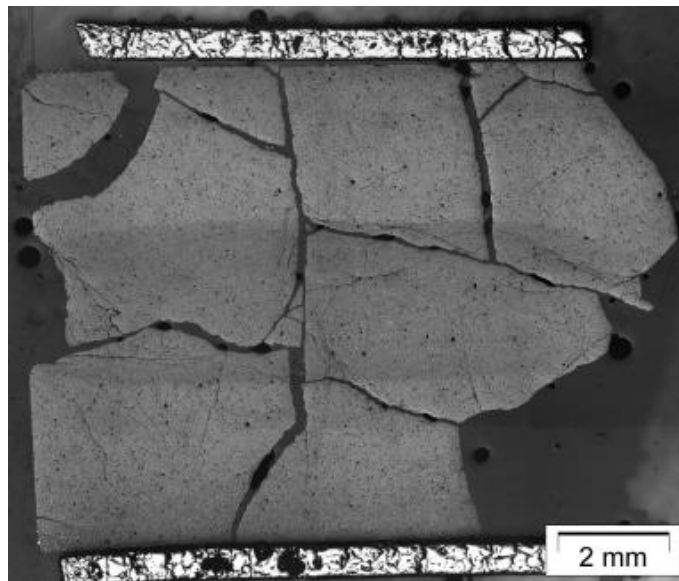


Figure 17: IF1500 Sample optical microscope image

2.2.4. VERDON 1

The VERDON-1 test was part of the VERDON-ISTP program, in which four tests have been performed to study FP release in severe accident conditions (Gallais-During et al., 2014). The original VERDON 1 sample, presented in **Figure 18**, consisted in two FX0GAC-E04 pellets and two depleted and un-irradiated UO₂ half-pellets at each side, the whole in the original M5 cladding. The annealing sequence, which conditions are presented in **Table 15**, consisted in three stages under different atmospheres: the first one under neutral atmosphere (He), the second one under an oxidizing H₂/H₂O mixture, and the third one under a reducing H₂/H₂O mixture.

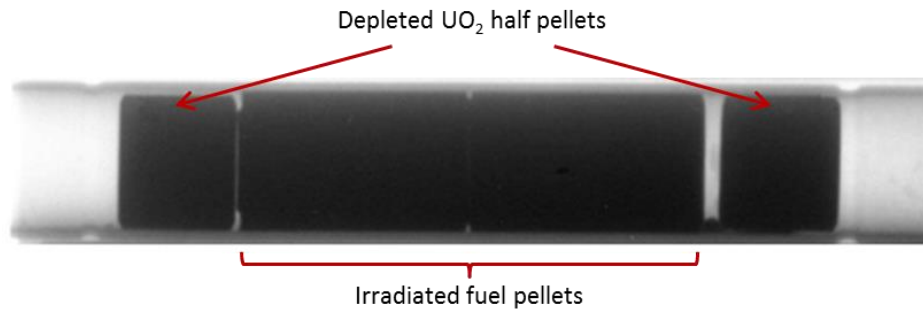


Figure 18: VERDON 1 original sample

	Temperature	Atmosphere	Oxygen potential
Phase 1	Ambient to 673 K Plateau at 673 K : 1h	Neutral Carrier: He	Fixed by FP redox couples
Phase 2	673 K to 1773 K Plateau at 1773 K : 1h	Oxidizing H ₂ O = 25 mg.s ⁻¹ H ₂ = 0.45 mg.s ⁻¹ Carrier: He	From -400 kJ.mol ⁻¹ (673 K) to -244 kJ.mol ⁻¹ (1773 K)
Phase 3	1773 to 1873 K Plateaus every 100°C (10 min) from 2273 K up to the end of sequence	Reducing H ₂ O = 0.3 mg.s ⁻¹ H ₂ = 0.33 mg.s ⁻¹ Carrier: He	From -365 kJ.mol ⁻¹ (1773 K) to -279 kJ.mol ⁻¹ (2873 K)

Table 15: VERDON 1 test conditions

FP behaviour during VERDON 1 was consistent with that of the VERCORS tests series (Gallais-During et al., 2014). The release kinetics of FP representative of each category (volatile, semi-volatile, low-volatile and non-volatile) are presented in **Figure 19**. Particularly, there was a complete release of volatile FP such as Cs and I, as well as of the fission gases Xe and Kr. Other volatile FP such as Te and Sb were completely released as well. The release kinetics of Cs and I could be perfectly superposed, and are also quite similar to those of the fission gases. However, the release kinetics of Te and Sb were delayed compared to that of Cs and I.

Each FP belonging to the semi-volatile category presented its own particular behaviour which was, as already observed in previous tests, highly dependent of the atmosphere conditions. Mo release started at the oxidation plateau (1773 K, oxidizing atmosphere) and got up to 40% before stopping by the end of the oxidation plateau. Mo release restarted when the H₂ flux was stopped, around 2673 K. Ba release started later, around 2273 K, and achieved 80% by the end of the test surpassing that of Mo (60%). Regarding low-volatile and non-volatile FP, no releases were measured on-line during the test except for Nb, which attained at final released fraction of around 10%. The global released fraction of Xe, Kr, Zr, Nb, Mo, Ru, Sb, Te, I, Cs, Ba, La, Ce, Nd, Eu and Np are presented in **Table 16**.

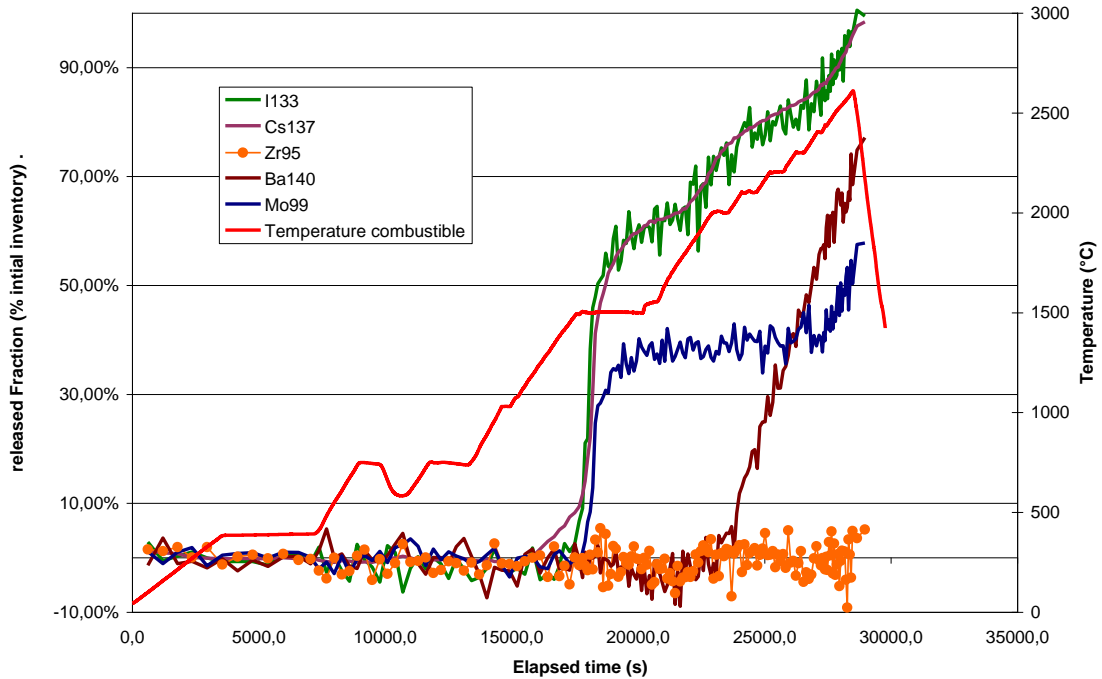


Figure 19: FP release kinetics in VERDON 1

Element	Released Fraction (%)
Fission gases ^a	100
Ba	70-75
Ce	0
Cs	99
Eu	0
I	93
La	0
Mo	64-65
Nb	10
Nd	0
Np	2
Ru	1-3
Sb	76-95
Te	99
Zr	0

Table 16: FP global released fractions during VERDON 1 test. ^aKr, Xe

The VERDON 1 sample was recovered after the test and two samples were prepared: Samples A2 and B. These two samples are presented in **Figure 20**. As observed, the original cladding disappeared and the fuel pellets were clearly degraded after the test, due to which half of one pellet (Sample A2) shattered during recovery. Both samples were prepared in a different way in order to perform different post-test examinations: Sample A2 was metallized in order to improve its conductivity and perform EPMA analyses, while sample B was embedded in an epoxy resin in order to perform a metallographic analysis (optical microscopy) and XRD. Both samples were polished up to half their diameter after embedding. The metallographic analysis and XRD results on sample B and EPMA results on sample A2 are presented later in this chapter.

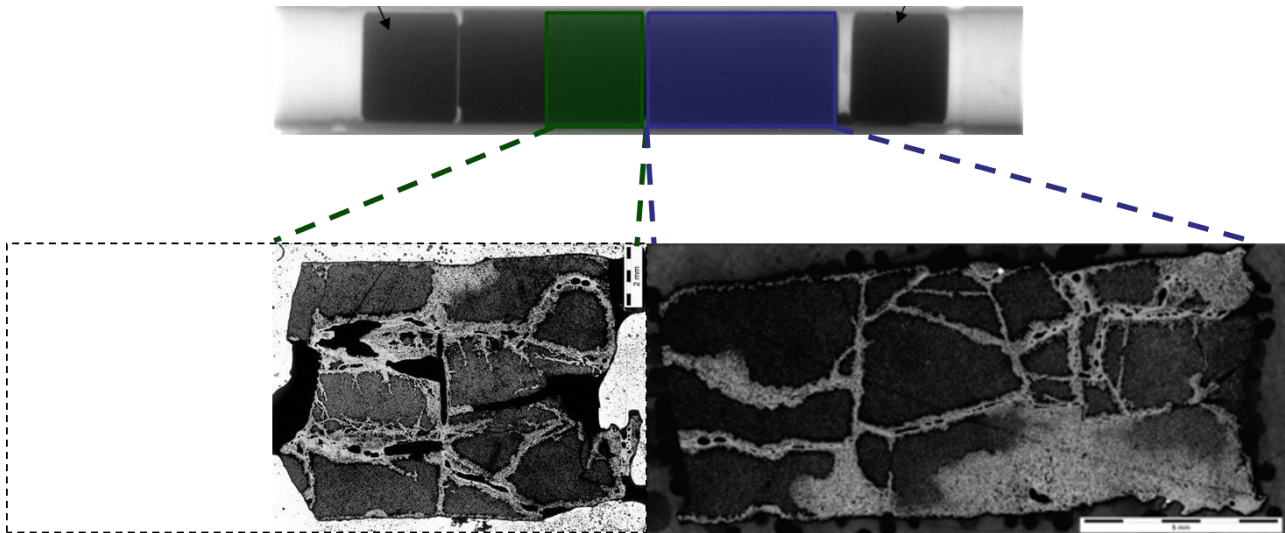


Figure 20: Samples A2 (left) and B (right), prepared from the VERDON 1 sample after test.

2.3. Experimental characterization of irradiated fuel samples

An analysis of the behaviour of the four FP of interest (barium, caesium, molybdenum and ruthenium) is presented in this section. Firstly, the characterisation results of the T_0 -IF sample are presented, followed by those of the IF1500 one and finally the VERDON 1 sample.

2.3.1. T_0 -IF Sample: Initial state

2.3.1.1. *Fuel micro-structure*

SEM-BSE images of the periphery and centre of the T_0 -IF sample are presented in **Figure 21**, extracted from (Pujol et al., 2004). It was observed that the porosity in the periphery was higher than in the rest of the sample, representing 15% of the total area, with pores size ranging from 0.2 to 2 μm . Porosity decreases towards the half-radius region of the sample, representing only 1.5 to 3.8% of the total area. It increases again in the centre of the sample, representing 8% of the total area, with pores sizes ranging from 1 to 2 μm .

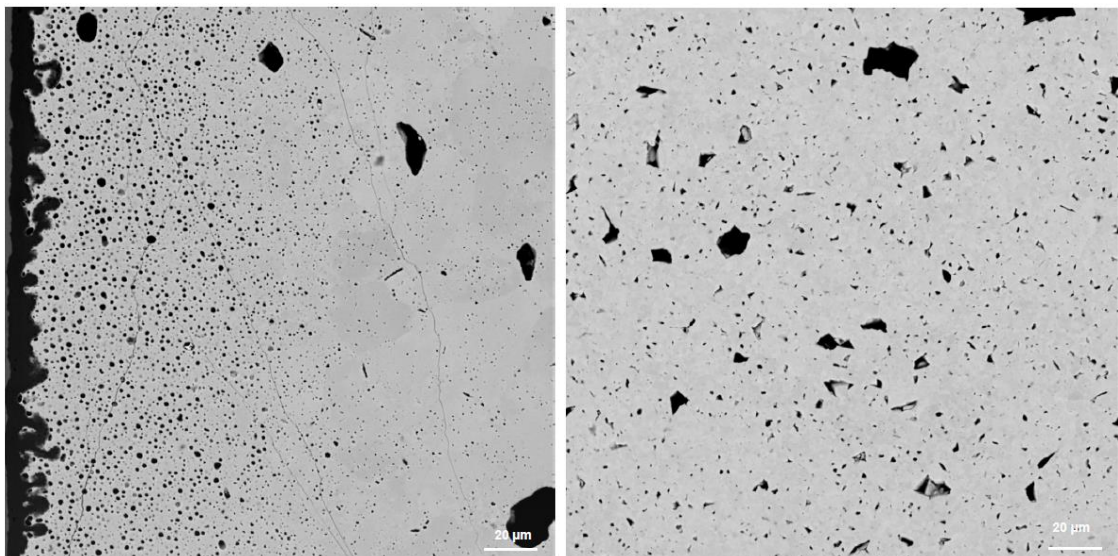


Figure 21: SEM-BSE images of the periphery (left) and centre (right) of T_0 -IF sample

2.3.1.2. Barium

The localization of barium in this sample was determined by SIMS and EPMA analyses. ^{138}Ba and ^{90}Zr ion maps obtained by SIMS in three different regions of the sample (periphery, half-radius and centre) are presented in **Figure 22**. No precipitates of Ba or Zr were observed in these ion maps, which was also confirmed by EPMA quantitative analyses, presented in **Figure 23**. Nevertheless, an increased concentration of Ba and Zr is observed from the periphery of the fuel (around 0.6 and 1.2 wt%, respectively) up to around 400 μm towards the centre of the sample (0.2 and 0.6 wt%, respectively). The latter is consistent with the Nd profile presented in **Figure 14**.

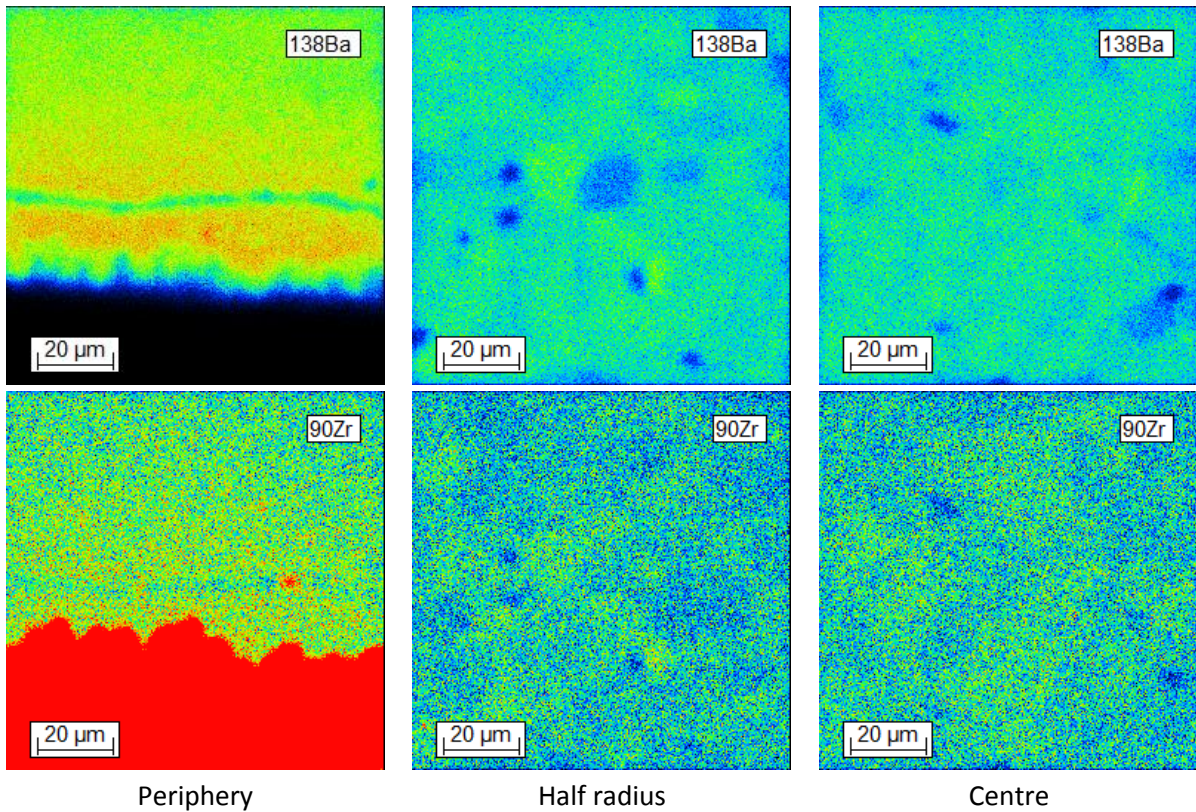


Figure 22: Ba and Zr ion maps obtained at the periphery, half radius and centre of the sample

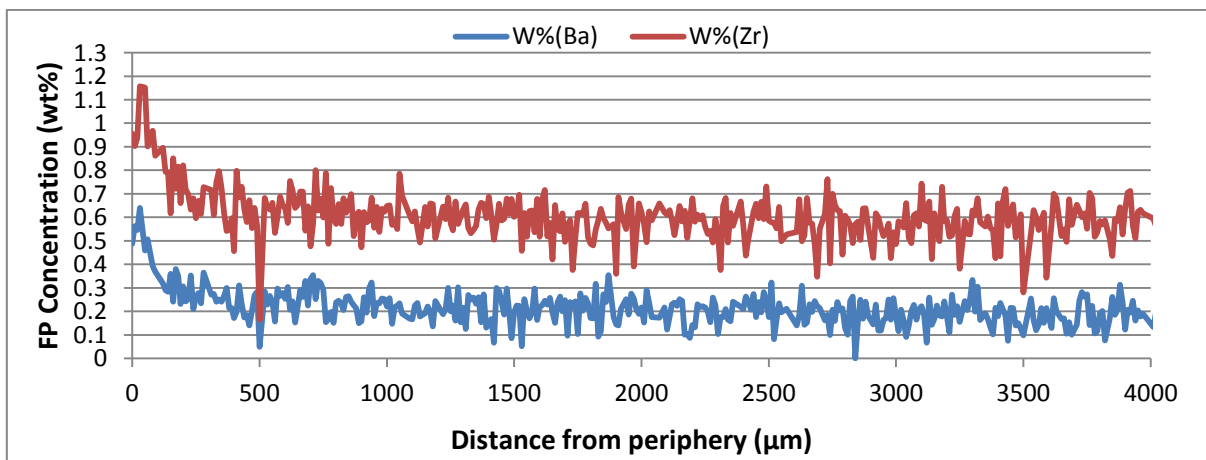


Figure 23: Ba and Zr concentration profiles determined by EPMA

2.3.1.3. Caesium

Caesium localization has been determined through EPMA and SIMS analysis. EPMA analyses, which results are presented in **Figure 24**, were performed on a sample obtained by fracture of an un-annealed FX0GAC-E04 pellet. As observed in these images, many Cs precipitates were found in the sample, with an Equivalent Circle Diameter (ECD) ranging from 4 to 7 μm . These precipitates disappeared progressively when impacted by the electronic beam. Mo and O X-ray maps were also acquired. No Mo-Cs association was observed and, besides, O X-ray map do not reveal any kind of precipitate. Regarding SIMS analyses, which were performed in three different regions (periphery, half radius and centre) of a polished FX0GAC-E04 and are presented in **Figure 25**, no Cs precipitates were observed. Nevertheless, it is observed an accumulation of this FP in the fuel cracks, close to the periphery.

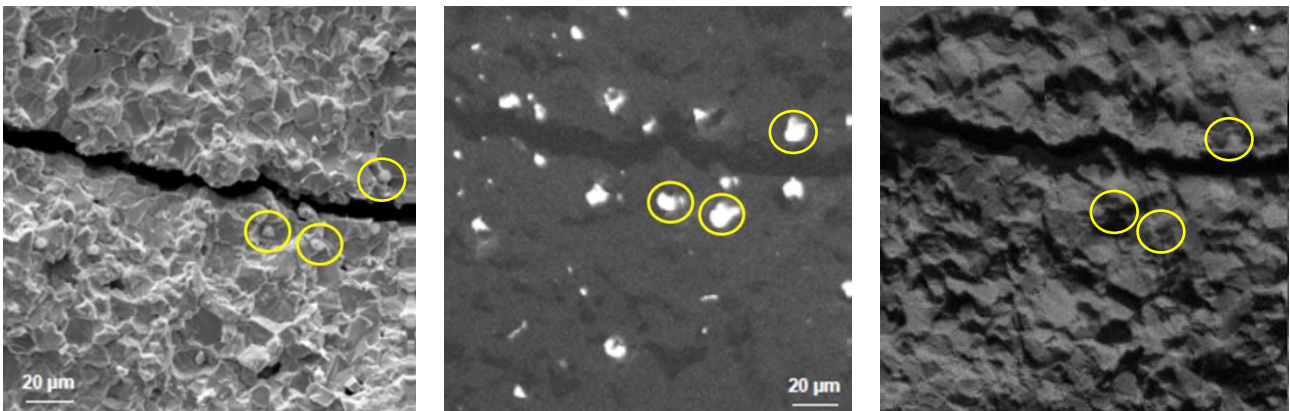


Figure 24: T_0 -IF sample fractography (left) along with Cs (middle) and O (right) X-Ray maps

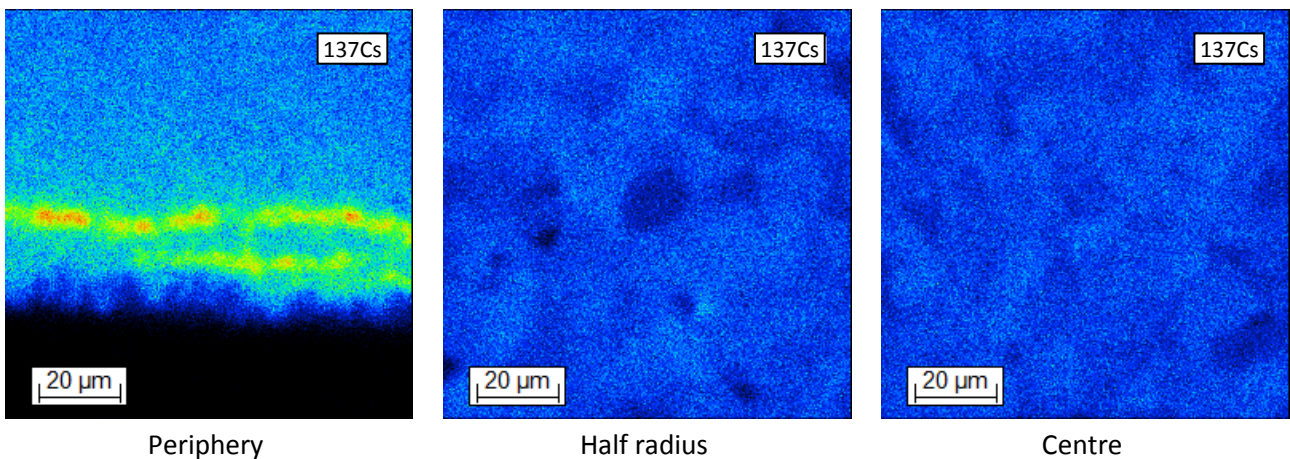


Figure 25: ^{137}Cs SIMS ion maps from the periphery, half radius and centre of T_0 -IF sample

2.3.1.4. Molybdenum and ruthenium

Mo and Ru distribution was determined through SIMS analyses in three different regions (periphery, half radius and centre) of a polished and un-annealed FX0GAC-E04 sample. Results, presented in **Figure 26**, indicate the presence of many Mo-Ru precipitates in the periphery and centre of the fuel, though no precipitates are observed in the half radius region of the sample. No Mo association other than with Ru and Tc was observed in the sample. EPMA quantitative analyses performed from the periphery to the centre of a polished sample and presented in **Figure 27**. These results confirm Mo distribution, since precipitates are

only observed close to the periphery and in the centre of the pellet, and Mo association, since no other than Mo-Ru-Pd is observed.

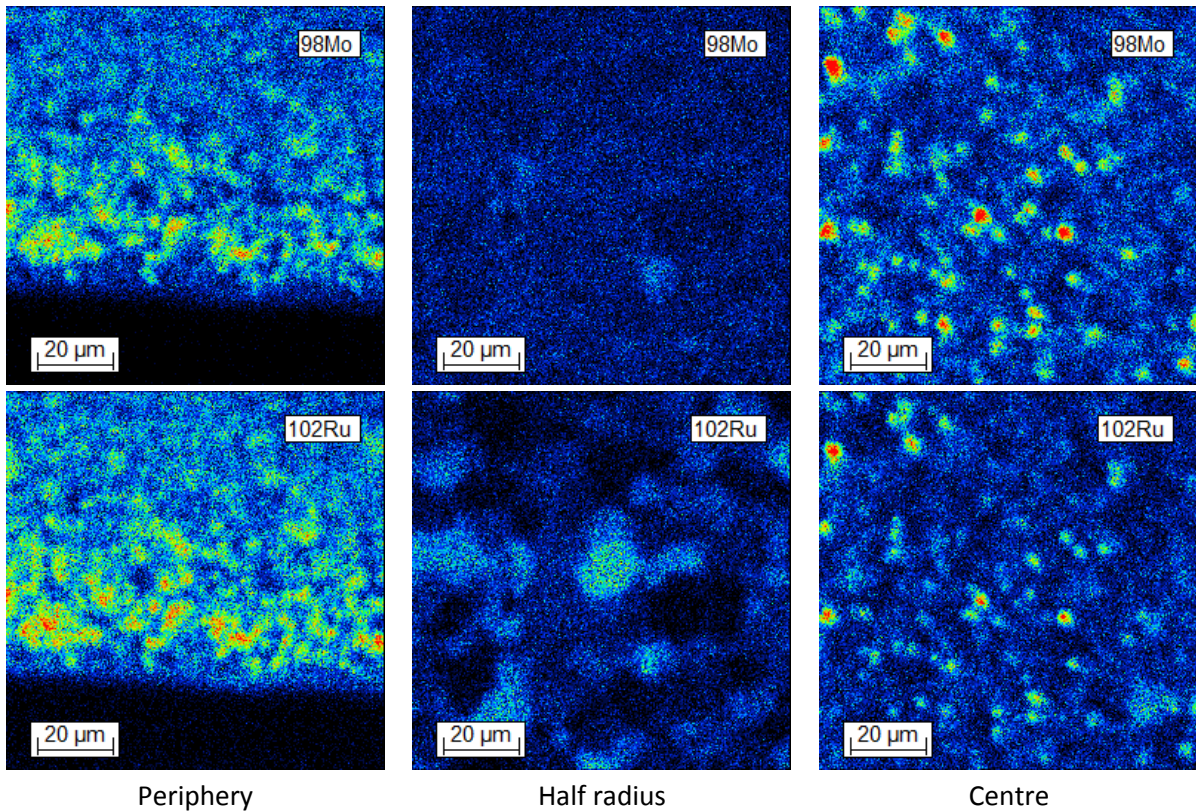


Figure 26: ^{99}Mo and ^{102}Ru ion maps from the periphery, half radius and centre of T_0 -IF sample

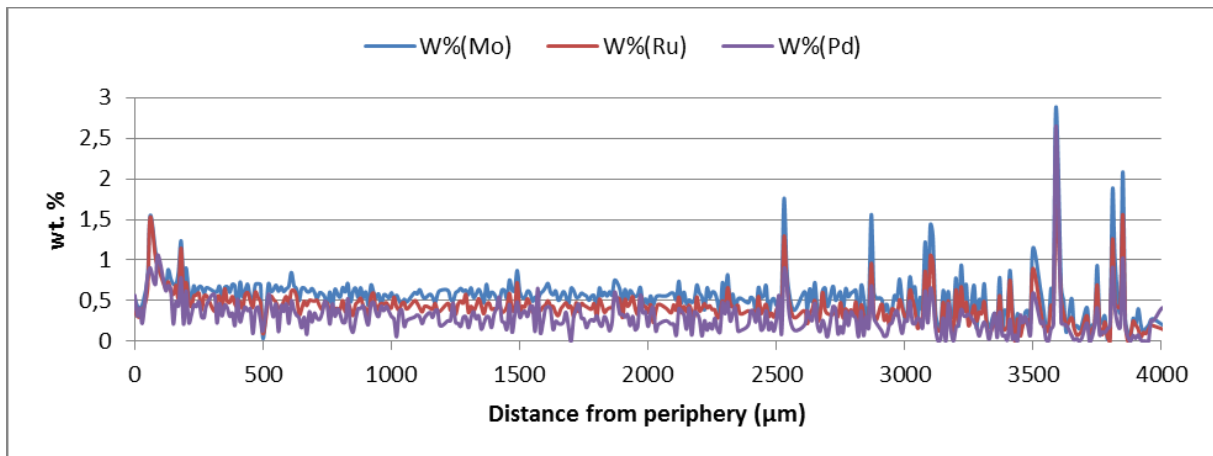


Figure 27: Mo, Ru and Pd concentration profiles in T_0 -IF Sample

2.3.2. IF1500 Sample: Intermediate state of a severe accident

2.3.2.1. Fuel micro-structure evolution

SEM-BSE images corresponding to the periphery and centre of the IF1500 sample are presented in **Figure 28**. As for T_0 -IF sample, an internal ZrO_2 layer is observed in the periphery, along with an increased porosity compared to the centre of the fuel. IF1500 sample porosity, both in the periphery and centre, is superior to that of T_0 -IF sample. Indeed, pores represent 21.5% and 18% respectively, of the total analysed

area in these images. The pores ECD are 0.9 ± 0.6 and 0.7 ± 0.3 μm for the periphery and centre regions, respectively. A partial interconnection of pores is observed as a consequence of the annealing test. Porosity at the centre of the sample is similar to that observed at the mid radius region.

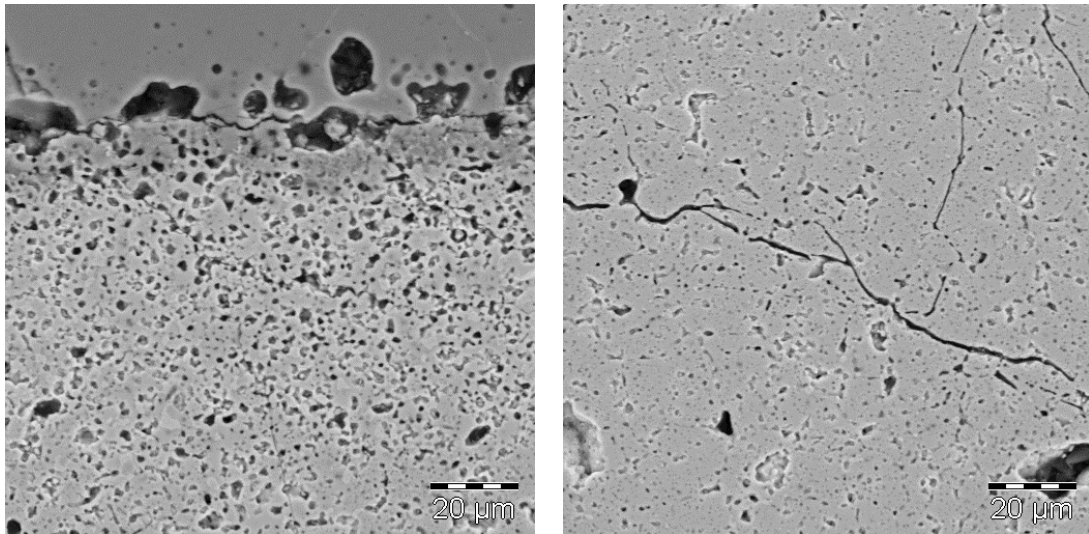


Figure 28: SEM-BSE images from the centre (right) and periphery (left), IF1500 Sample

2.3.2.2. Barium

Barium distribution in the IF1500 sample was determined through EPMA analyses. Again, three different zones were analysed (periphery, half radius and centre) but only two are presented here (periphery and centre) since results obtained in the centre and half radius of the sample were quite similar.

Many Ba-Zr precipitates were observed in the centre of the sample, as presented in **Figure 29**. Indeed, the superposed X-ray maps of Ba (green) and Zr (red) indicate a clear Ba-Zr association (yellow). Nevertheless, some precipitates containing Zr but no Ba were also observed, as well as precipitates containing Ba but no Zr. The observed precipitates present an ECD of 1.5 ± 0.7 μm . Regarding the periphery of the sample, results are quite interesting. Indeed, Ba and Zr X-ray maps, presented in **Figure 30**, indicate an important accumulation of Ba right next to the cladding on the fuel's side, coinciding with the internal ZrO_2 layer. At the same time, many Ba and Zr precipitates are observed close to the periphery, though Ba and Zr do not share, mostly, the same location. Ba precipitates close to the periphery present an ECD of 2.1 ± 0.9 μm .

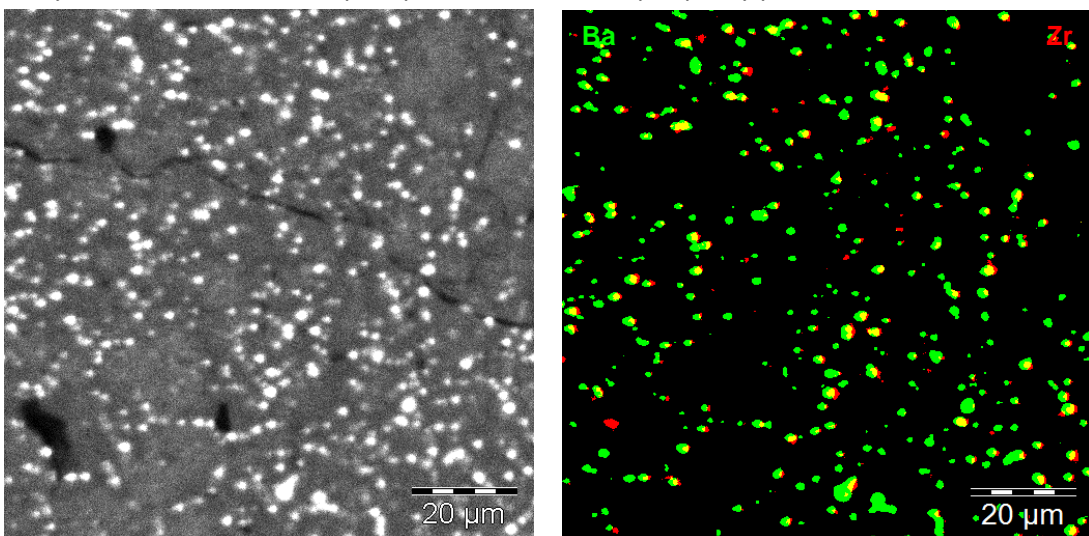


Figure 29: Ba (left) and Ba/Zr (right, superposed) X-ray maps, IF1500 Sample centre

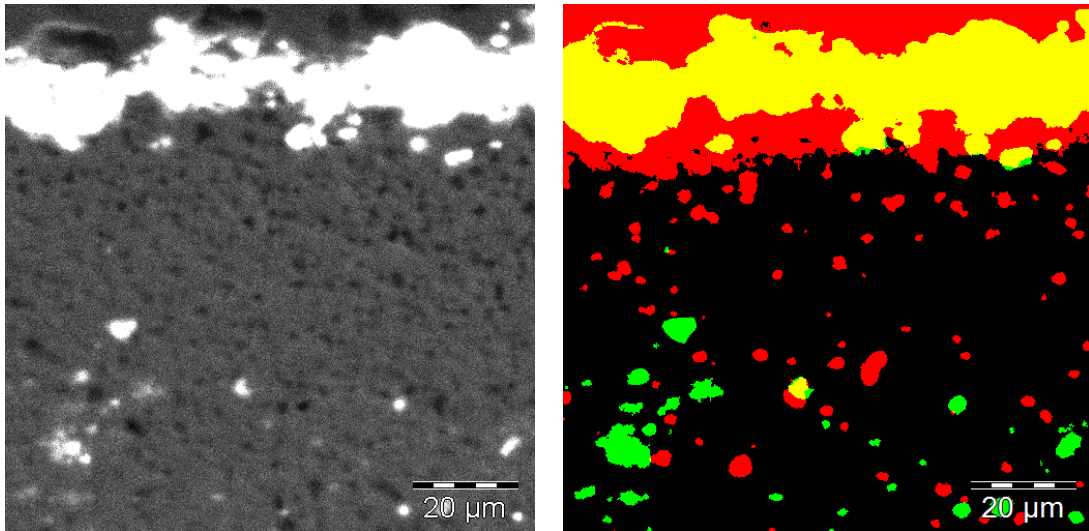


Figure 30: Ba (left) and Ba (green) - Zr (red), superposed X-ray maps, IF1500 Sample periphery

2.3.2.3. *Caesium*

Cs distribution in the IF1500 sample was determined by EPMA analysis at the centre and periphery of the sample. Results are presented in **Figure 31** and **32**, respectively. Though no Cs precipitates are observed in the centre of the sample, further image analysis showed that Cs and Xe would share the same location, as indicated by the green circles. Many Cs precipitates are clearly observed close to the periphery of the sample, associated with Xe. The latter precipitates present an EDC of $1.5 \pm 0.3 \mu\text{m}$. No association with any FP other than Xe was observed. No Cs or Xe accumulations were observed in the half-radius region of the sample.

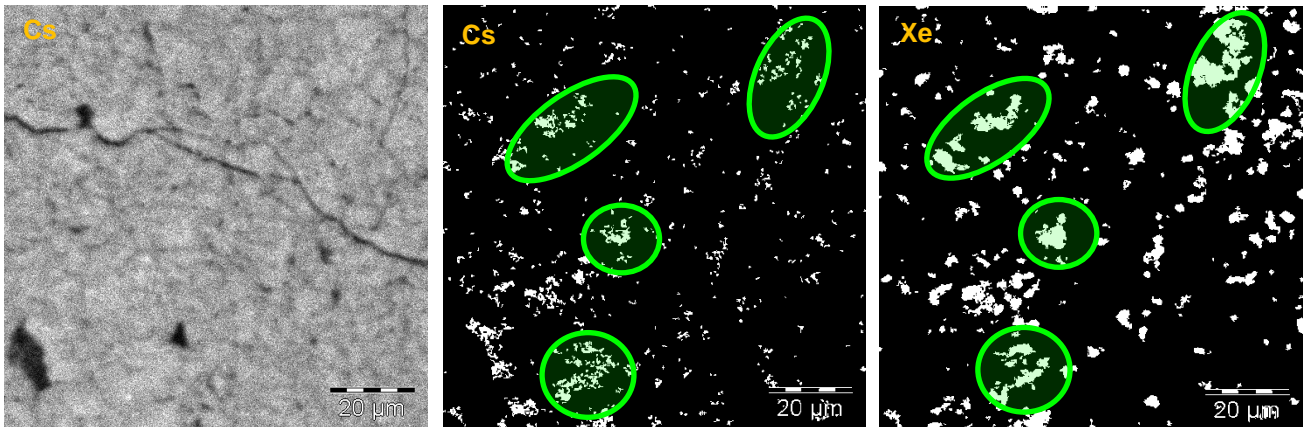


Figure 31: Cs and Xe X-ray maps, centre of IF1500 sample

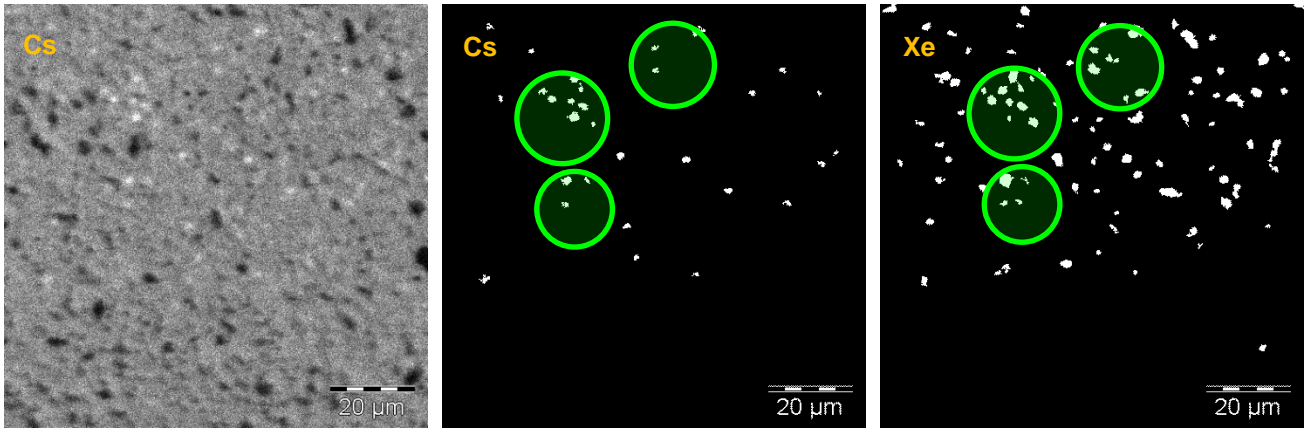


Figure 32: Cs and Xe X-ray maps, periphery of IF1500 sample

2.3.2.4. Molybdenum and Ruthenium

Mo distribution in the IF1500 sample was also determined by EPMA analyses. Many precipitates were observed in the whole sample, but only the results corresponding to the centre and periphery are presented here, in **Figures 33** and **34**, respectively. Mo was found associated to Ru, Rh, Tc and Pd, though many precipitates containing Mo, Ru, Rh and Tc but no Pd were observed, as indicated by the Mo-Pd superposed X-ray maps presented in these figures. Precipitates located at the periphery are twice larger than those at the centre and half radius regions. Indeed, precipitates at the centre of the sample presented an ECD of $1.1 \pm 0.6 \mu\text{m}$, those at the half radius region an ECD of $1.2 \pm 0.4 \mu\text{m}$, and those at the periphery an ECD of $2.4 \pm 1.5 \mu\text{m}$. The only Mo-Ru association observed was that of the white inclusions.

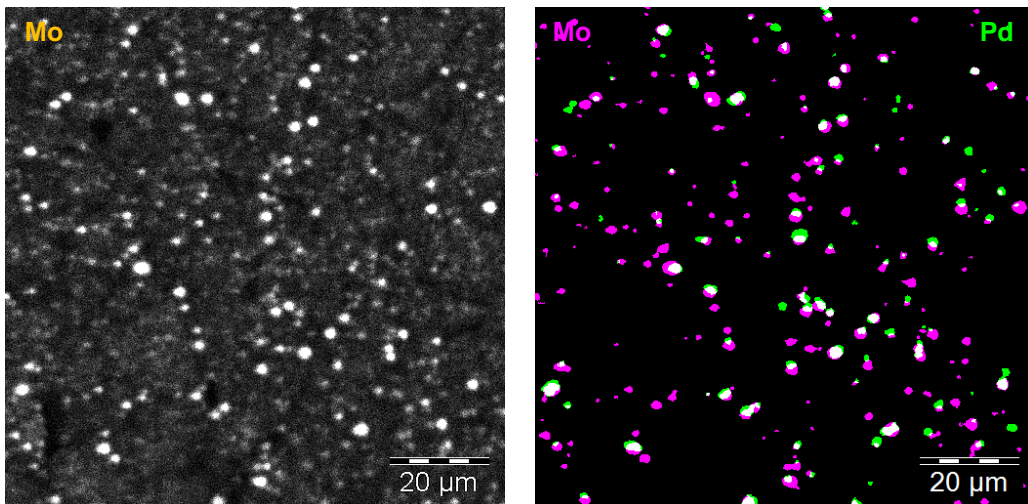


Figure 33: Mo (left) and Mo/Pd (right) superposed X-ray maps, IF1500 sample centre

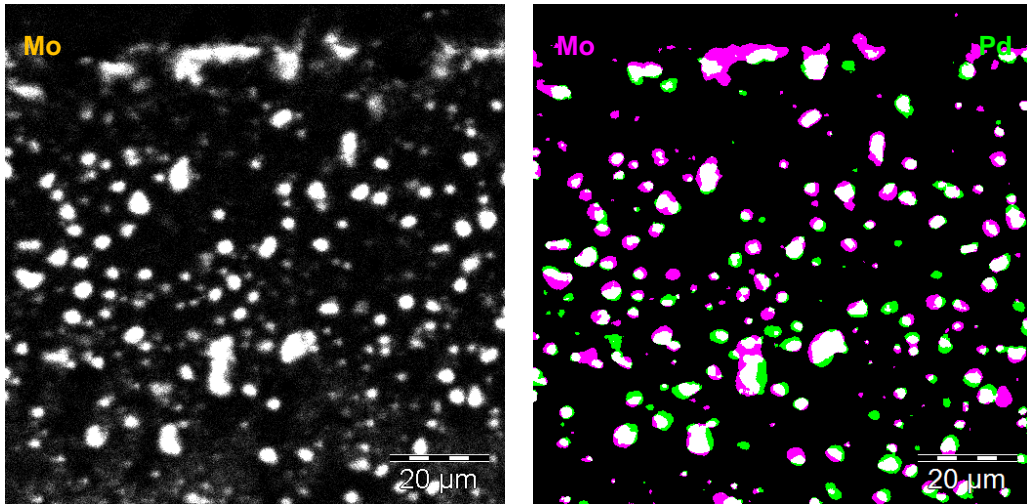


Figure 34: Mo (left) and Mo/Pd (right) superposed X-ray maps, IF1500 sample periphery

2.3.3. VERDON 1 Sample: Advanced state of a severe accident

2.3.3.1. *Fuel micro-structure evolution*

The fuel micro-structure evolution was studied thanks to a metallographic analysis performed on VERDON 1 - Sample B. Three main regions were observed, as presented in **Figure 35**: A predominant dark-grey one of elevated porosity, a light-grey one with moderate porosity; and second light-grey region of low porosity. Many white precipitates were observed in the regions of high and moderate porosity. Regarding the region of low porosity, no small precipitates were found but instead a few large precipitates with an ECD sometimes superior to 40 µm, as observed in **Figure 36**. The pores area fraction in the elevated porosity region is almost twice than in the moderate porosity one: 42% (ECD = 4.7 ± 4 µm) vs. 25% (ECD = 3.8 ± 2.9 µm). The precipitates area fraction is almost the same in these two regions (0.5 and 0.4% for the moderate and elevated porosity regions, respectively) though the precipitates ECD is different. Indeed, the metallic precipitates observed in the elevated porosity region presented a mean ECD of 0.8 µm, while those from the moderate porosity region and ECD of 1.1 µm.

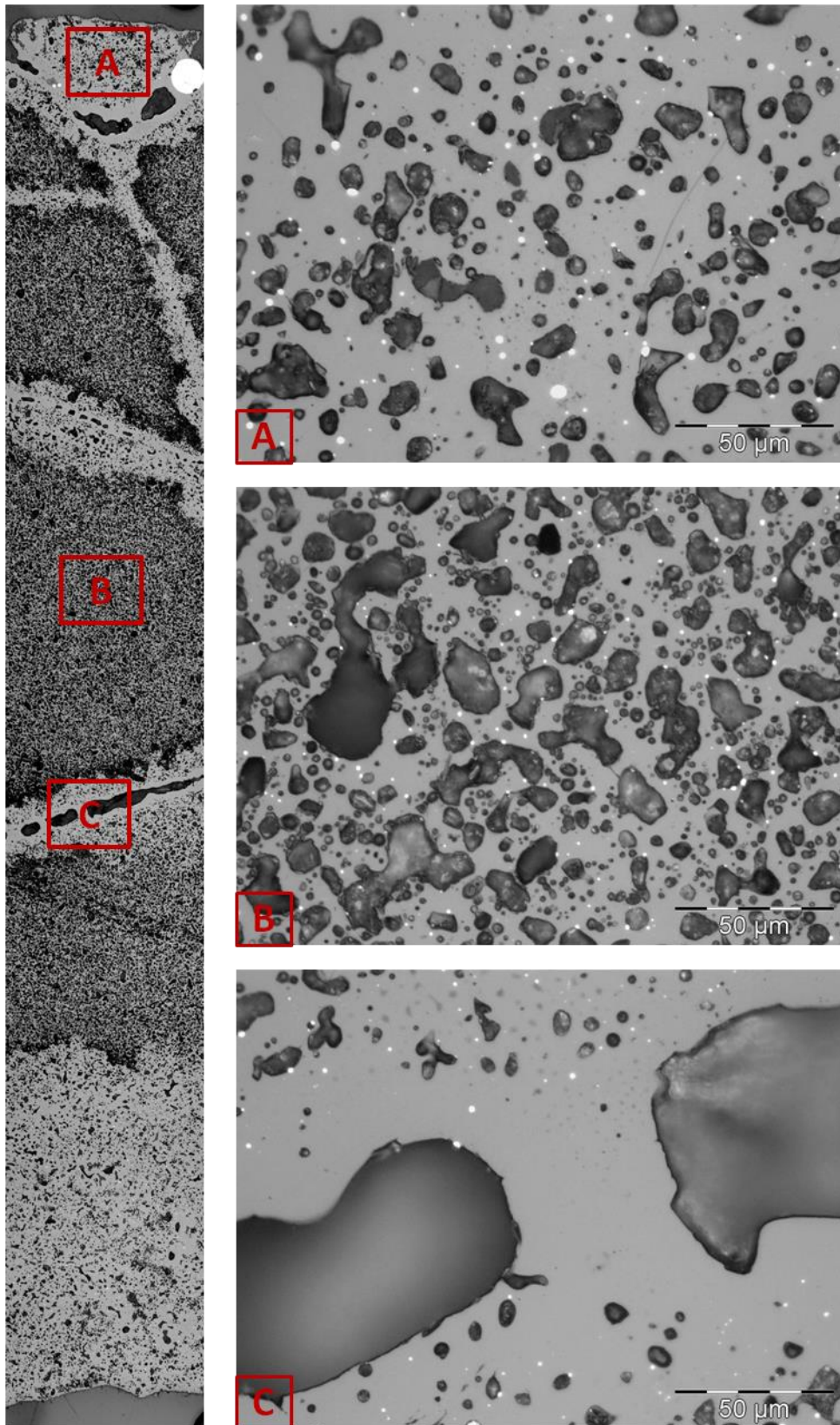


Figure 35: Sample B OM image. The three zones are observed: a moderate porosity zone, (A), an elevated porosity one (B) and a low porosity one (C)

EPMA analyses were performed on sample A2. The obtained results were important for determining the evolution observed during VERDON 1 test. A SEM-SE image of a fissure located close to the periphery of the sample where the three regions are observed is presented in **Figure 36**, along with the corresponding Mo, U and Zr X-ray maps. In these images it is clearly observed that there are important quantities of Zr in the low porosity compared to the elevated porosity one, while U content is lower in the low porosity zone compared to the high one. The latter is better observed thanks to quantitative analyses performed. O, U, Pu and Zr quantitative profiles analyses were acquired in this region, along the orange line presented in the SEM-SE image (**Figure 36**, top left). This line scan, which results are presented in **Figure 37**, is 250 μm long and consists of point analyses every 3 μm . The limits of each region are indicated by the dashed red lines on U concentration profile. According to these results, zirconium concentration increases from traces in the elevated porosity region to about 17 at.% in the centre of the fissure (low porosity region) On the contrary, uranium concentration, which is around 33 at.% in the elevated porosity region, gradually decreases down to around 17 at.% in the centre of the fissure. Regarding oxygen, its concentration remains uniform and equal to 66 at.% in the three covered zones. Plutonium profile is quite interesting. Indeed, its behaviour is similar to that of Zr: Its concentration increases slightly from around 0.4 at.% in the elevated porosity region to 0.5-at.% in the centre of the fissure.

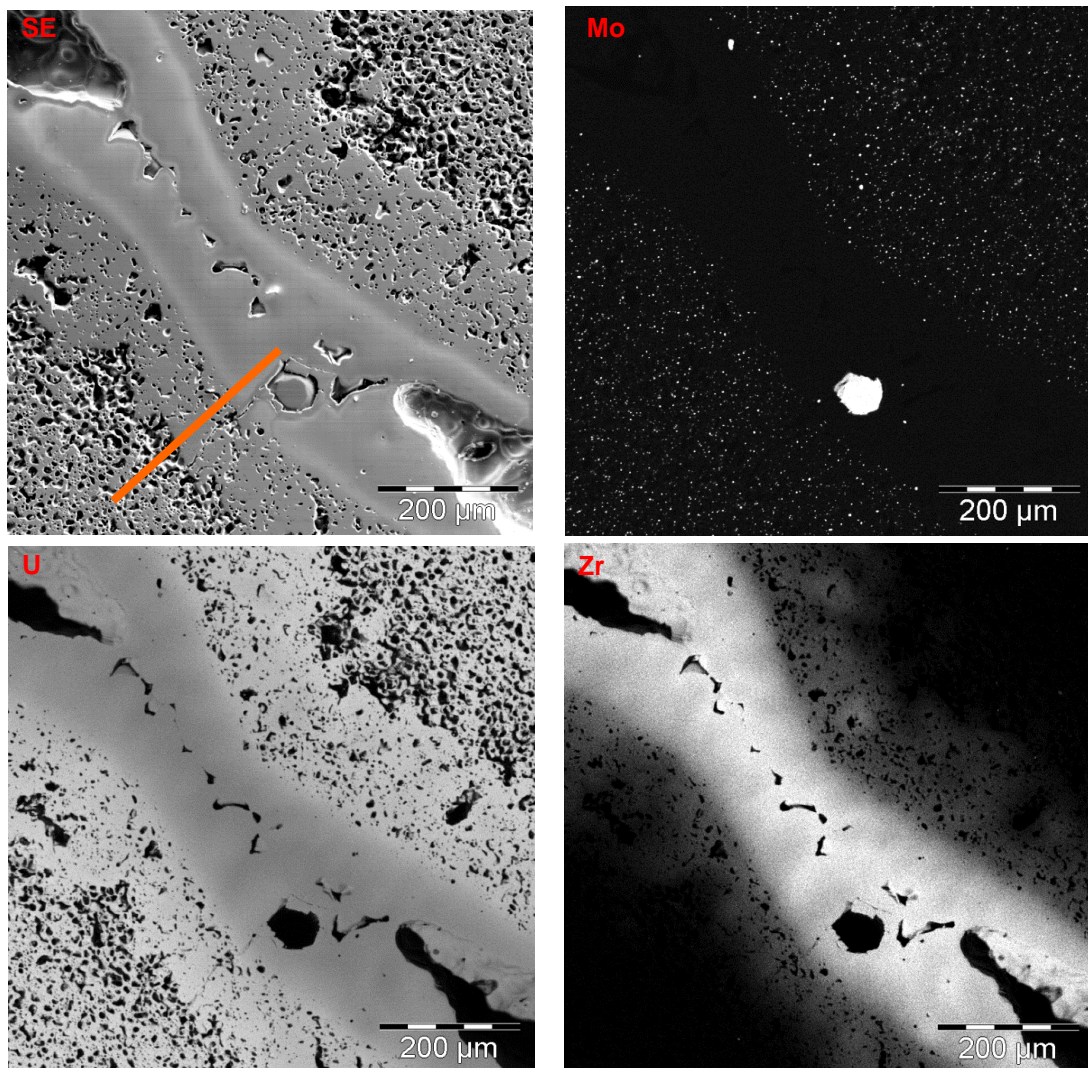


Figure 36: SEM-SE image and Mo, U and Zr X-ray maps, fissure close to the periphery, Sample A2

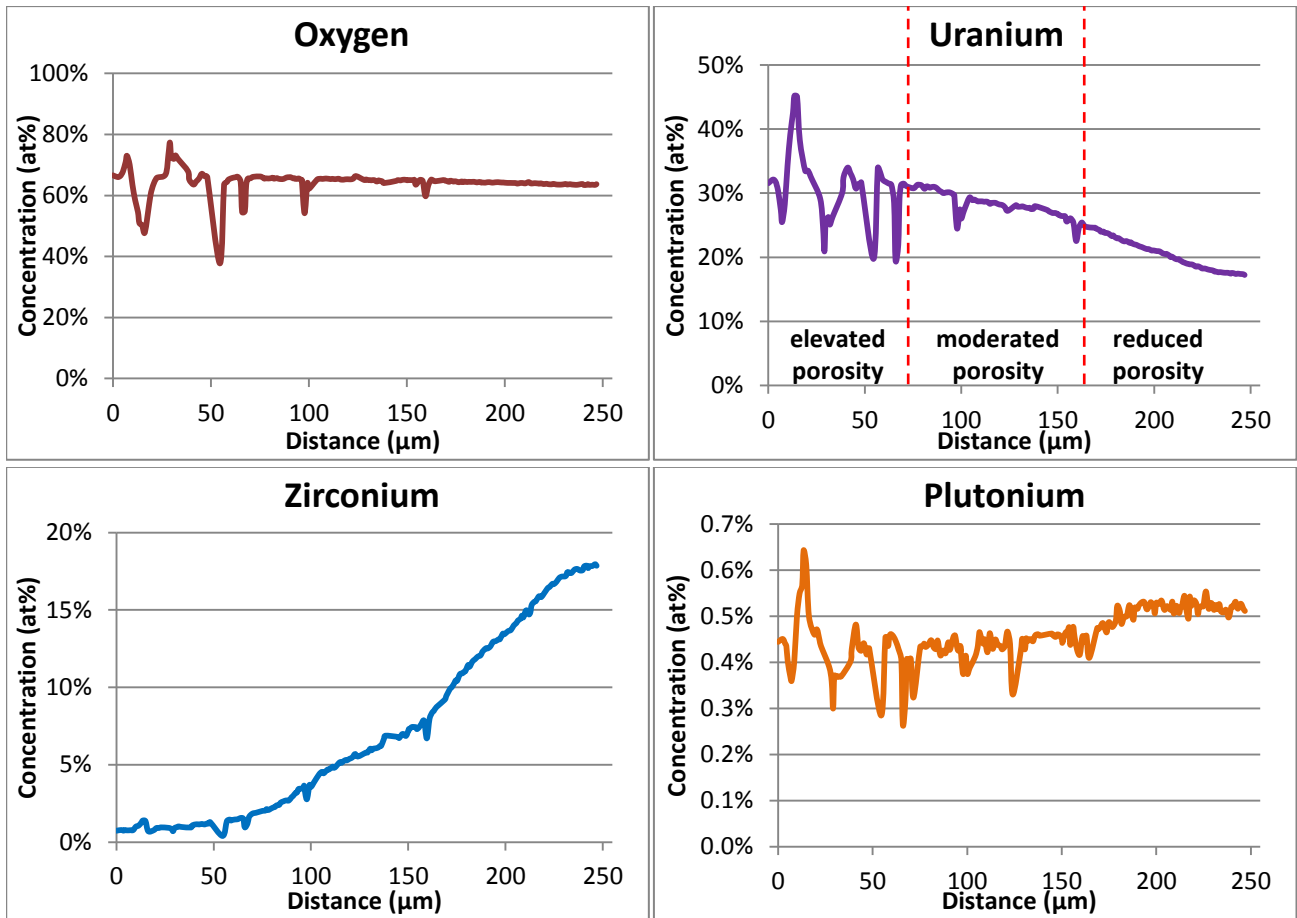


Figure 37: O, U, Zr and Pu quantitative analyses covering the three porosity regions, from the elevated porosity zone towards the low porosity one

A similar analysis was performed at the periphery of the sample. **Figure 38** presents a SEM-SE image of the periphery along with the corresponding Zr X-ray map. Quantitative analyses were also performed, as indicated by the orange line. U, Zr, O, Pu and Nd quantitative profiles are presented in **Figure 39**. According to these profiles, Pu concentration in the periphery decreased almost three times compared to the initial state. Indeed, Pu concentration at the fuel periphery in the T_0 -IF sample was 4.3 wt% while it was 1.3 wt% at the periphery of the VERDON 1 sample A2. As it will be explained later, these results would indicate that a cladding-fuel interaction took place during the last phase of the experimental sequence. Due to this interaction, the UO_2 at the periphery of the sample melted and penetrated through the cracks, carrying with it the Pu located mainly at the periphery.

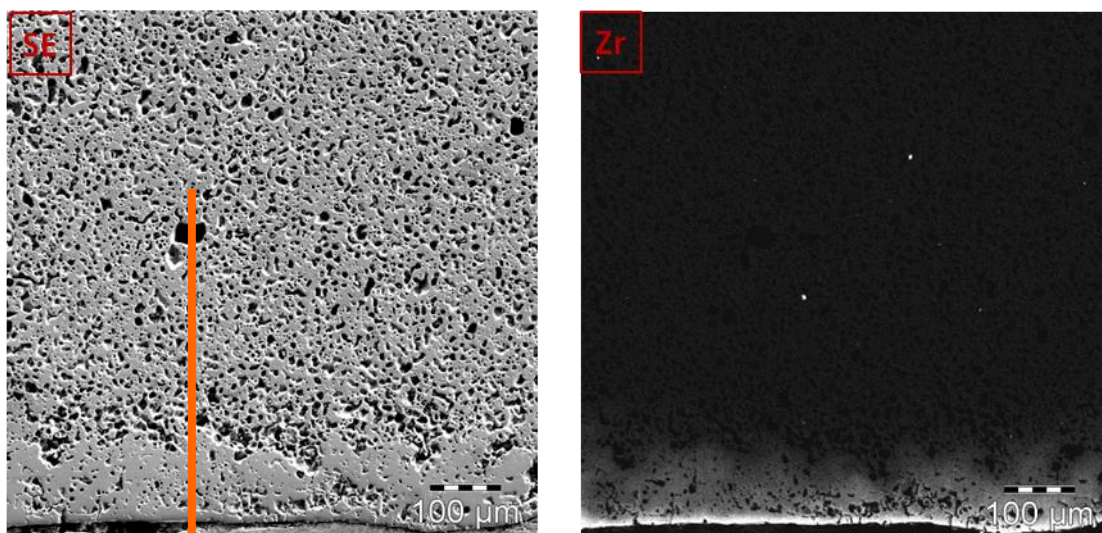


Figure 38: SEM-SE image (left) and Zr X-ray map (right), periphery of sample B

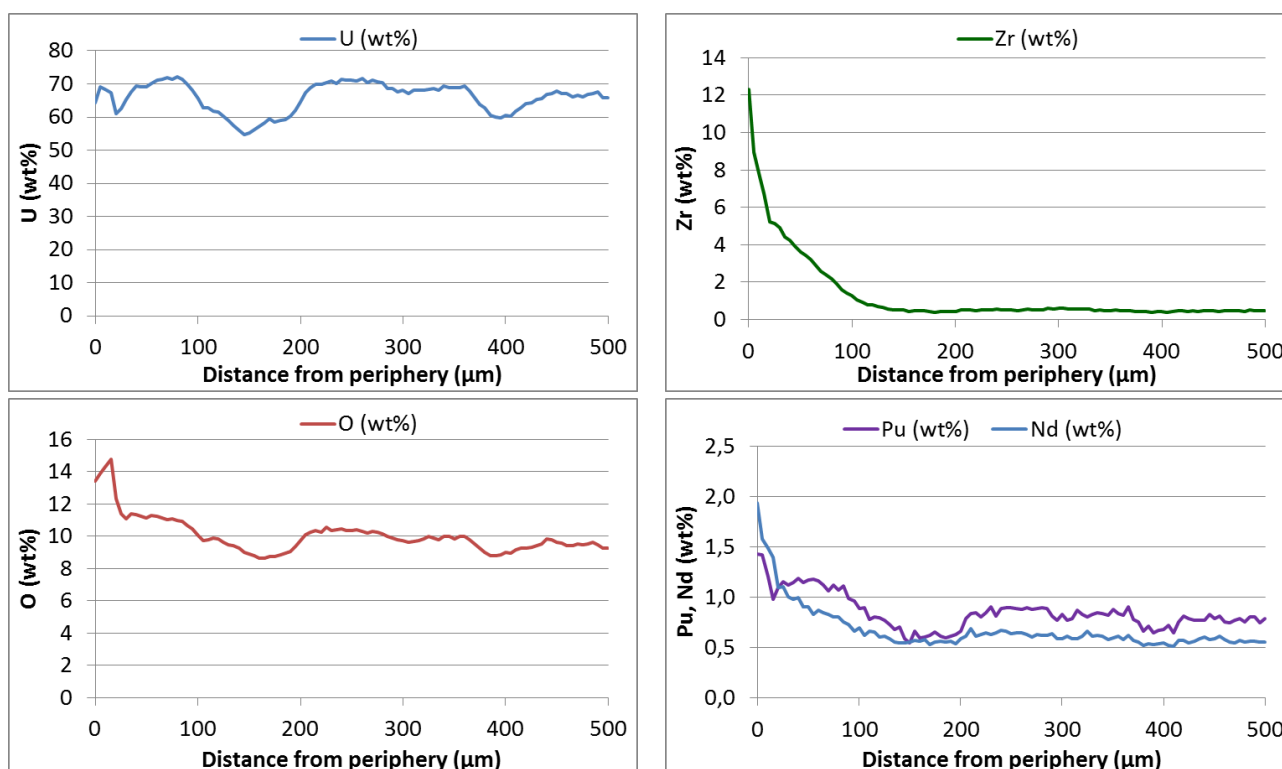


Figure 39: U, Zr, O, Pu and Nd concentration profiles, periphery of Sample B

2.3.3.2. XRD

Three different zones were analysed by XRD as indicated in **Figure 40**. These zones are representative of the high, moderate and low porosity regions described above: Zone 1 includes almost exclusively the dark region of elevated porosity; Zone 2, of similar size, includes mainly the region of moderate porosity; finally the Zone 3, smaller than the first two, includes mainly the low porosity region. The three collected diffractograms are different, particularly that of Zone 3, which highlights their different chemical composition. The experimental and fitted data obtained from Zones 1, 2 and 3 are presented in **Figures 41**, **42** and **43** respectively.

Three different phases have been considered in order to reproduce the experimental data: MoRu₂Pd, representative of the metallic precipitates, the UO₂ matrix and a U-Zr-O phase, depicted as (U_{0.5}Zr_{0.5})O₂. Only the UO₂ and the U-O-Zr phases were identified in Zone 3, though some metallic precipitates are indeed observed in SEM images. The fit was performed using the TOPAS 4.2 software and the theoretical lattice parameters considered were obtained from EVA 17.0.0.2 software, both from Bruker-AXS. The three diffractograms are presented together in **Figure 44**, along with the MoRu₂Pd phase lines. It is observed that the diffraction angles of the MoRu₂Pd phase are different for each zone, and so it is not possible to make a direct association. Nevertheless, some peaks observed for Zone 3 may correspond to the MoRu₂Pd diffraction lines, though they do not correspond to the most intense lines. The theoretical and the calculated lattice parameters are presented in **Table 17**.

The considered phases reproduce quite well the experimental data, with the exception of some lines that, according to EVA, could correspond to Ba compounds such as BaO or BaZrO₃. Nevertheless, their signal intensity is too low to properly identify the phases. It was observed that the calculated lattice parameters for the UO₂ matrix, the metallic precipitates and the U-Zr-O phase are different for each region and different to the theoretical values.

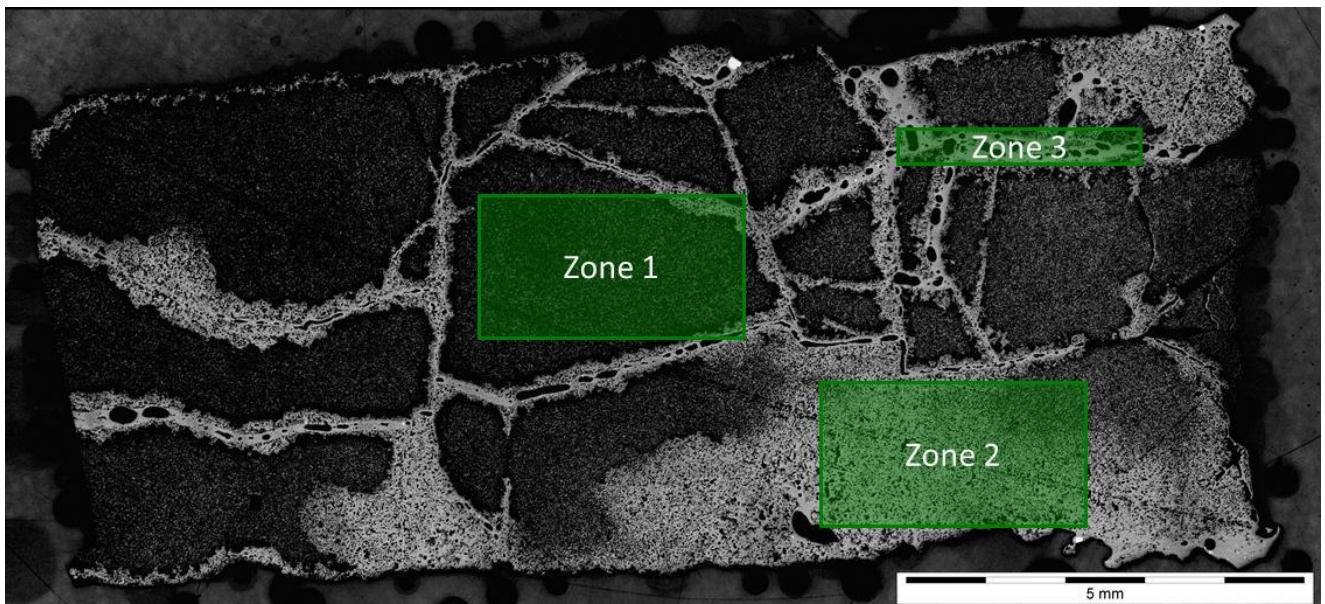


Figure 40: Zones analysed by XRD, Sample B

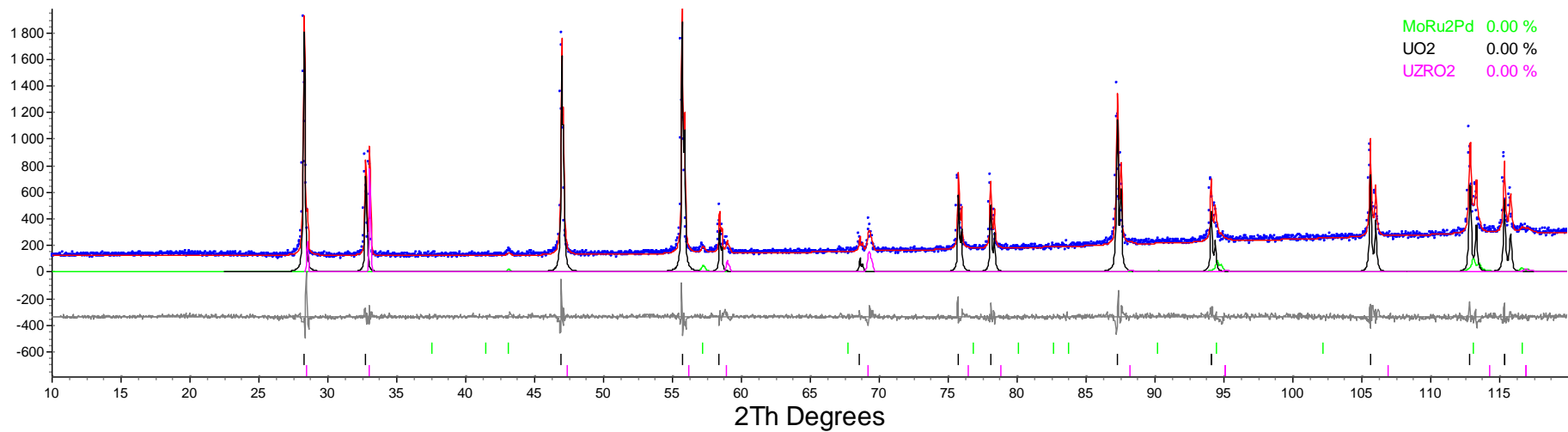


Figure 41: Zone 1 diffractogram, Sample B

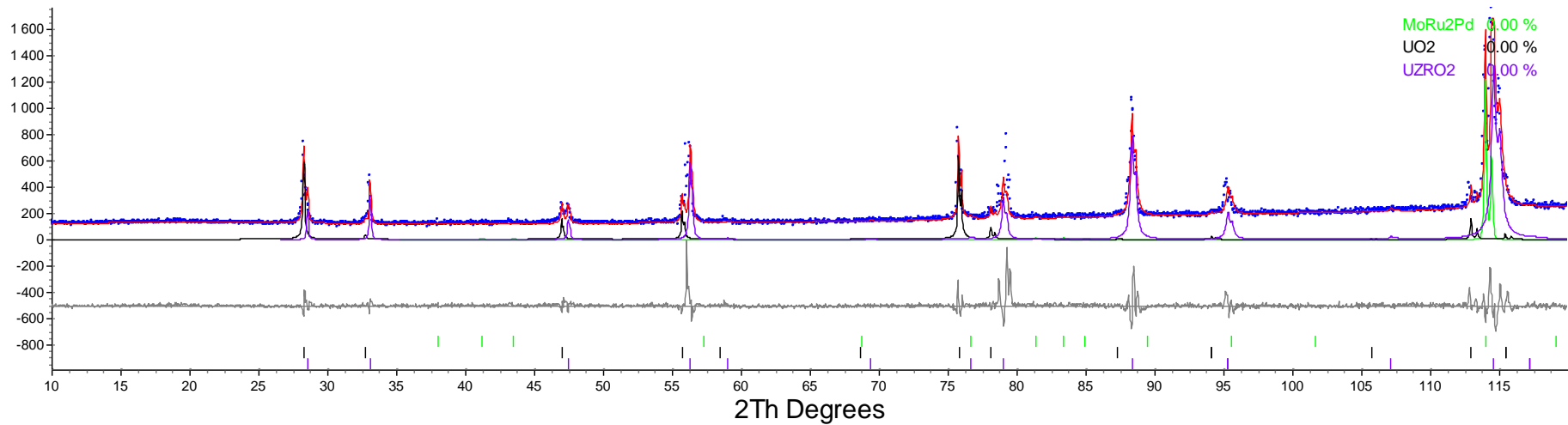


Figure 42: Zone 2 Diffractogram, Sample B

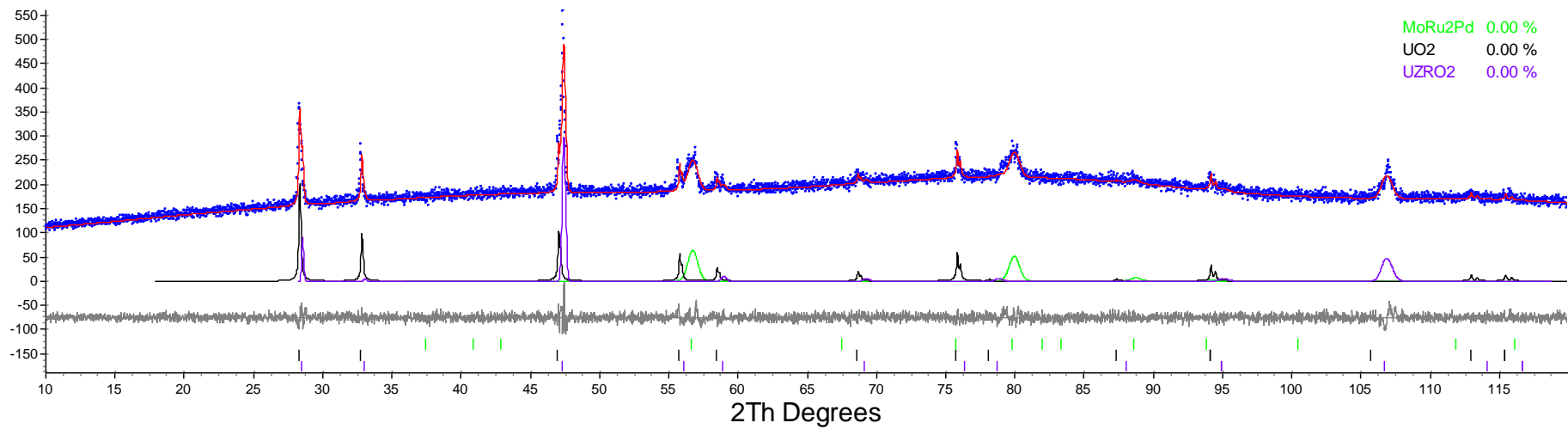


Figure 43: Zone 3 Diffractogram, Sample B

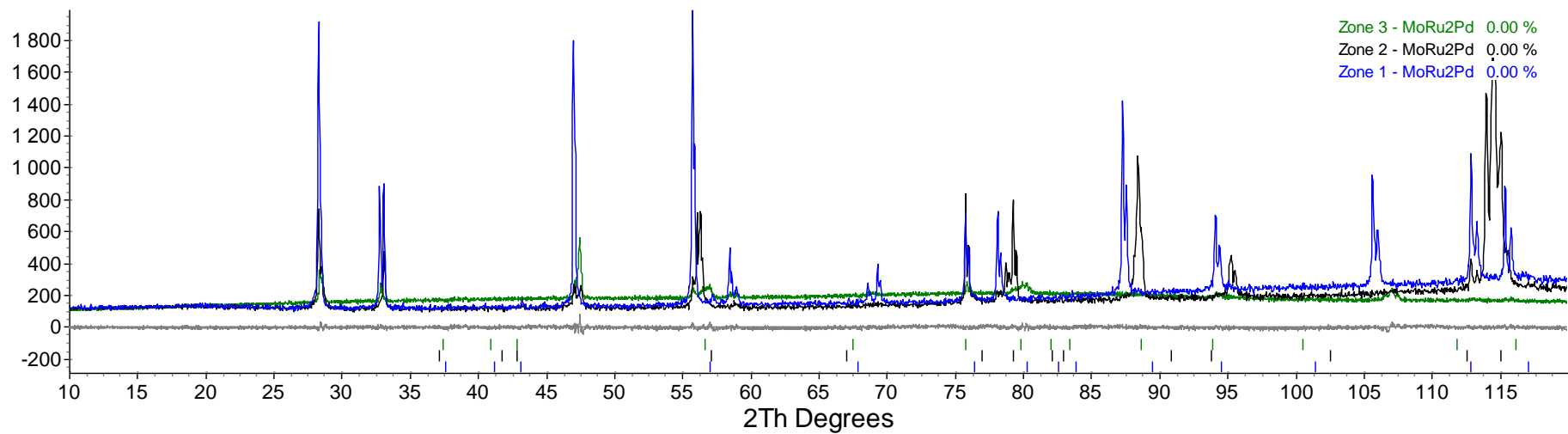


Figure 44: Zones 1, 2 and 3 diffractograms - MoRu₂Pd lines

Phase	Crystallographic Structure	Theoretical lattice Parameters (Å)	Calculated lattice parameters (Å)		
			Zone 1	Zone 2	Zone 3
MoRu ₂ Pd	Hexagonal (P63/mmc)	a= 2,748	a= 2,781±5E ⁻⁴	a= 2,806±5E ⁻⁵	--
		c= 4,383	c= 4,332±2E ⁻³	c= 4,176±1E ⁻⁴	--
UO ₂	FCC (Fm3m)	a= 5,467	a= 5,47±5E ⁻⁵	a= 5,468±2E ⁻⁴	a= 5,467±2E ⁻⁴
(U _{0,5} Zr _{0,5})O ₂	FCC (Fm3m)	a= 5,42	a= 5,424±2E ⁻⁴	a=5,416±2E ⁻⁴	a= 5,430±3E ⁻⁴

Table 17: Theoretical and estimated lattice parameters (Å) of the phases identified by XRD, Sample B

2.3.3.3. Barium

Though most barium was released during VERDON 1 test (80% of the initial inventory, according gamma spectroscopy analyses) some precipitates were found in the elevated porosity region (highlighted in green), as observed in the X-ray maps presented in **Figure 45**. Nevertheless, Ba was not associated to Zr (precipitates highlighted in orange). No precipitates of Ba or Zr were found in the moderate porosity region, as observed in the X-ray maps presented in **Figure 46**. No Ba precipitates were found either through EPMA quantitative analyses performed in the transversal section of the sample, which presented in **Figure 47**. Indeed, though there are some regions highly concentrated in Zr, no association with Ba was observed.

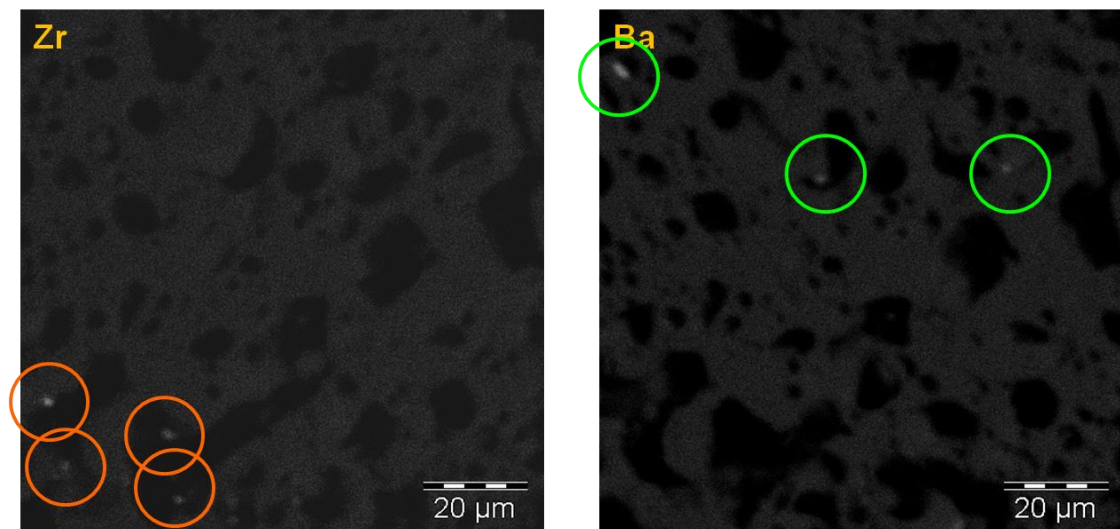


Figure 45: Zr and Ba X-ray maps, Elevated porosity region, Sample B

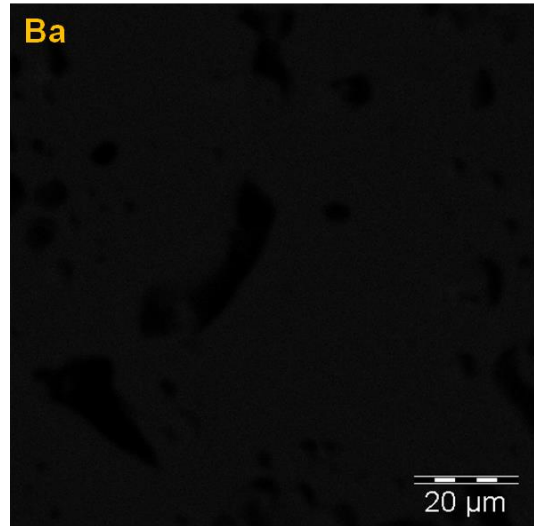
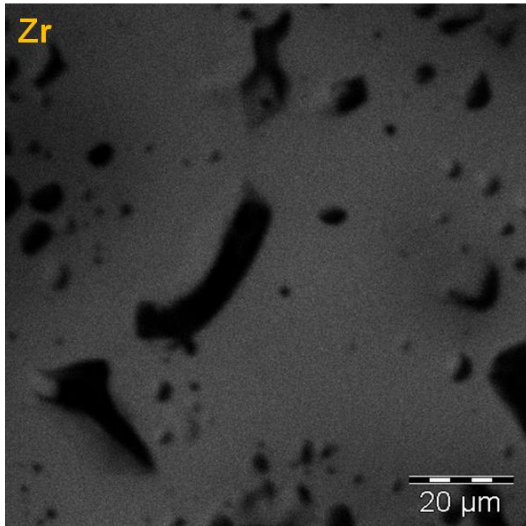


Figure 46: Zr and Ba X-ray maps, Moderate porosity region, Sample B

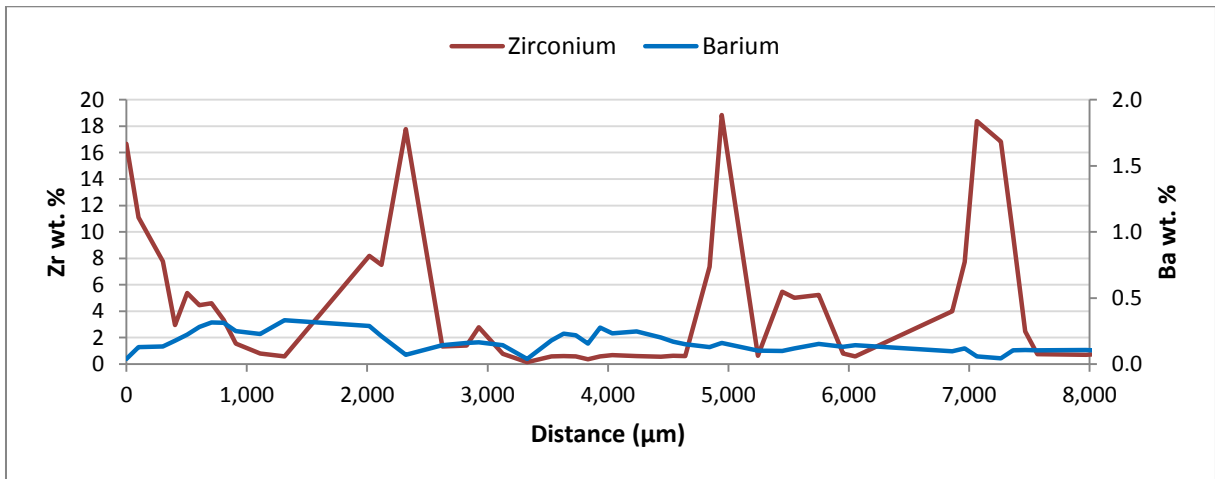


Figure 47: Zr and Ba transversal quantitative profiles, Sample A2

2.3.3.4. Caesium

As presented in **Section 2.2.4** where the VERDON 1 sample was described, volatile species such as Cs, I and Xe were completely released from the fuel sample. This was confirmed by EPMA X-ray maps and quantitative analyses, presented in **Figures 48** and **49**, respectively. Indeed, Cs and Xe measured concentrations correspond to the EPMA detection limit.

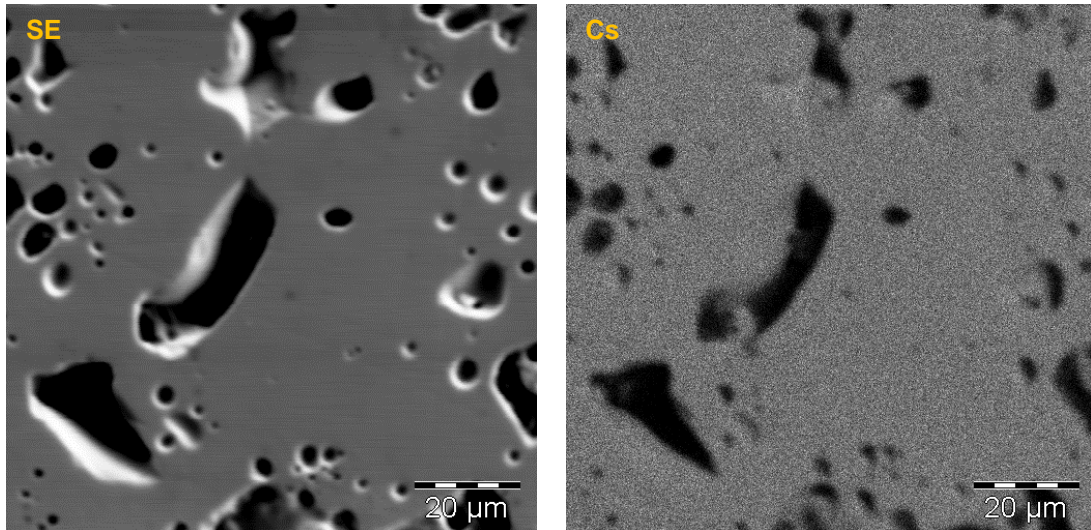


Figure 48: SEM-SE image and Cs X-ray map, moderate porosity region, Sample B

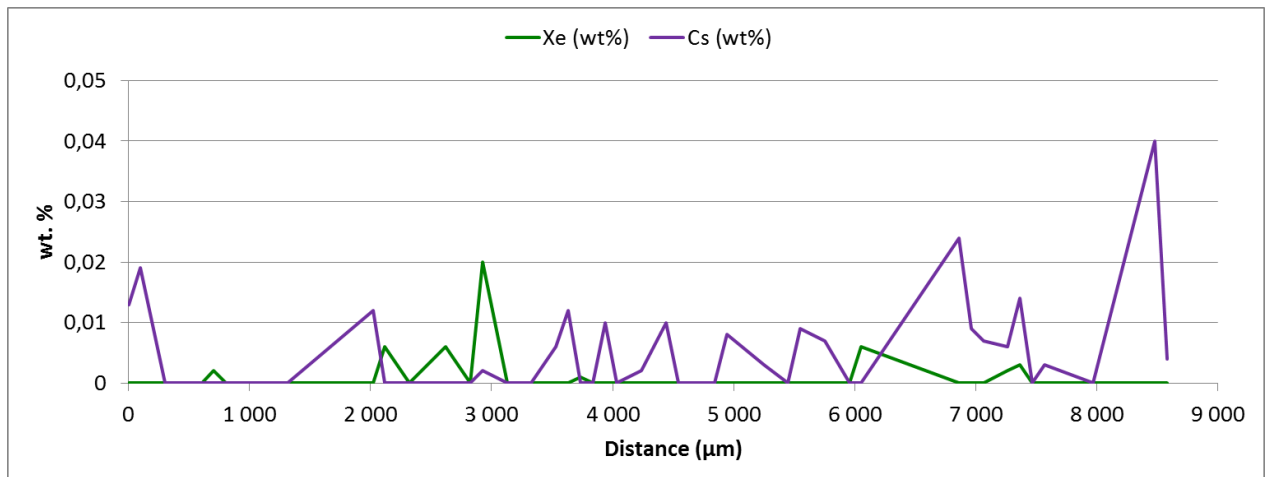


Figure 49: Xe and Cs transversal quantitative profiles, Sample A2

2.3.3.5. Molybdenum and ruthenium

SEM analyses performed in Sample B showed the presence of small, round precipitates at the grain boundaries in the low-porosity region (as observed in **Figure 50**) and in the sample matrix and grain boundaries of the moderate and elevated porosity regions. A SEM-SE image and Mo-Pd X-ray maps are presented in **Figure 51**, which correspond to the low porosity region. Large Mo precipitates, with an ECD superior to 40 μm, were also found in the low porosity region. Two of these large sized precipitates were found in Sample A2, one close to the periphery and the other in the centre of Sample B2. Their size allowed acquiring quantitative profiles of Mo, Ru, Pd, Rh and Tc, which are presented in **Figure 52**. Tc concentration was determined by subtraction (considering that any other

FP or O were present), since only Mo, Ru, Pd and Rh were actually measured. As observed in these quantitative profiles, Ru is the main constituent of these precipitates. Mo concentration varied according to the position of the precipitate in the sample. Indeed, it was observed that Mo concentration in the precipitate located near the centre of the sample was around 25 wt%, while it was around 10 wt% in the one located near the periphery.

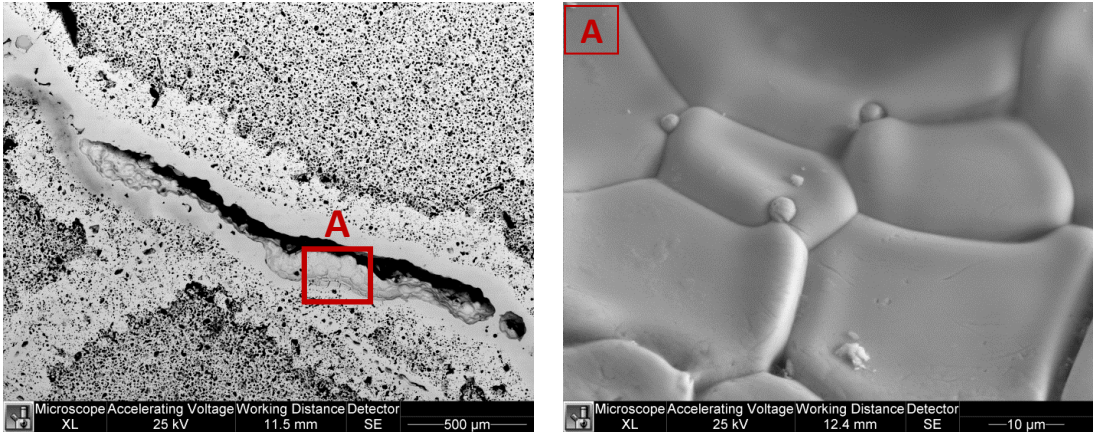


Figure 50: Zone 2 SEM-SE images, Sample A2

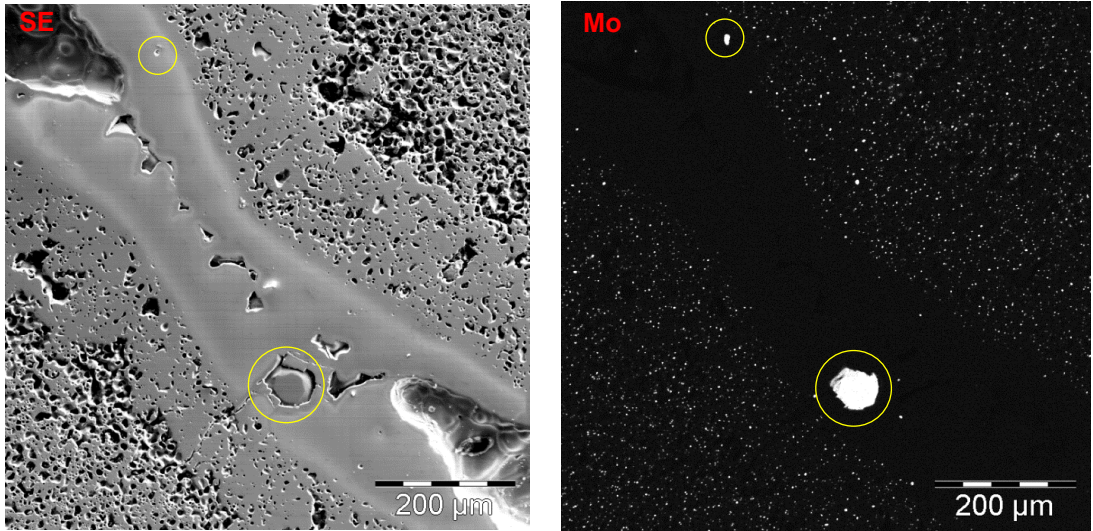


Figure 51: SEM-SE image and Mo X-ray map, low porosity region, Sample A2

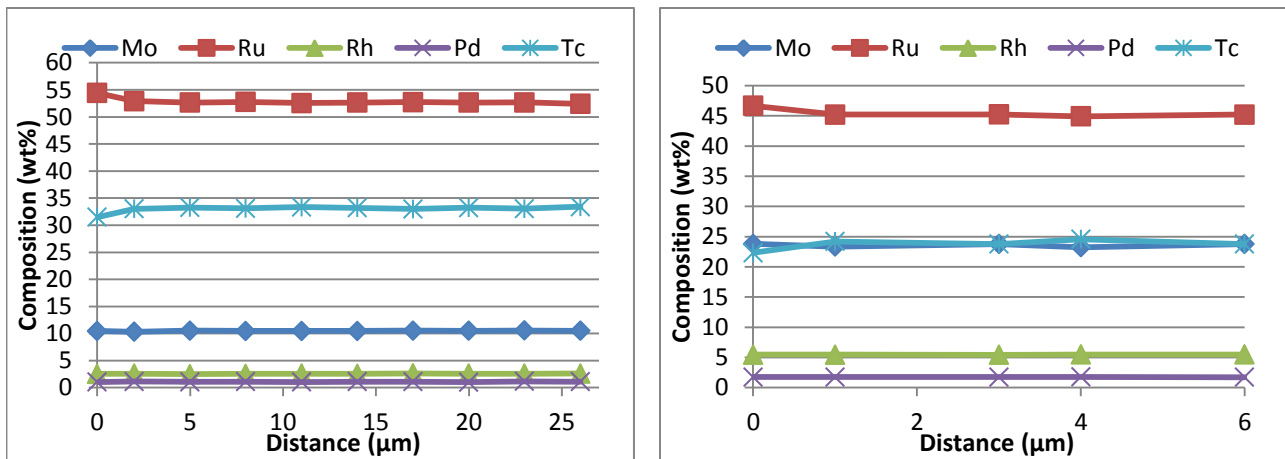


Figure 52: Quantitative profiles in large metallic precipitates located near the periphery (left) and centre (right) of Sample A2

EPMA analyses performed in the moderate porosity region are presented in **Figure 53**. These analyses showed that Ru was always associated to Mo, and so its X-ray maps are not presented here. Palladium, on the contrary, was present only in some of them, as observed in the superposed X-ray.

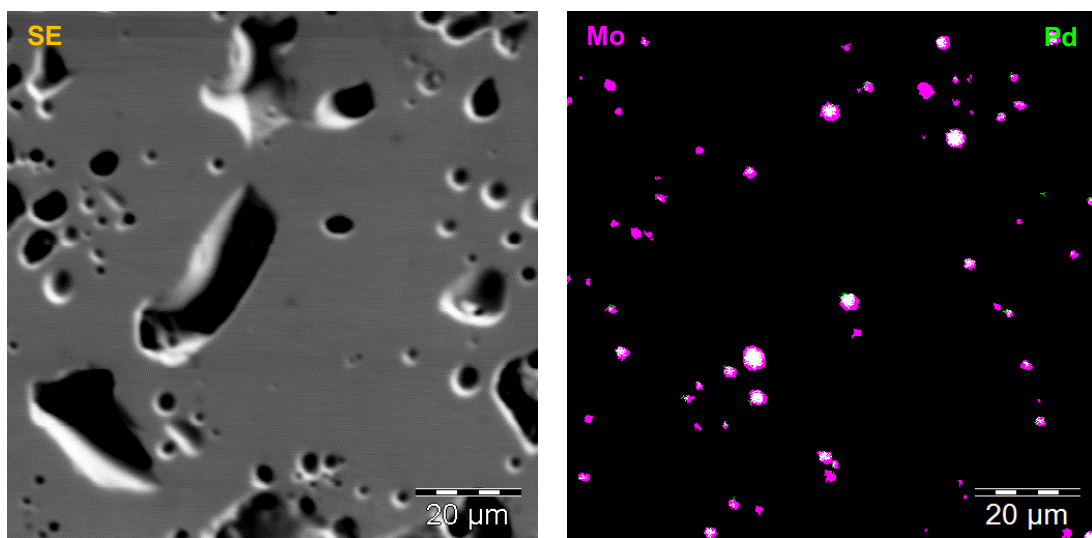


Figure 53: SEM-SE and Mo-Pd superposed X-ray maps, moderate porosity region, Sample A2

2.4. Discussion: Results vs. mechanism

2.4.1. Fuel micro-structure evolution

Studying the evolution of the fuel micro-structure is of main importance to understand FP release behaviour. Indeed, one of the main hypotheses of the proposed mechanism is the pores interconnection between 1373 and 1673 K. This interconnection would create a path through the fuel, increasing FP release rate. It was observed that porosity indeed increased from one sample to another: it went from 15% to 21.5% (at the periphery), and from 8% to 18% (at the centre), for T₀-IF and IF1500 samples, respectively. VERDON 1 samples porosity did not show a difference regarding periphery or centre, but instead it depended on the region (high or moderate porosity). So, porosity represented 42% in the elevated porosity region and 25% in the moderate one. Pores size also evolved with temperature. Indeed, their ECD increased from $0.8 \pm 0.4 \mu\text{m}$ to $0.9 \pm 0.6 \mu\text{m}$ at the periphery but decreased from $1.0 \pm 0.5 \mu\text{m}$ to $0.7 \pm 0.3 \mu\text{m}$ at the centre of T₀-IF and IF1500 samples, respectively. Regarding VERDON 1 samples, pores ECD were $4.7 \pm 4 \mu\text{m}$ at the elevated porosity region and $3.8 \pm 2.9 \mu\text{m}$ at the moderate one. Then, these results would validate the hypothesis of pores' interconnection at high temperatures, creating a path which enhances FP release from the sample.

Particularly for the VERDON 1 samples, quantitative analyses allowed to interpret what happened during the test and why three zones of different porosity exist. According to the pseudo binary ZrO₂-UO₂ phase diagram presented in **Figure 54**, extracted from (Piluso et al., 2005), an indifferent point (the analogue to liquid-vapour azeotrope) exists at $X_{\text{ZrO}_2}=0.58$ (atomic fraction). According to the U and Zr quantitative profiles, presented in **Figure 55**, the molar fractions measured at the centre of the region of low porosity were 0.174; 0.178 and 0.637, for U, Zr and O respectively. With these results a Zr/U ratio of 1.02 is obtained, not far from the indifferent point composition. Moreover, its fusion temperature, 2850 K, and the temperature attained by the end of VERDON 1 test, 2884 K, were close enough as to form a liquid solution, thanks to the dissolved FP and a possible oxygen sub-stoichiometry. It is assumed then that ZrO₂ from the cladding diffused into the periphery of the fuel pellets. When a composition matching or close to the indifferent point was attained, the solution melted and penetrated into the pellets through the cracks, carrying the elements normally located in the HBS, such as Pu.

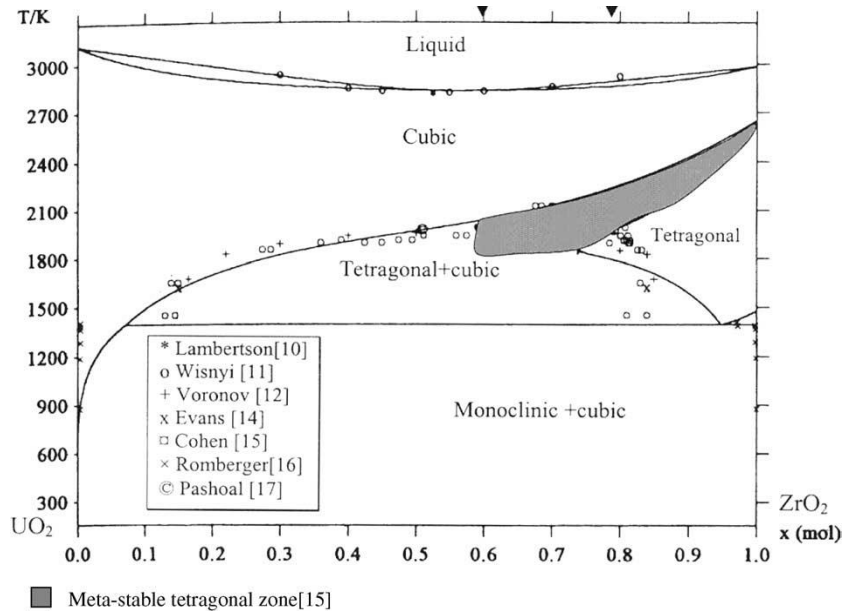


Figure 54: $\text{UO}_2\text{-ZrO}_2$ pseudo binary phase diagram from (Piluso et al., 2005)

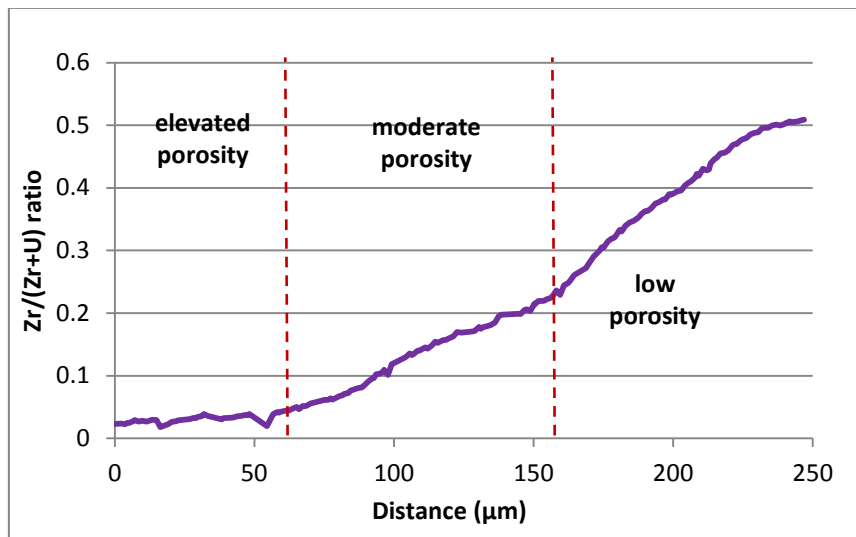


Figure 55: $\text{Zr}/(\text{Zr}+\text{U})$ ratio evolution from the elevated porosity zone towards the low porosity one

2.4.2. Barium

According to bibliography (Kleykamp, 1985), under normal operation conditions and high burn-up (72 GWd.t^{-1} in our case) barium would be found in oxide precipitates with perovskite structure called the “Grey Phase”. This phase is depicted as $(\text{Ba}, \text{Cs}, \text{Sr})(\text{Mo}, \text{Pu}, \text{Zr}, \text{U}, \text{RE})\text{O}_3$, where RE stands for Rare Earths. As Ba, Zr and U are the main chemical components of this oxide phase, the lattice parameter would range from $a=4.39 \text{ \AA}$ (for BaUO_3) to $a=4.19 \text{ \AA}$ (for BaZrO_3). The lattice parameter may be further reduced by incorporation of BaMoO_3 , present in oxidizing conditions (Kleykamp, 1985). According to (Kleykamp, 1985), rare earths such as Ce and Y are also present in the grey phase but are only detected in high-burn up fuels. Nevertheless, characterization tests performed on the $\text{T}_0\text{-IF}$ sample are opposed to these observations. Indeed, as observed in the ion maps presented in **section 2.3.1.2**, no precipitates of Ba were observed in the sample, not even in the HBS zone where the local burn-up attained values of 150 GWd.tn^{-1} . According to (Kleykamp, 1985), the perovskite

phase could be observed in high burn-up fuel or in fuel submitted to high temperatures. Kleykamp performed his observations on FBR fuel pins, where temperature in operation conditions ranges from 873 K (in the periphery of the fuel) to 2273 K (in the fuel pellets centre. The temperature attained in PWR fuels is lower. Indeed, the temperature of the fuel pellets ranges from 623 K in the periphery up to around 1373 K in the centre. However, it is also reported that the maximal Ba solubility in UO_2 is 0.6 at.% (or 0.3 wt.%) at 2273 K (Kleykamp, 1993; Paschoal et al., 1987), as indicated in the UO_2 -BaO phase diagram presented in **Figure 56**. EPMA quantitative analyses indicate that Ba concentration at the periphery of the sample (HBS) is 0.6 wt.%.

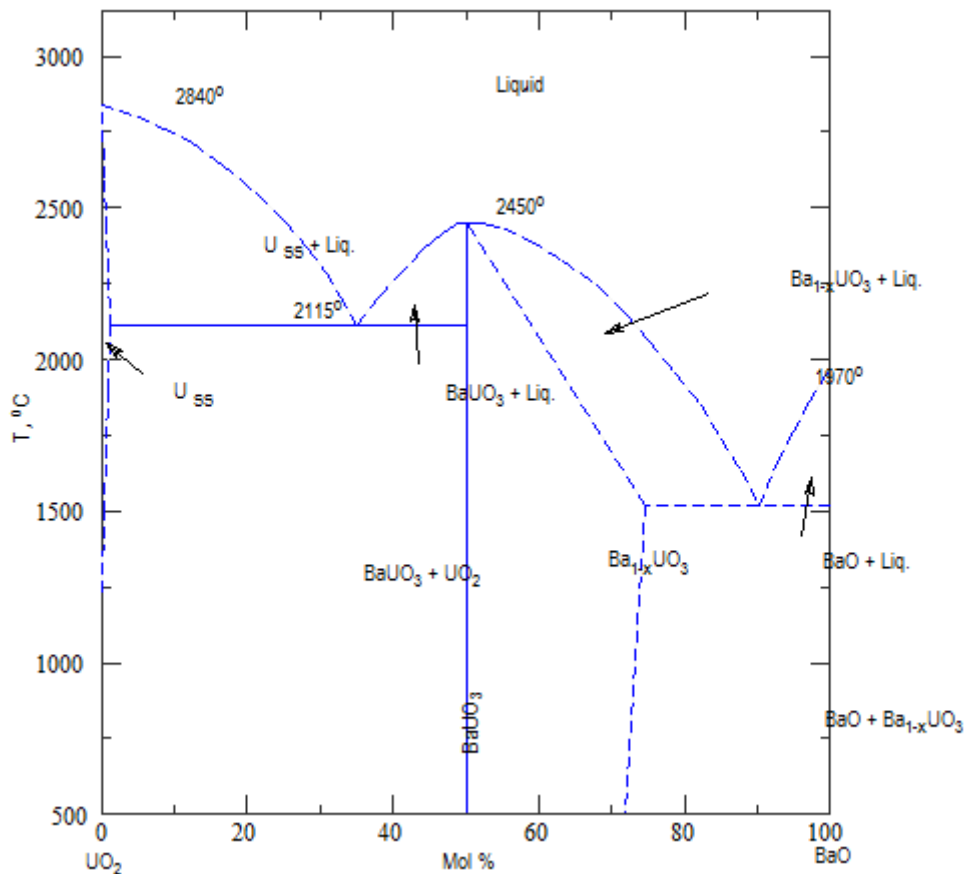


Figure 56: UO_2 -BaO pseudo binary phase diagram extracted from (Paschoal et al., 1987)

Though no Ba precipitates have been observed even at high burn up (periphery of T_0 -IF sample), after the annealing test up to 1773 K (IF1500 sample) many Ba-Zr precipitates were observed in the whole sample. We suppose then that Ba is soluble in the UO_2 matrix even at very high concentrations but this is a metastable state, and Ba precipitates as BaZrO_3 or BaO at high temperatures. Regarding the periphery of the IF1500 sample, an accumulation of Ba was observed at the fuel-cladding interface. Ba precipitates are also observed close to the cladding, but apparently they are not associated with Zr. As presented in Chapter 1, a similar Ba-cladding interaction has already been observed in the post test examinations performed on the VERCORS 5 sample. Indeed, it was observed that 15% of the initial Ba inventory remained in the cladding after the test (Ducros, 1994b). Nevertheless, the apparent dissociation of the Ba-Zr precipitates close to the periphery would indicate that the local oxygen potential conditions induced the BaZrO_3 dissociation into BaO or Ba. Ba mobility increased, migrated towards the periphery but was retained by the cladding. In this case, the cladding acted as a

physical and not a chemical barrier, considering that the annealing sequence was performed under reducing conditions and so the Zr from the cladding remained metallic. The latter has been confirmed by EPMA observations. The BaZrO_3 dissociation at the periphery but not at centre of the sample would imply a local oxygen potential which was lower than in the rest of the sample. According to the Ellingham diagram presented in **Figure 57**, extracted from (Kleykamp, 1985) there is no FP redox couple that would act as an “oxygen pump” inducing a lower oxygen potential. Then, the oxygen potential would have been fixed only by the atmosphere, meaning that if the annealing test had continued for a longer time than the duration of the test, all BaZrO_3 present in the sample would have dissociated.

At an advanced state of a severe accident (VERDON 1 post-tests samples) it was observed that, although Ba was released up to 80%, some precipitates were still found in the fuel matrix, but no association with Zr or other FP was observed. The atmosphere during the final stage of the VERDON test was reducing, and BaZrO_3 was dissociated at high temperature with Ba being released under a mobile form (either BaO or Ba).

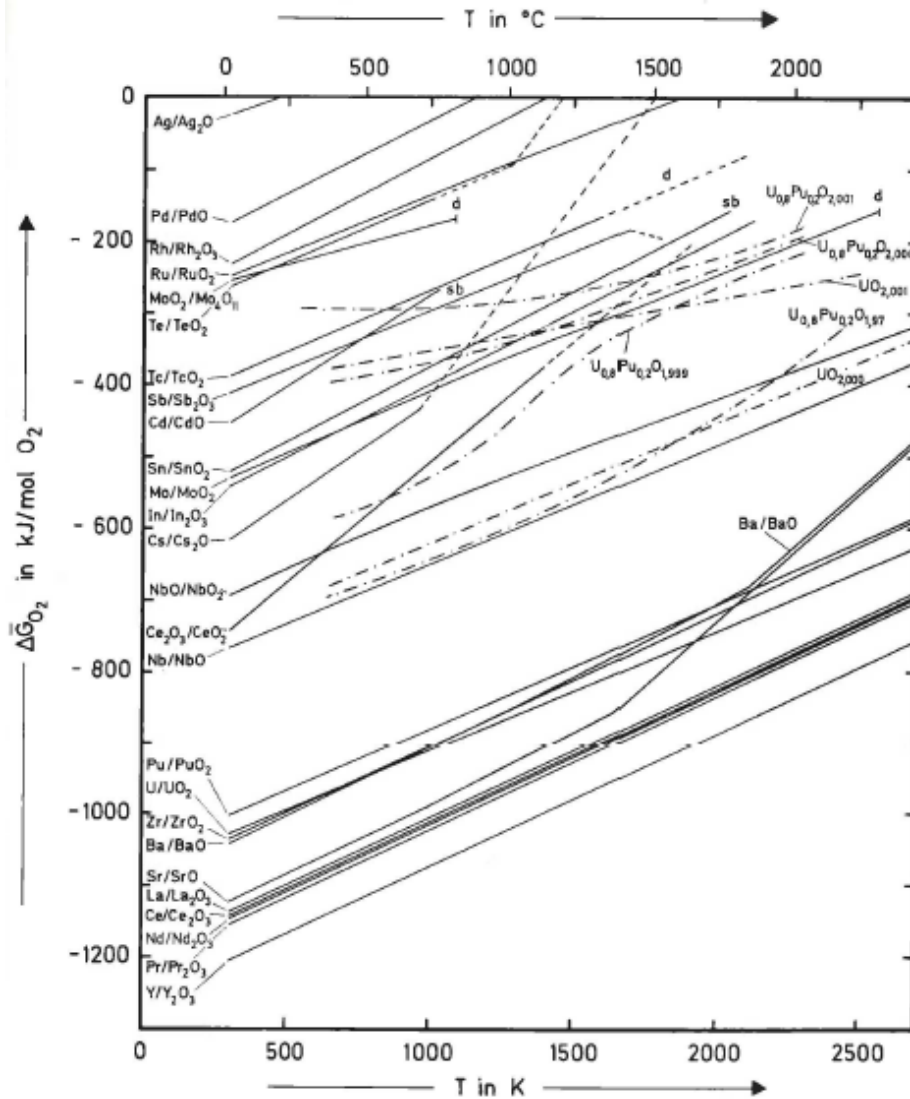


Figure 57: Ellingham diagram extracted from (Kleykamp, 1985)

2.4.3. Caesium

According to bibliography, Cs should be found in many precipitates, associated with U, O, I, Te, and even in the perovskite phase, (Ba, Cs, Sr)(Mo, Pu, Zr, U, RE)O₃ (Kleykamp, 1985). At the initial state, analysis results seem to be contradictory. Indeed, while no Cs precipitates have been observed through SIMS analyses presented in **Figure 25**, many ones were observed in the EPMA results presented in **Figure 24**. This could be due to the preparation of the samples: SIMS observations were performed on a polished sample, while EPMA ones were performed on a fractography. Then, Cs precipitates would have been removed mechanically during the polishing process or due to the temperature increase. Nevertheless, a Cs accumulation is observed in the fuel cracks close to the periphery, which would imply that Cs could be found in more than one chemical form, with high mobility. Since no association with Mo or Te was observed in EPMA results, Cs could be associated with U, O or I, though O X-ray maps did not indicate the presence of precipitates. According to observations done on the IF1500 sample, Cs behaviour would seem quite straight. Whatever the initial association was in normal operation conditions, the respective compound was dissociated and Cs behaved as a gas, explaining the association with Xe both in the periphery and centre of the sample. Cs was completely released at higher temperatures, as observed in the VERDON 1 post-test characterisations.

2.4.4. Molybdenum and Ruthenium

According to the mechanism described in Chapter 1, Mo and Ru are assumed to form metallic precipitates along with Pd, Tc and Rh. Mo could also be found in MoO₂ precipitates. According to bibliography, Mo could also be found in the perovskite phase (Kleykamp, 1985). T₀-IF sample results confirm the existence of metallic precipitates in the periphery and centre of the fuel. Since both, the IF1500 sample annealing test and the final stage of the VERDON 1 test were performed under reducing atmosphere, little evolution was observed regarding Mo and Ru chemical form. Indeed, the only association observed was Mo-Ru-Rh-Pd-Tc. According to gamma spectrometry measures performed during the VERDON 1 test, around 65% of the initial inventory of Mo was released, while only 1 to 3% of the Ru one. Most of Mo release took place during the oxidizing phase of the VERDON 1 annealing sequence, which would imply a release under an oxidized form, MoO₂ or Cs₂MoO₄. The large precipitates observed in the low-porosity region of the samples could be attributed to the presence of a UO₂-ZrO₂ liquid solution. Indeed, the metallic precipitates mobility was enhanced in the liquid medium allowing them to coalesce forming those large precipitates. This would explain why no small metallic precipitates were observed in this region. The size of the large precipitates enabled to perform quantitative analyses. According to them, Mo concentration in the precipitates located at the centre of the sample was higher than that of precipitates closer to the periphery: 25 and 10 wt%, respectively. This would reinforce the hypothesis of Mo release as Mo_(g). Indeed, the release mechanism during the final phase of the annealing test would have been purely diffusive: Mo, located in the metallic precipitates, passed to gaseous state and diffused through the interconnected pores towards the periphery. Since the pores interconnection is not total, some Mo remained in the metallic precipitates even at the imminent fusion of the fuel pellets. This behaviour is in good agreement with the mechanism presented in Chapter 1.

2.5. Conclusion

Results obtained in this Irradiated Fuels work axis have been used to verify and to refute some of the hypothetical chemical phases proposed by the mechanism. Firstly, the existence of Ba precipitates at the normal operation conditions of a PWR reactor has been refuted. Actually, no oxide precipitates corresponding to the perovskite phase, as described in bibliography, have been observed in this high PWR fuel, even at very high burn up (150 GWd.t^{-1} , at the periphery). It is concluded then that this kind of precipitates only appear at higher temperatures, between 1373 K (temperature at the centre of a fuel pellet under the normal reactor operation conditions) and 1773 K (maximal temperature attained during the Intermediate State test). Regarding Cs, it was observed that some precipitates indeed exist at the initial state, though their chemical form could not be accurately determined, since it is believed that U and O X-ray signals from the fuel matrix masked that of the precipitates (assuming that Cs chemical state was Cs_2UO_4). It was determined, though, that Mo and Te were not associated to Cs. At high temperature these precipitates dissociate and Cs behaves as a gas, diffusing through the open UO_2 matrix porosity in a similar way to Xe. Regarding Mo and Ru, many metallic precipitates were observed at the periphery and in the centre of the sample. These two FP were always associated to Pd, Rh and Tc. Since the annealing test that reproduced an intermediate state of a severe accident and the final stage of the VERDON 1 test were performed under reducing atmosphere, no oxidized species of Mo or Ru were detected.

Further investigations on FP behaviour require a complementary approach, since the characterisation techniques available for irradiated fuels enable the determination of their distribution but not of their chemical state. The need of a powerful characterisation technique to obtain the missing information led to the model materials experimental axis. Indeed, X-ray absorption spectroscopy allows not only to determinate FP chemical state but also their local environment, though it is yet unavailable for large irradiated fuel samples. To overcome this, we decided to use model materials doped with stable FP in concentration representative of a desired irradiated fuel burn up. Model materials enable a further study of FP behaviour in severe accident conditions and to validate and refute more hypothetical phases proposed in the release mechanism. These materials, the performed annealing tests, the used characterization techniques and obtained results are presented in the next chapter.

Chapter 3: Model Materials

3.1. Introduction	89
3.1.1. X-ray Absorption Spectroscopy	90
3.2. Samples description	92
3.2.1. Samples set I	92
3.2.2. Samples sets II and III	93
3.3. Thermodynamic Analysis	94
3.4. FP Behaviour	96
3.4.1. Sample Set I	96
3.4.2. Sample set II	102
3.4.3. Sample set III	118
3.5. Discussion	130
3.5.1. Tests performed under reducing atmosphere	130
3.5.2. Tests Performed under oxidizing atmosphere	133
3.6. Conclusions	135
3.6.1. Barium behaviour	136
3.6.2. Caesium behaviour	136
3.6.3. Molybdenum behaviour	136
3.6.4. Ruthenium behaviour	137

Chapter 3: Model Materials

3.1. Introduction

As explained in Chapter 1, a whole description of FP behaviour (such as oxidation state, chemical phases and solubility) requires characterisation techniques which are not yet available for large irradiated nuclear fuel samples. Model materials, called SIMFUEL, came up as a possible alternative. Indeed, these materials are made from natural UO_2 powder milled with several stable FP in concentrations representative of a desired burn-up and then sintered. The resulting ceramic samples present a microstructure and a FP distribution representative of irradiated fuels (Lucuta, 1991a) but without their radioactivity (except for the inherent natural uranium one). They are easier to handle and allow the use of characterization tools not present in hot laboratories. All the SIMFUEL samples were acquired from the Chalk River Laboratories, Canada. The use of SIMFUELS presents the following advantages:

- The possibility of decoupling thermodynamics/chemistry from irradiation. Indeed, model materials allow to study the FP chemistry at an "early state", without the impact of irradiation.
- The access to Synchrotron radiation based characterization techniques, such as X-ray Absorption Spectroscopy (XAS), which allow to accurately determine FP oxidation state and their local environment, thus allowing to characterize the chemical phases.
- Ease of manipulation, since these samples do not need to be handled in hot laboratories.

The advantages cited above have allowed performing an extensive experimental study of FP behaviour in severe accident conditions. Particularly, the interactions proposed by the release mechanism which are highlighted in **Figure 58** were studied, both under reducing and oxidizing conditions. Three different samples sets have been studied: a first set consisting in two SIMFUEL samples of which one was submitted to an annealing test at high temperature and reducing conditions; a second set consisting in five SIMFUEL samples of which four were submitted to annealing tests up to different temperatures also in reducing conditions; and a third set consisting also in five SIMFUEL samples of which four were submitted to annealing tests up to similar temperatures than those of set II but under oxidizing conditions. Every annealing test performed in this axis were carried out at the DURANCE experimental loop, described in **Appendix V**. This chapter is then organized in three main parts, according to the results obtained in the different sample sets.

Firstly the samples sets and the characterization analyses performed are briefly described in **Section 3.2**. A thermodynamic analysis of the expected results after each annealing test is presented in **Section 3.3**. The obtained results on FP behaviour are then presented in **Section 3.4**, in the following order: **samples set I** first, then **samples set II** and finally **samples set III**. These results are discussed in **Section 3.5** and conclusions are made in **Section 3.6**.

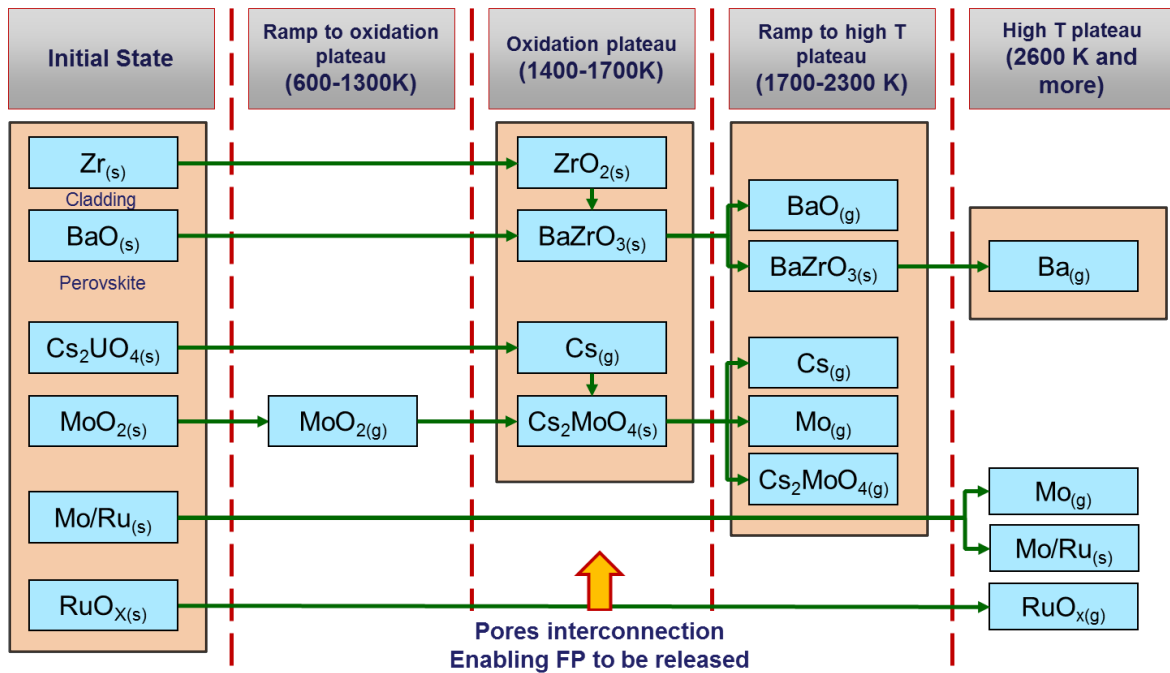


Figure 58: Hypothetical interactions and phases to be verified in this axis

3.1.1. X-ray Absorption Spectroscopy

Since the X-ray Absorption Spectroscopy (XAS) was the main characterization technique used in SIMFUEL samples, a brief description of its physical principle (Newville, 2004) and of the interpretation of the obtained results is presented.

3.1.1.1. XAS description

X-ray Absorption Spectroscopy (XAS) is an element specific characterization method which allows determining electronic properties (density of excited state and oxidation state) of an atom and its local environment (Z , distance, coordination number and disorder). XAS refers to the details of how X-rays are absorbed by an atom at energies near and above the core-level binding energies of that atom. Specifically, XAS is the modulation of an atom's X-ray absorption probability due to the chemical and physical state of the atom. It is based on the photoelectric effect: when X-rays of a particular energy strikes an atom, it may excite core electrons (with a well-defined binding energy) and as a function of its kinetic energy promote them to an unoccupied orbital (valence state) level and then eject them into the continuum where it will interact with electrons of the surrounding elements.

The representation of the absorption coefficient as a function of the incident energy is called the X-ray absorption spectrum. When the energy of the incident beam matches the binding energy of a core electron and a transition is achieved, there is a sharp rise in the absorption coefficient causing an absorption edge (E_0). The X-ray absorption spectrum is typically divided into two regimes: X-ray Absorption Near-Edge Spectroscopy (XANES, -30/+30 eV relative to the absorption edge) and Extended X-ray Absorption Fine-structure Spectroscopy (EXAFS). Though the two have the same physical origin, this distinction is convenient for the interpretation. XANES is strongly sensitive to

formal oxidation state and coordination chemistry (e.g., octahedral, tetrahedral coordination) of the absorbing atom, while the EXAFS is used to determine the distances, coordination number, and species of the neighbours of the absorbing atom.

By tuning the incident beam energy to the energy of a particular binding energy of a core atom (levels 1s, 2s, 2p, etc., each one with a defined energy), different absorption edges can be analysed. Therefore, when the energy of the incident beam matches that of the 1s electron, the K-edge is analysed, and when it matches the energy of levels 2s or 2p, the L edge is analysed. L_1 edge corresponds to level 2s, L_2 edge corresponds to level $2p_{1/2}$ and L_3 edge corresponds to level $2p_{3/2}$.

The metallic molybdenum absorption spectrum collected at the K-absorption edge is presented in **Figure 59** for illustration. Particularly for Mo^0 , the K absorption edge is located at 20000 eV. The XANES and EXAFS regions are also represented.

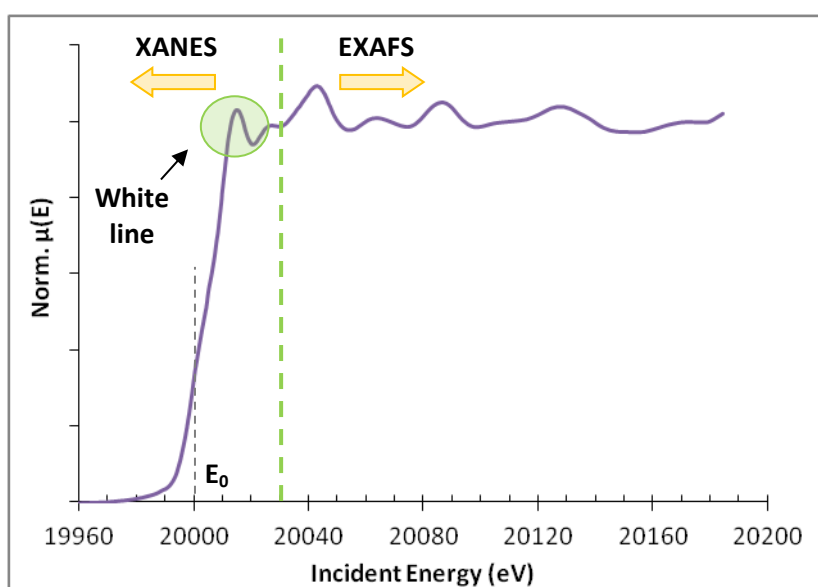


Figure 59: metallic Mo K-edge absorption spectrum

3.1.1.2. Interpretation of XAS results

Absorption edge, E_0

Mathematically, the position of the absorption edge (E_0) is calculated as the first zero crossing of the second derivate of the $\mu(E)$ function. The edge energy is affected by the density of empty state of the absorbing atom, which is influenced by the oxidation state: the sharp rise of $\mu(E)$ will occur at a higher energy the more positive the oxidation state of the atom is, since it is increasingly difficult to remove an electron from an atom that bears a higher positive charge. The absorption edge energy is then linked to the oxidation state of the absorbing atom: by analysing the energy shift of the absorption edge, the oxidation state of the absorbing atom can be determined.

White line

The rising absorption edge might lead to a very intense peak, which is referred to as the "white line". Formally, for Mo K edge the white line is created due to 1s transitions to 4 or 5d empty states. If all d

levels are occupied, then there is no transition and no white line is observed. Nevertheless, in this manuscript the first intense feature observed in XANES spectra is also called white line, despite if the absorbing atoms has its d levels occupied or not, in a way to compare XANES spectra and therefore the first coordination sphere of the analysed elements. Mathematically, the white line position is calculated as the zero crossing of the first derivate of the $\mu(E)$ function. The white line of Mo K-edge absorption spectrum is also indicated in **Figure 59**.

3.2. Samples and annealing tests description

As described above three different samples set have been studied. These sets, the annealing tests conditions and the employed characterization techniques are described below. Every annealing test to which were submitted samples from set I, II and III, were carried out in the DURANCE experimental loop. This loop description is available in **Appendix V**. Further information on how SIMFUEL samples were fabricated is available in **Appendices III**, and information regarding the characterization methods is available in **Appendices VI**.

3.2.1. Samples set I

This sample set consisted in two SIMFUEL samples doped with 11 FP: Ba, Ce, La, Mo, Nd, Pd, Rh, Ru, Sr, Zr and Y. Their estimated concentrations, presented in **Table 18**, match that of an UO_2 fuel irradiated up to 76 GWd.t^{-1} . The fabrication process of these samples, provided by the Chalk River Laboratories (Canada) is described in **Appendix III** according to (Lucuta, 1991a).

Samples composition (at.%)										
Ba	Ce	La	Mo	Sr	Y	Zr	Rh	Pd	Ru	Nd
0.26	0.61	0.20	0.51	0.13	0.06	0.60	0.03	0.42	0.64	0.91

Table 18: FP concentrations in sample set I

Annealing test conditions

The annealing sequence, representative of an intermediate state of nuclear severe accident, consisted on a temperature ramp ($0.2^\circ\text{C.min}^{-1}$) up to 1973 K, maintained for 1 h under reducing atmosphere (flowing Ar + 4% H_2). These conditions were chosen in order to verify the overall behaviour of the FP present in the sample. Therefore, not only the FP of interest were studied but all of them, aiming at evaluating the representativeness of SIMFUEL samples. Particularly, the main aspect to verify was the destruction of the $BaZrO_3$ phase, as assumed by the release mechanism at around 2100K.

Characterization

Since this samples set was intended to demonstrate the aptitude of SIMFUEL samples, XAS characterization was performed on most elements present in the sample. Then, K-edge absorption spectra were acquired for Mo, Ru, Y and Zr (from 17000 to 22000 eV), while the L-edge absorption spectra were acquired for U, Nd and Ce (from 5200 to 6300 eV for Nd and Ce, 17000 eV for U). Ba HERDF (High Energy Resolution Fluorescence Detection) XANES spectra were collected at the L3 absorption edge (5247 eV) using a CAS (Crystal Analyser Spectrometer) (LLorenz et al., 2014). A further description of the XAS acquisitions conditions is available in **Appendix VI**.

3.2.2. Samples sets II and III

Samples studied in sets II and III were SIMFUEL samples (same as set I) implanted with ^{133}Cs , at the *Institut de Physique Nucléaire de Lyon*. The implantation conditions are available in **Appendix III**. A SIMS implantation profile, also presented in **Appendix III**, indicates that most Cs is found 124 nm below the samples surface. The estimated concentration of FP in these SIMFUEL samples is presented in **Table 19**.

Samples composition (at. %)											
Ba	Ce	Cs	La	Mo	Sr	Y	Zr	Rh	Pd	Ru	Nd
0.26	0.61	0.35	0.20	0.51	0.13	0.06	0.60	0.03	0.42	0.64	0.91

Table 19: FP concentration in Samples Sets II and III

Annealing test conditions

Four different annealing tests were performed for each sample set, aiming at studying the intermediate stages of a severe accident proposed by the mechanism, which could not be studied using irradiated fuels. These annealing tests, resumed in **Figure 60**, consisted in different temperature ramps ($0.2^\circ\text{C}\cdot\text{min}^{-1}$) up to different temperatures (573, 1473, 1773 and 1973 K) under different atmospheres: Reducing (R) for samples set II and Oxidizing (O) for samples set 3.

Reducing atmosphere was applied by a constant flow of Ar + 4% H_2 , while oxidizing one was assured by the constant flow of high-purity Ar, containing traces of O_2 . Besides the annealed samples, implanted and un-annealed samples are also available in each set. Therefore, the samples studied in this chapter are:

- Samples **T₀-R** and **T₀-O**, implanted and un-annealed samples representative of the initial state for each set;
- Samples **R300** and **O300**, annealed up to 573 K for 3h under reducing and oxidizing conditions, respectively;
- Samples **R1200** and **O1200**, annealed up to 573 K for 2 h and then up to 1473 K for 30 min;
- Samples **R1500** and **O1500**, annealed at 573 K for 2h, then at 1473 K for 30 min and finally at 1773 K for 15 min;
- Samples **R1700** and **O1700**, which were annealed at 1973 K without intermediate temperature plateaus and maintained for 10 min.

The duration of the temperature plateaus at 1773 K and 1973 K (15 and 10 min, respectively) was chosen in order to limit Cs release (a volatile species) so that the intermediary compound could be studied. The oxygen potential (μ_{O_2}) was calculated using FactSage for each test, considering the composition of the inlet gas. These calculated values are presented in **Table 20**.

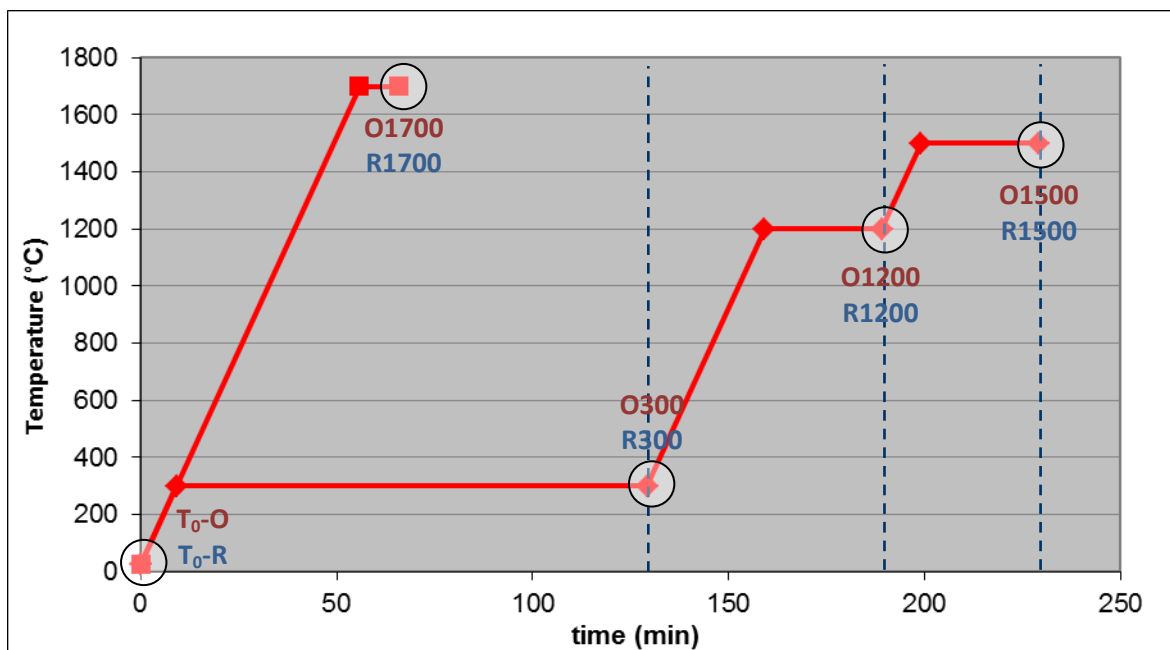


Figure 60: Annealing tests performed with samples sets II and III

	Calculated oxygen potentials (kJ.mol _{O₂} ⁻¹)			
Temperature	573 K	1473 K	1773 K	1973 K
Sample Set II	-490	-484	-480	-478
Sample Set III	-350	-210	-216	-230

Table 20: Calculated oxygen potentials for each annealing test

Samples characterization

Samples from sets II and III were also characterized by SEM-EDS at the CEA Cadarache and by XAS at the MARS beamline, SOLEIL Synchrotron. XANES spectra were collected at the Mo K absorption edge and at the Cs L₃ absorption edge. Particularly for samples T₀-R and R300 of set II, XANES spectra were also collected using a micro-focused beam (5 x 6 μm²) at the Mo K absorption edge.

3.3. Thermodynamic Analysis

As described above, thermodynamic estimations have been performed using the FactSage software, described in **Appendix IV**. A so-called predominance diagram was calculated considering a system composed of Mo, Ba, Cs, Zr, U and O, in a ratio representative of the concentration of the samples presented in **Table 19**. This diagram, which predicts the most stable chemical species in equilibrium as a function of the oxygen potential and temperature, is presented in **Figure 61**. Seven regions of interest were identified, separated by lines in the diagram. Each line indicates that a chemical reaction takes places. The red one, taken as reference, indicates the Mo/MoO₂ equilibrium. The most stable chemical species for each region are presented in **Table 21**. Each sample is indicated in the predominance diagram, blue corresponds to reducing tests and orange to oxidizing ones. Due to experimental problems sample O1500 could not be exploited, so this sample will not be considered further in the study. It must also be kept in mind that the SGPS database used for these calculations only considers pure compounds and not solid solutions.

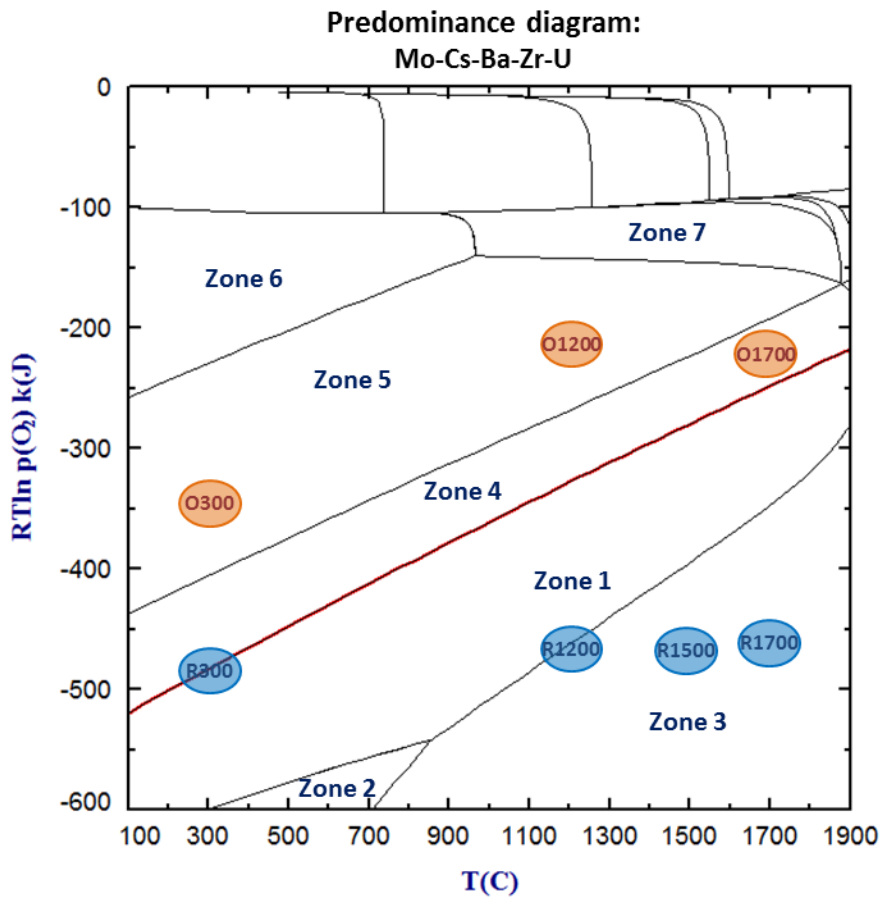


Figure 61: Predominance diagram for the Mo-Cs-Ba-Zr-U system

Zone	Most stable chemical species
1	ZrO_2 , Mo^0 , Cs_2MoO_4 , $BaZrO_3$, UO_2
2	ZrO_2 , Mo^0 , Cs_2UO_4 , $BaZrO_3$, UO_2
3	ZrO_2 , Mo^0 , $BaZrO_3$, UO_2 + gas(Cs_g)
4	ZrO_2 , MoO_2 , Cs_2MoO_4 , $BaZrO_3$, UO_2
5	ZrO_2 , MoO_2 , Cs_2MoO_4 , $BaMoO_4$, UO_2
6	ZrO_2 , Cs_2MoO_4 , $BaMoO_4$, MoO_3 , UO_2
7	ZrO_2 , Cs_2MoO_4 , $BaMoO_4$, UO_2 + gas(MoO_x)

Table 21: chemical species in equilibrium for each zone

The following assumptions can be made from the predominance diagram:

- Sample **R300** would be located between zones 1 and 4 and the chemical species in equilibrium would be ZrO_2 , Mo^0 , MoO_2 , Cs_2MoO_4 , $BaZrO_3$ and UO_2
- Sample **R1200** would be located between zones 1 and 3, and the chemical species in equilibrium would be ZrO_2 , Mo^0 , Cs_2MoO_4 , $BaZrO_3$, UO_2 and Cs^0 present in the gas phase, which means that a partial decomposition of Cs_2MoO_4 would take place.
- Samples **R1500** and **R1700** are both located in zone 3, meaning that the chemical species would be ZrO_2 , Mo^0 , $BaZrO_3$ and UO_2 , with Cs released from the samples as Cs^0 .

- Samples **O300** and **O1200** would be located in zone 5, and the chemical species would be ZrO_2 , MoO_2 , Cs_2MoO_4 , $BaMoO_4$ and UO_2 .
- Finally, sample **O1700** would be located in zone 4 so the chemical species would be ZrO_2 , $BaZrO_3$, MoO_2 , Cs_2MoO_4 and UO_2 .

3.4. FP Behaviour

The experimental observations on the FP of interest for this study (Ba, Cs, Mo and Ru) are presented here. Firstly the results from sample set I (the only ones which were not implanted with Cs) are presented, then those from sample set II and finally those from sample set III. A brief analysis of the samples overall evolution after tests is also included for each set.

3.4.1. Sample set I

3.4.1.1. Fuel micro-structure

SEM-SE images of samples set I before (T_0 sample) and after test (AT sample) are presented in **Figure 62**. Two main types of precipitates were observed in both samples. On one hand, precipitates containing mainly Ba and Zr and, on the other, precipitates containing mainly Mo and Ru. After the test, white precipitates on the surface and the grain boundaries etching were observed. The latter is quite common in UO_2 ceramics submitted to high temperatures (Mott and Williams, 1953). Quantitative analyses were performed on the UO_2 matrix of these two samples, results of which are presented in **Table 22**. According to them, the main FP dissolved in the matrix would be Zr, Ba, La, Ce and Nd. The concentration of these FP was not significantly modified after the annealing test at 1973 K under reducing atmosphere.

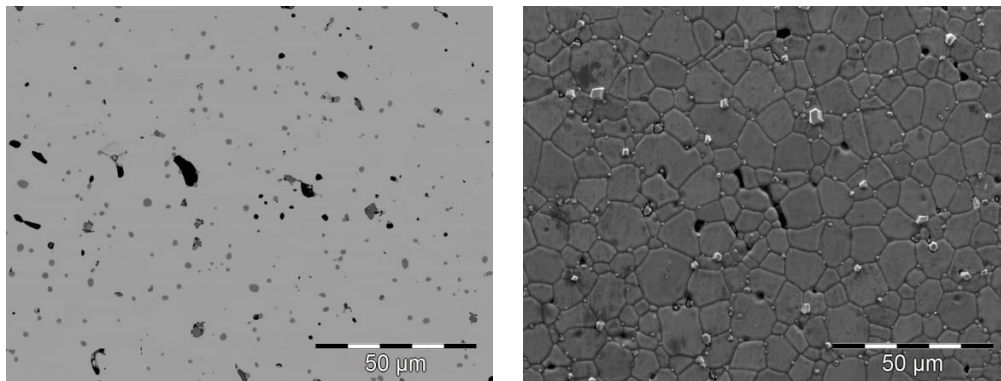


Figure 62: SEM images of the samples before (T_0 , left) and after (AT, right) annealing test

Element	Sample	
	T_0	AT
O	68.9 ± 0.5	69.0 ± 0.9
Zr	0.4 ± 0.1	0.3 ± 0.2
Ba	0.2 ± 0.1	0.1 ± 0.1
La	0.3 ± 0.1	0.2 ± 0.2
Ce	0.3 ± 0.0	0.3 ± 0.1
Nd	0.3 ± 0.2	0.4 ± 0.1
U	29.2 ± 0.2	29.4 ± 0.9

Table 22: Main FP dissolved in set I samples UO_2 matrix

3.4.1.2. Barium and zirconium

Barium and zirconium X-ray maps are presented in **Figure 63**. Though not presented here, the same distribution was observed for Sr, Y and Ce. As observed in these images, these FP are always found together. Quantitative analyses performed on these precipitates are presented in **Table 23**. These results indicate that oxygen and uranium are also present, which indicates that these five FP (Ba, Zr, Ce, Sr and Y) are in oxidized form.

After the test, an increased number of precipitates was observed but also an important reduction in their equivalent circle diameter (ECD) and the area contribution of these precipitates (the percentage of surface occupied by precipitates of the total surface of the analysed field), as presented in **Table 24**. The Ba/Zr ratio decreased by 13% after the test.

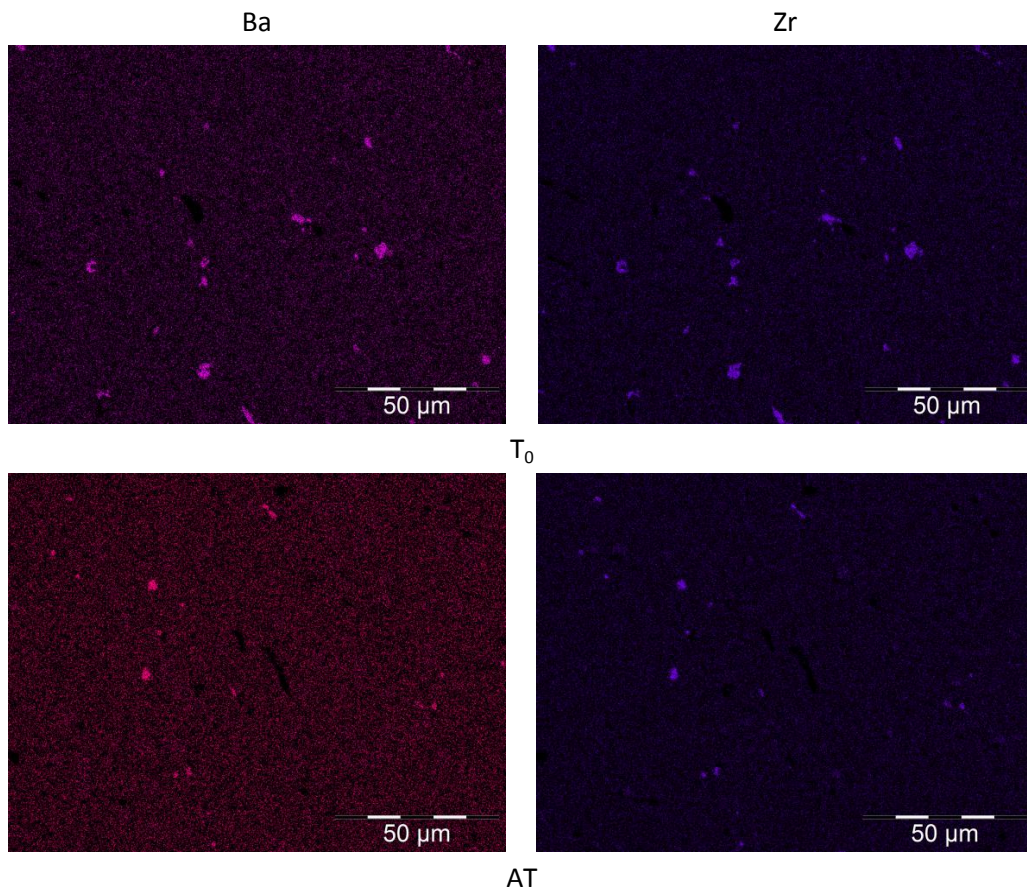


Figure 63: Ba (left) and Zr (right) X-rays maps collected in samples T₀ (top) and AT (bottom) from set I

Element	Concentration (at.%)	
	T0	AT
O	66.1 ± 0.7	70.3 ± 7.4
Sr	2.3 ± 0.3	2.5 ± 1.5
Y	0.2 ± 0.2	0.1 ± 0.1
Zr	12.3 ± 1.3	12.8 ± 3.6
Ba	12.3 ± 1.0	11.1 ± 3.2
Ce	0.2 ± 0.1	0.0 ± 0.1
U	6.7 ± 2.3	3.3 ± 0.9

Table 23: Oxide precipitates quantitative analysis

Sample	Area contribution (%)	ECD (μm)	Ba/Zr ratio
T ₀	0.64	2.45	1.0 ± 0.1
AT	0.29	0.83	0.87 ± 0.2

Table 24: Characteristics of oxide precipitates containing Ba and Zr in samples T₀ and AT

Barium HERFD-XANES and zirconium XANES spectra ($\mu(E)$) collected in both samples are presented in **Figure 64**, along with the BaO, metallic Zr, ZrO₂ and Sm₂Zr₂O₇ references spectra. Zr spectra have been shifted vertically for better illustration. The absorption edge (E_0) and white line positions of each spectrum are reported in **Table 25**.

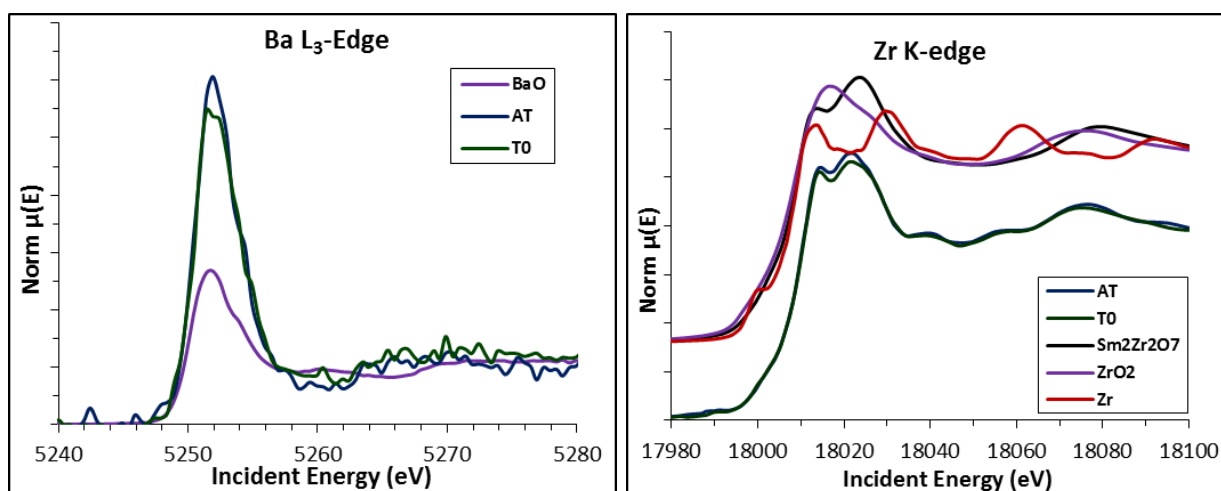


Figure 64: Ba L₃-edge (left) HERDF-XANES and Zr K-edge (right) XANES spectra measured on SIMFUEL samples and references

Zr K-edge			Ba L3-edge		
Sample	E ₀ (eV)	White line (eV)	Sample	E ₀ (eV)	White line (eV)
Zr	17998.0	18013.8	BaO	5250.3	5251.8
ZrO ₂ (tetragonal)	18013.5	18021.7	-	-	-
Sm ₂ Zr ₂ O ₇	18013.3	18018.1			
T ₀	18014.2	18018.3	T ₀	5250.4	5252.0
AT	18013.5	18018.2	AT	5250.5	5251.1

Table 25: E₀ and white line positions of samples and references spectra collected at the Ba L₃-edge and Zr K-edge. Incertitude: ± 0.5 for Ba spectra, ± 0.8 for Zr ones

As observed, both Ba and Zr spectra are not strongly modified after the annealing test. The E₀ position is similar for both samples within the experimental errors, indicating that the Ba and Zr oxidation state do not change before and after annealing. Particularly for Zr, spectra indicate a local environment close to that of the pyrochlore Sm₂Zr₂O₇ (Martin et al., 2009; Zhang et al., 2007). This local environment is characteristic of the perovskite structure (ABO₃) as well. Indeed, both structures are face-centred cubic, where Zr atoms are surrounded by O in an octahedron configuration. The (Z-O) interatomic distance for BaZrO₃ is 2.09 Å (Giannici et al., 2011), while for Sm₂Zr₂O₇ it is approximately 2.06 Å (Xiao et al., 2010). These results would support the existence of the BaZrO₃ chemical form.

3.4.1.3. Molybdenum and ruthenium

Mo and Ru X-ray maps are presented in **Figure 65**. The composition of these precipitates is presented in **Table 26**. Two main differences were observed after the annealing test. The first one is the apparition of a second phase, richer in molybdenum. Indeed, according to the quantitative analyses, the average Mo/Ru ratio of precipitates in sample T₀ was equal to 0.76. After the test, most precipitates of size superior to 1.5 μm exhibited a Mo/Ru ratio of 6.0 ± 1.4 (precipitates designed as Mo(Ru)) while the smaller ones a Mo/Ru ratio equal to 1.0 ± 0.0. Nevertheless, most of these latter precipitates exhibited a Ru concentration slightly higher than that of Mo, and so they are designed as Ru(Mo) precipitates. The characteristics of Mo-Ru precipitates before and after test are presented in **Table 27**. After the annealing test, it was observed that the area contribution of Mo-Ru precipitates increased around 45% and their ECD decreased about 50%.

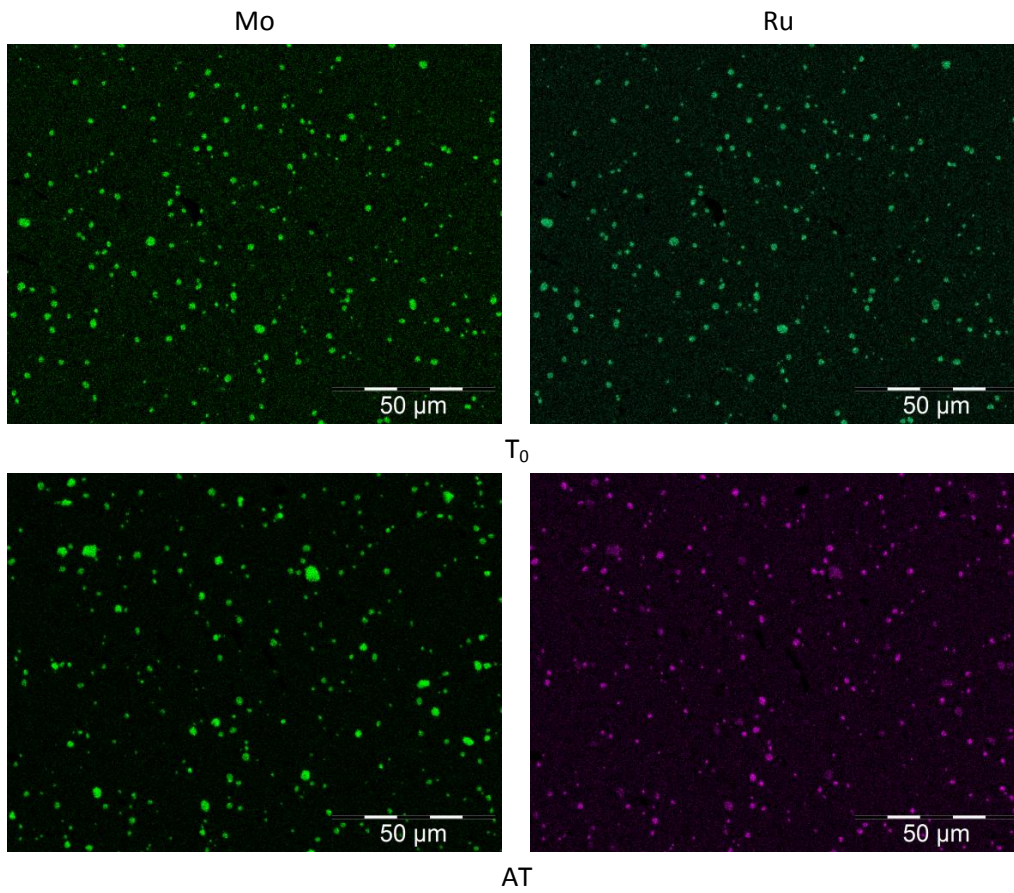


Figure 65: Mo (left) and Ru (right) X-ray Maps, samples T_0 and AT

Element	Concentration (at. %)		
	T_0	AT	
		Mo(Ru)	Ru(Mo)
Mo	32.4 ± 1.0	85.0 ± 2.9	49.4 ± 1.3
Ru	42.6 ± 0.8	14.8 ± 2.9	49.3 ± 1.1
Rh	0.4 ± 0.5	0.0 ± 0.1	0.6 ± 0.5
Pd	24.5 ± 1.0	0.1 ± 0.2	0.8 ± 0.4

Table 26: Metallic precipitates chemical composition

Sample	Area contribution (%)	ECD (μm)	Mo/Ru ratio
T_0	1.9	2.4	0.8 ± 0.0
AT	2.7	1.3	Mo(Ru)= 6.0 ± 1.4 Ru(Mo)= 1.0 ± 0.0

Table 27: Characteristics of metallic precipitates, before and after test

Molybdenum and ruthenium normalized XANES spectra ($\mu(E)$) are presented in **Figure 66**, along with metallic Mo, MoO_2 , MoO_3 , Ru and RuO_2 reference spectra. Spectra have been shifted vertically for better illustration. The absorption edge (E_0) and the white line positions of each spectrum are reported in **Table 28**.

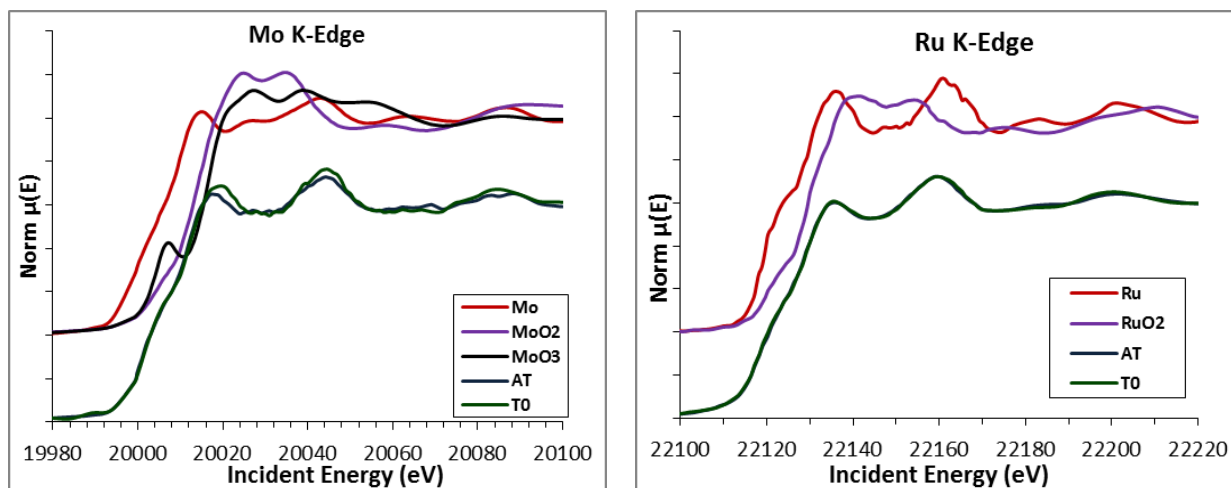


Figure 66: Mo (left) and Ru (right) K-edge XANES spectra collected on set I samples and references.

Mo K-edge			Ru K-edge		
Sample	E_0 (eV)	White line (eV)	Sample	E_0 (eV)	White line (eV)
Mo	20000.0	20016.1	Ru	22117.0	22134.9
MoO ₂	20004.3	20027.4	RuO ₂	22124.3	22140.1
MoO ₃	20004.3	20026.7	-	-	-
T ₀ sample	20001.4	20019.4	T ₀ sample	22117.4	22135.9
AT sample	20000.7	20017.8	AT sample	22117.2	22135.9

Table 28: Absorption edge (E_0) and white line position of samples and references spectra collected at the Mo and Ru K-edges. Experimental incertitude: ± 0.8

As observed, the Mo K-edge spectra of SIMFUEL samples are modified by the annealing sequence, contrary to the Ru K-edge ones. Indeed, as reported in **Table 28**, the white line position of Mo XANES is shifted by 1.6 ± 0.8 eV to lower energy after annealing.

The second main difference observed after the test is that palladium disappeared almost completely from these precipitates after annealing. Indeed, Pd mean concentration in the T₀ sample is 24.5 at.%, while after the test it was reduced to 0.1 and 0.8 at.% in the Mo(Ru) the Ru(Mo) and precipitates, respectively.

3.4.1.4. Summary of observations on sample set I

Two main observations have been made in this sample set, where an un-implanted sample was submitted to an annealing test under reducing atmosphere (Ar + 4% H₂) up to 1973 K for 1 h:

- The presence of two main types of precipitates: oxide ones containing mainly Ba and Zr, and metallic ones containing mainly Mo and Ru. The oxide character of the Ba-Zr precipitates and the metallic one of the Mo-Ru precipitates was confirmed by XAS analyses.
- The BaZrO₃ chemical form was confirmed by XAS analyses. It was observed that the Ba/Zr ratio decreased after an annealing test at 1973 K, for 1 h and under reducing atmosphere.
- The separation of the metallic precipitates after being submitted to 1973 K for 1h under reducing atmosphere, into two intermetallics with different composition. These different

precipitates are denoted as Mo(Ru), more concentrated in Mo, and Ru(Mo), slightly more concentrated in Ru.

3.4.2. Sample set II

Five SIMFUEL samples have been analysed in this set: sample T₀-R which was not submitted to any annealing test, and samples R300, R1200, R1500 and R1700, which were annealed at 573, 1473, 1773 and 1973 K, respectively, under reducing atmosphere. All these samples were implanted with Cs before tests.

3.4.2.1. Fuel micro-structure evolution

SEM-BSE images of samples R300, R1200, R1500 and R1700 are presented in **Figure 67**. SEM results for sample T₀-R are similar to those of Sample R300 and so they are not presented here. Little evolution is observed from sample R300 to R1200 and from this one to sample R1500. Nevertheless, sample R1700 exhibits precipitates which are similar in shape and size to those observed in sample AT from set I (also annealed at 1973 K).

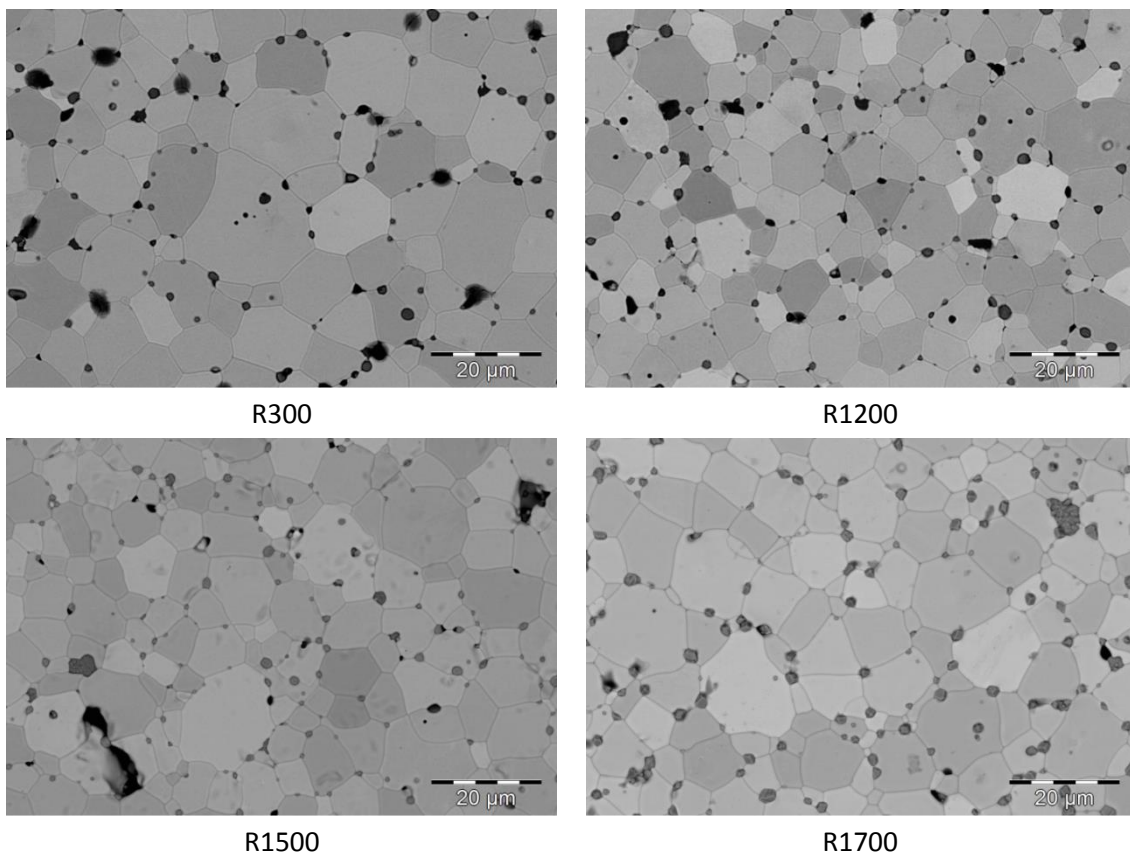


Figure 67: SEM-BSE images of samples R300, R1200, R1500 and R1700, from set II

Quantitative analyses were performed on the samples matrix, which results are presented in **Table 29** and **Figure 68**. Only results corresponding to the main FP dissolved in the samples matrix (Sr, Zr, Ce, Cs and Nd) are presented. As observed, FP concentration in the samples matrix is not significantly modified after tests, with the exception of Cs. Indeed, the concentration of this FP decreases after annealing above 1473 K.

Element	Sample				
	T0-R	R300	R1200	R1500	R1700
O	66.8 ± 1.1	67.4 ± 0.6	67.2 ± 0.7	66.6 ± 0.6	66.9 ± 0.6
Sr	0.3 ± 0.1	0.4 ± 0.1	0.3 ± 0.1	0.3 ± 0.2	0.4 ± 0.1
Zr	0.3 ± 0.2	0.4 ± 0.1	0.4 ± 0.1	0.4 ± 0.1	0.4 ± 0.1
Cs	0.3 ± 0.2	0.5 ± 0.1	0.4 ± 0.2	0.3 ± 0.2	0.2 ± 0.1
Ce	0.4 ± 0.2	0.4 ± 0.2	0.4 ± 0.2	0.5 ± 0.2	0.4 ± 0.2
Nd	0.5 ± 0.2	0.5 ± 0.2	0.5 ± 0.2	0.4 ± 0.2	0.5 ± 0.2
U	30.5 ± 0.9	29.7 ± 0.6	29.9 ± 0.6	30.8 ± 0.6	30.4 ± 0.7

Table 29: FP concentration in SET II samples fuel UO₂ matrix

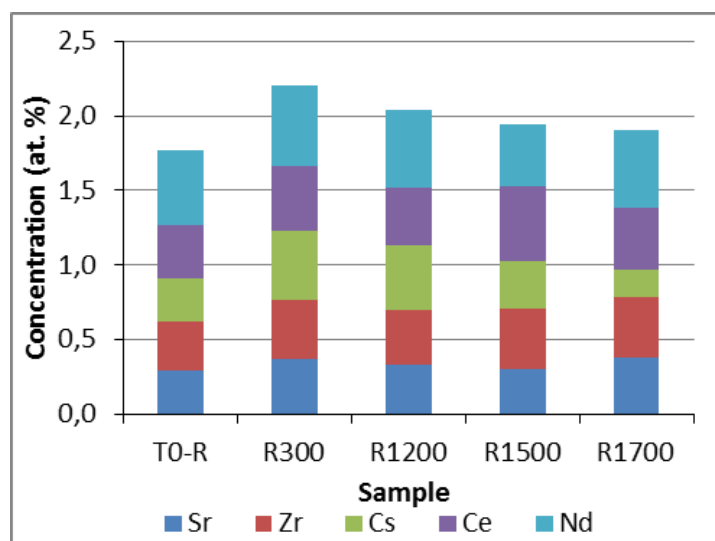


Figure 68: Sr, Zr, Cs, Ce and Nd concentration evolution in set II samples matrix

3.4.2.2. Barium and zirconium

Barium and zirconium X-ray maps obtained for samples R300, R1200, R1500 and R1700 (annealed at 573, 1473, 1773 and 1973 K, respectively) are presented in **Figure 69**. Results obtained for sample T₀-R are similar to those of sample R300 and so they are not presented here. As observed, Ba and Zr are always associated even at high temperatures. The same distribution was observed for Ce, Sr and Y, in a similar way to set I samples.

Quantitative analyses were performed on these precipitates and the obtained results are presented in **Table 30** and **Figure 70**. The overall evolution observed for these precipitates is resumed in **Table 31**. It was observed that the initial ECD, area contribution and Ba/Zr ratio in these precipitates decreased after tests. Indeed, the initial ECD of these precipitates decreased from 2.2 to 1.5 μm in sample R1200, 1.3 μm in sample R1500 and 1.7 μm in sample R1700. The total surface occupied by these precipitates also decreased from an initial 1.7% to 0.6% after annealing at 1973 K, as well as the Ba/Zr ratio, presented in **Figure 71**, which decreased from 1.8 in R300 sample to 1.5 in sample R1200, 1.0 in R1500 and finally 1.1 in sample R1700.

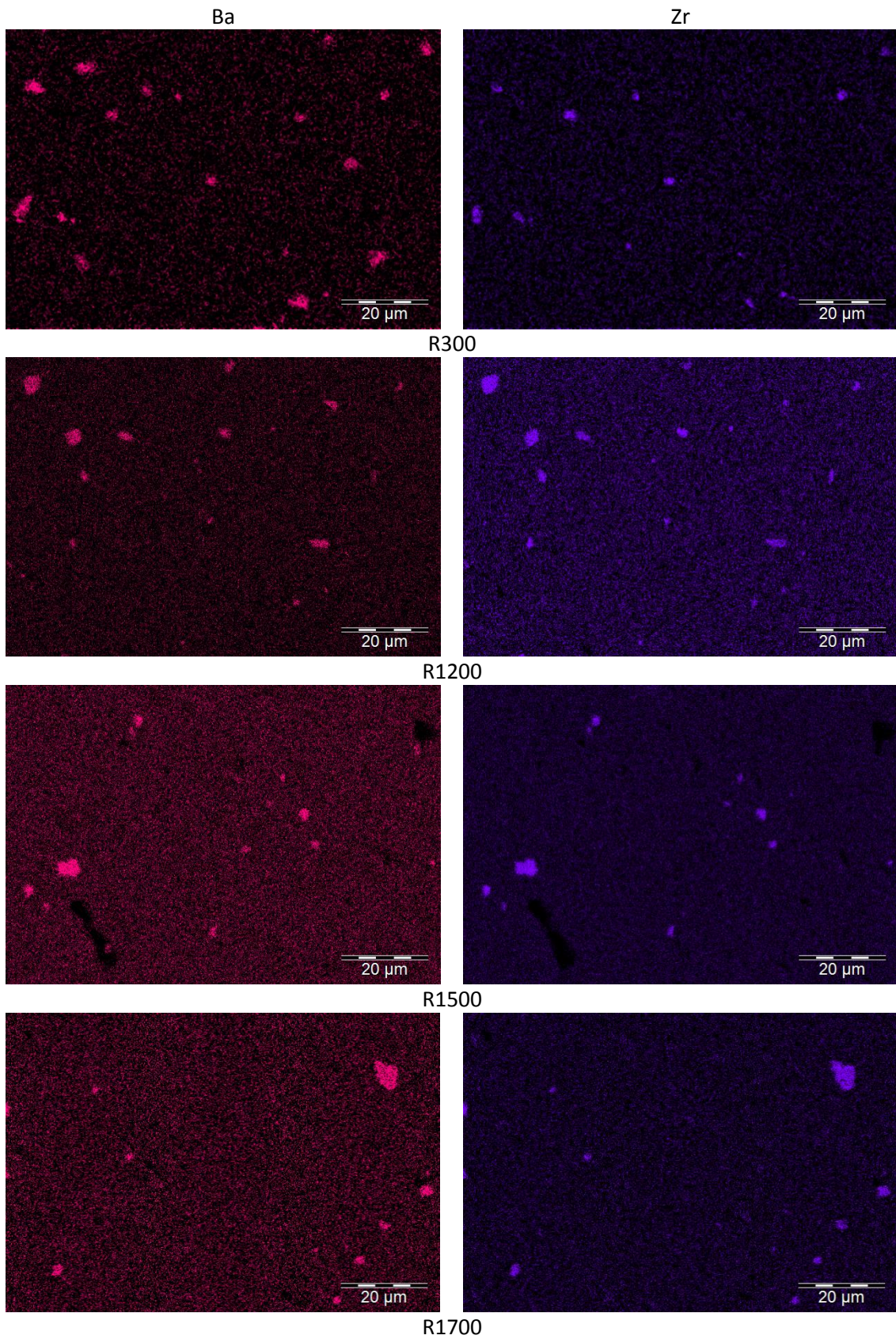


Figure 69: Barium (left) and zirconium (right) X-ray maps of Samples Set II.

Element	Sample				
	T0-R	R300	R1200	R1500	R1700
O	66.4 ± 8.2	60.7 ± 7.6	64.4 ± 5.3	56.0 ± 2.3	56.4 ± 2.9
Sr	2.9 ± 2.1	3.3 ± 0.7	1.9 ± 1.3	4.1 ± 0.3	3.3 ± 0.4
Zr	10.0 ± 6.6	12.9 ± 5.8	12.6 ± 3.6	18.2 ± 1.1	17.1 ± 1.3
Ba	16.0 ± 3.7	18.3 ± 1.9	16.9 ± 1.3	17.8 ± 1.4	18.4 ± 1.5
Ce	0.1 ± 0.1	0.0 ± 0.0	0.1 ± 0.1	0.1 ± 0.1	0.1 ± 0.1
U	4.7 ± 2.4	4.8 ± 2.1	4.2 ± 1.1	3.7 ± 0.8	4.6 ± 1.2

Table 30: FP concentration in oxide precipitates from set II samples

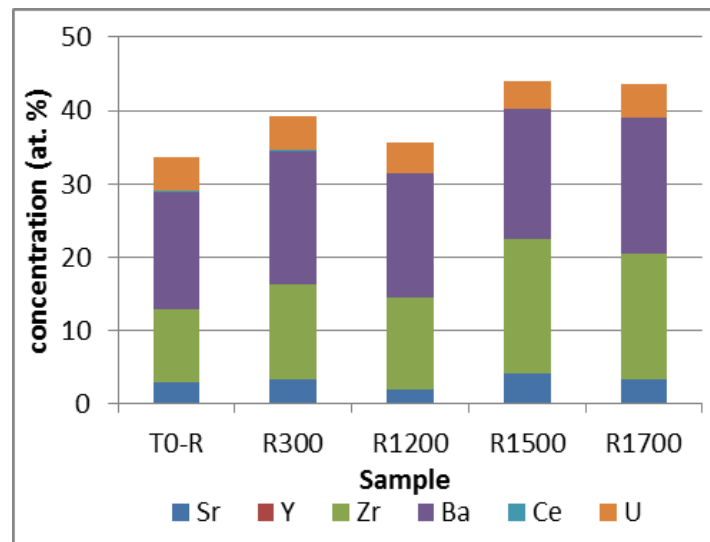


Figure 70: Sr, Zr, Ba and U concentration evolution in oxide precipitates of set II samples

Sample	Area contribution (%)	ECD (μm)	Ba/Zr ratio
R300	1.7	2.2	1.8 ± 1.1
R1200	0.6	1.5	1.5 ± 0.5
R1500	0.7	1.3	1.0 ± 0.1
R1700	0.6	1.7	1.1 ± 0.1

Table 31: Oxide precipitates characteristics in samples from set II

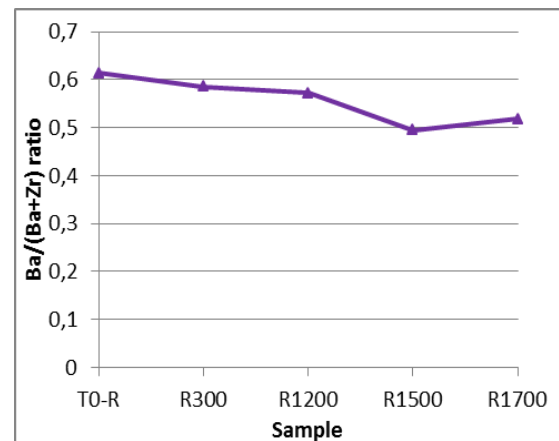


Figure 71: Ba/(Zr+Ba) ratio evolution in oxide precipitates of set II samples

3.4.2.3. Molybdenum and ruthenium

Molybdenum and ruthenium distribution in the samples was also determined by SEM-EDS analyses. Results, presented in **Figure 72**, indicate the presence of many precipitates all over the samples, composed of Mo, Ru, Rh and Pd. The concentration of these FP in each sample is presented in **Table 32**. In a similar way to samples from set I, it was observed the separation of the metallic phase into two, Mo(Ru) and Ru(Mo), which present a different Mo/Ru ratio. This phase separation took place between 1473 and 1773 K, since only one type of precipitates was observed in sample R1200. Results also indicate that the Mo/Ru ratio of the Mo(Ru) phase increased around 50% from 1773 K to 1973 K, along with the precipitates size and area contribution. Indeed, as presented in **Table 33**, the Mo/Ru ratio in phase Mo(Ru) was 4.1 in the precipitates of sample R1500, and 6.6 in those of sample R1700, and the precipitates ECD and area contributions increased from 0.9 μm and 1.3% in sample R1500 to 1.6 μm and 4.7% in sample R1700, respectively.

Element	Sample						
	T ₀ -R	R300	R1200	R1500		R1700	
				Ru(Mo)	Mo(Ru)	Ru(Mo)	Mo(Ru)
Mo	44.6 ± 1.0	44.1 ± 0.8	43.0 ± 0.9	49.2 ± 2.7	78.3 ± 6.0	49.6 ± 2.1	82.8 ± 5.8
Ru	53.4 ± 1.0	54.1 ± 1.1	54.9 ± 0.8	48.9 ± 2.7	20.5 ± 5.9	48.0 ± 2.4	16.3 ± 5.6
Rh	0.0 ± 0.0	0.1 ± 0.4	0.1 ± 0.3	0.1 ± 0.3	0.0 ± 0.0	0.0 ± 0.0	0.0 ± 0.0
Pd	2.0 ± 0.1	1.7 ± 0.3	2.0 ± 0.4	1.8 ± 0.3	1.2 ± 0.3	2.4 ± 0.5	0.9 ± 0.3

Table 32: FP concentration in metallic precipitates of samples from set II

Sample	Area contribution (%)	ECD (μm)	Mo/Ru ratio
R300	1.7	1.2	0.8 ± 0.0
R1200	1.9	0.8	0.8 ± 0.1
R1500	1.3	0.9	Mo(Ru) = 4.1 ± 1.2 Ru(Mo) = 1.0 ± 0.1
R1700	4.7	1.6	Mo(Ru) = 6.6 ± 5.8 Ru(Mo) = 1.0 ± 0.1

Table 33: Metallic precipitates characteristics, sample Set II

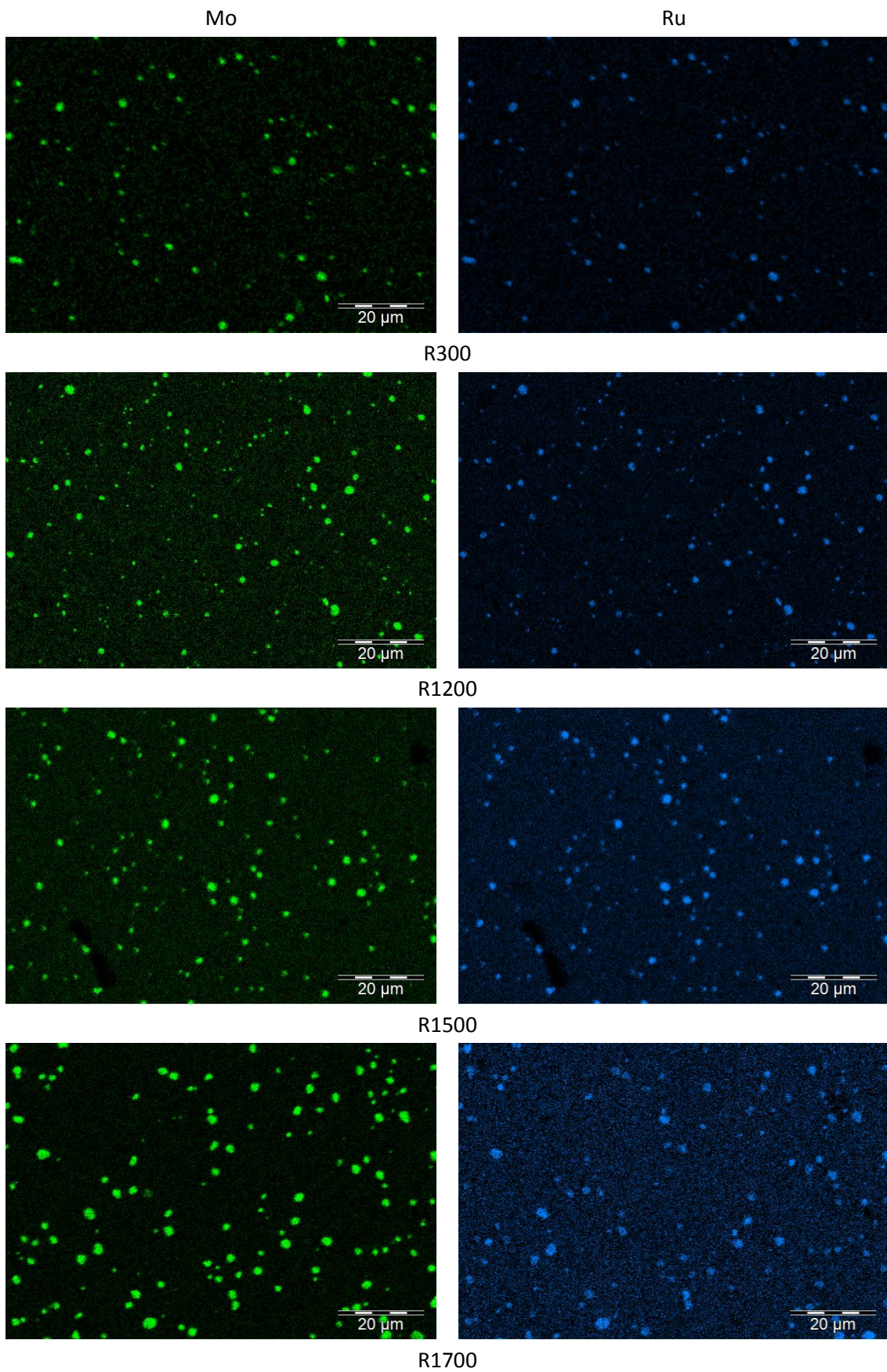


Figure 72: Mo (left) and Ru (right) X-ray maps, Sample set II

Every quantitative results obtained on the metallic precipitates in samples from set II are presented in the binary Mo-Ru system presented in **Figure 73**, extracted from (Gürler, 1999; Kleykamp, 1989a, 1988). Two main phases are observed in this diagram, below 1915°C. These phases are β (bcc structure more concentrated in molybdenum) and ϵ (hcp structure, slightly more concentrated in Ru). There is also a σ phase (tetragonal structure) between 1915 and 1143°C. As observed, metallic precipitates in samples T₀-R, R300 and R1200 present a composition similar to the ϵ phase. Regarding samples R1500 and R1700, the two phases observed correspond to the β and ϵ phases. These results also indicate that one of the precipitates analysed in sample R1500 presents a composition which correspond to the σ phase, and that many precipitates found in sample R1700 present a Mo concentration which is higher than the β solvus line (limit of solubility of Ru in Mo in the absence of other elements).

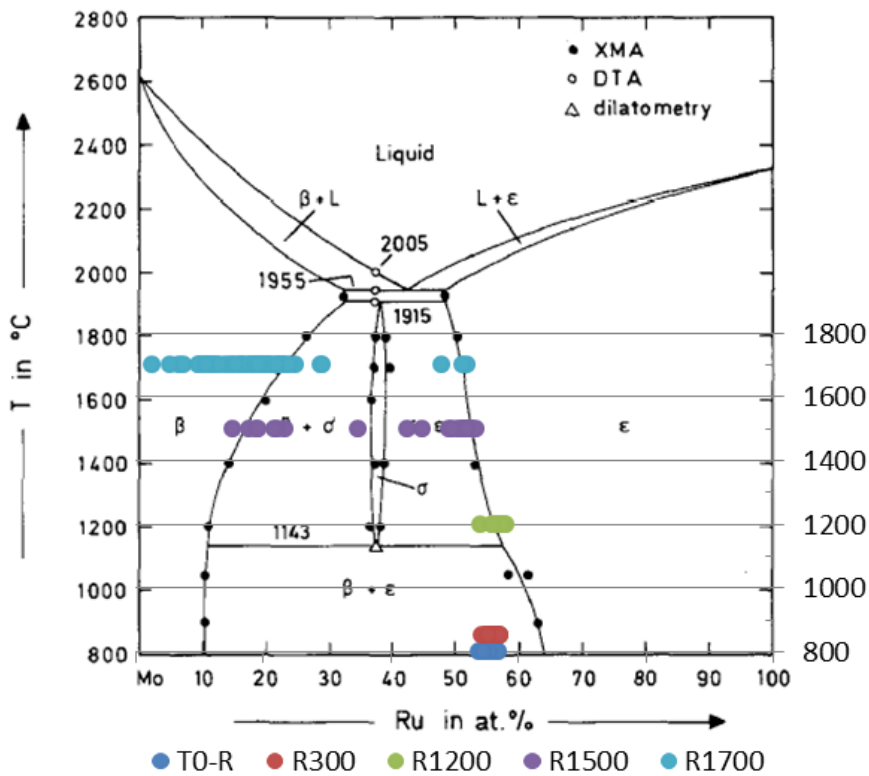


Figure 73: Quantitative analyses performed on samples set II metallic precipitates, represented in the Mo - Ru binary phase diagram extracted from (Kleykamp, 1989a).

Mo characterization by X-ray Absorption Spectroscopy

XAS analyses have been performed at the Mo K absorption edge (20000 eV) using both macro (300 x 300 μm^2) and micro beams (5 x 6 μm^2) on this samples set. Macro beam analyses were performed on the five samples of this set, while micro beam ones have only been performed on sample T₀-R. Results obtained using the micro beam are presented first, followed by those using the macro beam.

Micro-beam XAS

Micro XAS analyses have been performed on three different Mo precipitates in sample T₀-R, in order to accurately characterize Mo chemical form and compare the results to the average Mo spectrum (collected on sample T₀-R using a macro beam). The XANES spectra collected on these precipitates

(P1, P2 and P3) in sample T₀-R are presented in **Figure 74**, along with the T₀-R average Mo spectrum and the metallic Mo reference spectrum. The E₀ and white line positions of each spectrum are indicated in **Table 34**. As observed, the XANES spectra of the three precipitates are quite similar to that of the matrix and to the metallic Mo reference as well. There are, though, some important differences between the precipitates and sample matrix spectra compared to metallic Mo spectrum. These differences are:

- The shoulder in the precipitates and sample matrix spectra around the absorption edge position (indicated by the green circle on the metallic Mo reference spectrum);
- An energy shift of the white line and main features position towards higher energy (better illustrated in **Table 34**).
- The absence of the first feature after the white line in the precipitates and sample matrix spectra, compared to the metallic Mo reference one (indicated by the orange circle on the metallic Mo spectrum).

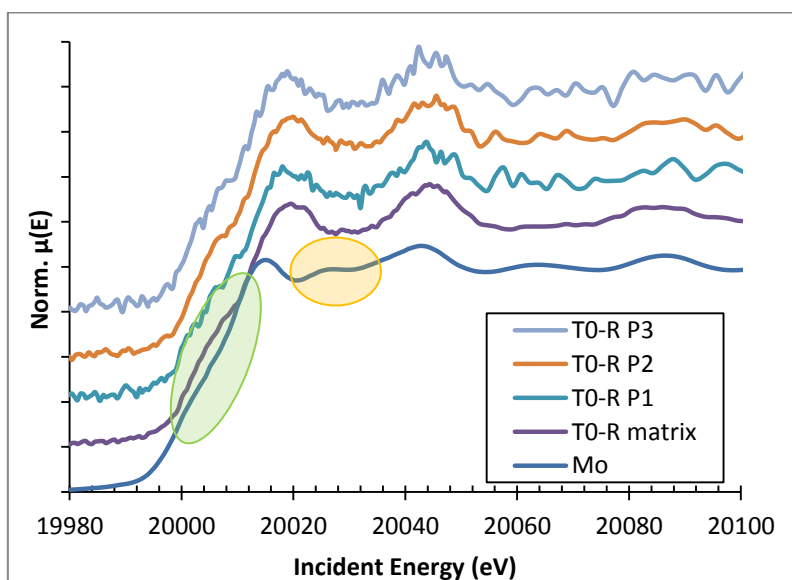


Figure 74: XANES spectra collected on sample T₀-R matrix and precipitates

Mo K-edge		
Target	E ₀ (eV)	White line (eV)
Mo	20000.0	20015.0
T ₀ -R	19999.8	20019.5
T ₀ -R P1	20000.2	20017.9
T ₀ -R P2	20000.0	20019.8
T ₀ -R P3	20001.2	20019.0

Table 34: E₀ and white line positions of sample T₀-R matrix and precipitates XANES spectra. Incertitude: ± 0.8 eV

A linear combination fit has been performed on the precipitates XANES spectra in order to estimate Mo chemical form, using the following references: metallic Mo, MoO₂, MoO₃ and Cs₂MoO₄. The obtained results are presented in **Table 35**. The R-factor presented in this table is a measure of the quality of the fit: the lower the R-factor value is, the better the spectrum was reproduced by the

reference ones. The mathematical expression of this factor and its meaning is presented in **Appendix VI**.

Precipitate	Reference weight				R factor
	Mo	MoO ₂	MoO ₃	Cs ₂ MoO ₄	
T ₀ -R P1	0.72	0.00	0.28	0.00	0.00494
T ₀ -R P2	0.69	0.00	0.31	0.00	0.00561
T ₀ -R P3	0.76	0.00	0.24	0.00	0.00547

Table 35: Linear combination fit results for sample T₀-R precipitates

As observed, the three precipitates present a very similar composition. These results indicate that Mo is mainly metallic, that important quantities of MoO₃ are present and that there is no MoO₂. A brief discussion of these results is required and some assumptions must be made before going further in the study of Mo chemical state in samples from set II, since these estimations are wrong from a thermodynamic point of view. Indeed, according to the Mo - O phase diagram presented in **Figure 75**, extracted from (Zhang et al., 2014), there cannot be Mo⁰ in equilibrium with MoO₃. If chemical equilibrium was not attained during the fabrication of the samples, then the three Mo oxidation states (0, 4+ and 6+) could have been present. Considering also that Mo is in metallic state in these precipitates (as indicated by the E₀ position of Mo spectra in these precipitates), it is assumed that the presence of MoO₃ is estimated by the software in an attempt to reproduce the differences observed between the precipitates spectra and the metallic Mo reference spectrum. These differences are attributed to the presence of Ru which is, along with Mo, the main component of these precipitates. Indeed, as described above, most precipitates observed would correspond to the ε phase of the Mo-Ru phase diagram, which presents an hcp structure. Pure metallic molybdenum presents a bcc structure. Then, the presence of Ru would modify the local environment of Mo, and this effect is observed in the precipitates Mo spectra.

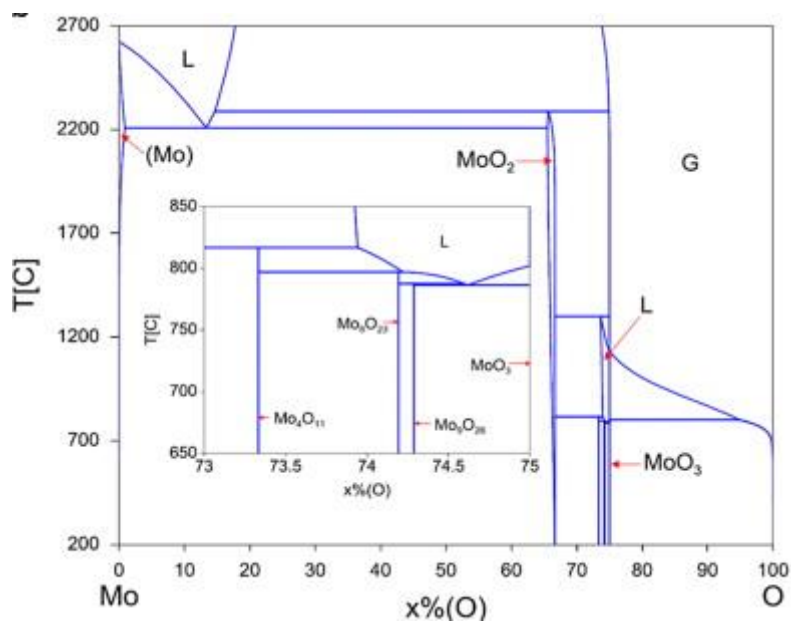


Figure 75: Mo - O phase diagram. According to this diagram, MoO₃ cannot exist in equilibrium with metallic Mo (Zhang et al., 2014)

The precipitates XANES spectra have been used, along with the metallic Mo, MoO₂, MoO₃ and Cs₂MoO₄ references spectra, to estimate Mo chemical state in sample T₀-R (which spectrum was collected using a macro-beam). The linear combination fit results are presented in **Table 36**. As observed, the overall composition of the sample would be the same as the precipitates: 70% of metallic Mo and 30% of MoO₃. Besides, the precipitates spectra reproduce quite well the sample one. The linear combination fit results using the precipitates spectra as reference would indicate that metallic Mo and MoO₃ are also present. As explained above, these estimations could be due to the presence of Mo-Ru precipitates with a composition corresponding to the ϵ , β or even the σ phases. Then, most Mo present in the sample would be metallic, in association to Ru, Pd and Rh in metallic precipitates. Nevertheless, it is observed that MoO₂ would also be present when using T₀-R P1 spectrum to fit the sample spectrum. MoO₂ would then be present dissolved in the sample matrix.

Sample	Reference weight							R factor
	Mo	MoO ₂	MoO ₃	Cs ₂ MoO ₄	T ₀ -R P1	T ₀ -R P2	T ₀ -R P3	
T ₀ -R	0.70	0.00	0.30	0.00	-	-	-	0.00462
	0.05	0.09	0.04	0.00	0.82	-	-	0.00078
	0.01	0.00	0.02	0.00	-	0.97	-	0.00035
	0.09	0.00	0.10	0.00	-	-	0.81	0.00095

Table 36: Linear combination fit results for sample T₀-R using precipitates XANES spectra. Incertitude: 2%

^aThe reference spectrum was not considered in the linear combination fit.

Macro-beam XAS

The XANES spectra collected on the five samples of this set, using a macro beam (300 x 300 μm^2) are presented in **Figure 76**, along with three reference compounds: Cs₂MoO₄, MoO₂ and metallic Mo. The absorption edge and white line positions are presented in **Table 37**. These results show that Mo oxidation state remained invariant after annealing tests. Indeed, the E₀ of every sample spectra is similar to that of metallic Mo, within experimental errors. Nevertheless, the white line positions of samples T₀-R, R300, R1200 and R1500 present an energy shift to higher energy, of about 4.6 eV, compared to that of the metallic Mo reference. The white line position of sample R1700 spectrum is shifted to lower energy and it is also observed the apparition of some features that are also present in the metallic Mo reference. The latter is better observed in the superposed XANES spectra of samples R1500, R1700 and the Mo metallic reference, presented in **Figure 77**, where these features are highlighted by green circles.

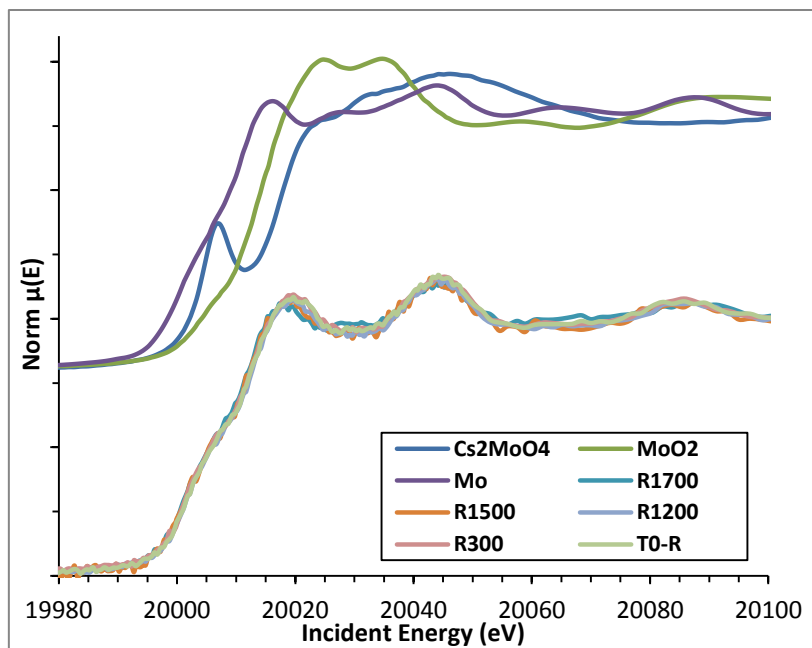


Figure 76: Mo XANES spectra, Sample Set II

Mo K-edge		
Sample	E_0 (eV)	White line (eV)
T ₀ -R	19999.8	20019.5
R300	20000.6	20019.5
R1200	20000.5	20019.5
R1500	20001.2	20019.6
R1700	20000.6	20017.8
Mo ⁰	20000.0	20015.0
MoO ₂	20005.0	20025.0
MoO ₃	20004.6	20026.8
Cs ₂ MoO ₄	20003.8	20045.5

Table 37: E_0 and white line positions of Mo spectra collected on set II samples and references. Incertitude: ± 0.8 eV

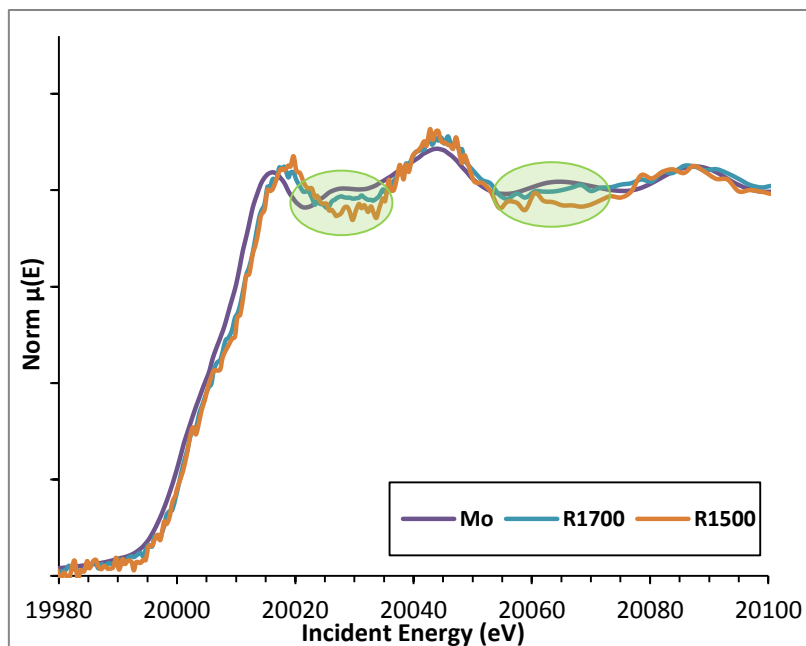


Figure 77: Samples R1500, R1700 and Mo reference superposed spectra, highlighting the modification of Mo local environment at 1973 K.

A linear combination fit has been performed in order to determine Mo chemical state. The samples spectra have been used along with the available reference to perform the linear combination fits. The obtained results are presented in **Table 38**. Particularly for sample T₀-R, two different calculations have been performed: one using metallic Mo, MoO₂, MoO₃, Cs₂MoO₄ and the T₀ sample (unannealed, unimplanted SIMFUEL sample from set I), the other one using the same reference spectra but without considering MoO₃. As observed, the R factors obtained for these two calculations are similar. This would imply that Cs₂MoO₄ would be created as a consequence of Cs implantation. Sample R300 spectrum is very well reproduced by sample T₀-R one, and sample R1200 spectrum is also well reproduced by sample R300 spectrum. This would mean that the annealing tests under flowing Ar + 4% H₂ did not produce an important impact on the Mo chemical state. Samples R1500 and R1700 results indicate that there is an important contribution of the metallic contribution to the samples spectra. This is consistent with the quantitative analyses results. Indeed, many precipitates with a concentration corresponding to the β phase, which presents the same structure as metallic Mo (bcc) were observed in these two samples. It is also observed that sample AT spectrum (unimplanted SIMFUEL sample from set I, submitted to 1973 K in reducing atmosphere) reproduces perfectly sample R1700 spectrum, meaning that there is no difference between these two samples.

Sample	Reference weight										R factor
	Mo	MoO ₂	MoO ₃	Cs ₂ MoO ₄	T ₀	AT	T ₀ -R	R300	R1200	R1500	
T ₀ -R	0.00	0.00	0.09	0.00	0.91	- ^a	-	-	-	-	0.00023
	0.00	0.04	-	0.05	0.91	-	-	-	-	-	0.00025
R300	0.03	0.00	0.00	0.00	-	-	0.97	-	-	-	0.00015
R1200	0.00	0.00	0.00	0.01	-	-	-	0.99	-	-	0.00015
R1500	0.11	0.00	0.00	0.00	-	-	-	-	0.89	-	0.00037
R1700	0.19	0.02	0.01	0.01	-	-	-	-	-	0.76	0.00033
	0.00	0.00	0.00	0.00	-	1.00	-	-	-	-	0.00032

Table 38: Mo spectra linear combination fit results of samples from set II. Incertitude: 2%

^aThe reference spectrum was not considered in the linear combination fit.

3.4.2.4. Caesium

Since Cs was implanted in the samples by the Ion implantation method, SIMS analyses were performed in order to determine its distribution, but only on sample unannealed T₀-R. Cs ion maps were acquired at the surface of the sample and at the bottom of the crater created after the acquisition of implantation profiles. These images, presented in **Figure 78**, show that Cs precipitates are indeed created after implantation. These precipitates presented an ECD of 3.15 μm and a area contribution of 1.2%. No particular association of Cs to other FP was detected using this characterization technique.

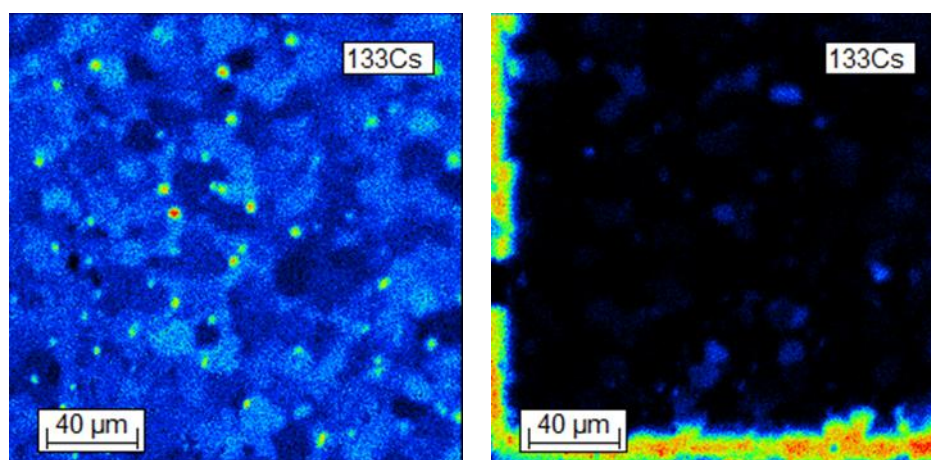


Figure 78: ¹³³Cs ion images at the surface and bottom of the crater, T₀-R sample

Cs X-ray maps were also collected on samples from set II. These X-ray maps, presented in **Figure 79**, do not show the presence of any Cs precipitate.

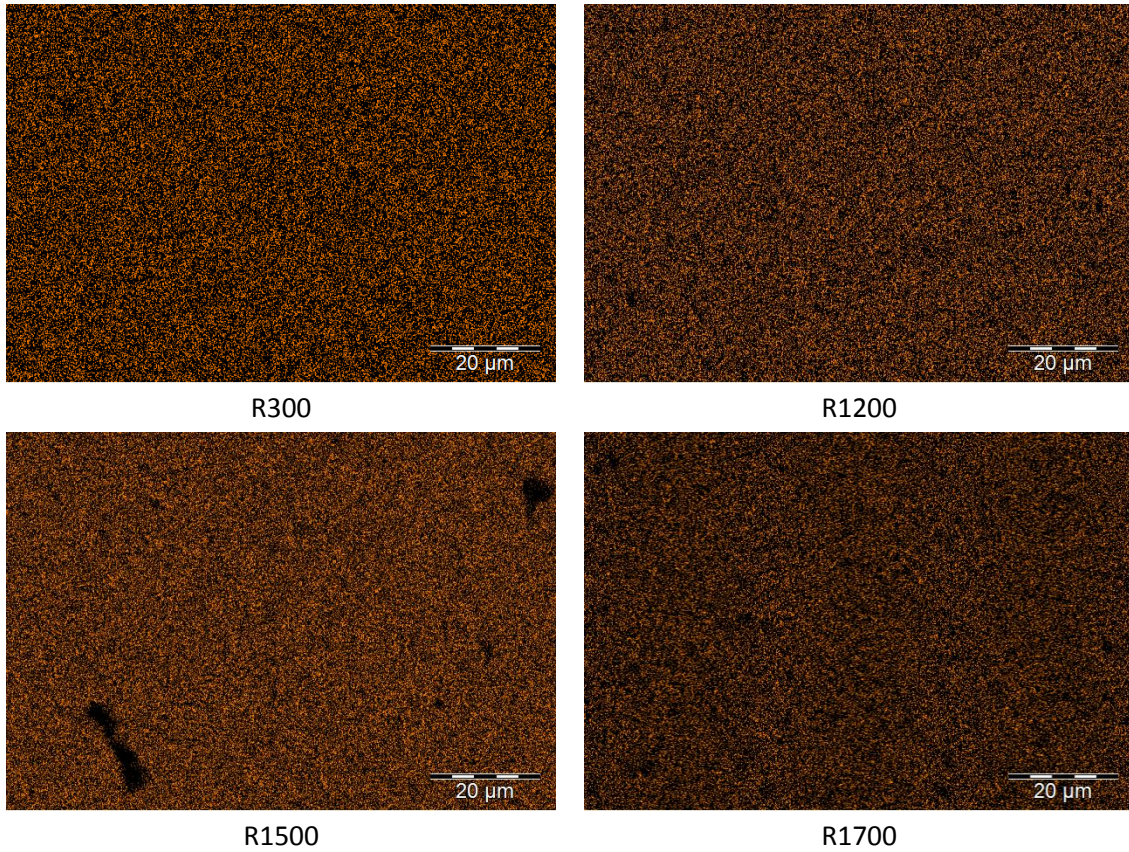


Figure 79: SEM-BSE images and corresponding Cs X-ray maps, Samples Set II

Caesium XANES were acquired at the L_3 absorption edge (5012 eV) for samples R300, R1200 and R1500 and two reference compounds, Cs_2MoO_4 and Cs_2UO_4 . No Cs signal was detected in sample R1700, meaning that this FP was no longer present after the annealing test at 1973 K. Indeed, the linear fit combination results performed on the Mo XANES spectrum of sample R1700 indicate that there is virtually no difference between this sample and the unimplanted AT sample from set I. The collected spectra are presented in **Figure 80** and the corresponding E_0 and white lines energy positions are presented in **Table 39**. Spectra have been shifted vertically for a better illustration.

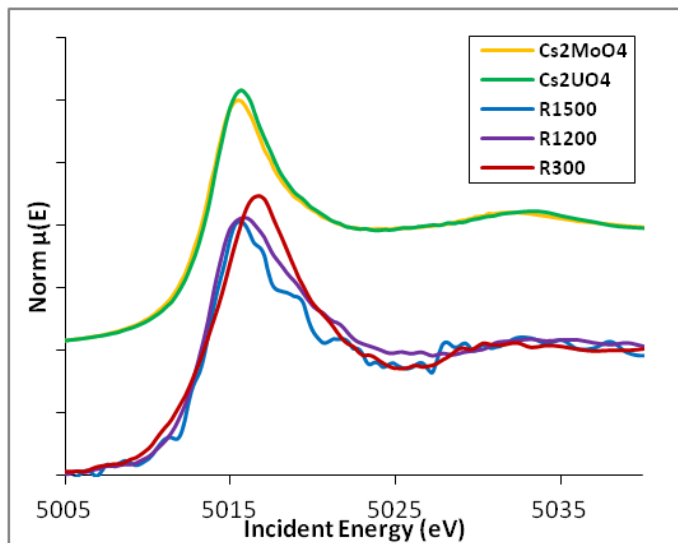


Figure 80: Cs XANES spectra, Sample Set II

Cs L3-edge		
Sample	E_0 (eV)	White line (eV)
Cs_2UO_4	5013.7	5015.6
Cs_2MoO_4	5014.0	5015.5
R300	5014.7	5016.8
R1200	5013.8	5015.9
R1500	5013.8	5015.5

Table 39: Cs absorption edge position and White line position, Sample Set II. Incertitude: ± 0.5 eV

Although a Cs^0 reference was not available at the time the experience took place, according to (Elam et al., 2002), the metallic Cs E_0 position is 5012 eV. XANES results show that the E_0 and white line positions of sample R300 Cs spectrum are shifted to higher energies compared to the references. After the annealing tests, these positions are shifted to lower energies and are similar to that of Cs_2UO_4 and Cs_2MoO_4 , within experimental errors, which would confirm the oxidation state as Cs^{+1} . It is also observed that Cs XANES white line intensity in sample R300 is higher than that of the references. The latter is better observed in the superposed XANES spectra of samples R300 and Cs_2MoO_4 , presented in **Figure 81**. The characteristics of sample R300 Cs spectrum (E_0 and white line positions and white line intensity) indicate that Cs is in a different chemical state (or electronic configuration) than the available references, and so a linear fit combination was of no use. Samples R1200 and R1500 linear combination fits results using the reference spectra are presented in **Table 40**. The best fit results are highlighted in the table.

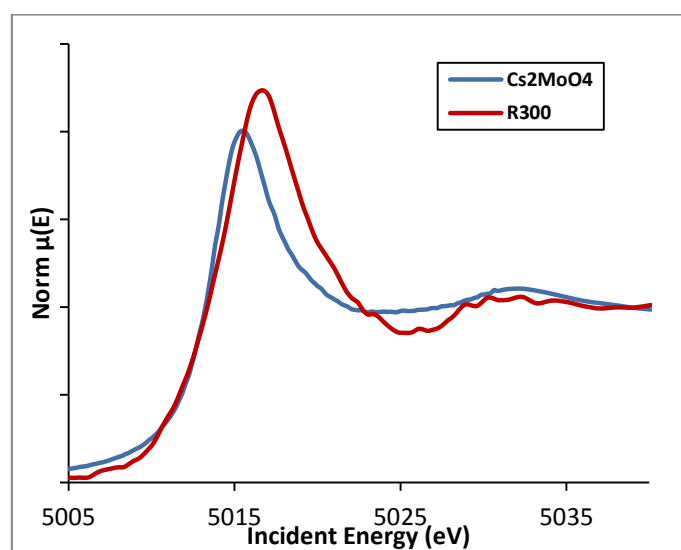


Figure 81: sample R300 and Cs_2MoO_4 superposed L3 XANES spectra, samples Set II

Sample	Reference weight				R factor
	Cs_2UO_4	Cs_2MoO_4	R300	R1200	
R1200	0.92	0.08	- ^a	-	0.0060
	0.00	0.56	0.44	-	0.0024
R1500	0.20	0.80	-	-	0.0075
	0.00	0.58	-	0.42	0.0062

Table 40: Linear combination fit of Cs spectra, sample Set II. Incertitude: 2%

^aThe reference spectrum was not considered in the linear combination fit.

According to these results the main species in sample R1200 would be Cs_2UO_4 , while Cs_2MoO_4 would be the main one in sample R1500. When including samples R300 and R1200 for fitting samples R1200 and R1500 respectively, these results indicate that Cs_2MoO_4 is the main species in both samples. Nevertheless, both references XANES spectra are very similar, which indicates that Cs local environment is almost the same in both compounds.

3.4.2.5. *Summary of observations on samples set II*

The main observations performed on samples from set II are related to Mo and Cs chemistry:

-Two different molybdenum metallic phases have been observed in samples R1500 and R1700, which differ in their Mo/Ru ratio. The Mo/Ru ratio of the precipitates more concentrated in Mo was further modified at 1973 K. Indeed, this ratio increased 50% from sample R1500 to sample R1700.

-Mo XANES spectra collected using a micro beam on three precipitates of sample T₀-R were very similar to the Mo spectra collected in the matrix of these samples, using a macro beam. It was observed that Ru, also present in the metallic precipitates, modifies the Mo local structure.

-Mo XANES collected using a macro beam on samples T₀-0, R300 and R1200 were similar and no annealing test effect was observed. The spectra collected on samples R1500 and R1700 would indicate a more important contribution of metallic Mo, which was attributed to the apparition of precipitates with a composition corresponding to the β phase of the Mo-Ru phase diagram.

-Cs precipitates have been observed in sample T₀-R by SIMS analyses, though they were not observed by SEM-EDS analyses. No particular associations of Cs to other FP could be determined. XAS analyses performed at the Cs L₃ absorption edge on samples R1200 and R1500 indicate that this FP is indeed in oxidized state (Cs⁺¹) though the exact chemical form could not be identified. XAS analyses performed on sample R300 Cs indicate the existence of a chemical form other than Cs₂MoO₄ or Cs₂UO₄. No Cs signal was detected in sample R1700.

3.4.3. Sample set III

3.4.3.1. Fuel micro-structure evolution

SEM analyses were performed on samples O300, O1200 and O1700. Results obtained on sample T₀-O were similar to those of sample O300, and so they are not presented here. A SEM-BSE image of sample O300 is presented in **Figure 82**. As observed in this image, the annealing test at 573 K under pure argon did not produce a significant impact in the sample. Indeed, results for sample O300 are similar to those of Sample R300, annealed under reducing atmosphere.

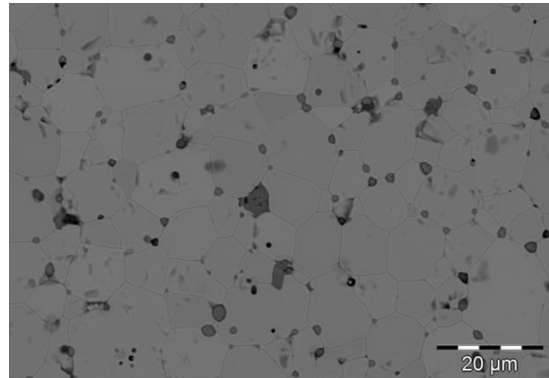


Figure 82: SEM-BSE image of sample O300, sample set III

A SEM-BSE and a SEM-SE image of sample O1200 are presented in **Figure 83**. Two different precipitates, which present a very different morphology (highlighted by the red and green squares on the image), are observed on the surface of this sample. This different morphology is better appreciated in the SEM-BSE and SE images presented in **Figure 84**. As it will be demonstrated latter, these are oxide precipitates which contain also Ba and Sr. Metallic inclusions were also observed, which present many micrometric pores. SEM-BSE and SE images of these precipitates are presented in **Figure 85**.

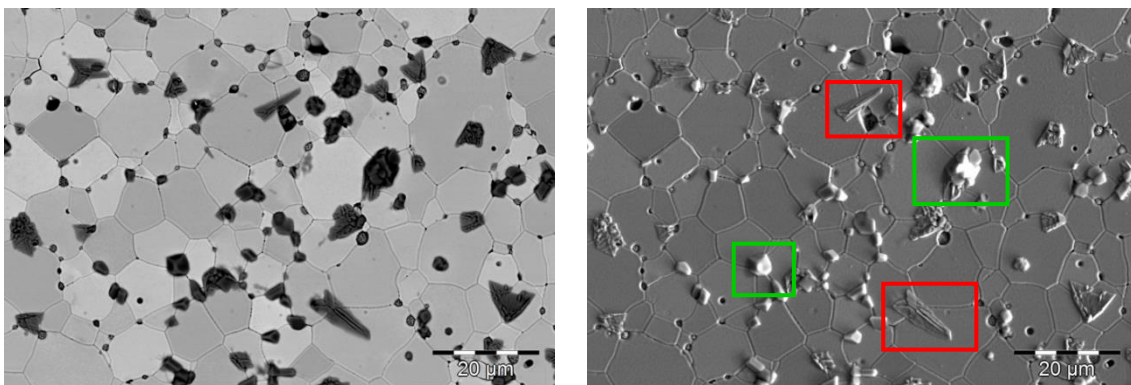


Figure 83: SEM-BSE (left) and SEM-SE (right) image of sample O1200, sample set III

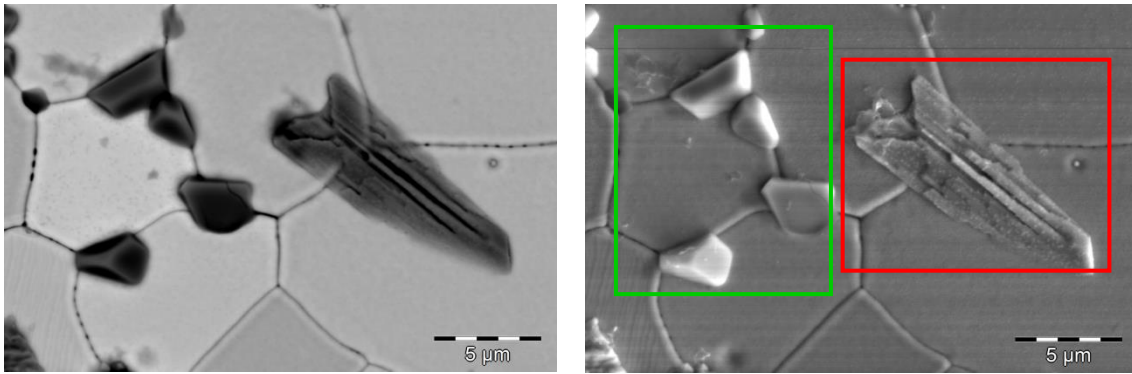


Figure 84: SEM-BSE (left) and SEM-SE (right) image of oxide precipitates present in sample O1200, sample set III

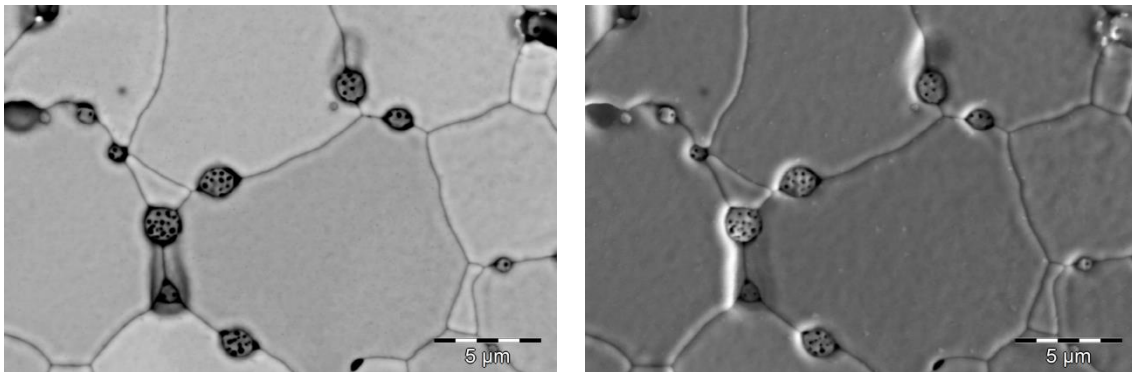


Figure 85: SEM-BSE (left) and SEM-SE (right) image of metallic inclusions present in sample O1200, sample set III

SEM analyses performed on sample O1700, presented in **Figure 86**, showed the presence of two types of precipitates. Metallic precipitates on one hand and large dendritic precipitates on the other. As it will be demonstrated further below, the latter precipitates have a similar composition to the amorphous precipitates observed in sample O1200.

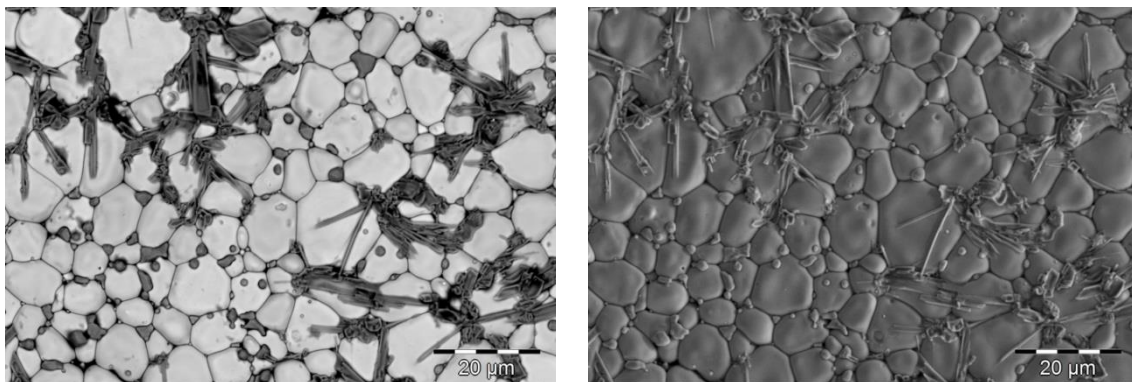


Figure 86: SEM-BSE (left) and SEM-SE (right) images of sample O1700, Samples Set III

Quantitative analyses were performed in the matrix of samples T₀-O, O300, O1200 and O1700. The main FP found present in these samples matrices are Mo, Ce, Sr, Cs, Nd and Zr, and the evolution of their concentration is presented in **Table 41** and **Figure 87**. After the annealing tests it was observed an increased concentration of Zr and Mo in the samples matrix, particularly in sample R1700. On the contrary, Ce, Cs and Sr concentration decreased.

Element	Sample			
	T ₀ -O	O300	O1200	O1700
O	67.3 ± 1.6	70.1 ± 0.9	67.5 ± 0.5	67.5 ± 2.1
Sr	0.3 ± 0.1	0.3 ± 0.1	0.3 ± 0.1	0.1 ± 0.1
Zr	0.4 ± 0.1	0.3 ± 0.1	0.4 ± 0.2	0.8 ± 0.2
Mo	0.2 ± 0.1	0.4 ± 0.1	0.3 ± 0.2	0.7 ± 0.3
Cs	0.4 ± 0.2	0.1 ± 0.1	0.3 ± 0.1	0.2 ± 0.1
Ce	0.4 ± 0.1	0.1 ± 0.1	0.1 ± 0.1	0.1 ± 0.1
Nd	0.4 ± 0.2	0.5 ± 0.1	0.5 ± 0.1	0.4 ± 0.2
U	30.1 ± 1.4	27.6 ± 0.7	29.8 ± 0.3	29.5 ± 2.0

Table 41: Main FP concentration in set III samples matrix

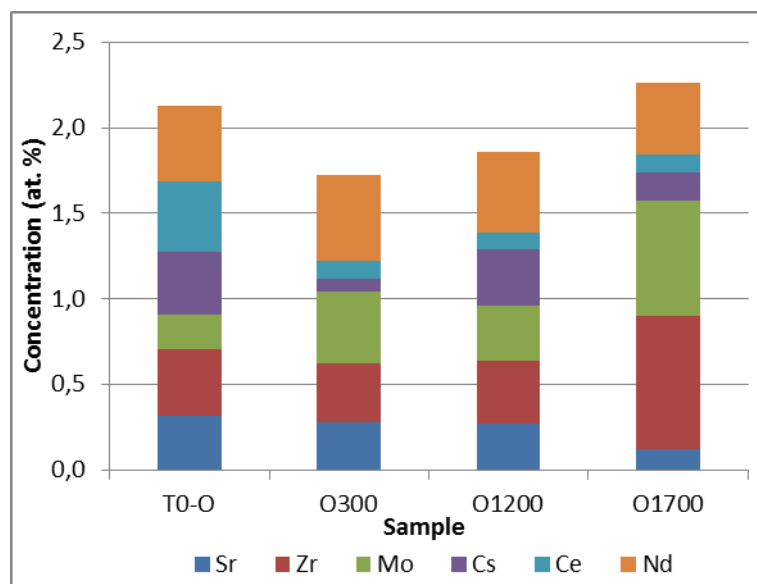


Figure 87: Evolution of FP concentration in set III samples matrix

3.4.3.2. Caesium

Cs X-ray maps collected on samples T₀-O, O300, O1200 and O1700 are presented in **Figure 88**. No Cs precipitates or any particular association to other FP are observed in these X-ray maps. Nevertheless, it has already been determined by SIMS analyses that Cs precipitates do exist at least in sample T₀-R, which implantation conditions are identical to those of sample T₀-O.

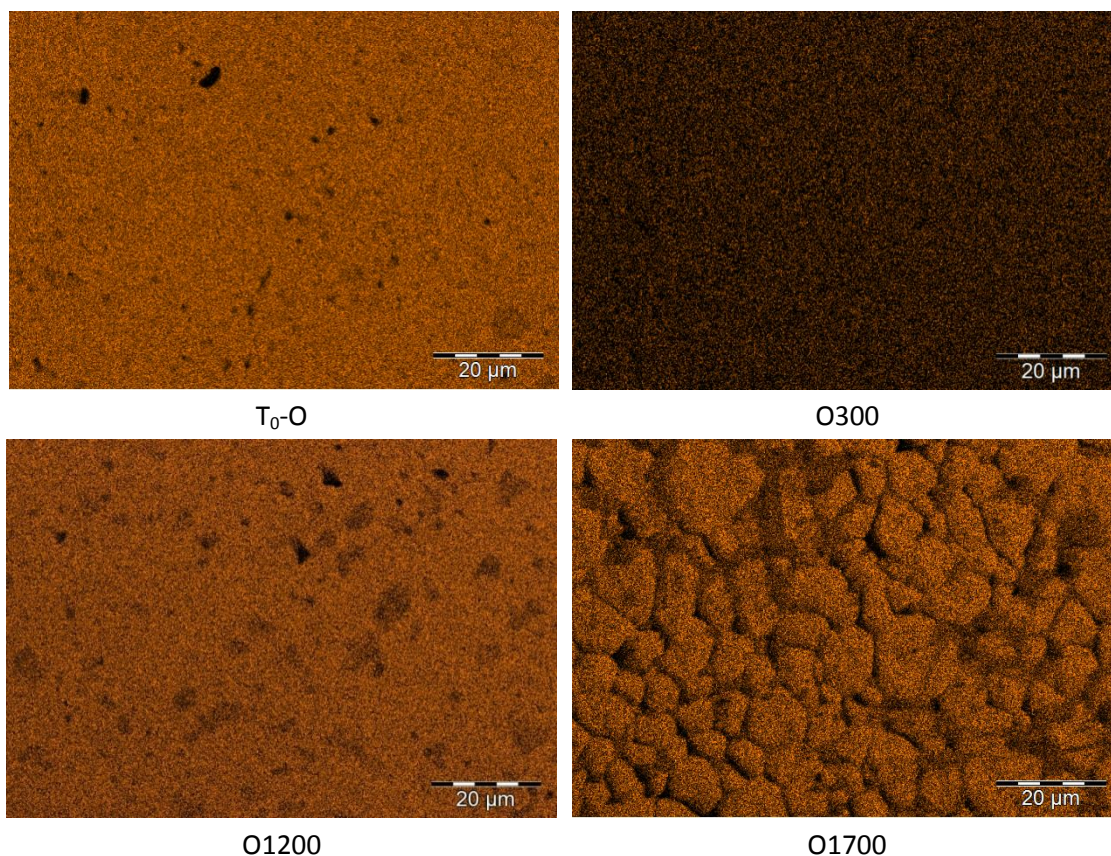
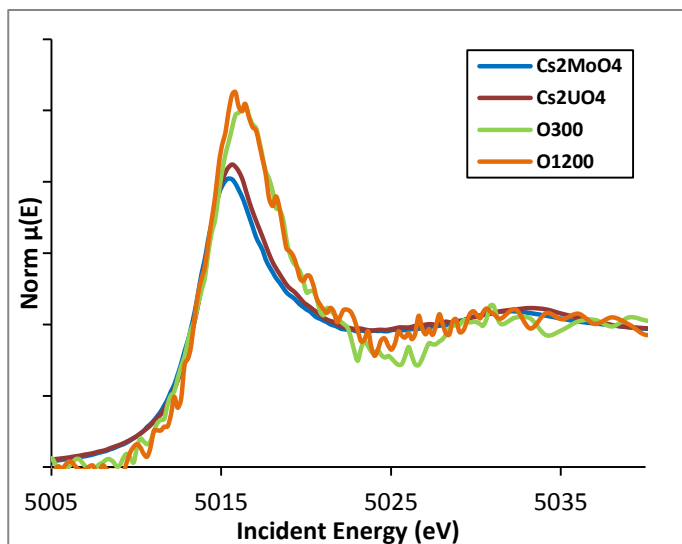


Figure 88: Cs X-ray maps acquired on samples from set III

Caesium XANES spectra were acquired for samples O300, O1200 and O1700, along with two reference compounds, Cs₂MoO₄ and Cs₂UO₄, at the L₃ absorption edge (5012 eV). Only results collected on samples O300 and O1200 are presented in **Figure 89**, since no Cs signal was detected in sample O1700. The absorption edge and white line positions of each spectrum are presented in **Table 42**.



Cs L ₃ -edge		
Sample	E ₀ (eV)	White line (eV)
Cs ₂ UO ₄	5013.7	5015.6
Cs ₂ MoO ₄	5014.0	5015.5
O300	5014.8	5016.3
O1200	5014.6	5015.8

Table 42: Cs spectra E₀ and white line positions, samples from set III. Incertitude: ± 0.5 eV

Figure 89: Cs XANES spectra collected on samples from set III

As previously explained, Cs⁰ absorption edge is located at 5012 eV, according to (Elam et al., 2002). XANES results show that the E₀ and white line positions of both samples, O300 and O1200 are shifted to higher energies compared to both reference spectra, in a similar way to sample R300 of set II. The white line intensity of these samples is also higher than that of the references. Due to these characteristics linear combination fits could not be performed. Contrary to sample R1200 (annealed at 1473 K in reducing conditions), the E₀ and white line positions of the Cs spectra did not shift to lower energy after the annealing test at 1473 K in oxidizing conditions.

3.4.3.3. Oxide Precipitates

Barium and zirconium X-ray maps collected on samples T₀-O, O300, O1200 and O1700 are presented **Figure 90**. According to these results the oxides precipitates in sample O300 are similar to those observed in R300 sample, though these associations change at 1473 K. Indeed, as observed in these X-ray maps and the quantitative analyses presented in **Table 43**, only traces of Zr are present, Mo becomes the main component and Ru traces are also detected. The two oxide precipitates described in the fuel micro-structure evolution of these samples differ greatly in their Ba/Mo ratio, as observed in **Table 44**. The precipitates more concentrated in Mo, designed as **OP I**, present a Ba/Mo ratio equal to 0.8 while the other, designed as **OP II**, a Ba/Mo ratio of 0.1. The area contribution and ECD of oxides precipitates also increased significantly from sample O300 to sample O1200. Indeed, while the area contribution and ECD of the oxide precipitates in sample O300 were 0.7% and 1.5 μm, respectively, both type of oxide precipitates observed in sample O1200 present a combined area contribution of 9.2 %, with different ECD: 2.3 μm for **OP I** precipitates and 3.5 μm for **OP II** ones. Regarding sample O1700, only one type of oxide precipitates is observed, which present a dendritic shape and cover an important surface of the sample. Indeed, these precipitates represent the 23% of the analysed surface. Besides oxygen, these precipitates are mainly composed of Mo, though Ba and Sr are present but in a significantly lower concentration compared to the observed ones in sample O1200.

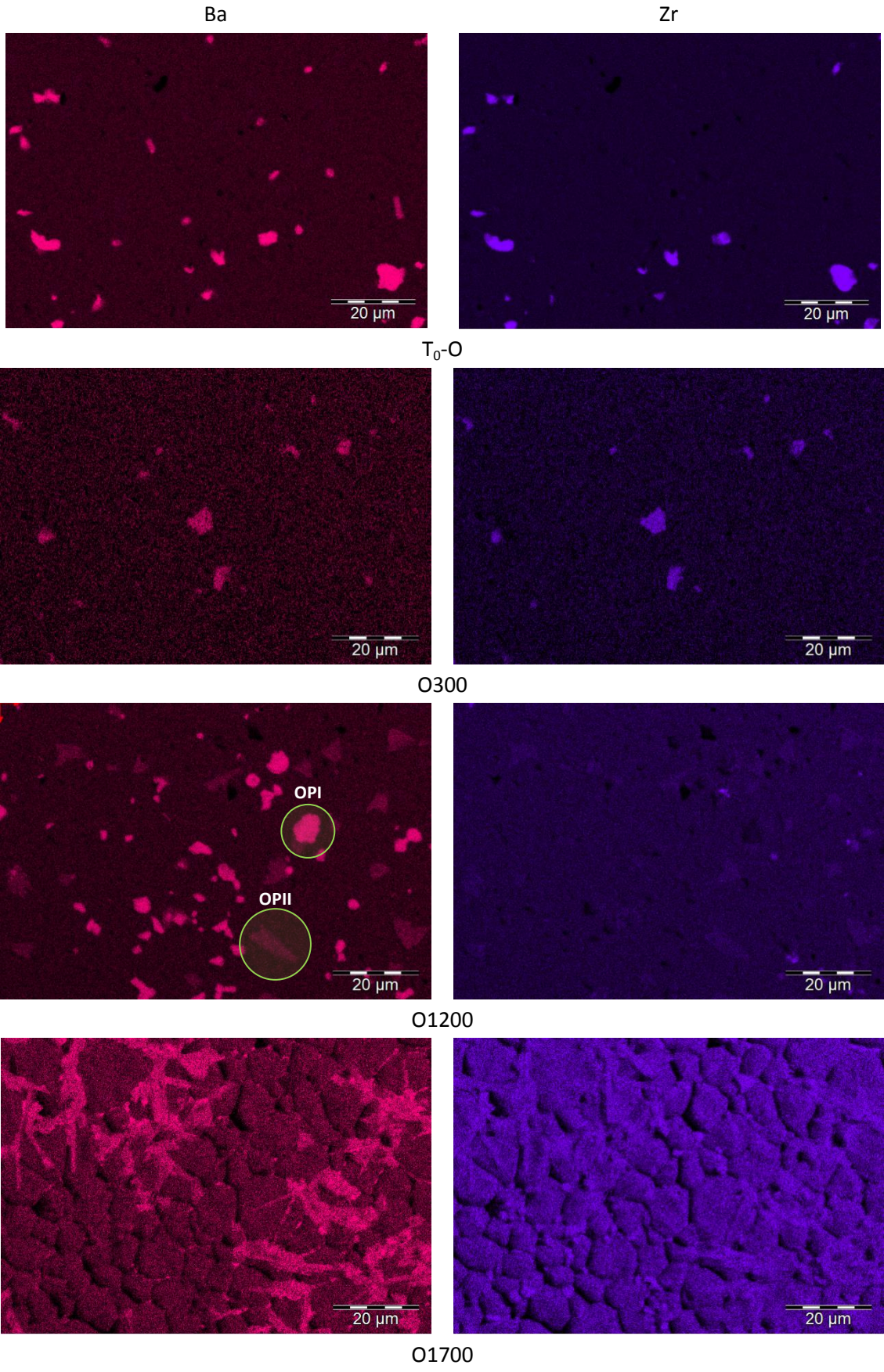


Figure 90: Ba (left) and Zr (right) X-ray Maps, Sample Set III

Element	Sample				
	T ₀ -O	O300	O1200		O1700
			OP I	OP II	
O	60.1 ± 4.4	59.7 ± 1.8	62.1 ± 6.6	55.5 ± 4.8	56.1 ± 9.0
Sr	3.1 ± 1.0	3.0 ± 0.6	3.6 ± 0.7	1.5 ± 0.3	1.7 ± 0.4
Zr	15.2 ± 3.4	15.2 ± 1.8	0.4 ± 1.0	0.1 ± 0.1	0.0 ± 0.1
Mo	0.3 ± 0.1	1.0 ± 1.4	17.4 ± 2.6	27.0 ± 2.2	36.2 ± 7.5
Ru	0.0 ± 0.0	0.6 ± 1.5	0.4 ± 1.0	0.4 ± 0.6	0.7 ± 0.6
Ba	17.3 ± 1.5	15.8 ± 1.7	14.2 ± 3.0	3.9 ± 0.5	4.6 ± 1.6
U	3.9 ± 0.7	4.4 ± 0.9	1.5 ± 1.6	11.0 ± 4.3	0.4 ± 0.5

Table 43: FP concentration in oxide precipitates, Sample Set III

Sample	Surface contribution (%)	ECD (μm)	Ba/Zr ratio	Ba/Mo ratio
T ₀ -O	2.6	2.6	1.2 ± 0.4	63.3 ± 15.3
O300	1.0	1.4	1.0 ± 0.1	31.8 ± 18.0
O1200	4.8	2.3	84.0 ± 89.8	0.8 ± 0.1
	4.6	3.5	64.7 ± 0.0	0.1 ± 0.0
O1700	23.0	3.9	36.9 ± 12.0	0.1 ± 0.0

Table 44: Oxide precipitates characteristics, Sample Set III

3.4.3.4. Metallic Precipitates

Mo and Ru distribution in the samples was also determined by SEM-EDS analyses. The acquired X-ray maps for samples T₀-O, O300, O1200 and O1700 are presented in **Figure 91**. As previously described, Mo is present in the oxide precipitates along with Ba, Sr and traces of Zr and Ru. Nevertheless, metallic precipitates containing mainly Mo and Ru are still observed. The composition of these precipitates is modified as result of the annealing tests under oxidizing atmosphere, as observed in the quantitative analyses results presented in **Table 45**. According to these results, Mo concentration in the metallic precipitates is significantly reduced from sample O300 to sample O1200, from 45.2 to 6.1 at.%, while Ru one increased from 52.9 to 91.1 at.%, respectively. After the annealing test at 1973 K under oxidizing conditions (sample O1700) the phase separation of the metallic precipitates is observed, similarly to samples R1500 and R1700, annealed at 1773 K and 1973 K under reducing conditions, respectively. Two types of precipitates are observed, denominated as phases Ru(Mo) (with a Mo/Ru ratio equal to 1) and Mo(Ru) (with a Mo/Ru ratio equal to 4.6). As observed in **Table 46**, the size and area contribution of the Mo/Ru precipitates decreased from 1.3 μm and 2.2% in sample O300 to 0.8 μm and 1.5% in sample O1200, respectively. This reverts after the annealing test at 1973 K, and the precipitates size and area contribution increase to 1.2 μm and 3.9%, respectively.

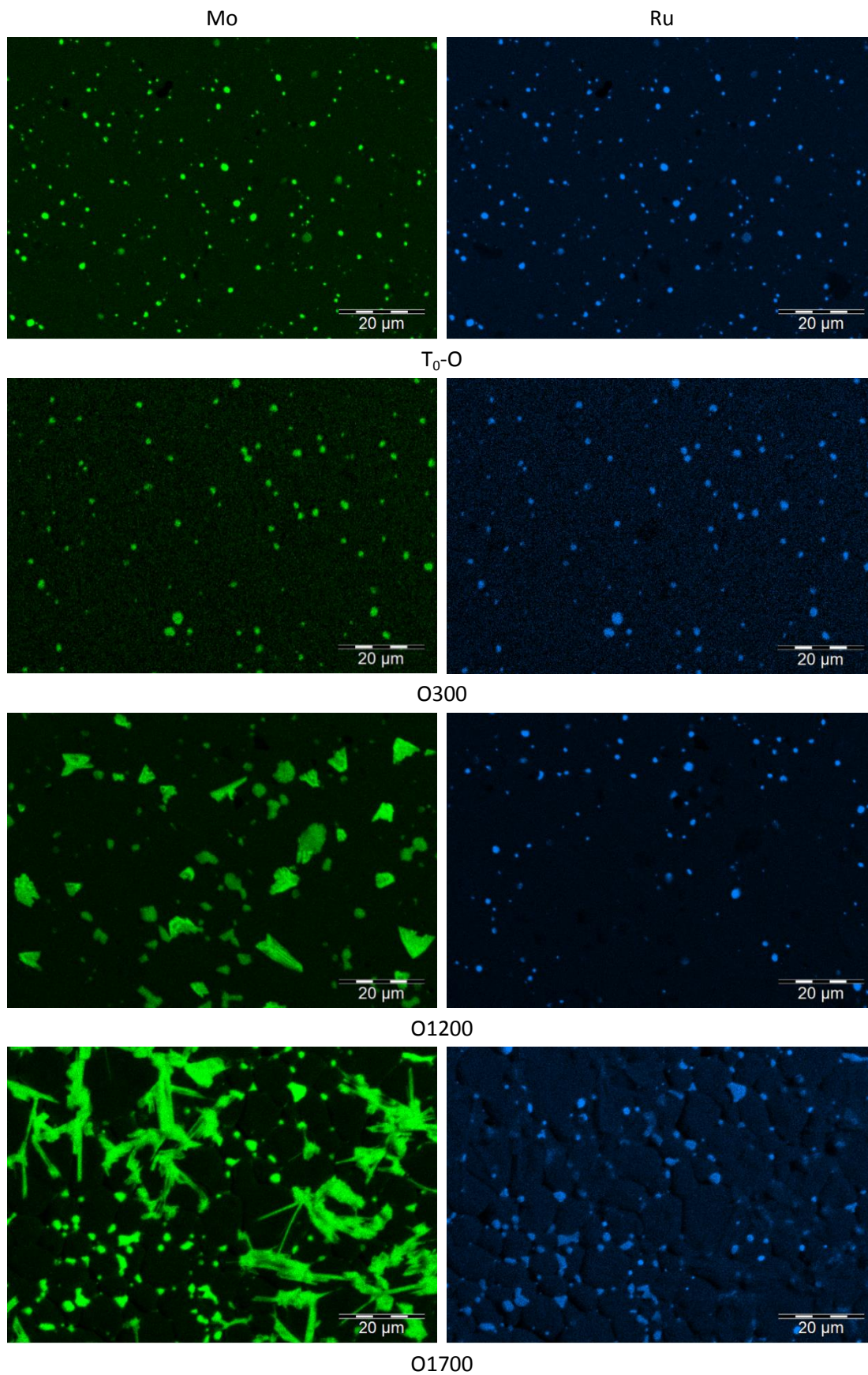


Figure 91: Mo (left) and Ru (right) X-ray maps collected on samples from set III

Element	Sample				
	T ₀ -O	O300	O1200	O1700	
				Ru(Mo)	Mo(Ru)
Mo	44.7 ± 0.3	45.2 ± 0.8	6.1 ± 3.9	48.9 ± 6.5	80.8 ± 3.7
Ru	53.2 ± 0.3	52.9 ± 0.8	91.1 ± 4.8	49.1 ± 6.5	18.2 ± 3.6
Rh	0.0 ± 0.0	0.0 ± 0.0	0.4 ± 1.1	0.0 ± 0.0	0.0 ± 0.0
Pd	2.2 ± 0.3	1.8 ± 0.2	2.3 ± 0.6	2.0 ± 0.5	1.0 ± 0.2

Table 45: FP concentration in metallic precipitates of samples from set III

Sample	Area contribution (%)	ECD (μm)	Mo/Ru ratio
T₀-O	2.1	1.3	0.8 ± 0.0
O300	2.2	1.3	0.9 ± 0.0
O1200	1.5	0.8	0.1 ± 0.0
O1700	3.9	1.2	Mo(Ru) = 4.6 ± 1.1
			Ru(Mo) = 1.0 ± 0.3

Table 46: Characteristics of the metallic precipitates on samples from set III

In a similar way to samples from set II, quantitative results of each analysed Mo precipitate in these samples has been represented on the Mo-Ru binary phase diagram, in **Figure 92**. As observed, results obtained on samples T₀-O, O300 and O1200 indicate that the metallic precipitates present a composition which is consistent with that of the ε phase. The phase separation of the metallic precipitates is observed in sample O1700. Indeed, the Mo/Ru ratio in both type of precipitates are consistent with the ε and β phases ones. Of the precipitates analysed in the O1700 sample, only one presented a composition which would be consistent to the σ phase.

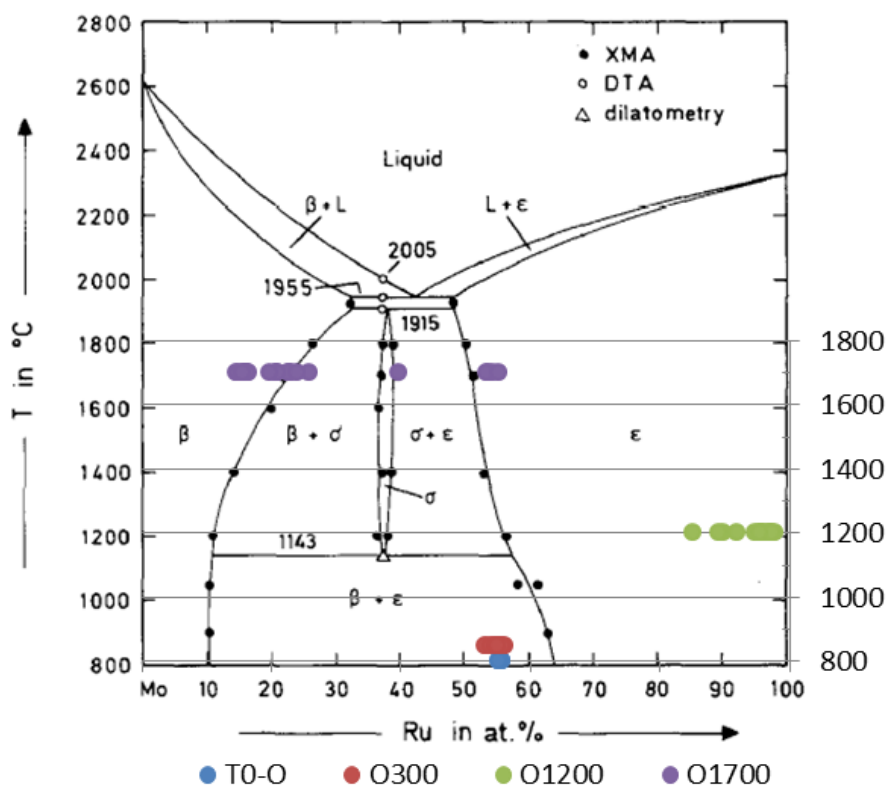


Figure 92: Quantitative analyses performed on samples set III metallic precipitates, represented in the Mo - Ru binary phase diagram extracted from (Kleykamp, 1989a)

Mo characterization by X-ray Absorption Spectroscopy

Mo XANES spectra were collected at the K absorption edge (20000 eV) for samples T₀-O, O300, O1200 and O1700 and four reference compounds: metallic Mo, Cs₂MoO₄, MoO₃ and MoO₂. These spectra are presented in **Figure 93** and the corresponding E₀ and white line positions are presented in **Table 47**. According to these results, an important evolution of the Mo chemical state after tests is observed. Indeed, while T₀-O sample spectrum presents an absorption edge position similar to that of metallic molybdenum, the other spectra are shifted to higher energy. Samples O300, O1200 and O1700 present an energy shift of their E₀ position of 1.4, 4.3 and 1.2 eV compared to metallic Mo one. At 1473 K (sample O1200) the apparition of a pre-peak at 20008 eV is observed. The E₀ position of sample O1700 is shifted back to lower energy compared to sample O1200.

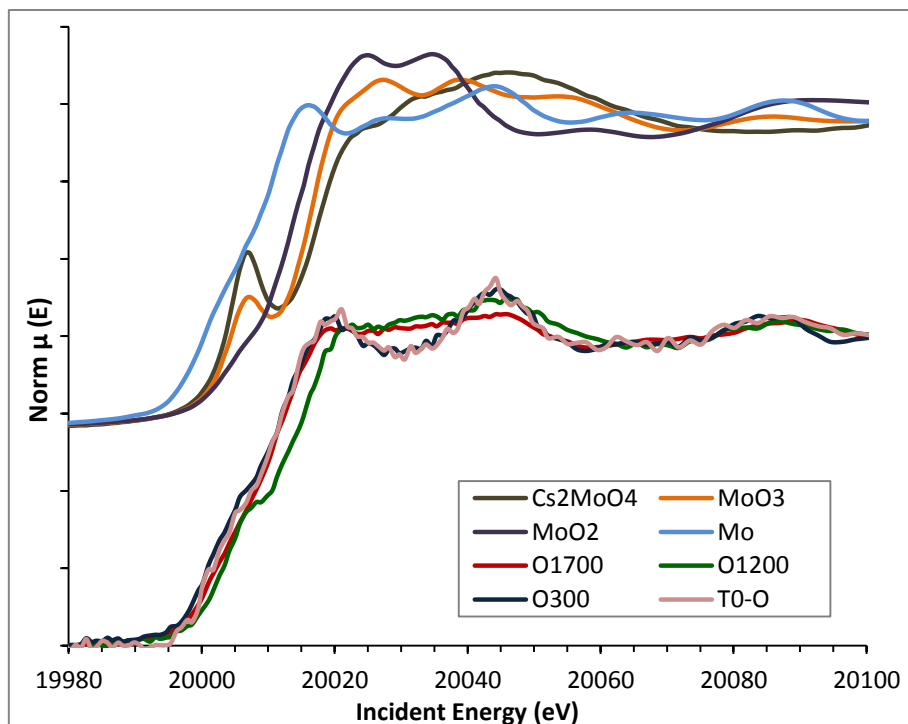


Figure 93: Mo XANES spectra, Samples Set III

Mo K-edge		
Sample	E_0 (eV)	White line (eV)
T₀-O	2000.2	20020.7
O300	20001.4	20019.3
O1200	20004.3	20023.0
O1700	20001.2	20019.1
Mo	20000.0	20016.6
MoO₂	20005.0	20025.0
MoO₃	20004.6	20026.8
Cs₂MoO₄	20003.8	20045.5

Table 47: Mo XANES spectra E_0 and white line positions, set III samples. Incertitude: ± 0.8 eV

A linear combination fit has been performed in order to estimate Mo chemical state in samples from set III, Mo reference compounds spectra, as well as T₀-R (implanted, unannealed sample from set II) and AT (unimplanted, annealed at 1973 K sample from set I) samples spectra. The obtained results are presented in **Table 48**. As expected, sample T₀-O is similar to sample T₀-R, and sample O300 is similar to sample T₀-O. Nevertheless, it is also observed an increased contribution of the metallic Mo (8%) and Cs₂MoO₄ (6%) reference spectra. As described previously for samples from set II and since no MoO₂ is detected, these little contributions could be attributed to the modification of Mo local environment in the metallic precipitates by the presence of Ru. Then, the annealing test at 573 K under oxidizing atmosphere did not produce a major impact on Mo chemical state. Sample O1200 results highlight the evolution of Mo chemical state in oxidizing conditions. As observed, there is an important contribution of the oxidized Mo spectra: 24% of MoO₂, 10% of MoO₃ and 27% of Cs₂MoO₄.

The remaining 39% would correspond to sample O300, which could be attributed to metallic Mo (since, as observed, Mo is mostly metallic in this sample).

Regarding sample O1700, it is observed an important contribution of metallic Mo (39%). This would imply that an important fraction of the oxidized Mo in sample O1200 would have reduced and returned to the metallic precipitates. The latter is in good agreement with SEM-EDS observations. It is also observed a decreased fraction of Mo under the MoO₂ chemical form in sample O1700, compared to sample O1200.

Sample	Reference weight								R factor
	Mo	MoO ₂	MoO ₃	Cs ₂ MoO ₄	T ₀ -R	T ₀ -O	O300	O1200	
T ₀ -O	0.00	0.06	0.00	0.00	0.94	-	-	-	0.00049
O300	0.08	0.00	0.00	0.05	-	0.87	-	-	0.00036
O1200	0.00	0.24	0.10	0.27	-	-	0.39	-	0.00049
O1700	0.39	0.19	0.00	0.00	-	-	-	0.41	0.00112

Table 48: Samples from set III Mo XANES spectra fit results. Incertitude: 2%

^aThe reference spectrum was not considered in the linear combination fit.

3.4.3.5. Summary of observations on sample set III

Important observations have been performed on samples from set III, regarding the behaviour of Mo, Ru and Ba under oxidizing conditions.

- The oxide precipitates composition, which originally contained mainly Ba and Zr, changed above 1473 K in oxidizing conditions. Two different oxide precipitates were observed at 1473 K, of which Mo was the main constituent, followed by Ba and Sr and traces of Zr and Ru. These two types of precipitates presented a very different Ba/Mo ratio: 0.8 in one hand and 0.1 in the other. Only one type of oxide precipitate was observed in sample O1700, in which Mo was also the main constituent but Ba and Sr were also present along with traces of Ru. It was observed that Zr was no longer present. These precipitates covered around 24% of the sample surface. XAS analyses indicate the oxidized Mo in sample O1200 is under the Mo⁺⁶ form, while the oxidized Mo in sample O1700 is mainly under the Mo⁺⁴ form.
- Metallic precipitates were also present in set III samples, with Mo and Ru as the main constituents, even though the annealing tests were performed under oxidizing atmosphere. The composition of these precipitates changed at 1473 K, where a drastic reduction of Mo content was observed. Indeed, most precipitates presented a Ru content superior to 80 at.%. The phase separation of the metallic precipitates is observed at 1973 K, and three different compositions are observed, which are consistent with the β (more concentrated in Mo), σ (an intermediary phase slightly more concentrated in Mo) and the ε phases (slightly more concentrated in Ru).
- Cs chemical state could not be identified in samples from set III, due to the absorption edge and white line positions, as well as the white line intensity of the collected spectra. Contrary to samples from set II, the energy shifts and white line intensities did not return to the expected values after the annealing tests at 1473 K, under oxidizing atmosphere.

3.5. Discussion

The annealing tests and associated characterizations performed in this work axis have highlighted the complex behaviour of FP in the nuclear fuel when submitted to severe accidents conditions. Firstly, observations performed on samples submitted to reducing conditions will be discussed, followed by the oxidizing tests one.

3.5.1. Tests performed under reducing atmosphere

Annealing tests performed under reducing atmosphere did not produce a major impact on the fuel micro-structure of the samples. Regarding unimplanted samples from set I, the grain boundaries etching is observed, along with the apparition of white precipitates. The UO_2 grain boundaries etching is a common phenomenon in ceramic materials submitted to high temperatures (Mott and Williams, 1953). Regarding the Cs implanted samples, the grain boundaries etching is already observed even before any annealing tests due to the ion beam effect. According to SEM-EDS quantitative analyses the main FP dissolved in the UO_2 matrix are Sr, Zr, Cs, Ce, La and Nd. According to the thermodynamic analysis, Zr chemical species would be ZrO_2 , which is highly soluble in UO_2 . FP concentration in the UO_2 matrix is not modified after annealing under reducing atmosphere, with the exception of Cs. Indeed, Cs concentration in the samples matrices tends to decrease above 1473 K, which would imply the partial release of this FP.

3.5.1.1. Barium zirconate destruction

Many Ba precipitates were found in samples set I and II, containing also Ce, Zr, Sr and Y. According to the considered release mechanism and our thermodynamic estimations presented in Section 3, the involved Ba chemical species would be BaZrO_3 . According to XAS results, Ba and Zr spectra confirm the oxidations states Ba^{+2} and Zr^{+4} , as well as an octahedral Zr local environment, where Zr atoms are surrounded by six oxygen atoms (similar to that of the perovskite structure). These results would support the BaZrO_3 chemical form.

The initial Ba/Zr ratios observed in samples T_0 -R and R300 were 1.0 and 1.8, respectively. This ratio decreased to 0.8 and 1.1 in samples AT and R1700, respectively (both annealed at 1973 K). The size and number of precipitates also decreased. Indeed, these precipitates presented an ECD equal to 2.45 and 2.2 μm for samples T_0 and R300, respectively, which decreased down to 0.83 and 1.7 μm for samples AT and R1700, respectively. Their area contribution also decreased, from 0.64 and 1.7 % in samples T_0 and R300, to 0.29 and 0.60 % in samples AT and R1700, respectively. These results would imply a partial destruction of the involved chemical phase at high temperatures and reducing conditions, in good agreement to the proposed release mechanism, presented in **Section 3.1**. The XANES spectra collected on samples from set I are not strongly modified by the annealing process: the absorption edge position is similar for both samples within the experimental errors, indicating that Ba and Zr oxidation states do not change after the annealing test. Then, even if the presumed chemical form, BaZrO_3 is partially destroyed and BaO is released, the local structure around Ba and Zr would not change significantly.

3.5.1.2. *Molybdenum - ruthenium phase separation*

Regarding Mo and Ru, SEM-EDS analyses indicate the presence of many precipitates in samples set I and II (annealed under the same reducing conditions), which also contained some Rh and Pd. While only one type of precipitates was observed in samples T_0 , R300 and R1200, it was observed the apparition of two other type of precipitates at high temperatures, in samples AT (1973 K), R1500 (1773 K) and R1700 (1973 K). Besides, it was observed that the number of precipitates and their area contribution increased as a function of temperature. Indeed, initially the ECD and area contribution of these precipitates were 1.2 μm and 1.7% respectively in sample R300, which increased up to 1.6 and 4.7% in sample R1700. Though the ECD of these precipitates in sample AT was lower than that of T_0 sample, the number of precipitates increased implying an augmentation of the area contribution, from 1.9% in T_0 sample to 2.7% in AT one. The Mo/Ru ratio of these precipitates was also modified as a consequence of temperature. For tests performed below 1773 K the Mo/Ru ratio remained constant and equal to 0.8 (samples T_0 , R300 and R1200). Once this phase is separated at 1773 K (sample R1500) this ratio is modified: some precipitates present a Mo/Ru ratio equal to 1 while the others a ratio equal to 4.1. This ratio is further modified at higher temperatures. Indeed, at 1973 K the Mo/Ru ratios were 1 and 6.0 for sample AT and 1 and 6.6 for sample R1700. Particularly for sample R1500, a third type of precipitate was observed, which presented a Mo/Ru ratio equal to 1.6. The quantitative analyses performed on the Mo-Ru precipitates of samples from set II were placed on the Mo-Ru binary phase diagram. The only type of precipitates present below 1773 K would correspond to a ϵ phase. Above 1773 K three different Mo/Ru ratios were detected among the precipitates. These compositions are consistent with the β (richer in Mo), σ (slightly richer in Mo) and the ϵ phases (slightly richer in Ru). Most analysed precipitates of sample R1700 presented a composition consistent with the β phase, along with an ECD and area contribution superior to that of the precipitates with a composition similar to the ϵ phase. These observations would indicate that Mo could have diffused from the bulk of the samples, thus enriching the precipitates located at the surface and that Ru did not diffuse at all or, if it did, lesser than Mo.

According to XAS analyses performed on samples from set I, Mo would be mainly in metallic state, both in T_0 and AT (1973 K) samples. The Mo K-edge spectrum is slightly modified by the annealing process, contrary to the Ru K-edge one. Indeed, the white line position of Mo XANES is shifted by 1.0 ± 0.8 eV to lower energy after the annealing at 1973 K, while Ru spectrum does not change at all. This indicates that the local structure around Mo evolves during annealing, but not the Ru one. Micro beam analyses performed on Mo-Ru precipitates in sample T_0 -R also indicate that Mo is in metallic state. These Mo spectra presented some differences though, compared to the metallic Mo reference. These differences are doubtlessly related to Mo local environment, which is modified by the presence of Ru. Indeed, pure metallic Mo and the β phase of the Mo-Ru binary system present a bcc structure (Kleykamp, 1988), while the ϵ and σ phases present a hcp (Kleykamp, 1988) and tetragonal (Grånäs et al., 2008) structures, respectively.

Mo spectra is not significantly modified up to 1773 K, but at 1973 K an energy shift of the white line position towards lower energy and the apparition of features on the XANES spectra are observed. These new features are also observed on the pure metallic Mo reference spectrum. This would imply that Mo local environment evolves between 1773 K and 1973 K to become similar to the pure metallic Mo one. Moreover, when the quantitative analyses results are placed on the binary system

diagram, some precipitates are even richer in Mo than the β phase in equilibrium with the σ and ϵ ones. All these results would support the assumption that Mo mobility increases above 1773 K and migrates from the bulk of the sample towards the surface, while Ru remains immobile. This would explain the enrichment of the metallic precipitates over the equilibrium $\epsilon/\sigma/\beta$ compositions, the augmentation of the precipitates ECD and their area contribution.

3.5.1.3. *Caesium behaviour*

Caesium X-ray maps acquired on samples T₀-R, R300, R1200, R1500 and R1700 show that this FP is mainly dissolved in the UO₂ matrix, since no precipitates or particular association to other FP were observed. Nevertheless, SIMS analyses which were only performed on sample T₀-R (right after implantation and without any annealing test), show the existence of Cs precipitates. These precipitates present an ECD of 3.15 μm . The implantation profiles also obtained by SIMS (refer to **Appendix III**) indicate that most Cs is located around 124 nm underneath the surface of the sample. These different results obtained by SEM-EDS and SIMS analyses could be due to the different interaction spheres of both techniques. Indeed, 15 keV electrons (acceleration tension employed in SEM-EDS analyses) may travel up to 1 μm in the sample from the surface, while ion beams (SIMS analyses) penetrations is in the order of nanometres. As it was determined by SIMS profile analyses, most Cs is found 124 nm from the surface.

According to thermodynamic estimations, Cs should be found as Cs₂MoO₄ in samples R300 and R1200, and should have been totally released in samples R1500 and R1700. Though no Cs signal was detected during the XANES acquisition on sample R1700, results show that this FP is still present at 1773 K in reducing conditions (sample R1500). The absorption edge and white line positions of sample R300 Cs XANES spectrum present a shift towards higher energy compared to reference spectra. Higher energy positions of the absorption edge indicate higher oxidation states. Nevertheless, only two oxidation states exist for Cs: 0 and +1, and since Cs is already as Cs⁺¹ both in Cs₂UO₄ and Cs₂MoO₄, the observed absorption edge position for R300 spectrum could be a consequence of Cs implantation. Indeed, it has already been observed that the implantation of elements in a matrix could induce abnormal states (Stöcker et al., 2014). Then, by implanting Cs ions in a UO₂ matrix, abnormal states could be produced which affect Cs absorption edge position and the intensity and position of the white line. These states would disappear at high temperatures, which would explain the shift towards lower energies of the absorption edge and white line positions in samples R1200 and R1500. The XANES spectra of both Cs reference compounds (Cs₂UO₄ and Cs₂MoO₄) are very similar and so Cs chemical form in our samples cannot be determined directly by the linear combination of the spectra. Nevertheless, Cs XANES spectra in these samples indicate that Cs is present whether as Cs₂UO₄ or Cs₂MoO₄, and since Mo XANES spectra indicate that Mo is mostly metallic in the five samples of set II (all annealed under reducing atmosphere), then Cs would be found as Cs₂UO₄. The absence of Cs XANES signal at 1973 K would imply the complete release of this FP from the sample. The latter is also confirmed by SEM-EDS quantitative analyses. According to thermodynamic estimations Cs₂UO₄ exist at very low oxygen potentials, below -600 kJ/mol_{O₂} at 573 and 1473 K. The oxygen potential attained during the annealing tests of samples R1200 and R1500 were -484 and -480 kJ.mol_{O₂}⁻¹, respectively. Then, these results could mean that if Cs₂UO₄ was indeed created, it was not due to chemical equilibrium but as a consequence of the implantation itself.

3.5.2. Tests Performed under oxidizing atmosphere

Tests performed under oxidizing atmosphere highlighted the complex interactions that take place between FP. Though no significant evolution was observed from sample T₀-O to sample O300, many precipitates were observed in samples O1200 and O1700. According to SEM-EDS quantitative analyses, the main FP dissolved in the UO₂ matrix were Sr, Zr, Mo, Cs and Nd. The concentration of these FP was modified after test, particularly for Zr and Mo. Indeed, though their concentration is similar in samples O300 and O1200 (of around 0.4 at.% each), it increases to 0.8 and 0.7 at.% for Zr and Mo, respectively. This would imply a dissolution of Zr and Mo oxidized species in the UO₂ matrix.

3.5.2.1. *Molybdenum - barium in oxide precipitates*

The evolution of the oxide precipitates in tests performed under oxidizing atmosphere was quite interesting. Indeed, the main components of these precipitates were initially Ba, Zr, Sr and U, in samples T₀-O and O300. Two different oxide precipitates were observed in sample O1200 which differed both in aspect and composition. The main difference of these precipitates was the Mo/Ba ratio: on one hand, some precipitates (designed as OP I) presented a Mo/Ba ratio equal to 0.8 and a mean ECD value of 2.3 μm. These precipitates represented the 4.8% of the sample surface. On the other hand, some precipitates (designed as OP II) presented a Mo/Ba ratio of 0.1 and a mean ECD equal to 3.5 μm. These precipitates represented the 4.6% of the sample surface. Sr and U were still found, but in lower concentration: Sr and U concentration in OP I precipitates was 3.6 and 1.5 at.% respectively, while in OP II precipitates the concentrations were 1.5 and 11 at.%, respectively. Traces of Zr and Ru were observed in these precipitates, as observed in the quantitative analyses.

According to thermodynamic estimations, the chemical species in equilibrium in sample O1200 would be ZrO₂, MoO₂, Cs₂MoO₄, BaMoO₄ and UO₂, which is consistent with the experimental observations. Indeed, the initial BaZrO₃ compound would have reacted with oxidized Mo giving ZrO₂ and BaMoO₄. Then ZrO₂ would have dissolved in the matrix, which would explain why almost no Zr is found in the oxide precipitates and why its concentration in the O1200 sample UO₂ matrix increased. Mo oxidation is clearly observed in the SEM-BSE and SE images presented in **Figure 85**, where small pores are observed in the metallic precipitates.

XAS results of sample O1200 indicate that Mo is mainly oxidized (61%, if considered that the contribution of sample O300 spectrum to the linear combination fit is representative of Mo in the metallic precipitates). Of this oxidized Mo, 60% would be as Mo⁺⁶ and the remaining 40% would be as Mo⁺⁴. These two different oxidation states would explain the existence of the two different oxide precipitates in sample O1200. Indeed, the precipitates containing a Ba/Mo ratio equal to 0.8 would be mainly composed of BaMoO₄ (Mo as Mo⁺⁶). If the Sr composition is also considered (Ba and Sr are both alkaline earth metals, so they present a similar behaviour), then the (Ba+Sr)/Mo ratio would be equal to 1, meaning that those precipitates are mainly composed of BaMoO₄ and SrMoO₄. The second type of oxide precipitates observed in sample O1200 would be mainly composed of MoO₂. Nevertheless, Ba and Sr were also detected in those precipitates ((Ba+Sr)/Mo ratio equal to 0.2), implying that MoO₂ is capable of dissolving considerable quantities of these FP oxidized species (whether BaMoO₄ and SrMoO₄ or BaO and SrO). XAS analyses using micro beams would be required in order to validate these assumptions.

Another possible explanation would be the demixing of the MoO_3 - $(\text{BaMoO}_4\text{-SrMoO}_4)$ phase. Indeed, according to the MoO_3 - SrO pseudo binary phase diagram extracted from (Zhukovskii et al., 1972) and presented in **Figure 94**, above 940 K MoO_3 would be in equilibrium with a solid solution of $\text{MoO}_3(\text{SrMoO}_4)$. An eutectic point exists at 940 K, below which the solid solution separates into MoO_3 and SrMoO_4 . Considering that Sr and Ba have a similar behaviour, the molar ratio observed in the different precipitates $(\text{Ba+Sr})/\text{Mo}$ equal to 1 and $(\text{Ba+Sr})/\text{Mo}$ equal to 0.2 would correspond to the phases in equilibrium presented in this phase diagram. Nevertheless, pure oxidized Mo precipitates have not been observed in this sample.

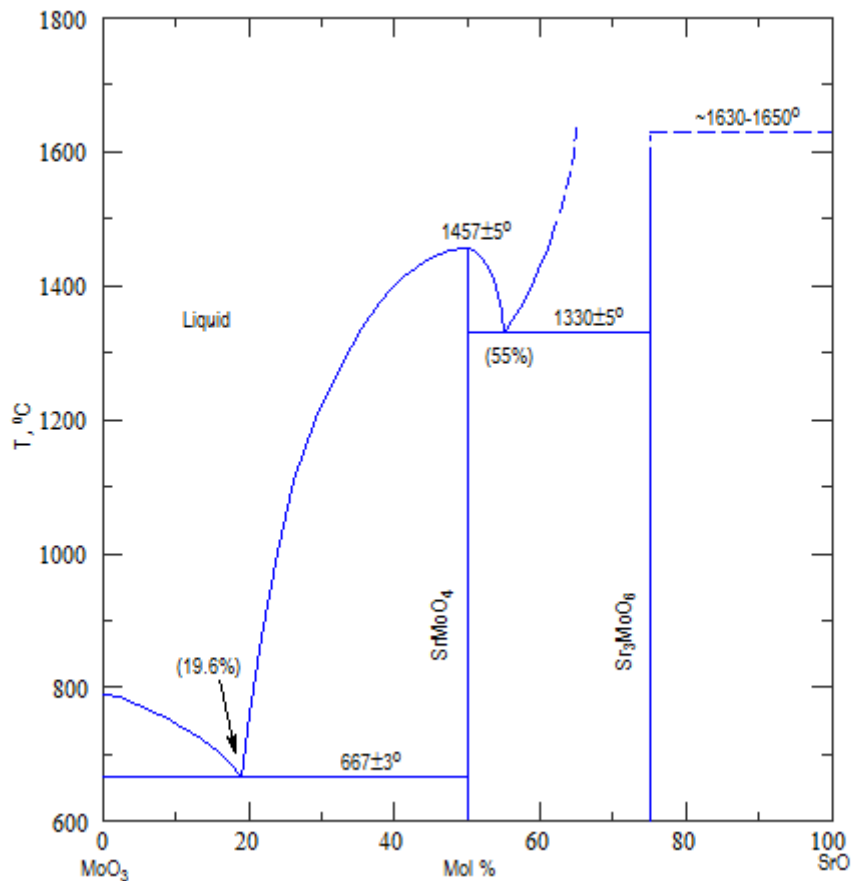


Figure 94: MoO_3 - SrO pseudo binary phase diagram extracted from (Zhukovskii et al., 1972)

Only one type of oxide precipitates was observed in sample O1700. These precipitates presented a dendritic shape and covered a quarter of the sample surface. According to quantitative analyses, Mo would be the main constituent of these precipitates, followed by Sr and Ba. The $(\text{Ba+Sr})/\text{Mo}$ ratio of these precipitates was calculated to be 0.17, similar to the second type of precipitates observed in sample O1200. According to XAS results obtained in sample O1700, oxidized Mo would be mainly Mo^{4+} . This would imply that the oxides precipitates are mainly composed of MoO_2 , with oxidized species of Ba and Sr dissolved. These precipitates would then be similar to the second type of precipitate observed in at 1473 K in oxidizing conditions.

3.5.2.2. Molybdenum - ruthenium

Quantitative analyses performed on metallic precipitates of the sample annealed at 1473 K indicate that Ru became the main component. Indeed, every analysed precipitate was constituted of more than 80% of Ru. Mo initially present in these precipitates would have oxidized and reacted with the initial Ba-Zr precipitates, giving place to the oxide precipitates observed in this sample. The phase separation of the metallic precipitates was observed after annealing at 1973 K (sample O1700), in a similar way to samples from set II. According to thermodynamic estimations, the test conditions of sample O1700 would have been close to the Mo/MoO₂ equilibrium. It is considered then that Mo present in the oxides precipitates observed in sample O1700 was partially reduced and went back to the metallic phase. The important presence of Mo in the surface, both in oxide and metallic precipitates would support the assumption of Mo mobility at high temperatures. The existence of three molybdenum oxidation states (0, 4+ and 6+) in samples O1200 and O1700 would imply that chemical equilibrium was not attained during the annealing tests.

3.5.2.3. Caesium

Similarly to samples from set II, no Cs precipitates or particular associations to other FP were observed through SEM-EDS characterization of samples from set III. Nevertheless, since the implantation conditions of samples set II and III were the same and Cs precipitates were observed through SIMS analysis performed on sample T₀-R from set II, similar precipitates are believed to exist at least in T₀-O sample. According to thermodynamic estimations, only one chemical species, Cs₂MoO₄, should be present in these samples. This chemical species would be present even in sample O1700, annealed at 1973 K. Nevertheless, since no Cs signal could be measured in the XAS experiments this would imply that this FP would have been completely released at 1973 K. Cs XANES spectra collected in samples O300 and O1200 present an energy shift of the absorption edge and white line position to higher energy and a more intense white line compared to that of both reference compounds. As in sample R300, this could be attributed to the creation of metastable chemical state as a consequence of the implantation. Contrary to the test performed at 1473 K in reducing conditions (sample R1200), the metastable state did not disappear at 1473 K in oxidizing ones.

3.6. Conclusions

The behaviour of Ba, Cs, Mo and Ru in high burn-up simulated UO₂ nuclear fuels, or SIMFUELS, submitted to nuclear severe accident conditions has been studied. Three different samples sets were prepared, submitted to different conditions and characterized by SEM-EDS and XAS. Sample set I consisted in two samples, one of which was annealed at 1973 K, containing 11 FP each (Ba, Ce, La, Mo, Nd, Pd, Rh, Ru, Sr, Y and Zr). Sample set II and III consisted in 5 samples each, which contained 12 FP (the latter 11 FP + Cs, implanted by the ion implantation method). Samples of set II were submitted to reducing conditions while those of set III were submitted to oxidizing ones. The conclusions regarding barium, caesium, molybdenum and ruthenium behaviour are presented below.

3.6.1. Barium behaviour

According to the release mechanism presented in Chapter 1, barium would be initially found in micrometric oxide precipitates known as the perovskite phase (Kleykamp, 1985). In our samples, it was indeed observed that Ba was initially present in oxide precipitates which also contained Ce, Sr, Y and Zr. These precipitates, with an average size of about 2 μm , were evenly distributed in samples annealed under reducing conditions. XAS analyses performed on samples from set I indicated that Ba chemical form was indeed BaZrO_3 . This compound was partially destroyed and Ba released in reducing atmosphere at temperatures above 1773 K, as indicated by SEM-EDS results from samples set I and II. This behaviour is in good agreement with the proposed mechanism.

In oxidizing conditions it was observed that BaZrO_3 was also destroyed, with Ba interacting with oxidized Mo to likely form BaMoO_4 . Nevertheless, further experimentations are required to accurately characterize Ba chemical state. Zr was initially also present in these Ba-Mo precipitates (at 1473 K) but then was dissolved, likely as ZrO_2 according to thermodynamic estimations, in the fuel matrix (at 1973 K).

3.6.2. Caesium behaviour

Caesium, being a volatile FP, cannot be added during the SIMFUELS fabrication process since it would be released during the sintering stage. By using the ion implantation method this difficulty was overcome. Studying Cs behaviour was one of the main objectives for samples set II and III. Through SIMS analyses it was observed that Cs precipitates are formed after implantation, though this result could not be supported by SEM-EDS analyses. Indeed, no Cs precipitates were detected in any implanted sample through SEM-EDS analyses, before or after annealing tests. It has been reported in bibliography that the implantation of ions in a matrix would create metastable oxidation states. This phenomenon was observed in our samples, as indicated by the Cs XANES spectra collected on the sample submitted to 573 K under reducing atmosphere. At higher temperatures and reducing conditions Cs_2UO_4 is assumed to exist, since all Mo in the sample would be in metallic state. Nevertheless, thermodynamic estimations indicate that the attained oxygen potentials in tests performed for samples from set II were not reducing enough as to induce the formation of Cs_2UO_4 . Therefore, it is assumed that Cs_2UO_4 indeed exists in samples annealed under reducing atmosphere, but only as a direct consequence of the ions implantation and not to thermodynamic equilibrium. A Cs metastable state was also observed in samples O300 from set III. This state persisted even in sample O1200, contrary to sample R1200, both annealed at 1473 K. Therefore, Cs behaviour could not be studied in SIMFUEL samples submitted to oxidizing conditions. It is believed, though, that similar metastable states would be created during irradiation in nuclear fuels.

3.6.3. Molybdenum behaviour

Molybdenum was observed to be initially present in metallic precipitates along with Ru, Rh and Pd. These precipitates, known as white inclusions, have already been observed in irradiated fuels (Kleykamp, 1985). When submitted to reducing conditions and high temperatures it was observed a phase separation of the initially homogeneous metallic precipitates into two different phases, which differed in their Mo-Ru ratio. The metallic phase separation is predicted by the Mo-Ru binary diagram system. Three different phases may be found in equilibrium, which are β (richer in Mo, with

a bcc crystal structure), σ (slightly richer in Mo, with a tetragonal crystal structure) and ϵ (slightly richer in Ru, with a hcp crystal structure). A higher Mo mobility was observed at high temperatures, due to which most precipitates observed presented a β composition (sometimes even higher than the β phase solvus composition for the Mo-Ru binary) and increased ECD.

In oxidizing conditions, it was observed that Mo present in the metallic precipitates got oxidized and interacted with Ba and Sr. According to thermodynamic estimations, only BaMoO_4 and MoO_2 should be present in SIMFUEL samples from set III. It was observed though that two different Mo-Ba precipitates coexist at 1473 K, which present an important difference in their Mo/Ba-Sr ratios. XAS analysis allowed to assume that these precipitates are, on one hand, a solid solution of BaMoO_4 and SrMoO_4 (consisting with a (Ba+Sr)/Mo ratio equal to 1) and on the other a solid solution mainly composed of MoO_2 , with dissolved oxidized forms of Ba and Sr (or MoO_3 with dissolved Sr and Ba molybdates). XAS analyses at the Mo and/or Ba absorption edges using a micrometric X-ray beam would be required in order to identify the involved chemical compounds.

3.6.4. Ruthenium behaviour

According to the mechanism Ru would be present mainly in metallic precipitates which also contain Mo. As described for Mo, these precipitates were observed in our samples. XAS analyses confirmed Ru metallic state in samples from set I. As described above, a phase separation of the metallic precipitates occurs between 1473 and 1773 K. Regarding tests performed under oxidizing conditions, traces of Ru were observed to be present in oxide precipitates, in a concentration similar to Zr. The mechanism considers that Ru is released as RuO_x even at relatively low temperatures if submitted to an atmosphere oxidizing enough. Nevertheless, quantitative analyses would be required in order to determine if Ru was released from our samples.

Finally, it is concluded that SIMFUELS are a good complement to irradiated fuels for studying FP behaviour in severe accident conditions. Indeed, the evolutions observed for Ba, Mo and Ru are quite in good agreement with the proposed mechanism and experimental observation on irradiated fuel samples. Furthermore, their behaviour in oxidizing conditions could be studied. It was observed though that SIMFUEL representativeness to irradiated fuels is reduced at lower temperatures, particularly for Ba and Cs. Indeed, while no Ba precipitates are observed in the irradiated fuel sample representative of an initial state (before the severe accident), many precipitates are observed in SIMFUEL samples. Regarding Cs, the ion implantation method was required in order to study this FP chemistry, since it cannot be added during the samples fabrication process. It was observed though that metastable oxidation states were created through implantation, which are not representative of Cs chemistry, but could be representative of Cs state in irradiated nuclear fuels.

A comparison of the experimental results obtained in the Irradiated Fuels work axis and the model materials one is presented in the next and final chapter. Suggestions on how to improve SIMFUEL samples representativeness are also presented, along with experimental perspectives.

Chapter 4: Discussion

4.1. Introduction	141
4.2. Summary of samples and characterizations performed.....	141
4.2.1. Studied samples.....	141
4.2.2. Characterization methods	143
4.3. Experimental results comparison	144
4.3.1. Barium and zirconium.....	144
4.3.2. Barium, molybdenum and ruthenium.....	145
4.3.3. Caesium, uranium and molybdenum	146
4.3.4. Molybdenum and ruthenium	146
4.4. Comparison between experimental results and the release mechanism	147
4.4.1. Barium	147
4.4.2. Molybdenum	147
4.4.3. Caesium	148
4.4.4. Ruthenium	148
4.5. Summary of validated and refuted chemical phases.....	149
4.6. Modified release mechanism.....	149
4.6.1. Initial state	150
4.6.2. Stage at 1300K.....	151
4.6.3. Oxidation Plateau	151
4.6.4. Ramp to high temperature plateau.....	152
4.6.5. High temperature plateau.....	154

Chapter 4: Discussion

4.1. Introduction

In this Chapter the results presented in Chapters 2 and 3 will be compared. Chapter 2 described the irradiated fuels analyses and Chapter 3 the SIMFUELS one. These two research axes have been implemented in order to validate or refute, through experimental observations, the chemical phases proposed to be initially present in an irradiated fuel under normal operation conditions of a PWR nuclear reactor and their evolution during a severe accident initiated by the loss of the primary coolant fluid. These hypothetical phases and their evolution are recalled in **Figure 95**.

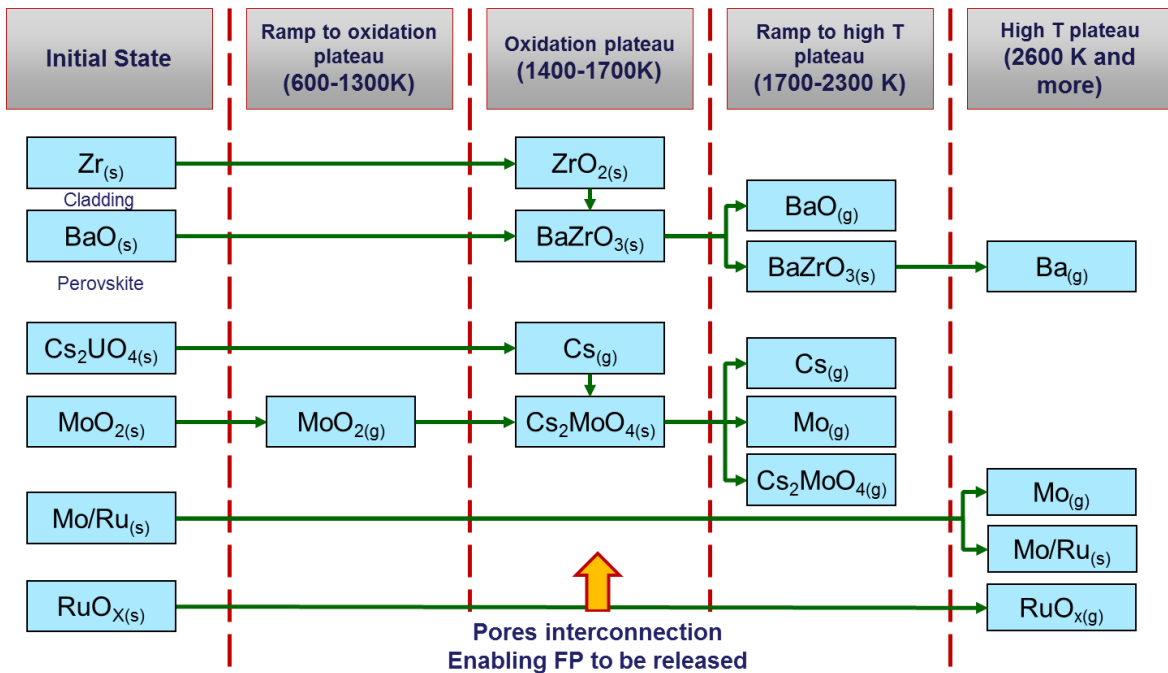


Figure 95: Hypothetical phases initially present in an irradiated fuel and their evolution during a nuclear severe accident

4.2. Summary of samples and characterizations performed

4.2.1. Studied samples

The two experimental work axes were meant to be complementary. Indeed, though the samples were different (irradiated fuel samples in one case and model materials representative of irradiated nuclear fuels in the other) the experimental loops and annealing tests performed were similar. Model materials, also known as SIMFUEL, allowed exploring further conditions compared to the irradiated fuels axe. Indeed, while the annealing tests using irradiated fuel samples were performed mainly under reducing atmospheres (flowing Ar + 4% H₂), model materials were submitted to both reducing and oxidizing (flowing Ar) conditions. The samples and tests conditions (atmospheres and final temperatures) are summarized in **Table 49**. Further information on the experimental loops and tests atmospheres is available in **Appendix V**.

Work axis	Sample	Atmosphere	Final Temperature (K)	Time at max temperature (min)
Irradiated Fuels	T ₀ -IF	-	-	-
	IF1500	Reducing	1773	35
	VERDON 1	Oxidizing then reducing	2873	0
Model Materials	T ₀	-	-	-
	AT	Reducing	1973	60
	T ₀ -R	-	-	-
	R300	Reducing	573	180
	R1200	Reducing	1473	30
	R1500	Reducing	1773	15
	R1700	Reducing	1973	10
	T ₀ -O	-	-	-
	O300	Oxidizing	573	180
	O1200	Oxidizing	1473	30
	O1700	Oxidizing	1973	10

Table 49: Summary of samples studied in this work

4.2.1.1. Irradiated fuels samples

Sample T₀-IF was not submitted to any annealing test. This sample is then representative of an initial state, before the severe accident starts. Sample IF1500 was annealed under reducing conditions, the temperature sequence consisting in a first plateau at 573 K which was maintained for 20 min, a second plateau at 1473 K, maintained also for 20 min and a last temperature plateau at 1773 K which was maintained time enough so that Cs release attained around 50% of the initial inventory. The exact duration of this last plateau was 35 min and the total Cs released fraction was measured to be 47%.

The VERDON 1 sample followed a quite complex annealing sequence, which reproduced the phenomena observed during a nuclear severe accident triggered by the loss of the primary fluid. The main characteristics of this sequence, which was presented in Chapter 2, were the implementation of a temperature plateau under oxidizing atmosphere (H₂O/H₂) in order to oxidize the cladding (at 1773 K); by the end of this temperature plateau the atmosphere was switched to reducing (H₂O/H₂) until the end of the test, where a temperature of 2873 K was attained. This temperature was maintained only a few seconds since on-line gamma spectrometry observation indicated the imminent sample collapse.

4.2.1.2. SIMFUEL samples

Samples from set I (T₀ and AT) are SIMFUEL samples doped with 11 FP (Ba, Ce, La, Mo, Nd, Pd, Rh, Ru, Sr, Y and Zr). T₀ sample was not submitted to any kind of annealing sequence while AT one was submitted to a single temperature plateau at 1973 K, which was maintained for 1 h.

Samples from sets II (T_0 -R, R300, R1200, R1500 and R1700) and III (T_0 -O, O300, O1200 and O1700) are SIMFUEL samples similar to those of set I but implanted in Cs. Samples T_0 -R and T_0 -O were not submitted to any annealing samples, and so they are representative of the initial state of an irradiated fuel before the severe accident starts. Samples R300 and O300 were annealed up to 573 K under reducing and oxidizing atmospheres, respectively. These temperatures were maintained for 3 h in an attempt to let the structure relax and arrive to chemical equilibrium after Cs implantation. Indeed, it has been reported in bibliography (Richard, 2012) that ion implantation (Cs in the case of these samples) leads to atoms displacement which distorts the crystal structures. Given the low temperature attained, these samples may be also considered as representative of an initial state before accidental sequence begins.

Samples R1200, R1500, R1700, annealed under reducing atmosphere and samples O1200 and O1700, annealed under oxidizing one, are representative of intermediate states of a nuclear severe accident sequence. These temperatures were chosen in order to check if the chemical phases proposed in the mechanism presented in **Figure 95** exist. Samples R1200 and O1200 were annealed up to 573 K and maintained at that temperature for 3h and then up to 1473 K for 30 min. Sample R1500 was annealed up to 573 K for 3 h, then up to 1473 K for 30 min and finally up to 1773 K for 15 min, under reducing atmosphere. The duration of the plateau at 1773 K, at which Cs is meant to be released, was chosen in order to limit this FP release and study the involved intermediary compound.

Finally, samples R1700 and O1700 were annealed up to 1973 K for 10 min under reducing and oxidizing atmosphere, respectively, without any intermediary temperature plateau. This final temperature and its duration were chosen in order to study FP behaviour at high temperature but attempting to limit Cs release.

4.2.2. Characterization methods

4.2.2.1. Irradiated Fuels

Irradiated fuel samples were characterized at the LECA-STAR facility, Cadarache centre. Characterizations performed include Secondary Ion Mass Spectroscopy (SIMS), Electron Probe Micro Analysis (EPMA), X-ray Diffraction (XRD), Scanning Electron Microscopy (SEM) and Optical Microscopy (OM).

Sample T_0 -IF was characterized through SIMS, EPMA, SEM and OM; sample IF1500 was characterized by SEM and EPMA and finally sample VERDON 1 was characterized by XRD, SEM and OM.

4.2.2.2. SIMFUEL samples

All SIMFUEL samples were characterized by SEM at the *Laboratoire Bernard François*, Cadarache, and by X-ray Absorption Spectroscopy (XAS) at the MARS beam-line, Soleil Synchrotron. Samples Set I, already described in Chapter 3 were also characterized by XRD but results were not exploited since the uranium diffraction lines masked those of the other chemical phases. Regarding XAS analyses, a total of five analysis campaigns were performed at the MARS beamline with different objectives for each SIMFUEL sample set. Particularly for samples from set I, acquisitions were performed at the K absorption edges of Mo (20000 eV), Ru (22117 eV), Zr (17998 eV) and Y (17038 eV) and at the L3 edges of U (17166 eV) and Ce (5723 eV). Ba L3 HERDF-XANES spectra were collected also at the L3

absorption edge (5247 eV). Regarding samples sets II and III, the Mo K and Cs L3 (5012 eV) absorption edges were analysed.

4.3. Experimental results comparison

Five different FP were studied during this work with the objective being to identify their behaviour in irradiated nuclear fuel samples, when submitted to high temperatures and oxidizing and reducing conditions. In this section the results obtained both in the irradiated fuels and model material samples will be compared to the proposed release mechanism and own thermodynamic estimations. Results will be discussed according to the observed association. Firstly, Ba and Zr interaction is discussed, followed by that of Ba and Mo, then Cs, U and Mo and finally Mo and Ru. Conclusions on FP initial chemical states and their evolution are also made in each sub-section.

4.3.1. Barium and zirconium

According to our thermodynamic estimations Ba and Zr should be present as BaZrO_3 in the range of 573 to 1773 K, in reducing conditions. SIMS and EPMA analyses performed on the irradiated T_0 -IF fuel sample, representative of a nuclear fuel in normal operation conditions of a commercial PWR, did not show although the presence of any Ba or Zr precipitate. It has been reported in bibliography that these precipitates, if they exist, are hard to detect by normal light-optical observations due to its poor contrast with the surrounding fuel, although they have been observed in Fast Reactors fuel pins (Kleykamp, 1985). On the contrary, such precipitates were observed on a similar sample which has been submitted to an annealing test up to 1773 K in reducing conditions (IF1500 sample). The latter precipitates were evenly distributed all over the sample, both at the centre and periphery. Particularly, it was observed an accumulation of Ba close to the periphery, at the fuel-cladding interface. Regarding SIMFUEL samples, this Ba-Zr association is already observed in samples from the very beginning, before any annealing test was performed. Besides Ba and Zr, other FP such as Sr, Ce and Y were also observed to be present in these precipitates. XAS analyses performed on samples from set I confirmed the BaZrO_3 chemical form. Indeed, Ba oxidation state and Zr local environment match that of BaZrO_3 . Taking into consideration the following facts regarding our irradiated fuels samples:

- The T_0 -IF irradiated fuel was submitted to six irradiation cycles (the maximum number of cycles to which nuclear fuel are submitted in commercial PWR) attaining a burn-up of 72 GWd.t^{-1} and so the FP concentration in this sample is the maximal concentration that can be attained;
- No Ba precipitates were observed even at the periphery of the fuel where the local burn-up is higher (150 GWd.t^{-1} in the case of the E04 sample);
- Ba precipitates were observed in an irradiated fuel sample after an annealing test at 1773 K, and they were also observed in FR fuel pins (Kleykamp, 1985), which operate at a higher temperature compared to PWR.

It is assumed then that the UO_2 matrix is capable of dissolving large amounts of Ba but it precipitates when submitted to high temperatures. The precipitation temperature would range from around 1373 K (temperature at the centre of a PWR fuel pellet) and 1773 K (temperature at which these

precipitates were observed). The reason why BaZrO₃ precipitates are early observed in SIMFUEL samples is related to their fabrication process: As described in **Appendix III**, the SIMFUEL samples fabrication process includes a sintering stage at 1923 K under reducing atmosphere. Then, these samples are already submitted to a first annealing sequence at a temperature higher to that of the hypothetical precipitation range, inducing the formation of BaZrO₃ precipitates.

Though Ba initial chemical state in SIMFUELS samples is therefore not representative of the initial state observed in irradiated nuclear fuels, these samples allow to study Ba behaviour at high temperatures. Indeed, the reduction of BaZrO₃ precipitates O1700 and Ba/Zr ratio at 1973 K under reducing atmosphere (sample AT from set I) would imply a partial destruction of this phase. XAS analyses demonstrated that Ba oxidation state did not change at the studied temperature, meaning that if the intermediate compound is still present in the sample it would be BaO (with Zr remaining as ZrO₂). Observation performed on the VERDON 1 sample would confirm this behaviour. Indeed, it was observed through on-line gamma spectrometry that this FP release started at around 2073 K (reducing atmosphere), attaining a final released fraction of 80% of Ba initial inventory at 2873 K. Only a few Ba precipitates were detected during the post-test examinations performed on this sample, but no longer in association to Zr. The cladding would also play a very important role. Indeed, if Ba reacts with the Zr produced by the fission of U atoms, then it can also react with the Zr from the oxidized cladding. The cladding would then act both as a chemical and a physical barrier, hindering Ba release, as it was observed in the irradiated fuel IF1500 sample.

Ba and Zr behaviour in oxidizing conditions could only be studied in SIMFUEL samples during this work. It was observed that the initial phase, BaZrO₃, interacts with oxidized Mo to form BaMoO₄ at least at 1473 K (sample O1200 from set III). Quantitative analyses performed on the matrix of this sample and on that of the sample annealed at 1973 K also in oxidizing conditions (sample O1700), indicate that Zr would dissolve in the fuel matrix, possibly as ZrO₂ which is highly soluble in UO₂ (Piluso et al., 2005). Zr was no longer found associated to Ba in the oxide precipitates observed in sample O1700. Similar annealing tests on irradiated fuel samples would be required in order to verify this behaviour.

4.3.2. Barium, molybdenum and ruthenium

Barium and molybdenum associations were only observed in SIMFUEL samples submitted to oxidizing conditions. Indeed, two different precipitates containing mainly Ba, Mo and Sr were observed through SEM-EDS analyses performed on sample O1200, submitted to 1473 K. These precipitates differed in shape and composition. On one hand, some precipitates presented a similar Mo to (Ba+Sr) atomic ratio and on the other hand, precipitates presented a Mo concentration five times higher than that of (Ba+Sr). Only one type of oxide precipitate is observed in the sample submitted to 1973 K under oxidizing conditions (sample O1700 from set III), which are similar in shape to those of high-Mo concentration observed at 1473 K. Quantitative analyses performed on these precipitates show a Mo/(Ba+Sr) ratio equal to 5.7 and traces of Ru and Zr. XAS analyses show that, in the sample annealed at 1473 K, oxidized Mo is present under the following chemical forms: MoO₃, MoO₂ and MoO₄²⁻. Regarding sample O1700, XAS analyses indicate that no more molybdates are present and the Mo oxidized forms are MoO₂ and MoO₃. These results lead to make the following conclusion: The precipitates observed in sample O1200, containing a Mo to (Ba+Sr) ratio equal to 1 would be composed of BaMoO₄ and SrMoO₄ (which are predicted by our thermodynamic

estimations) while the others would be composed mainly of MoO_2 and MoO_3 , with some dissolved Ba and Sr oxides (or even molybdates). Since only one type of Mo oxide precipitates are observed in the O1700 sample and no more molybdates are present, the chemical form would be MoO_2 and MoO_3 , with dissolved Ba and Sr oxides. XAS analyses using micro-focussed beams are required in order to validate these assumptions.

4.3.3. Caesium, uranium and molybdenum

In order to determinate Cs initial chemical state in irradiated fuels, EPMA and SIMS analyses were performed on the irradiated fuel sample T_0 -IF. Though no precipitates were observed through SIMS analyses, many precipitates were observed through EPMA ones. Mo and U X-ray maps did not show any particular association to Cs. These results imply that, at least in the T_0 -IF sample, Cs_2MoO_4 (predicted by own thermodynamics estimations) is not created during irradiation. On the contrary, the absence of U-Cs association does not mean that Cs_2UO_4 is not present. Indeed, since these precipitates are surrounded by UO_2 , the U signal from the matrix would mask that of the U in the Cs_2UO_4 precipitates. Determining Cs early chemical form was one of the main objectives of the analyses performed on the implanted samples. Many Cs precipitates were observed through SIMS analyses of the T_0 -R sample, though no association to Mo, U or any other FP could be identified.

Cs behaviour at higher temperatures was studied both in irradiated fuels and SIMFUEL samples. EPMA analyses performed on the IF1500 irradiated fuel sample (annealed at 1773 K in reducing conditions) showed that Cs and Xe were usually located together. This result would imply that, whatever the initial Cs chemical form was, it was decomposed and Cs behaved as a gas, diffusing through the porosity of the fuel along with Xe. XAS analyses performed both at the Mo K and Cs L_3 absorption edges on implanted SIMFUEL samples annealed in reducing conditions would indicate that Cs is present under the Cs_2UO_4 , at 1473 and 1773 K in reducing conditions. Nevertheless, this chemical form is believed to have been created as a consequence of ions implantation and not to thermodynamic equilibrium. Indeed, according to thermodynamic estimations Cs_2UO_4 would only exist at very reducing conditions, which were not attained during annealing tests. Cs abnormal chemical state after implantation persisted in oxidizing conditions, even at 1473 K. No more Cs was detected in SIMFUEL samples submitted to 1973 K and in the VERDON 1 sample.

4.3.4. Molybdenum and ruthenium

Mo and Ru precipitates were observed both in irradiated fuel (along with Tc, Pd and Rh) and in SIMFUEL (along with Pd and Rh) samples. XAS analyses performed on SIMFUEL samples from set I confirmed the metallic state of Mo and Ru. It was observed that the initially homogeneous metallic phase underwent a significant modification at high temperature. Indeed, the separation of this phase was observed at 1773 K and three different metallic phases were created, ones very rich in Mo (more than 80 at.%), other also rich in Mo, but not as much as the first ones (around 65%) and the other with a similar Mo and Ru content (Mo/Ru molar ratio equal to 1). This behaviour is predicted in the Mo-Ru binary phase diagram presented in (Kleykamp, 1989b). Indeed, the observed precipitates correspond to the β (significantly richer in Mo), σ (richer in Mo) and the ϵ (richer in Ru) phases. It was observed that some precipitates richer in Mo presented a concentration of this FP which was higher to that of the β phase solvus line. The latter observation, along with the increased precipitates ECD

and area contributions would imply an improved mobility of Mo at high temperatures, which is higher to that of Ru.

4.4. Comparison between experimental results and the release mechanism

In this section the conclusions made through experimental observations will be compared to the hypothetical FP initial states and evolutions proposed in the release mechanism. Firstly, barium initial state and evolution is compared, followed by that of Mo, Cs and finally Ru.

4.4.1. Barium

(Nicaise, 2004a) mechanism proposes that Ba is initially found as BaO precipitates. It was observed though that Ba remains dissolved in the UO₂ matrix even at very high burn-ups and precipitates only at high temperatures, between 1373 and 1773 K. Since Ba must be oxidized in order to be dissolved in the matrix (presumably as BaO), the proposed initial state is therefore partially validated.

The mechanism also considers that Ba reacts with Zr (both the FP and the one from the oxidized cladding) to form BaZrO₃. This Ba-Zr association has been observed in irradiated fuels and XAS analyses performed on SIMFUEL samples have confirmed this chemical state. It is also considered that BaZrO₃ is destroyed at high temperatures in reducing conditions and Ba is released. Observations performed on SIMFUEL samples are also in good agreement with this proposed evolution, and so the Ba evolution in reducing conditions is validated. Furthermore, experimental observations done on SIMFUEL samples have contributed to understand the behaviour of this FP in oxidizing conditions. Indeed, results obtained indicate that a Mo-Ba compound was created under oxidizing atmospheres, presumably BaMoO₄. This compound was initially considered in the first mechanism proposed by Nicaise in (Nicaise and Ozrin, 2003) but was later abandoned in further investigations (Nicaise, 2004a).

4.4.2. Molybdenum

(Nicaise, 2004a) proposed mechanism considers that Mo is initially present under two different chemical forms. In one hand, as metallic precipitates along with Ru, Rh, Pd and Tc. Similar precipitates have been observed both in irradiated fuels and SIMFUELS samples. Furthermore, XAS analyses at the Mo and Ru absorption edges confirmed the metallic state of Mo and Ru. On the other hand, the mechanism considers that Mo is also present as very small precipitates of MoO₂. XAS analyses performed on SIMFUEL samples representative of an initial state indicate that Mo is only present in metallic state. Nevertheless, the sintering stage of the SIMFUEL fabrication process would not let Mo to be oxidized, which implies a limited representativeness of these samples. Though Mo oxides were not observed in T₀-IF irradiated fuel sample, they could still be present. Indeed, EPMA and SIMS analyses can only determine FP distribution and not they chemical state. Therefore, MoO₂ could share the same location as the metallic precipitates, due to oxidation of Mo in the surface of these precipitates. Therefore, only the existence of Mo in metallic precipitates as proposed in the mechanism is validated, since MoO₂ has not been observed.

The mechanism also considers that oxidized Mo would react with Cs to give Cs₂MoO₄ around 1300 K. As described above this compound was not observed in the irradiated fuel sample, possibly due to the high temperature of the test (1773 K) at which it is supposed to dissociate. The presence of

Cs_2MoO_4 could not be determined by XAS analyses on SIMFUEL samples submitted to oxidizing conditions, since the metastable state created by the ions implantation persisted. The presence of this compound remains uncertain.

Finally, it is considered that, under reducing conditions, Mo is released as $\text{Mo}_{(g)}$. During the VERDON 1 test it was observed that Mo started being released during the cladding oxidation stage but stopped when the atmosphere was switched to reducing. Mo started releasing again at higher temperature (above 2500 K) under this reducing atmosphere. Observations performed on the VERDON 1 sample indicate that Mo is only found in metallic inclusions, implying that it was released directly from these precipitates, under the $\text{Mo}_{(g)}$ form. Besides, it was observed a significant boost of Mo mobility at high temperatures. This FP could then migrate towards the edges of the fuel pellets and be stripped off by the surrounding atmosphere. Therefore, this evolution proposed in the mechanism is validated.

4.4.3. Caesium

(Nicaise, 2004a) mechanism considers that Cs is initially found in precipitates as Cs_2UO_4 (besides other chemical compounds which contain Cs which have already been observed experimentally, such as CsI). Though Cs precipitates were observed in the T_0 -IF and implanted SIMFUEL samples, the other FP involved could not be determined. It was observed that at least initially there is no Cs-Mo association in this sample. As already explained for Mo, at around 1000 K the mechanism considers that Cs_2UO_4 is destroyed and Cs reacts with Mo to give Cs_2MoO_4 . The presence of this compound could not be verified through XAS analyses performed on SIMFUEL samples. Lastly, the mechanism considers that the destruction of these Cs chemical phases starts at around 1373 K. According to the Cs release profile presented in Chapter 2, obtained through on-line gamma spectrometry during the annealing tests performed on the IF1500 irradiated fuel sample, Cs release started at 1273 K and by 1773 K a total released fraction of 47% was attained. Since an accurate determination of Cs initial state and the intermediate compounds could not be performed, Cs chemistry in UO_2 remains uncertain.

4.4.4. Ruthenium

(Nicaise, 2004a) mechanism considers that most Ru is initially present in metallic precipitates along with Mo, Rh, Pd and Tc. It also considers that a small fraction of Ru is found in oxidized form. Observations performed in the E04 sample allowed to verify the initial distribution Ru-Mo-Pd-Rh-Tc and XAS analyses performed on SIMFUEL samples confirmed the metallic state of Ru. Nevertheless, no Ru oxides were observed to be present in SIMFUEL samples, though the mechanism states that these species would be created as a consequence of irradiation or in very oxidizing conditions. The proposed initial chemical state of Ru is then partially validated. Regarding Ru behaviour in oxidizing conditions at high temperatures, it was observed that traces of this FP were present in the oxide precipitates of SIMFUELS samples of set III which would imply the partial oxidation of this FP. XAS analyses at the Ru K edge would be required to accurately determine Ru chemical state.

4.5. Summary of validated and refuted chemical phases

Results obtained in both experimental axes have allowed to validate or refute most hypotheses made in the original (Nicaise, 2004a) release mechanism though some uncertainties still remain (highlighted in green, red, and orange respectively, in **Figure 96**). As observed, the remaining uncertainties are mainly related to the initial state of FP (highlighted in orange). The main reason for this is that the current characterizations techniques available for irradiated fuels allow determining FP distribution and associations but not their chemical state. Particularly for Ba, it was observed that precipitates of this FP do not exist in an irradiated fuel sample in normal operation conditions, even at very high burn-up (150 GWd.t^{-1}). Instead, this FP remains dissolved in the fuel matrix and may precipitate under the effect of temperature, between 1100 and 1773 K. If this FP is dissolved in the matrix, then it is forcefully under an oxidized form, such as BaO. Another main uncertainty is Cs overall behaviour in UO_2 . Indeed, though precipitates of this FP were observed in an irradiated fuel sample, the other FP to which it was associated could not be identified. XAS analysis aiming at determining its evolution as a function of temperature and atmosphere were not conclusive, since a metastable state was created through ion implantation. Regarding Mo and Ru, these FP were always observed together in the irradiated fuel sample, along with Pd, Rh and Tc. If Mo and Ru oxides are present in an irradiated nuclear fuel in normal operation conditions, they could be located next to the metallic precipitates. It must be kept in mind, though, that the mechanism was initially proposed for LWR moderate burn-up irradiated fuels (around 40 GWd.t^{-1}), while only high burn-up samples (72 GWd.t^{-1} for irradiated fuels and 76 GWd.t^{-1} for SIMFUELS) have been studied in this work.

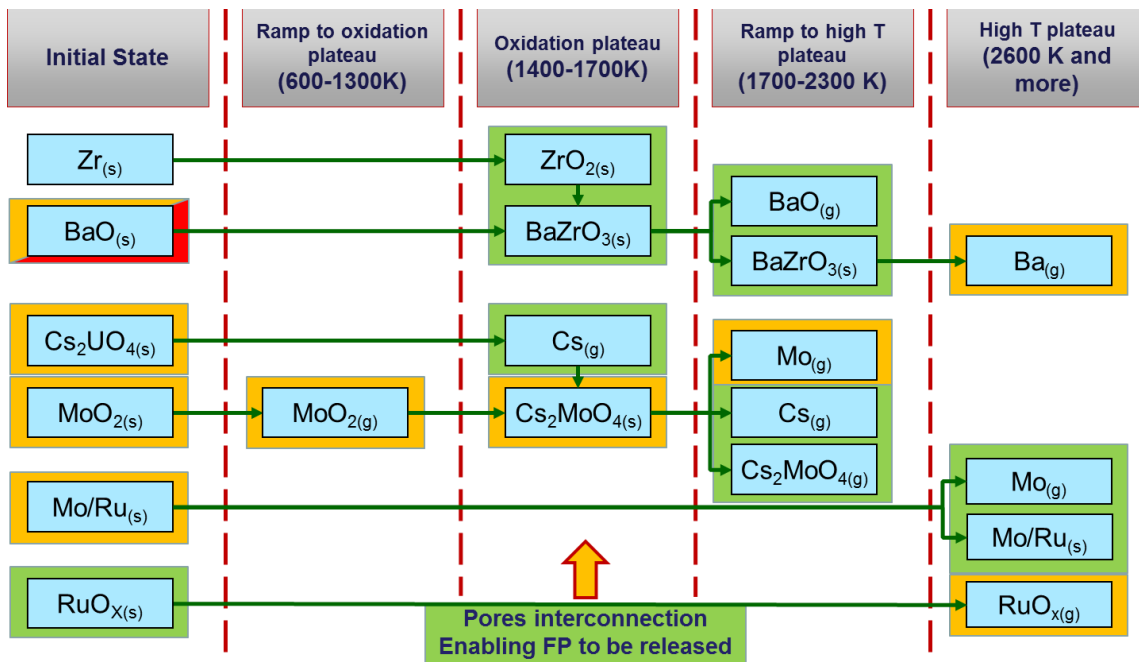


Figure 96: Release mechanism indicating the validated (green), refuted (red) and unanswered hypotheses (orange)

4.6. Modified release mechanism

Experimental observations done on irradiated fuels and SIMFUEL samples have allowed to propose a new release mechanism, considering both reducing and oxidizing conditions. The mechanism

proposed here is based on a VERDON type annealing sequence and considers the same stages considered in the mechanism presented in Chapter 1:

- An initial state, which is an irradiated nuclear fuel in normal operation conditions of a PWR,
- An intermediate stage at 1300 K under neutral atmosphere,
- An intermediate state between 1400 and 1800 K, under oxidizing atmosphere (oxidation plateau),
- A temperature ramp from the oxidation plateau up to around 2600 K,
- A high temperature plateau, around 2600 K.

Some hypotheses of the original release mechanism, which could not be completely validated, have been incorporated here. These assumptions are the existence of Cs precipitates in the initial state, as Cs_2MoO_4 , and its retention by reaction with MoO_2 to form Cs_2MoO_4 .

4.6.1. Initial state

The initial state considered here, represented in **Figure 97**, is similar to that of the initial mechanism presented in Chapter 1 with the exception of Ba. Indeed, experimental observations demonstrated that Ba can remain dissolved in the matrix even at high concentrations. Therefore, the initial precipitates are Cs_2UO_4 , MoO_2 , the intermetallic composed of Mo, Ru, Pd, Rh and Tc, known as white inclusions. Though not observed experimentally, Ru oxides are also considered to be present. The volatilization of these oxides, considered to be created during irradiation, would be responsible of the few percent of Ru release observed in analytical tests using irradiated fuel samples in reducing temperature (Pontillon and Ducros, 2010c).

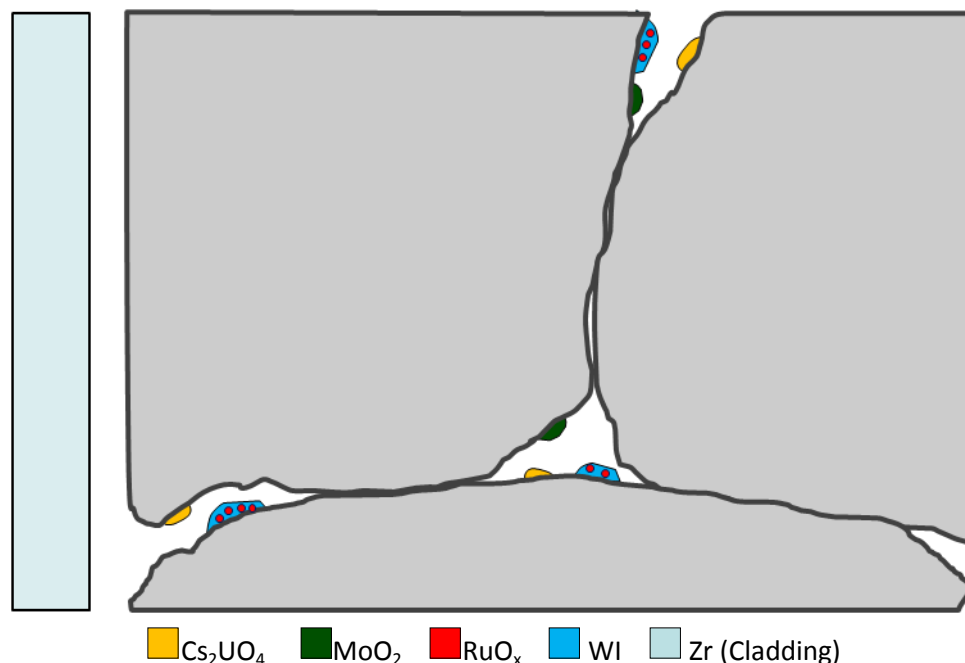


Figure 97: Representation of the Initial state, new release mechanism

4.6.2. Stage at 1300 K

As considered by the initial mechanism, MoO₂ are believed to volatilize at 1300K. Nevertheless, Mo is not released yet since the pores are not interconnected. This stage is represented in **Figure 98**.

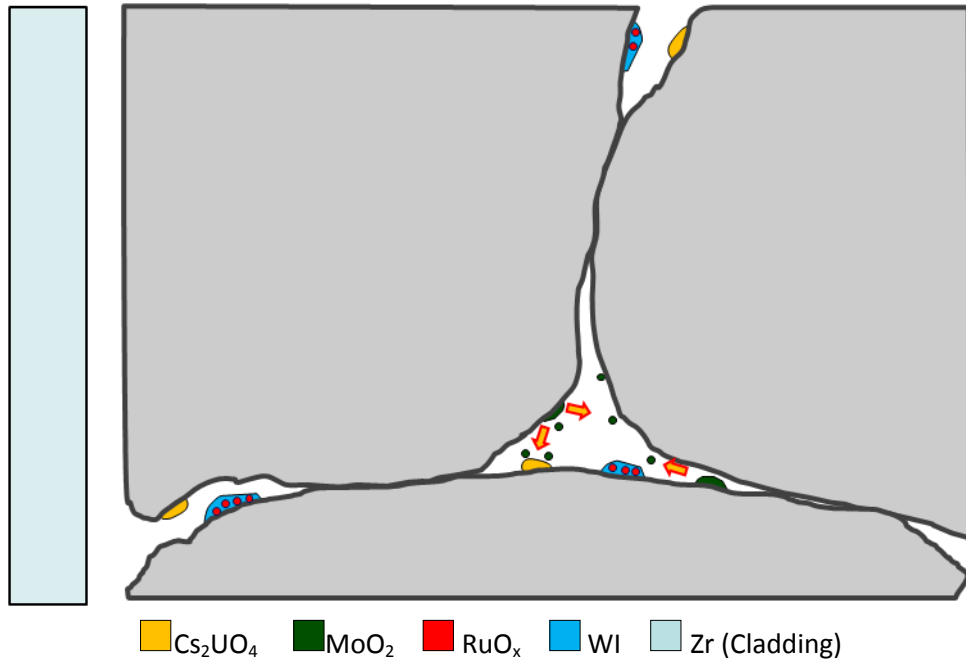


Figure 98: Representation of the stage at 1300K, new release mechanism

4.6.3. Oxidation Plateau

This stage, represented in **Figure 99**, considers a temperature evolution from 1400 to 1800 K under oxidizing atmosphere. This stage is normally implemented in VERDON type tests in order to oxidize the cladding so temperature can still be increased. Otherwise, the cladding could interact with the UO₂, even from around 1400-1500 K. As observed in the SIMFUEL experimental axis, at 1473 K and under oxidizing temperature Mo oxide precipitates were formed. These precipitates also contained Ba, and according to our thermodynamic estimations the chemical compound would be BaMoO₄. Experimental observations demonstrated that Ba precipitates between 1100 and 1773 K, as BaZrO₃. The oxidized Zr from the cladding could also react with Ba, and BaZrO₃ would be formed on the fuel side of the cladding. A partial interconnection of the pores was observed after the test in which the irradiated fuel sample was submitted to 1773 K under reducing atmosphere. This interconnection would enable the gaseous species to be released from the fuel. As Mo oxidizes from the metallic precipitates, it would start reacting with BaZrO₃ precipitates to form BaMoO₄. Regarding Cs, it is considered that the initial chemical form, Cs₂UO₄, is partially destroyed and Cs starts to be released as gas. Nevertheless, most Cs would react with MoO₂ to give Cs₂MoO₄, a less volatile species, and the release of this FP stops. The reaction taking place during this stage would be:

Oxidation of Mo present in the metallic precipitates, according to **Reaction 4.1**:



Destruction of Cs₂UO₄ and reaction with MoO₂, according to **Reactions 4.2** and **4.3**:



Precipitation of Ba as BaZrO₃ and reaction with MoO₂ giving BaMoO₄, according to **Reactions 4.4** and **4.5**:

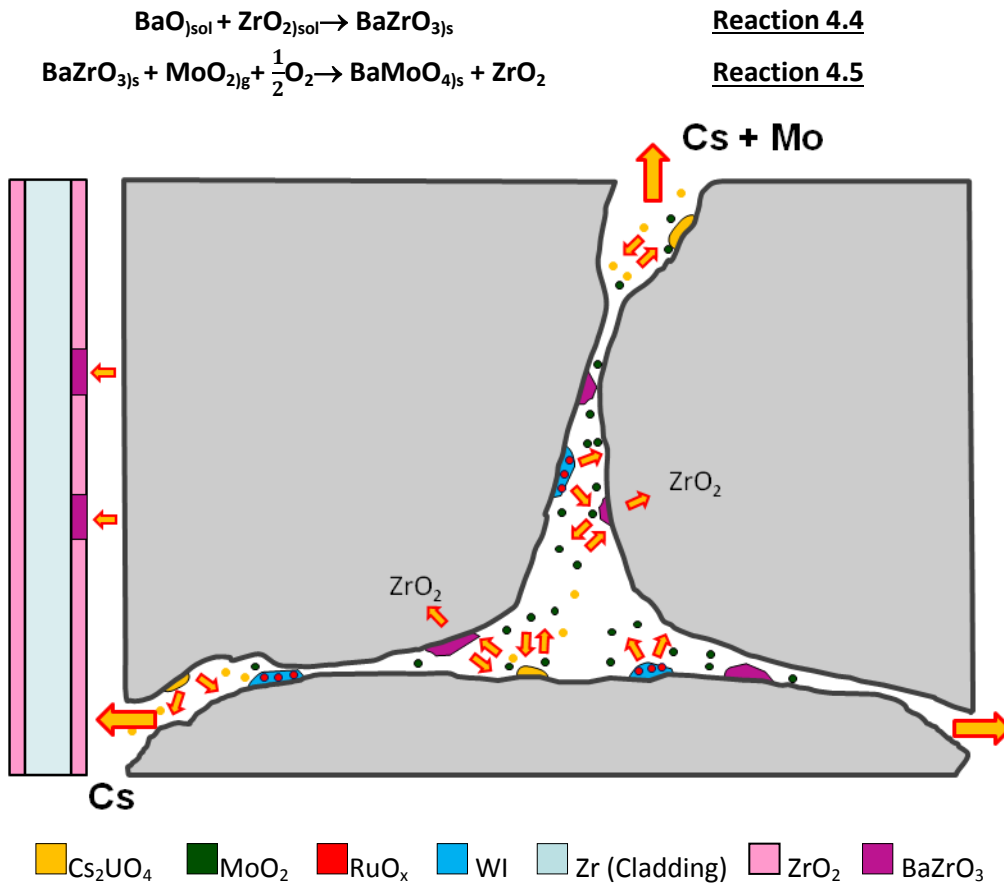


Figure 99: Representation of the oxidation plateau, from 1400 to 1800 K, new release mechanism

4.6.4. Ramp to high temperature plateau

At this point two different scenarios are considered, one in which the atmosphere is switched to reducing, the other in which the atmosphere remains oxidizing.

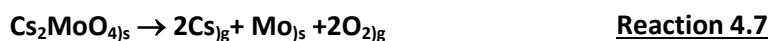
4.6.4.1. Reducing atmosphere

In this case it is considered that the atmosphere is switched to reducing right after the oxidation plateau (an atmosphere not reducing enough as to reduce the ZrO₂ from the cladding). In such scenario the existing MoO₂ would be reduced and would return back to the white inclusions. The Cs₂MoO₄ formed during the oxidation plateau would be partially destroyed but it would also volatilize, leading to the release of both Cs and Mo, under the Cs_g and Cs₂MoO_{4g} forms. As observed in tests performed on SIMFUEL samples under reducing atmosphere, BaZrO₃ is partially destroyed in these conditions and Ba is released as BaO_g. The reactions taking place in this stage would be:

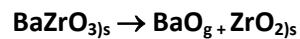
Reduction of MoO₂, according to **Reaction 4.6**:



Destruction of Cs₂MoO₄ and volatilization, according to **Reactions 4.7** and **4.8**:



Destruction of BaZrO₃, according to **Reaction 4.9**:



Reaction 4.9

The evolution proposed in this stage is represented in **Figure 100**.

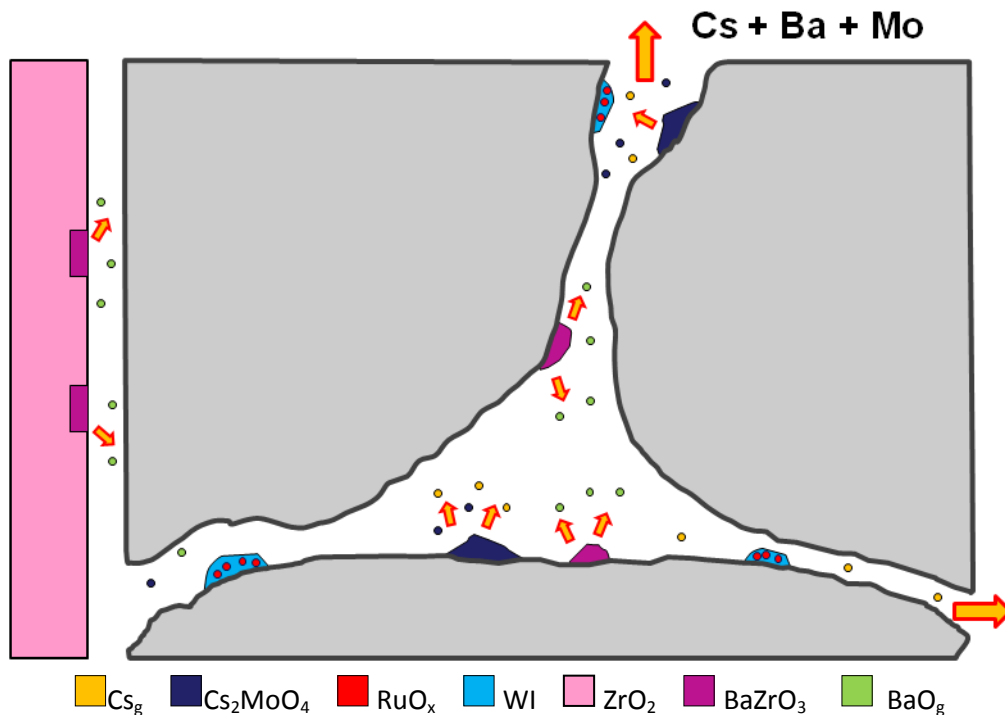
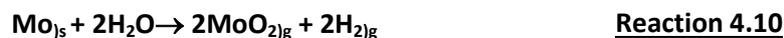


Figure 100: Representation of the ramp to high temperature plateau under reducing atmosphere, new release mechanism

4.6.4.2. Oxidizing atmosphere

During the ramp and under oxidizing atmosphere Mo would keep oxidizing from the metallic precipitates. Some Ru would also be oxidized but in a very lower proportion than Mo. Mo would be released as MoO₂ and would be partially dissolved in the existing oxide precipitates as well. Cs₂MoO₄ would be partially destroyed and volatilized, leading to the release of Mo and Cs. The reactions taking place in this stage would be:

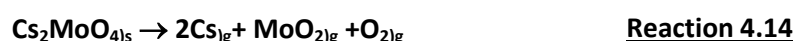
Oxidation of Mo and Ru in the metallic precipitates, according to **Reactions 4.10 and 4.11**:



Dissolution of Mo and Ru oxides in the oxide precipitates, according to **Reaction 4.12**:



The volatilization and partial destruction of Cs₂MoO₄, according to **Reactions 4.13 and 4.14**:



The evolution proposed here is represented in **Figure 101**.

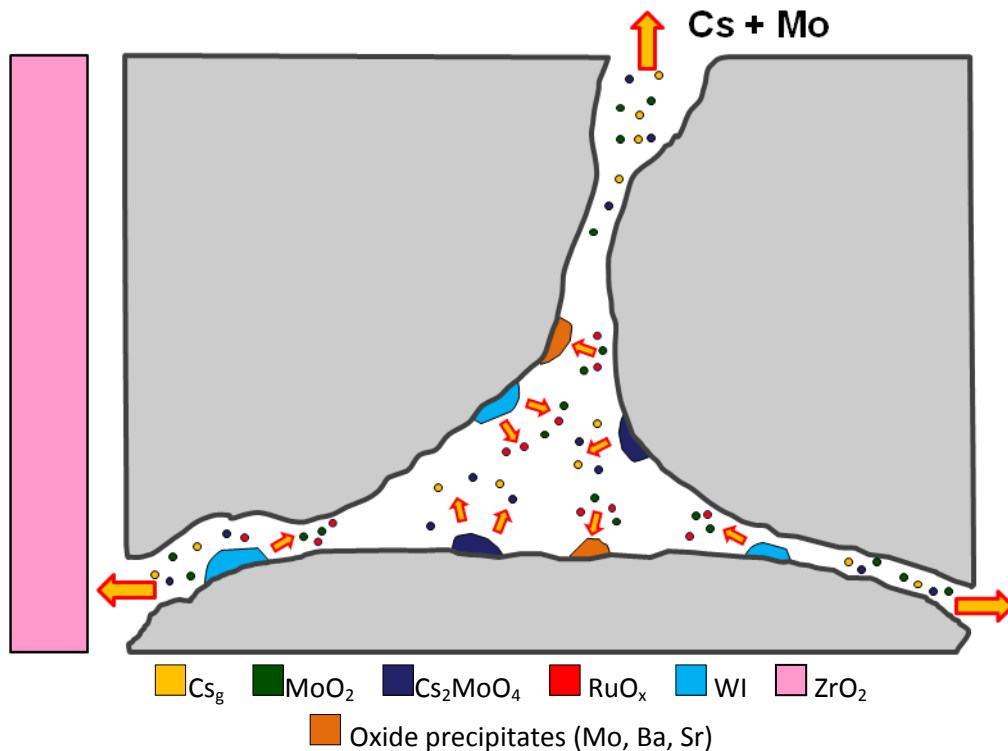


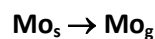
Figure 101: Representation of the ramp to high temperature plateau under oxidizing atmosphere, new release mechanism

4.6.5. High temperature plateau

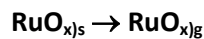
4.6.5.1. Reducing atmosphere

At the high temperature plateau (2600 K and more) under reducing atmosphere, the destruction of BaZrO_3 would continue and Ba would be released as BaO_g . Most ZrO_2 produced during the temperature ramp and this stage would dissolve back into the fuel matrix. Mo would be volatilized as Mo_g and be released, along with the Ru oxides. The reactions taking place in this stage would be:

Volatilization of Mo and Ru oxides, both present in the metallic precipitates, according to **Reactions 4.15** and **4.16**:



Reaction 4.15



Reaction 4.16

Destruction of BaZrO_3 , producing BaO_g (or Ba_g , depending on the reducing character of the atmosphere) which is released and ZrO_2 which is dissolved in the matrix (along as the ZrO_2 from the oxidized cladding), according to **Reactions 4.17** and **4.18**:



Reaction 4.17



Reaction 4.18

This evolution is represented in **Figure 102**.

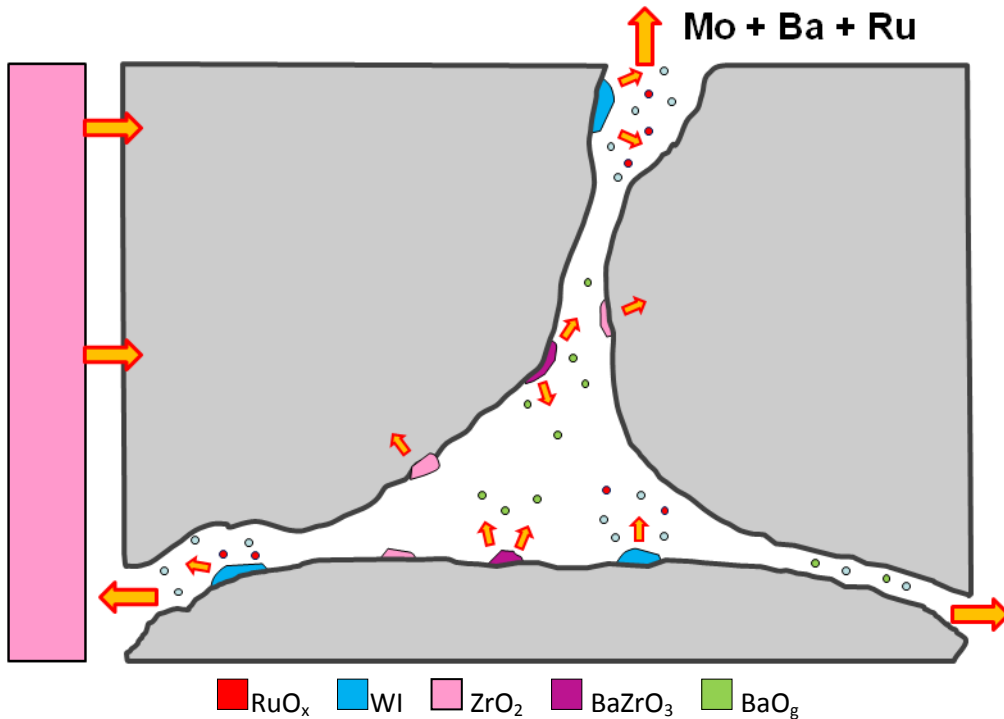


Figure 102: Representation of the high temperature plateau under reducing atmosphere, new release mechanism

4.6.5.2. Oxidizing atmosphere

During the high temperature plateau, under oxidizing atmosphere, Mo and Ru would keep being oxidized from the metallic precipitates and their released would continue. As observed during the VERCORS 5 test presented in Chapter 1, which was performed under oxidizing atmosphere, Ba release started during the high temperature plateau. This could be explained by the volatilization of BaMoO₄ from the oxide precipitates. Then, the reactions taking place during this stage would be: Oxidation of Mo and Ru located in the metallic precipitates, according to **Reactions 4.10** and **4.11**:



Volatilization of BaMoO₄ present in the oxide precipitates, according to **Reaction 4.19**:



This evolution is represented in **Figure 103**.

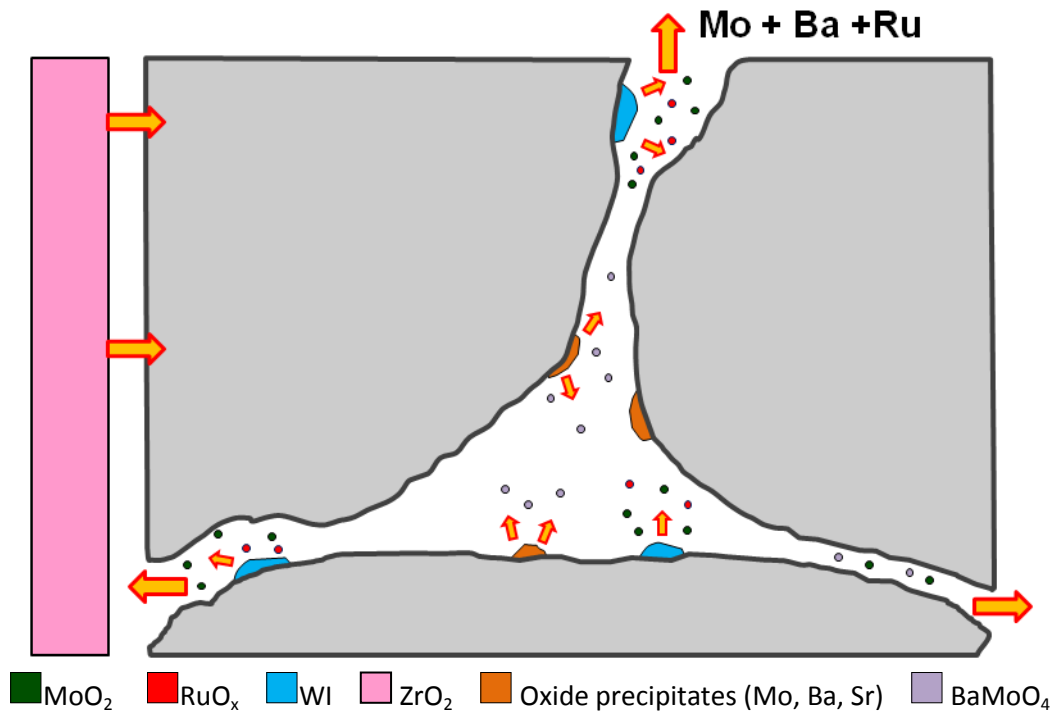


Figure 103: Representation of the high temperature plateau under oxidizing atmosphere, new release mechanism

The proposed evolution here would explain the behaviour observed in different tests using irradiated fuels, though it incorporates some assumptions proposed in the original mechanism, which require further experimental validation. These assumptions are the initial state of Cs as Cs₂UO₄ and its retention by reaction with MoO₂, as well as the existence of Ru and Mo oxides from the very beginning, assumed to be created during irradiation. Further tests using both irradiated fuels and SIMFUEL samples would be required to validate these hypotheses. Both proposed mechanisms are summarized in **Figures 104** (two last stages under reducing atmosphere) and **Figure 105** (two last stages under oxidizing atmosphere).

The final conclusion of this work and the perspectives are presented in the next and final chapter.

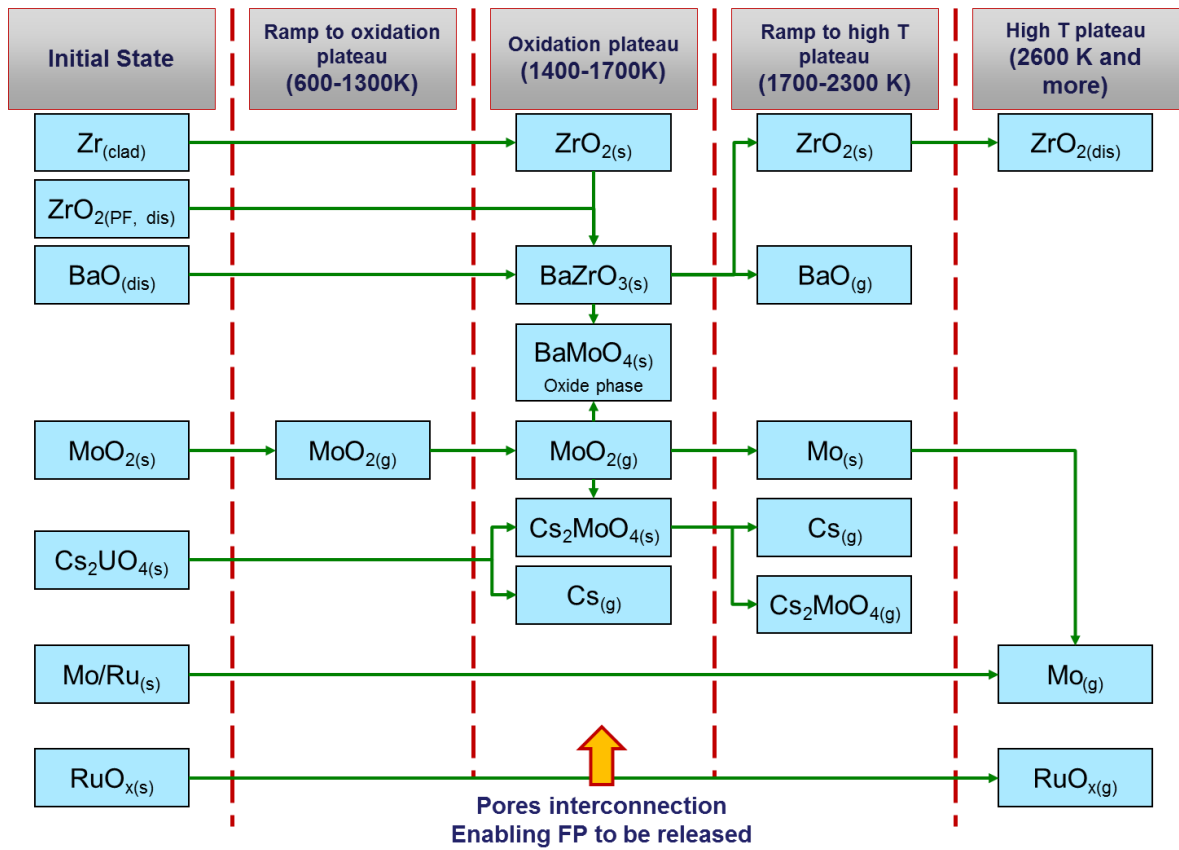


Figure 104: New release mechanism proposed, last two stages under reducing atmosphere

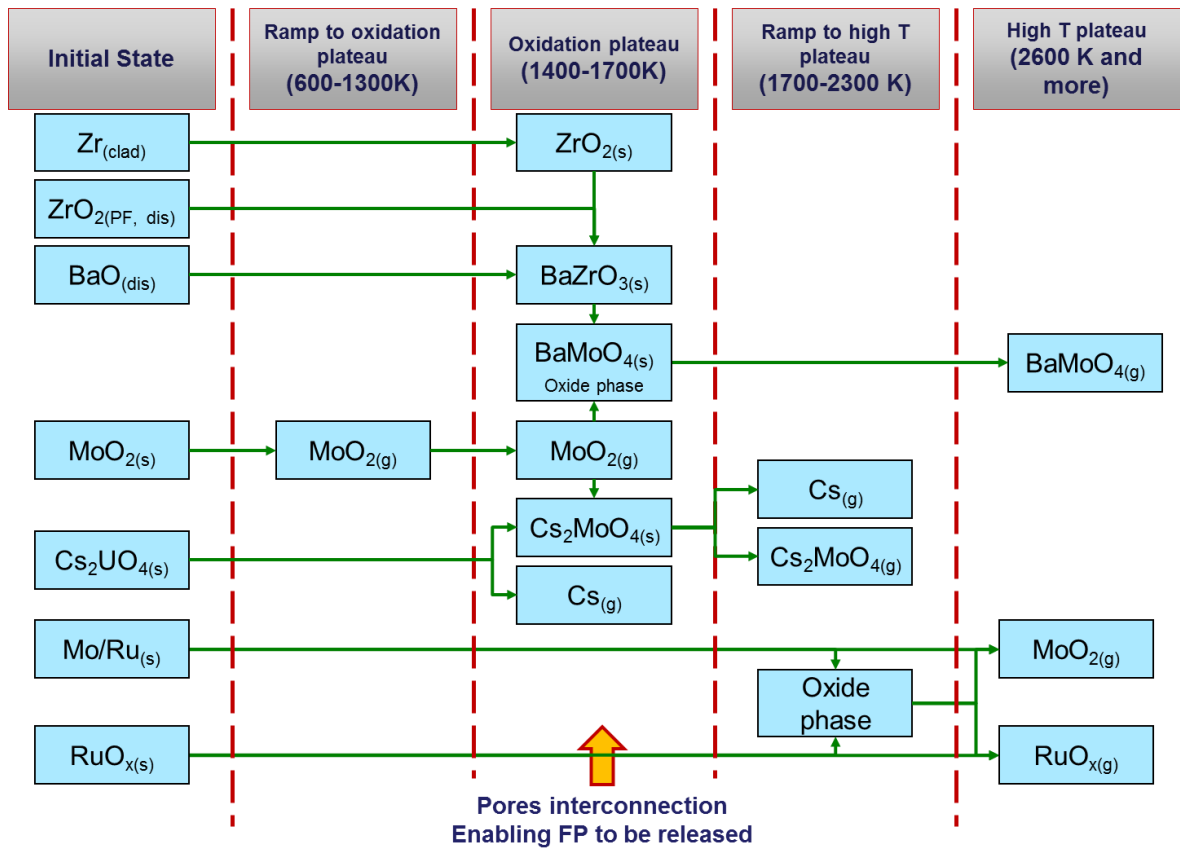


Figure 105: New release mechanism proposed, last two stages under oxidizing atmosphere

Conclusions and Perspectives

5.1. Conclusion.....	161
5.2. Perspectives	161
5.2.1. Annealing tests	162
5.2.2. Characterization	162
5.2.3. Improved samples	162

Conclusion and Perspectives

5.1. Conclusion

In order to study the behaviour of four different FP in irradiated nuclear fuel submitted to nuclear severe accident conditions, two complementary work axes have been implemented. These axes share a similar approach, which is performing annealing tests in conditions representative of nuclear severe accidents in terms of temperature and atmosphere, but differ in the type of samples. The first axis studied the behaviour of FP in irradiated nuclear fuel samples while the second focuses on their behaviour in model materials, representative of irradiated fuels. Though these model materials, known as SIMFUEL, do have some limitations such as the impossibility of reproducing phenomena linked to irradiation (e.g. the high burn-up structure), they allow to perform powerful characterization analyses, yet unavailable for large samples of irradiated fuels. One of such techniques is the X-ray Absorption Spectroscopy, which is element specific and allows identifying the oxidation state and coordination chemistry of an atom. The experimental results obtained in these two axes were compared to a release mechanism proposed in literature, aiming to validate or refute the considered initial chemical states and their evolution.

The original mechanism was modified taking into consideration the results obtained in both work axes, both under reducing and oxidizing conditions. The new mechanism considers the same stages proposed in the original one, which are an initial state (before the severe accident begins) an intermediate state at 1300 K, a temperature ramp followed by an oxidation plateau (from 1400 to 1800 K), a second temperature ramp towards a high temperature plateau (from 1800 to 2600 K) and a final stage which is a high temperature plateau (at 2600 K or more). Two different atmospheres have been considered for these last two stages: reducing (but not as strong as to reduce the oxidized cladding) and oxidizing (but not as strong as to oxidize the UO_2). The proposed evolutions are a combination of experimental observations performed on irradiated fuels and SIMFUELS samples, demonstrating that, despite a limited representativeness (particularly to the initial state), model materials are a very good complement to irradiated fuels in the study of FP behaviour in severe accident conditions. Some question remains unanswered yet, regarding mainly to these four FP initial state in irradiated fuel samples. Since the characterization techniques currently available for irradiated nuclear fuels allow determining their distribution and associations, their chemical state cannot be accurately determined. Nevertheless, characterization techniques available for model materials would provide the missing information, though new model materials, with increased representativeness to irradiated fuels, must be developed.

5.2. Perspectives

As stated above, some questions remain unanswered regarding FP initial state in irradiated fuel samples and their evolution during a severe accident. The required experimental approach and characterization analyses which would allow answering these questions are presented in this section. Particularly, the use of model materials samples fabricated through Spark Plasma Sintering (SPS) is discussed, which would allow to reproduce a microstructure similar to the high burn-up structure (HBS) of irradiated nuclear fuels and analyse volatile FP behaviour such as Cs, without performing an ion implantation on samples.

5.2.1. Annealing tests

The experimental approach adopted in this work proved to be adequate to study most FP initial state and evolution, with the exception of Ru behaviour. Indeed, the mechanism states that Ru is released under very oxidizing conditions which could not be studied in the DURANCE experimental loop. Indeed, according to the Ellingham diagram presented in (Kleykamp, 1985), Ru oxidation would take place at the following oxygen potentials, considering the studied temperatures in the SIMFUEL work axis: $-200 \text{ kJ.mol}_{\text{O}_2}^{-1}$ at 573 K and $-50 \text{ kJ.mol}_{\text{O}_2}^{-1}$ at 1473 K. These very oxidizing conditions would require the use of different, more refractory components of the experimental loop, starting with the crucible which is made of metallic Mo and would be completely oxidized in these conditions. Besides, during nuclear severe accidents the atmosphere is usually more oxidizing than the atmosphere studied in this work. Performing annealing tests under such conditions would also allow verifying the behaviour of FP such as Ba and Mo.

5.2.2. Characterization

A better identification of FP chemical phases could be achieved by performing specific XAS analyses. Indeed, the accurate identification of Mo chemical species observed in samples submitted to oxidizing conditions would require micro XAS analyses. Regarding Cs, in order to determine its initial state in SIMFUEL sample EXAFS spectra should be collected. Such experiments would allow determining if Cs is found as Cs_2UO_4 or Cs_2MoO_4 after implantation and in annealing tests performed at 573 K. Moreover, a better study of FP behaviour could be carried over by performing in-situ XAS analyses, with samples submitted to high temperatures and atmospheres representative of severe accident conditions. A device which would allow such experiments to be performed has been developed at the CEA Cadarache and is currently on a validation stage. In-situ acquisitions would allow following FP evolution in real time.

Another very interesting option would be to combine XPS (X-ray Photoelectron Spectroscopy) and XAS analyses. These techniques are based on the same principle (excitation of core electrons) and are thus atoms specific and provide information about the local structure and electronic structure around individual atomic sites in a system. Performing such techniques on SIMFUEL samples would allow a very accurate characterisation of FP chemical state. A first XPS test has been performed during this work in order to verify its aptitude to determine FP chemical state in SIMFUEL samples (low concentration, in a UO_2 matrix), at the *Plateforme Aquitaine de Caractérisation des Matériaux* (PLACAMAT), Bordeaux, France. The results of this analysis were quite satisfactory, since they demonstrated that most FP could be studied through XPS despite the interference of U atoms. Nevertheless, it was also observed that SIMFUEL samples require a special preparation and handling for these analyses, in order to prevent superficial contamination and/or oxidation, which would lead to abnormal results.

5.2.3. Improved samples

As described in Chapter 3, SIMFUEL samples present some limitations regarding their representativeness to irradiated nuclear fuels. This limitation is directly linked to the fabrication process, which includes a sintering stage at 1923 K under pure H_2 . This sintering stage, which constitutes a first annealing test, has two main back draws. Firstly, it prevents the addition of volatile

FP oxides during the fabrication process since they would be released at the sintering temperature and, secondly, the resulting chemical phases are not representative of the initial state of FP in irradiated nuclear fuels, as it was observed for barium. Adding volatile species to this kind of samples requires performing ion implantations which, as it has been observed in this work, does not reproduce the exact chemical states observed in irradiated fuels but is useful for studying their behaviour at high temperatures.

The use of a different fabrication process would overcome these limitations. Particularly, the SPS process stands out as a promising alternative. This process consist in submitting UO_2 powder doped in many FP to very intense electric currents, fusing the UO_2 fast enough as to prevent volatile FP from releasing. A first characterization of three different samples, prepared using this process at the Institute of Transuranium Elements (ITU, Karlsruhe, Germany) has been carried out during this work. These three samples consisted in UO_2 doped with Cs_2UO_4 , Cs_2MoO_4 and CsI at 1 wt. %, respectively. Through SEM-EDS and XAS analyses it was observed that the volatile species Cs and I remained in the samples and that the obtained UO_2 micro-structure was representative of that of high burn-up fuels.

Appendices

6.1.	Appendix I: The INES scale	167
6.2.	Appendix II: Experimental Research Programs on Fission Products release	169
6.2.1.	Analytical Tests	169
6.2.2.	Integral Test	178
6.3.	Appendix III: SIMFUEL samples preparation	181
6.4.	Appendix IV: Thermodynamic estimations	183
6.5.	Appendix V: Experimental loops	184
6.5.1.	VERDON	184
6.5.2.	MERARG	185
6.5.3.	DURANCE	187
6.5.4.	Tests atmospheres	187
6.6.	Appendix VI: Characterization methods	189
6.6.1.	Optical Microscopy	189
6.6.2.	Scanning Electron Microscope	189
6.6.3.	Electron Probe Micro Analysis (EPMA)	189
6.6.4.	Secondary Ion Mass Spectroscopy (SIMS)	189
6.6.5.	X-Ray Diffraction	190
6.6.6.	X-ray Absorption Spectroscopy	191
6.7.	Appendix VII: Résumé en Français	195
6.7.1.	Contexte de l'étude	195
6.7.2.	Objectif de la thèse et méthodologie	195
6.7.3.	Echantillons analysés	195
6.7.4.	Résultats Obtenus	196
6.7.5.	Nouveaux mécanismes	197
6.7.6.	Conclusions	200

6.1. Appendix I: The INES scale

Nuclear events are classified according to the INES scale (International Nuclear and radiological Event Scale) (AIEA, 2001). As indicated in **Figure 106** (adapted from [IRSN]), this scale categorizes nuclear events in 8 levels, from 0 to 7, in relation to their consequences. Events of **Level 0** are simple deviations from operation conditions, which do not have any importance from a security point of view. **Levels 1 to 3** correspond to nuclear incidents, with limited consequences such as contamination or operators exposure to radiation. **Levels 4 to 7** correspond to nuclear accidents which involve the release of radioactive materials. The TMI-2 accident has been classified as level 5, while the Chernobyl and Fukushima Dai-Ichi accidents have been classified as level 7.

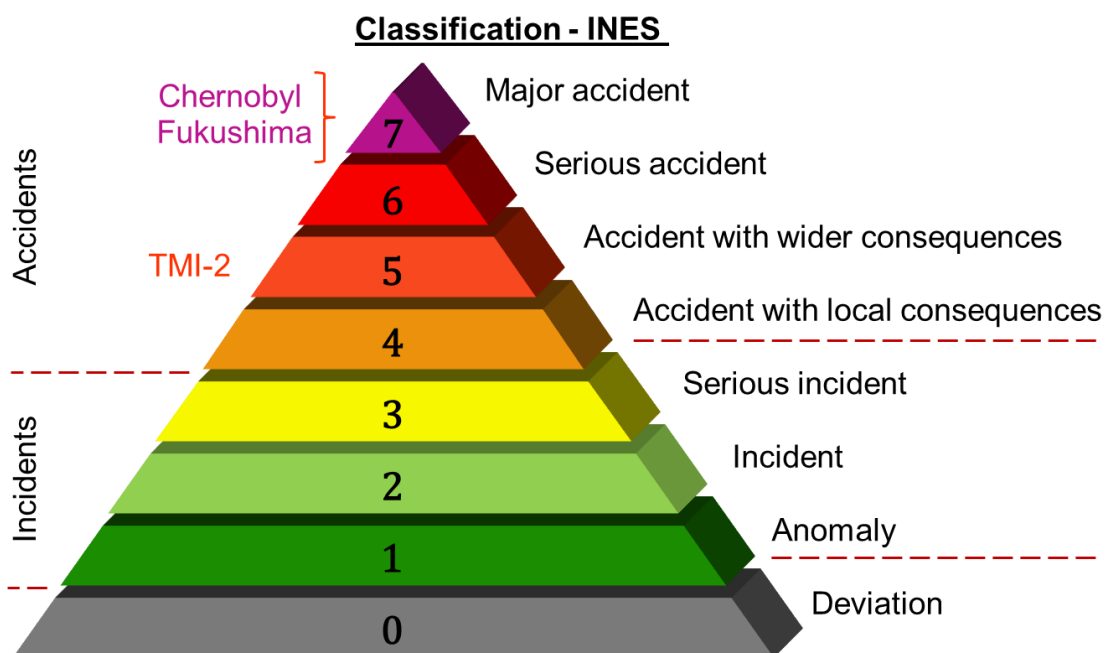


Figure 106: INES scale

Three factors are considered in order to classify the different nuclear events:

- Impact over population and environment, where the radiation doses on the population surrounding the place where event takes place and the unexpected release of materials on a big scale are considered.
- Impact on barriers and radiological controls, which concerns events happening inside facilities and which do not have a direct impact over the population or the environment. The unexpected presence of intense radiation sources and the release of important quantities of radioactive substances inside facilities are taken into account.
- Impact on the in-depth defence for events without a direct impact on the population or the environment, but for which the different measures aiming to prevent the accident did not work as expected.

A description of the consequences of each level on these three factors is presented in **Table 50**, adapted from [IRSN].

		Population and Environment	Barriers and Radiological controls at the Facility	In-depth Defence
7	Major Accident	Major release of radioactive materials with considerable effects on health and environment, requiring implementation of planned mitigation measures or more.		
6	Severe Accident	Important release of radioactive materials requiring implementation of planned mitigation measures		
5	Accident with extended consequences	Limited release of radioactive materials, probably requiring the implementation of some planned mitigation measures. Several radiation induced deaths	Severe damage to the reactor core. Release of major quantities of radioactive materials into the facility with high probability of public exposure. This could result from a critically accident or major fire	
4	Accident with local consequences	Minor release of radioactive materials, not requiring probably the implementation of mitigation measures other than monitoring of local food. At least one radiation induced death	Fuel damage or melting causing the release of more than 0,1% of the core radioactivity. Release of significant quantities of radioactive material within an installation with a high probability of significant public exposure	
3	Severe Incident	Exposure exceeding ten times the statutory annual limit for workers. Non-lethal deterministic health effects (burns, etc.) radiate on-induced	Radiation in a work area exceeding 50mSv.h ⁻¹ . Significant contamination in an area of intended installation will not be contaminated by design.	Narrowly avoided accident in a nuclear power plant with failure of all safety provisions. Loss or theft of high-activity sealed sources. Wrong delivery of high activity sealed source without adequate procedures to deal with.
2	Incident	Exposure of a member of the public exceeding 10 mSv.h ⁻¹ . Worker exposure exceeding the statutory annual limits	Radiation in a work area exceeding 50 mSv.h ⁻¹ . Significant contamination in an area of intended installation does not contaminant by its design.	Significant failures in safety provisions, without real consequences. Discovery of a sealed orphan source, device or package of high activity without adequate procedures to deal with.
1	Anomaly			Overexposure of a member of public above statutory annual limit. Minor problems related to safety components, while maintaining a strong in-depth defence. Loss or theft of a source, device or package of low activity
0	Deviation	No importance in terms of safety		

Table 50: Description of each level defined in the INES scale

6.2. Appendix II: Experimental Research Programs on Fission Products release

6.2.1. Analytical Tests

The main Analytical research programs that have been carried out using irradiated nuclear fuels are the HI/VI program in the USA, the CRL program in Canada, the HEVA and VERCORS programs in France and the VEGA program in Japan. All the tests were performed in hot-cells laboratories and are of reduced complexity than integral programs. As mentioned above, only fuel segments were employed which allowed a parametrical approach. Some tests were performed using fuel segments with and without the original cladding and in some cases samples were re-irradiated before tests, in order to recreate the short lived FP.

6.2.1.1. HI/VI

The HI/VI program (Lorenz and Osborne, 1995) was conducted at Oak Ridge National Laboratory (ORNL) on behalf of the NRC. Initiated in 1981, it continued until 1993. Pioneer in the field, it has long acted as reference

The generic name of this program is related to the different furnaces geometries in which the experiments were conducted. Indeed, the first series of tests (6 tests) were performed in an induction furnace in horizontal configuration (Horizontal Induction Series). Then, in order to eliminate problems related to the flow of the fuel sample and deposition of PF on the walls of the furnace, it was placed in a vertical configuration (Vertical Induction Series). A total of 7 tests have been performed in this configuration.

Sample Characteristics:

A diagram of the fuel samples employed in this program is represented in **Figure 107**. Samples consisted on UO_2 sections of approximately 15 cm long, containing about one hundred grams of oxide. Two Zircaloy plugs were pressed tight on both sides of the samples. Finally, a 1.6 mm diameter hole was drilled into the cladding at mid-height of the sample. This hole constituted a known sealing failure of controlled size, allowing exchange between fluids circulating during the test. Although it did not provide an exchange surface comparable to that of the HEVA/VERCORS samples which had both sides open, it is interesting to note that similar results were obtained on both programs.

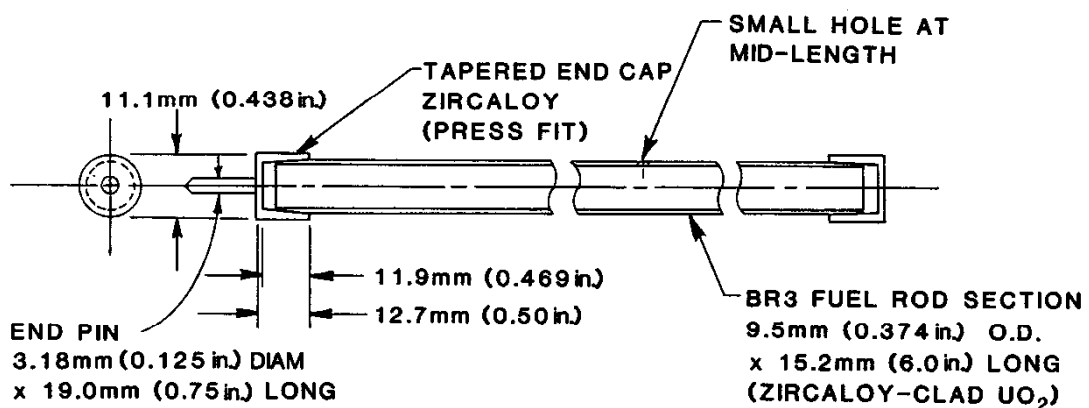


Figure 107: Sample employed on the VI series.

Experimental Loop Characteristics:

In both HI and VI series the furnaces were made of refractory ceramics (ZrO_2 and ThO_2). Thermal insulation was assured by fibrous zirconia and graphite felt.

A diagram of the furnace employed on the VI series is shown in **Figure 108**. **Figure 109** details the test loop.

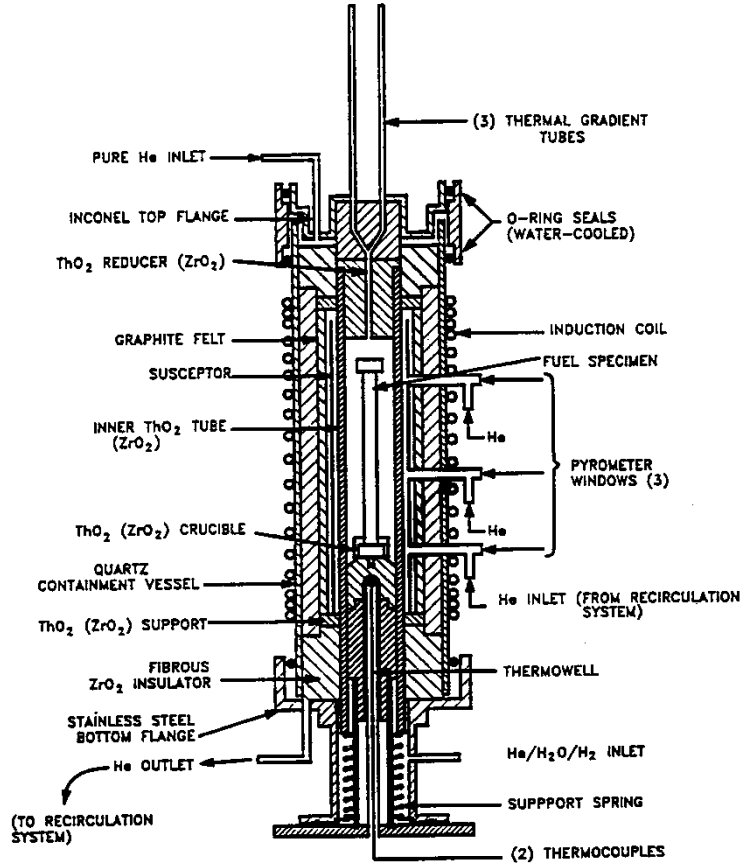


Figure 108: Furnace of the VI series.

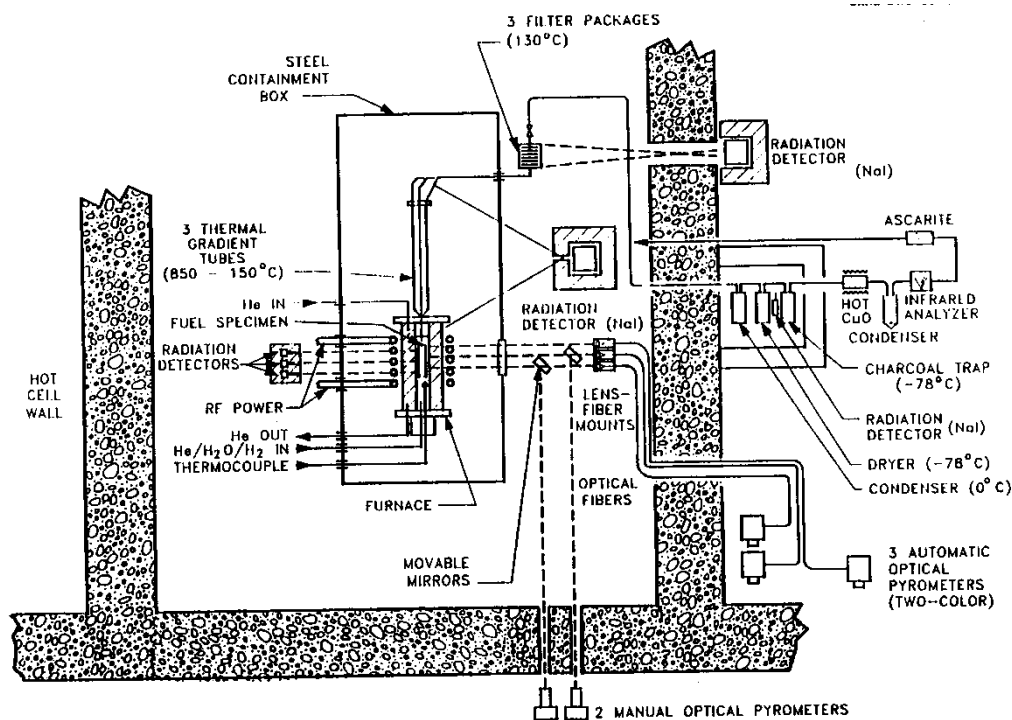


Figure 109: VI Configuration experimental loop.

In the furnace, FP were collected by means of three sequential devices, each one including:

- A temperature gradient tube (TGT) for condensable vapours
- A set of glass fibre filters for aerosols.
- Activated carbon cartridges for trapping volatile forms of iodine and fission gases.

For tests conducted under a steam atmosphere a condenser and a dryer were placed in order to remove the water before condensing the gases in a dry-ice trap.

The temperatures of the fuel rod were measured by bi-chromatic and disappearing filament pyrometers and thermocouples.

Hydrogen generated by the oxidation of the Zircaloy cladding was continuously measured during tests, since the VI-1 test.

NaI detectors provided online measurement of noble gases condensed in the cold traps (^{85}Kr), ^{134}Cs and ^{137}Cs deposited in the TGT and filters. From VI-4 onwards online gamma spectrometry measurement was installed at the bottom and at the top of the fuel, to monitor the possible collapse of the fuel rod.

Since re-irradiation of the fuel samples was not performed, the number of measurable PF was limited only to those of long half-life generated in the PWR. Gamma scans before and after the tests were performed on samples in order to characterize the distribution of detectable FP: ^{125}Sb , ^{134}Cs , ^{137}Cs and ^{154}Eu , as well as ^{106}Ru , ^{144}Ce and $^{110\text{m}}\text{Ag}$ for tests that employed fuel in a short time after extraction from the reactor.

The quantities of iodine deposited on the loop were evaluated by Neutron activation; Sr, Mo, Te, Ba, U and Pu were chemically analysed after rinsing the loop components with acid solutions. From VI-3 onwards, most of these elements were analysed by ICP. Attempts of U and Pu release evaluation were performed by alpha counting. Though these analyses are not as precise as the gamma spectrometry (since they were performed on components and not on the whole loop), they present a good consistency regarding the measurements from the VERCORS tests.

6.2.1.2. CRL

This program was conducted at the Chalk River Laboratories, Canada, from 1983 to 1992. More than 300 tests were performed, being the main objective to study of FP release under an air atmosphere, since this kind of scenario has a rather high probability of occurrence in the Canadian CANDU reactors (Cox et al., 1991; D.S. Cox et al., 1992; Hunt et al., 1986; Iglesias, 1989; Liu et al., 1994). In addition, such scenarios in PWR in severe accidents following the rupture of the lower head, in accidents occurring during fuel assemblies recharges, or accidents involving drying of spent fuel pools.

Sample Characteristics:

Samples were fuel fragments and segments from CANDU or PWR reactors, some of them with a Zircaloy cladding (73% of samples), masses ranging from hundreds of mg to a few grams. Some of the samples had been re-irradiated for several days before the tests.

Experimental Loop Characteristics:

Experimental device used (called MCE) is shown in **Figure 110**. Roughly speaking, the test loop is quite similar in principle to that of the VI and VERCORS series: The central element is a resistance furnace placed in a high activity cell, provided with an on-line gamma detector devoted to measure the FP release kinetics. A second detector was employed to monitor the release of fission gases out of the furnace. The main differences with the fore mentioned programs were the type of samples studied and the continuously controlled Oxygen potential (both at the inlet and outlet of the furnace), using specially developed probes at the CRL.

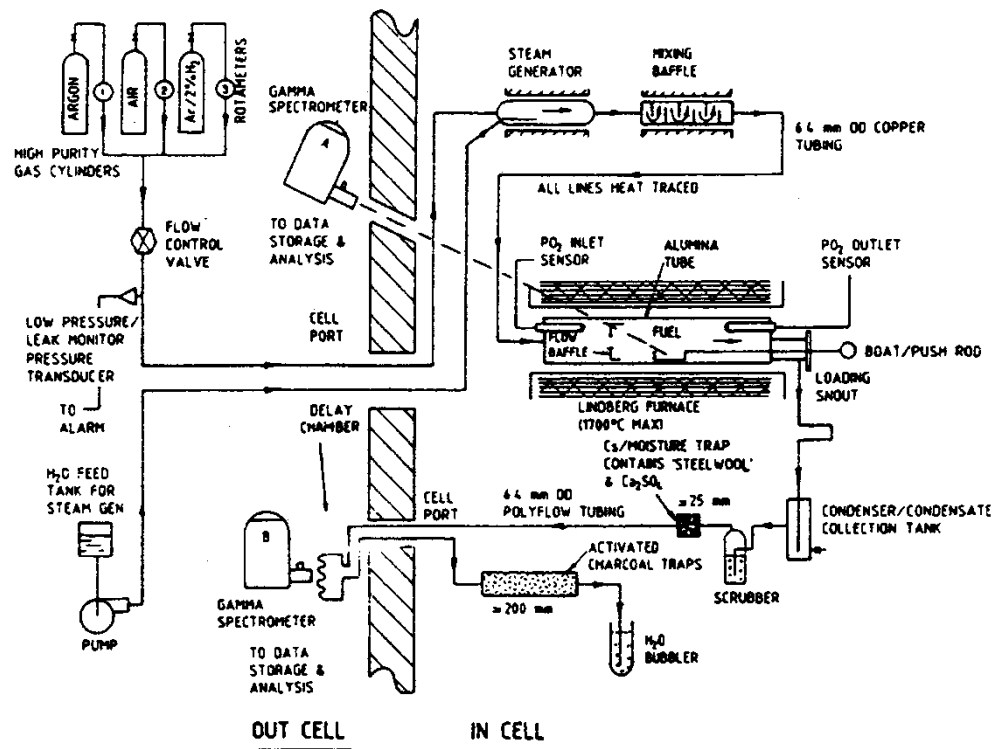


Figure 110: Experimental loop of the CRL series.

6.2.1.3. VEGA

The VEGA program was conducted at the JAEA (Japan Atomic Energy Agency). 10 tests in total were performed from 1999 to 2004 under inert and steam atmospheres. The main feature of this program is the study of FP release and fuel behaviour at high pressure (up to 1 MPa) and temperature (up to

3123 K), being the only program in the world to study such conditions. A model for FP release under pressure effect was developed from these results (Hidaka, 2011).

Sample Characteristics:

The samples were sections of PWR, BWR (both UO₂) and ATR (MOX) fuel about 60 mm long with a mass between 40 g and 100 g, most of them without cladding. Some samples were re-irradiated for 8 h at the Nuclear Safety Research Reactor (NSRR) to generate short-life radionuclides. Since the generated short-life radionuclides were insufficient and the duration of re-irradiation at NSRR could not be prolonged, samples were re-irradiated for 26 days at the Japan Research Reactor No. 3 (JRR-3) in the VEGA-6 and VEGA-7 tests.

Experimental Loop Characteristics:

The VEGA experimental loop is presented in **Figure 111**. It is a highly instrumented loop similar to that of VERCORS HT. It consists mainly of a gas supply system, a high-frequency induction furnace, three sets of thermal gradient tubes (TGTs), aerosol filters, a condenser, a noble gas trap, and a γ -ray measurement system.

The fuel specimen set in the tungsten or ThO₂ crucible is inductively heated to 3150 K (max) in inert or oxidizing atmosphere. The ThO₂ crucible was fabricated by rubber pressing and/or centrifugal slip casting technique through a lot of trial and error due to limited experiences. The bottom of the crucible is measured using pyrometers located below the furnace, which are adjusted so that the measured temperature is equal to the fuel temperature within an error of ± 50 K. The facility can be pressurized up to 1.0 MPa between the gas supply system and the valves just after the aerosol filters.

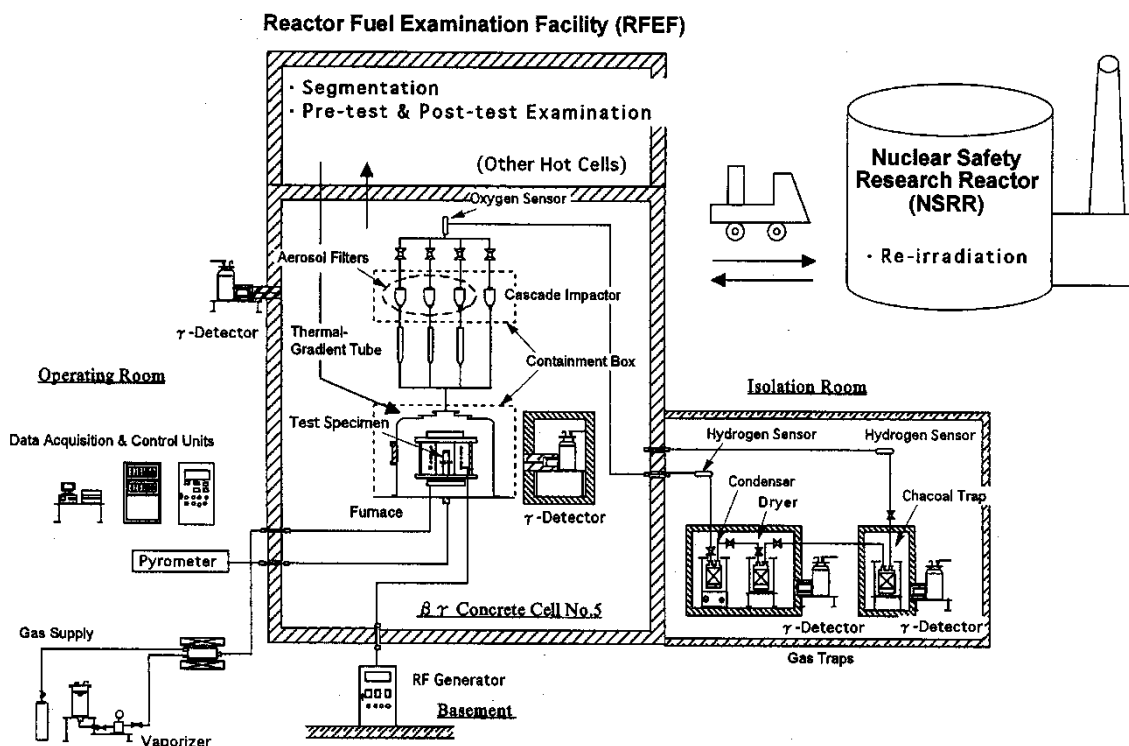


Figure 111: VEGA experimental loop

Experimental Sequence:

The usual typical annealing treatments performed consisted on several temperature plateaux maintained for a short time under a specific atmosphere that remained the same for the whole test. The Temperature evolution for the first test, VEGA-1 is shown in **Figure 112**.

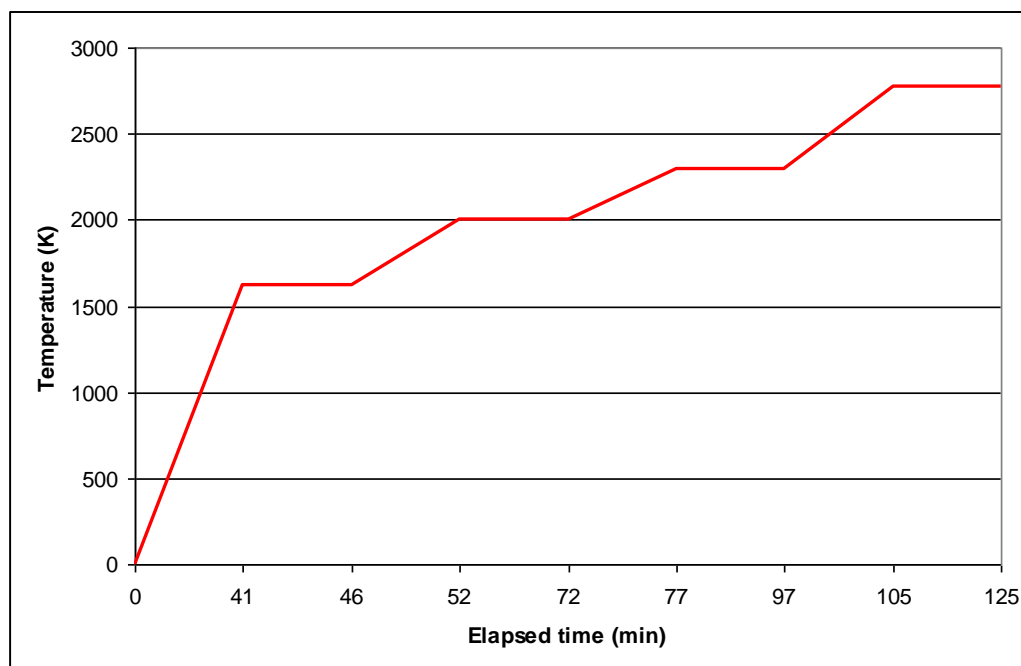


Figure 112: Temperature evolution on VEGA-1 test.

Regarding the tests samples, UO_2 fuel from Japanese PWR were employed for tests 1, 2, 3, 4 and 5. Test M1 and M2 were conducted employing MOX fuel fabricated in Japan, and irradiated at the Advanced Thermal Reactor (ATR). Tests 6, 7 and 8 were conducted employing UO_2 samples from Japanese BWR.

6.2.1.4. HEVA-VERCORS

The French research on nuclear severe accidents started with the HEVA program from 1983 to 1989 followed by the VERCORS, VERCORS HT and VERCORS RT from 1989 to 2002, and since 2011 with the VERDON program. All these programs have been conducted by the CEA.

The HEVA program, which consisted in 8 test, has permitted to study FP release up to a temperature of 2370 K (Leveque et al., 1991). In the VERCORS program (6 tests) temperatures up to 2600 K were achieved, which permitted to increase the FP database with FP of lower volatility. The VERCORS HT (for High Temperature, 3 tests) and VERCORS RT (for Release of Transuranics, 8 tests) permitted, using innovative experimental devices for the time, to reach temperature in the range of fuel fusion (Pontillon et al., 2010). This made possible to study the release of non-volatiles FP and Transuranics, to measure the kinetics of deposition of FP, to better characterize the chemical forms of iodine and finally to analyse the interaction of FP with structural materials (Leveque et al., 1991). Regarding the VERDON program, 4 tests have been carried out. One of the objectives of this program was to study the ruthenium behaviour in highly oxidizing conditions.

Sample Characteristics:

The samples employed on the VERCORS programs consisted on PWR fuel pellets in their original cladding, with depleted UO_2 half pellets at each side. A diagram of the sample employed in the tests is shown in **Figure 113**. This sample was composed of three PWR pellets in their original Zircaloy

cladding. Half pellets of depleted UO_2 were placed on both sides firstly, to maintain the fuel pellets in place after crimping the cladding and secondly, to eliminate the effects of neutron edges for eventual re-irradiation of the sample. The cladding remained open on each side to enable interaction with the surrounding atmosphere and mass transfer phenomena.

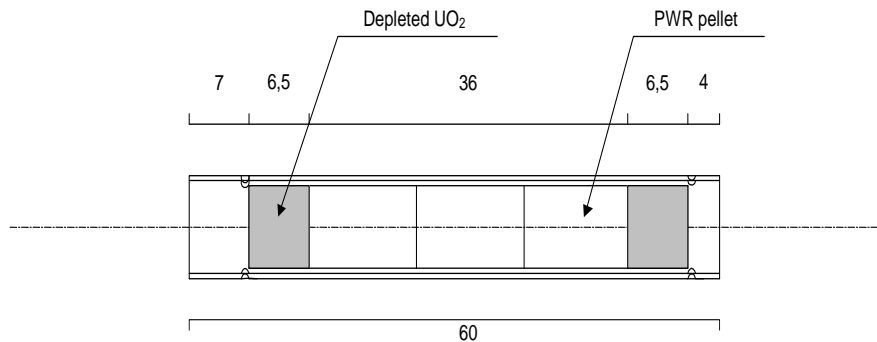


Figure 113: Sample used in VERCORS RT7 test

Samples were generally re-irradiated at a linear power density of about $10\text{-}20 \text{ W.cm}^{-1}$, in order to recreate short and medium half-life FP up to activity levels on the same order of magnitude as that of long period FP and thus obtaining optimum gamma spectrometry detectability for all FP.

Regarding the VERDON program, samples are similar but only with two irradiated fuel pellets instead of three, as showed in the radiography in **Figure 114**.

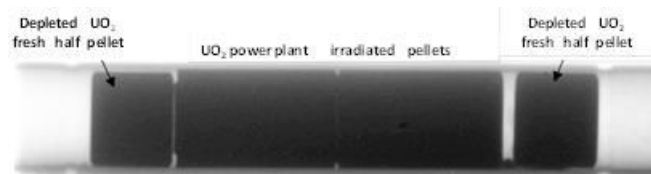


Figure 114: VERDON 2 sample radiography

Experimental Loop Characteristics:

HEVA-VERCORS:

Though the initial experimental loop used in the HEVA programme underwent several adaptations and updates to meet the experimental requirements, the loops used for these test are relatively similar. **Figure 115** shows the experimental loop for the VERCORS tests, which components are described below.

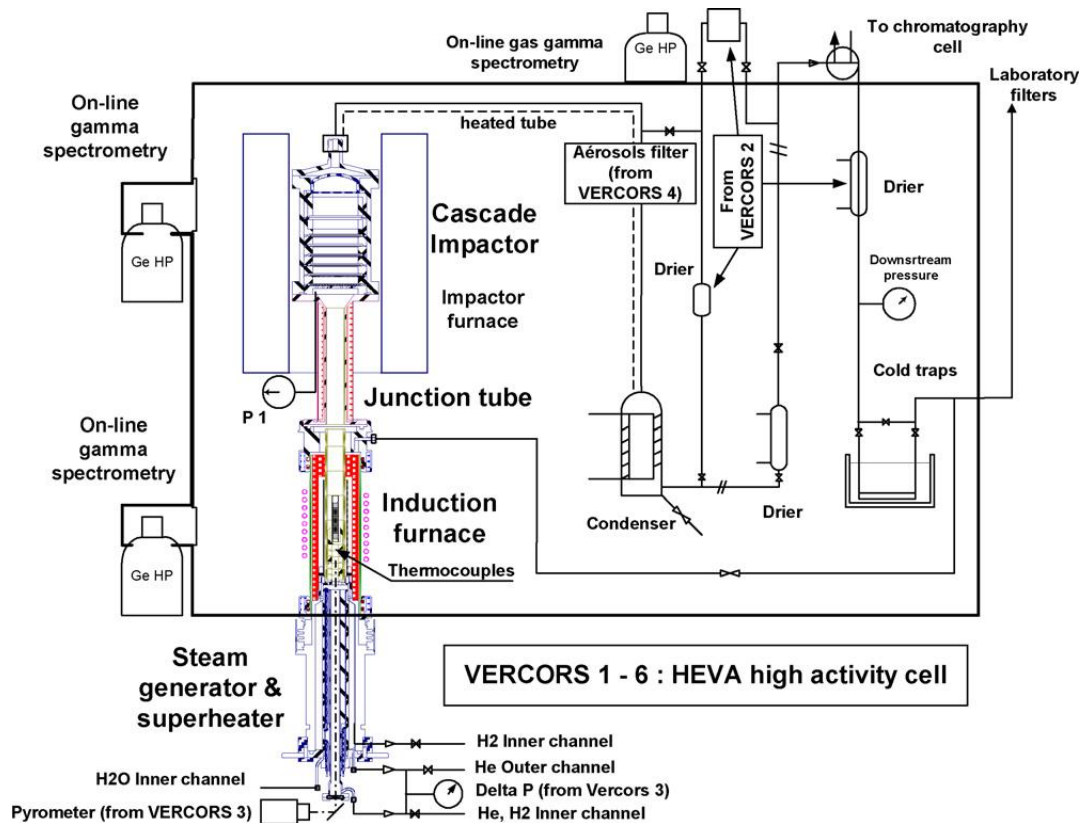


Figure 115: VERCORS 1-6 experimental loop

By following the path of the gases, the following elements may be distinguished:

- Supply of steam, hydrogen and helium, composing the injection fluid for the central part of the furnace flowing over the fuel sample.
- Additional supply of helium designed to protect the furnace susceptor against oxidation by the steam.
- Super-heater designed to preheat the gases to 1073 K before they arrive to the furnace.
- Induction furnace which includes (from the outside inwards):
 - Two concentric channels whose dynamic leak tightness was guaranteed by a stack of dense zirconia sleeves. Steam and hydrogen flowed through the inner channel containing the sample. The outer channel containing the susceptor was swept by helium at a slight overpressure in relation to the inner channel. The susceptor received the high frequency coupling and dissipated it as thermal energy.
 - Thermal insulator enveloping the two channels composed of a double envelope of zirconia and porous alumina.
 - The Quartz tube which set the limits of the furnace area.
 - Induction coils around the quartz tube.
- Junction area connecting the furnace to the impactor. The inner channel of this junction was made of zirconia.
- Cascade impactor (Andersen Mark II) placed in a resistance furnace at a temperature of 873 K. This impactor was composed of (upstream to downstream):
 - A succession of six impaction stages designed to collect the aerosols on the basis of decreasing diameters ranging from about 10 μm to 1 μm .
 - Two successive batteries of bead beds designed to collect sub-micrometric aerosols.

- A porous filter (grade-3): filtering 99.9% of 0.5 μm residual particles and 98% of 0.2 μm particles.
- Line heated at 573 K.
- Additional aerosol filter set at 400 K, used from the VERCORS 4 test onwards (porous filter identical to that of the impactor).
- Water trapping devices composed of a condenser and two driers placed in series. From VERCORS 2 onwards, a derivation from the main line, located between the two driers, made it possible to send a gas sample to a gas phase chromatograph to measure the hydrogen produced during cladding oxidation. At this point, there was also a capacity of 100 cm^3 for the on-line measurement of fission gases by gamma spectrometry.
- Two active charcoal traps assembled in parallel and cooled with liquid nitrogen to guarantee the complete collection of the fission gases.

VERCORS RT series:

The main objective for these tests was to improve the measurement precision of the FP released fractions and to extend the “release” database to include both FP that do not emit gamma rays but are important for safety (e.g., ^{90}Sr), and heavy nuclei (U, Np, Pu, Am and Cm) by means of post-test chemical analysis. In order to reach higher temperature, some components of the loop were modified:

- The furnace was modified:
 - The crucible, its supports and the column delimiting the inner channel and the outer channel were made of dense ThO_2 .
 - The new column was composed of two series of tubular sleeves in a staggered arrangement to guarantee the dynamic leak tightness between the two channels.
 - The susceptor was made of tungsten and formed an extractable sheath that supported both the column and the crucible. It made possible to run series of several tests by remote handling with no need for direct human intervention in the cell.
 - The thermal insulators between the susceptor and the quartz tube were made of porous ThO_2 (inner insulator) and porous ZrO_2 (outer insulator).
- A newly designed aerosol filter was placed in the position of the impactor.
 - The connecting tube (junction area linking the furnace to the impactor) was removed to reduce any upstream deposits.
 - The filter was annular to make it possible to obtain a direct pyrometric view of the fuel from the top.
 - From test RT5, a video camera was added to this pyrometric view. The camera was an essential tool that was complementary to the on-line gamma spectrometry in sight of the fuel, and it was used to identify the time at which the fuel sample relocated.
 - The filter was composed of five successive stages of bead beds and a grade-3 Porous disc. The device was heated to 400 K for the duration of the test.

Beyond the filter (and similarly to the previous VERCORS series) the line heated to 400 K led the gases to the steam condenser. Then an unheated line transported them to the online gas measurement (by gamma spectrometry, located between the two driers) and finally to the active charcoal traps for fission gases collection.

VERCORS HT series

In addition to the FP release objective, this loop was used to study FP transport as well as their potential interactions with Ag, In, Cd and B. These elements may be present during a severe accident due to degradation of neutron absorbers. The loop was provided with a thermal gradient tube (TGT) and a may-pack (selective trap for the various chemical forms of iodine).

The furnace design was very similar to that of the VERCORS RT loop. The only differences were in terms of the crucible geometry and the presence (for HT2 and HT3) of a series of cups underneath the crucible which were used as supports for the wires of Ag, In and Cd. Another cup containing B oxide was placed at pre-calculated positions so that emissions of its vapours would coincide with those of the FP and, in particular, iodine.

A view port was installed in the upper end of the TGT for tests HT2 and HT3, for direct pyrometric viewing and video recording of the fuel. The may-pack was of the same type for all the tests and was identical to that of the PHEBUS program. Beyond the may-pack there was a steam condenser followed by an unheated line transporting the gases to the gaseous phase micro-chromatograph (located between the two driers) and finally to the cooled active-charcoal traps for fission gas collection.

6.2.2. Integral Test

The objective of Integral Test programs were to study not only the release of FP from the reactor core but as well as the transport in the cooling circuits up to the containment and the possible interaction that may take place between the released FP and others materials, such as paintings. These tests were carried out in dedicated facilities that reproduced whole nuclear reactors at reduced scale. The most representative program of this category was the PHEBUS FP program, described below.

6.2.2.1. PHEBUS FP

The PHEBUS FP program was initiated in 1988 through an agreement between IRSN (at that time IPSN) and the European Commission, represented by its Joint Research Centre. The objective was to study the degradation of real core material, from the early phase of cladding oxidation and hydrogen production up to the late phase of melt progression and molten pool formation. The partnership was rapidly extended to the French utility EDF, the Atomic Energy of Canada Limited (AECL) and the CANDU owners Group (Canada), the US Nuclear Regulatory Commission (NRC), the Nuclear Power Engineering Company (NUPEC, then JNES, now NRA, Japan) the Japanese Atomic Energy Research Institute (now JAEA), the Korea Atomic Energy Research Institute (KAERI), the Swiss Federal Nuclear Safety Inspectorate (HSK now ENSI) and the Paul Scherrer Institute (PSI, Switzerland). After 5 years of design and construction, 5 tests were performed from 1993 to 2004.

The PHEBUS facility provided prototypic reactor conditions which allowed the study of basic phenomena governing from core degradation to the late phase (melt pool formation), hydrogen production, FP release and transport, circuit and containment phenomena and iodine chemistry (Schwarz et al., 1999b)(Clément and Zeyen, 2013).

Experimental Facility

The PHEBUS FP experimental facility is composed of a driver core and its cooling circuit, a pressurized water loop, an injection loop, a test section simulating the core of a Light Water Reactor (LWR), an

experimental circuit simulating the primary circuit of a LWR with a cold leg break and containment vessel simulating the containment building of a LWR (March and Simondi-Teisseire, 2013).

The PHEBUS reactor is of a pool type reactor with a central cavity where the in-pile test section is located. The core is cooled by a forced water flow at atmospheric pressure and at room temperature. A horizontal section of the experimental bundle as it was designed for the first test (FPT-0) is shown on **Figure 116**. It is a 1/5000 scale of a 900 MW PWR prototype reactor composed of a 20 fuel rods (800 mm fissile length) bundle, surrounded by a ceramic shroud fitted inside the pressure tube. The central position is occupied by an Ag-In-Cd control rod with a stainless steel cladding, inside a Zircaloy guide tube. Two Zircaloy grids with Inconel spacers are located at 220 and 740 mm, respectively from the bottom of the fuel column. The thermal shroud consisted of two concentric, high-density ZrO_2 tubes (Schwarz et al., 1999b).

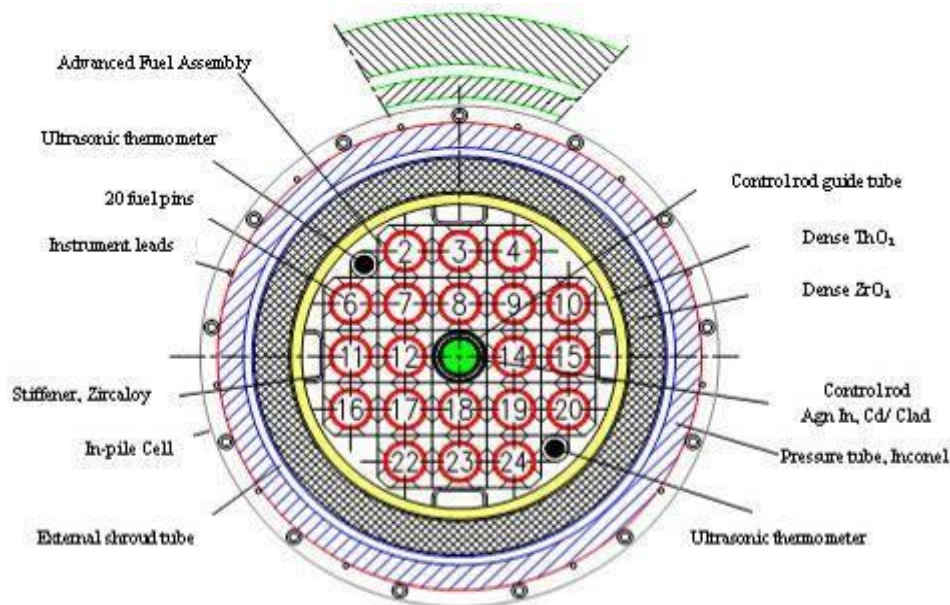


Figure 116: Horizontal section of the PHEBUS PF experimental device.

Previous to the test, the bundle was re-irradiated in the PHEBUS facility during a few days, in order to recreate the short-life FP inventory and to induce irradiation doses large enough to observe radiochemistry effects on the containment.

Radioactive materials exiting the bundle were conveyed through a hot line heated at 970 K to a steam generator simulated by a single inverted U-tube (scaling ratio 1/5000 for the number of tubes) and then to model containment through a cold leg heated at 420 K. The model containment was a 10 m^3 vessel simulating a reactor containment atmosphere, painted wall surfaces and a sump. The given scaling ratio is also valid for the volume of the containment atmosphere, the surface area of the painted condensing surfaces and the interfacial area between the sump and the atmosphere. A diagram of the facility is shown in **Figure 117**.

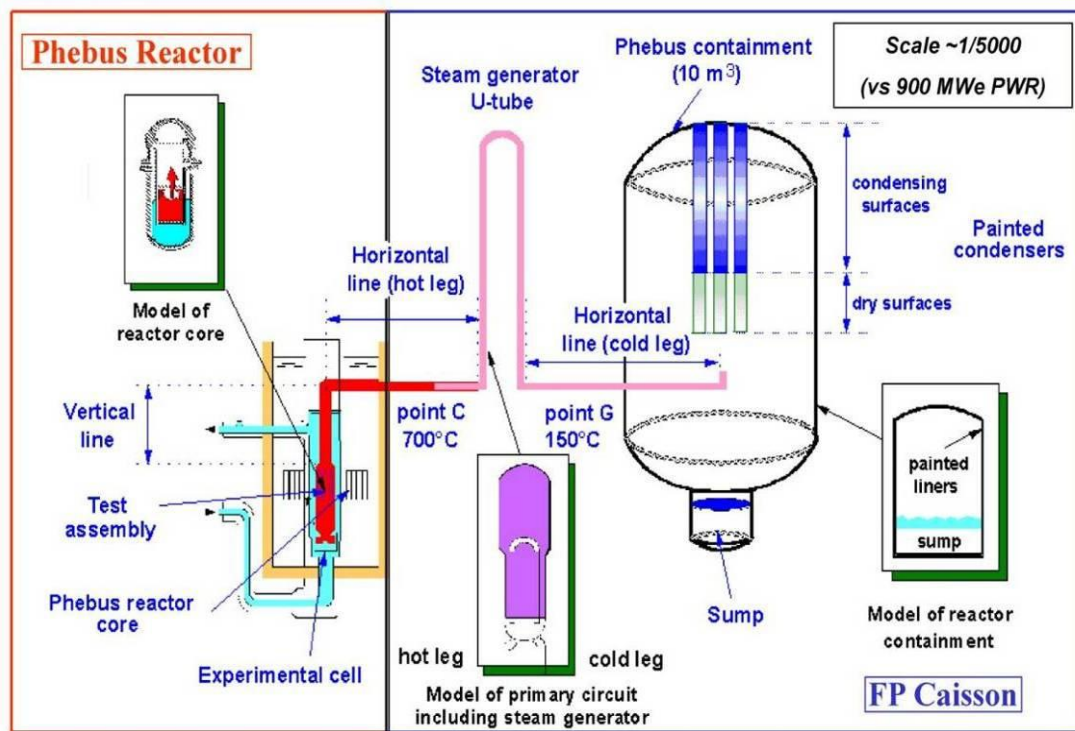


Figure 117: PHEBUS PF experimental facility

The FPT-4 experiment was different, since it was performed to study the release of low volatile FP and actinides from a pre-fabricated debris bed without trying to simulate a reactor cooling system or a containment vessel. The debris bed was made of irradiated fuel fragments and oxidised Zircaloy cladding shards typical of what was observed in the upper part of the TMI2 reactor pressure vessel.

A considerable amount of on-line and analytical off-line instrumentation was used on each test. The instrumentation is described in detail in (March and Simondi-Teisseire, 2013).

This facility therefore offers several advantages, compared to the other in-pile facilities, which include: a complete integral design (including a simulated primary circuit and containment vessel); complete instrumentation to assess the temporal and spatial progression of the core melt sequence, including on-line and sequential sampling of solid, liquid and gaseous effluents at various points in the experimental train (e.g., FP, aerosol and iodine speciation sampling); the possibility of conducting the experiment over extended periods of time (at high temperature); and complete pre and post-test examination (including gamma scanning, transmission and emission tomography).

6.3. Appendix III: SIMFUEL samples preparation

SIMFUEL samples were acquired from the Chalk River Laboratories, Canada. Samples contain 11 stable FP: Mo, Ru, Rh, Pd, Ba, Zr, Ce, Sr, Y, La and Nd; in concentrations representative of a 76 GWd.t⁻¹ Burn-up UO₂ irradiated fuel. The concentration of each FP is presented in **Table 51**.

Samples Composition (at. %)										
Ba	Ce	La	Mo	Sr	Y	Zr	Rh	Pd	Ru	Nd
0.26	0.61	0.20	0.51	0.13	0.06	0.60	0.03	0.42	0.64	0.91

Table 51: SIMFUEL samples composition

According to (Lucuta, 1991b), samples preparation was as follows: high-purity oxides (BaCO₃, CeO₂, La₂O₃, MoO₃, SrO, Y₂O₃, ZrO₂, RhO₃, PdO, RuO₂, Nd₂O₃, 99.999% purity) were dry-mixed with UO₂ powder, and then submitted to high-energy, wet, stirred-ball milling, in order to achieve an uniform dispersion. After spray drying, the oxides mix was submitted to conventional pre-compaction, granulation, pressing and a final sintering stage at 1923 K for 2 hours under flowing hydrogen. Under these conditions, an oxygen potential equal to -500 KJ.mol⁻¹ was attained.

The resulting samples have a density equal to about 97% of theoretical density of UO₂ and fuel grains with a mean size of 12 µm.

In order to study volatile FP behaviour such as Cs, the ion implantation method was adopted. SIMFUELS samples as described above were implanted at the *Institute de Physique Nucléaire de Lyon* (IPNL, Villeurbanne, France), under the following conditions: ¹³³Cs implantation at 800 keV, with a dose of 4.5E10¹⁵ atoms.cm⁻². Many Cs implantation profiles have been acquired through SIMS analyses, and are presented in **Figure 118**. The depths at which the maximal ¹³³Cs concentration values were observed for each implantation profile are presented in **Table 52**.

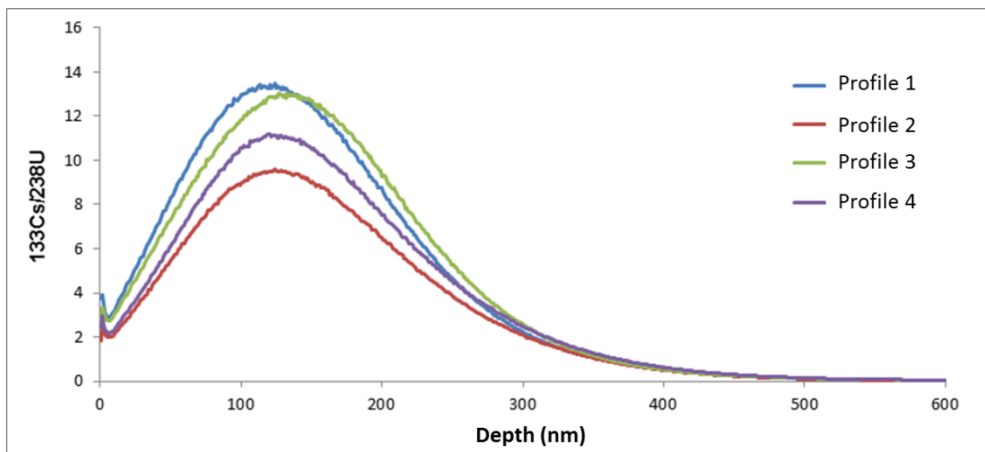


Figure 118: ¹³³Cs implantation profiles

	Profile 1	Profile 2	Profile 3	Profile 4
Depth (nm)	124	119	133	120

Table 52: Maximal ¹³³Cs implantation values

The implantation profile has been estimated considering the implantation conditions presented above, along with the Displacement Per Atoms (DPA) profile (presented in **Figure 119**). According to these results, Cs concentration is maximal at 155 nm from the surface, with an average

concentration of 0.355 at.%. The maximum value of DPA was estimated to be 35.5, located at 70 nm from the sample surface

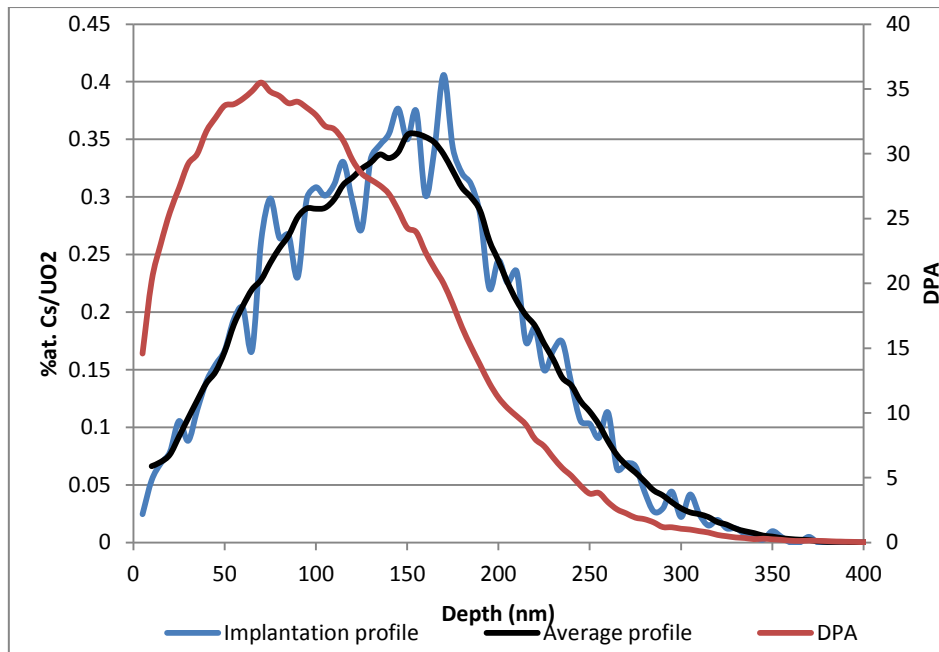


Figure 119: Estimated implantation Cs implantation profile and DPA

FP concentration after implantation was recalculated, and results are presented in **Table 53**. As observed, Cs implantation did not produce an appreciable modification of samples composition regarding the concentration of the other FP.

Samples composition (at. %)											
Ba	Ce	Cs	La	Mo	Sr	Y	Zr	Rh	Pd	Ru	Nd
0.26	0.61	0.35	0.20	0.51	0.13	0.06	0.60	0.03	0.42	0.64	0.91

Table 53: FP concentration in samples from Sets II and III

Finally, SIMFUEL samples were cut into quarter discs from 10 mm diameter, 500 µm thick discs.

6.4. Appendix IV: Thermodynamic estimations

Thermodynamic estimations were performed using the FactSage 6.3 software. FactSage is the product of the fusion of two software packages for computational thermochemistry: F*A*C*T/FACT-Win and ChemSage (Bale et al., 2009). The original F*A*C*T package was designed to simulate the thermochemistry of pyrometallurgical processing. With the migration to the Windows-based FACT-Win and then to FactSage the applications have been expanded to include hydrometallurgy, electrometallurgy, corrosion, glass technology, combustion, ceramics, geology, environmental studies, etc.

The database adopted for calculations was the SGPS pure substance database, provided with the software. This database does not consider solid solutions (metallic inclusions for example, which are composed of Mo, Pd, Rh, Ru and Tc) but it is useful for the prediction of the most stable chemical compounds in the studied conditions. The Mo-Cs-U-Ba-Zr-O₂ predominance diagram presented in Chapter 3 was performed using the Phase Diagram mode, considering a FP molar ratio identical to that of the SIMFUEL samples.

6.5. Appendix V: Experimental loops

6.5.1. VERDON

The VERDON laboratory (Ferroud-Plattet et al., 2009), located at the LECA-STAR facility, is constituted of 2 high activity cells (C4 and C5) and a glove-box. Cell 4 is dedicated to the sample reception, pre and post-tests gamma scanning and loop elements storage. Cell 5 contains the VERDON experimental loop itself, dedicated to the accidental sequence realisation and on-line γ -spectrometry measurements. The VERDON 1 loop, presented in **Figure 120**, consists mainly of an induction furnace where the sample is located, a fluid injection system, an aerosols filter, a May-Pack filter for iodine species, a condenser for recovering steam and a final safety filter.

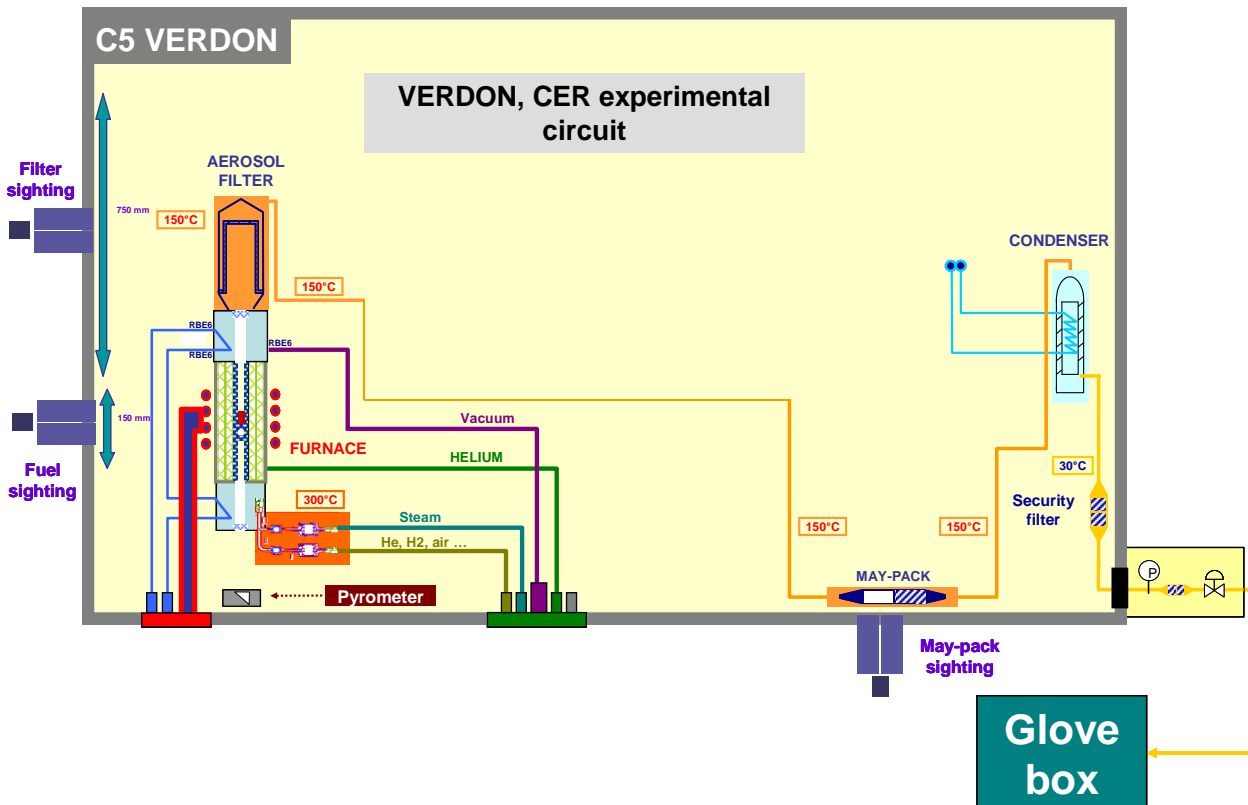


Figure 120: VERDON 1 experimental loop

The induction furnace presented in **Figure 121** is constituted of a coil surrounding a tungsten susceptor tube, which is the heating component of the furnace. A high frequency power supply generates a current in the coil. By electro-magnetic coupling, a current is generated into the susceptor and converted in thermal energy by the Joule effect. The fuel sample located inside the susceptor tube is then heated mostly by thermal radiation.

The external part of the furnace is constituted of a quartz tube sealed between two stainless steel bases thanks to two seals. The internal part can be schematically divided into two areas delimited by a ceramic column. This latter is constituted by a double stack of concentric dense ceramics; in the central area where the furnace temperature is the highest, the ceramics are manufactured using hafnium dioxide and at the ends, where the furnace temperature is the lower, they are in zirconium dioxide. The crucible, in which the fuel sample is introduced before the sequence, is located inside this ceramic column together with several cups allowing crucible's supporting and gases flow circulation. The susceptor and a double stack of concentric porous zirconia and hafnia are located outside of the ceramic column and are devoted to furnace insulation. A "susceptor gas" flow constituted of He circulates between the quartz tube and the

“ceramic column” through the porous insulators and along both sides of the susceptor tube. It is maintained in slight over-pressure regarding the experimental gas in order to create a protection of the susceptor tube (in tungsten) against oxidation from the experimental fluid.

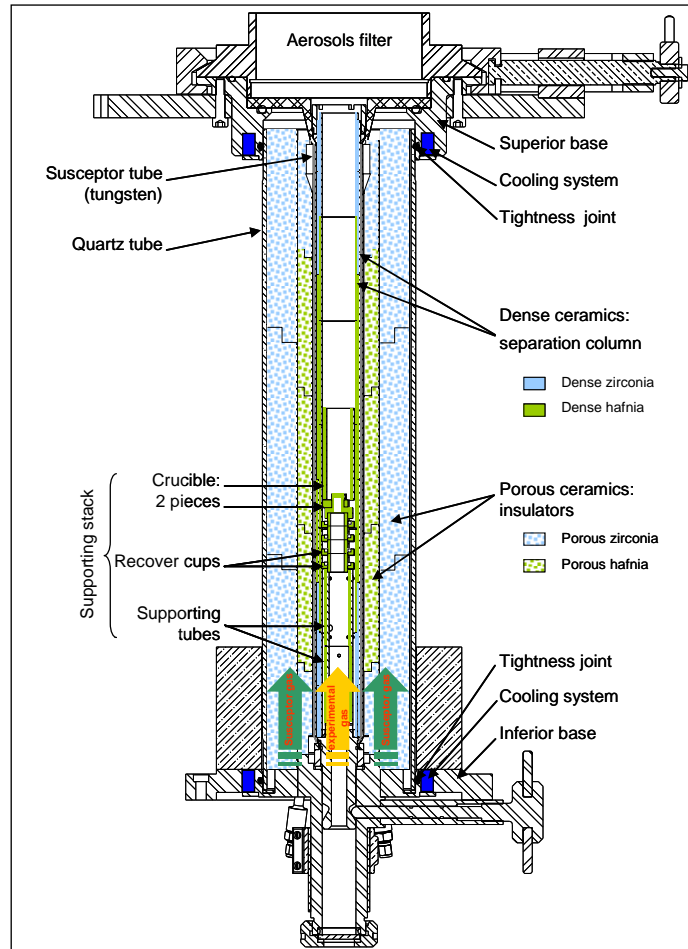


Figure 121: VERDON 1 Induction furnace

FP release kinetics are measured thanks to three complementary on-line gamma spectrometry stations and one micro gas chromatograph: One gamma station aimed directly to the fuel sample, allowing to follow qualitatively the remaining FP in the sample; the second gamma station aimed to the aerosol filter, allowing to identify the deposited species; the third gamma station was aimed to the may-pack filter.

6.5.2. MERARG

Irradiated fuel sample FRAG3 was submitted to an annealing test using the MERARG experimental loop, located in Cell 7 at the LECA-STAR facility, CEA Cadarache. The main components of the experimental loop, presented in **Figure 122**, are an electromagnetic induction furnace where samples are placed, a γ -Spectrometry unit followed downstream by a μ -Gas Chromatograph and a gas container.

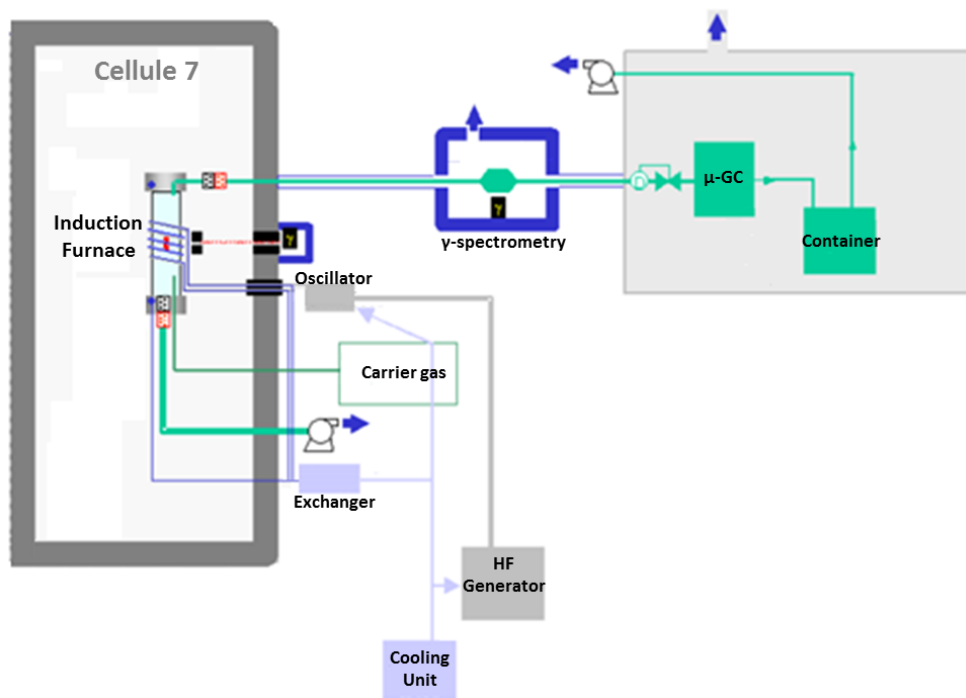


Figure 122: MERARG experimental loop

The main components of this experimental device are:

The induction furnace: The furnace is located in the high-activity cell. The irradiated fuel sample is placed in a metallic crucible which is placed at the centre of the induction spires. This crucible acts then as a susceptor, transforming the electromagnetic waves into heat. The sealed chamber of the furnace is constituted by a quartz tube within which the crucible is placed. The carrier gas (Ar + 4% H₂ for IS sample) which assures the atmosphere of the tests circulates constantly through the quartz tube at rather low flow, generally of 60 cm³.min⁻¹.

The gamma-spectrometry detector: The on-line gamma detector was directed to the crucible, in order to measure the Cs instantaneous release. A second gamma spectrometry detector, located between the furnace and the glove-box, measures on-line the fission gasses release (⁸⁵Kr).

Glove box and μ-GC: After the furnace the carrier gas is conducted to a glove box where, if necessary according to tests objectives, is analysed by a μ-Gas Chromatograph and is finally collected in a container. A picture of the MERARG furnace is presented in **Figure 123**.

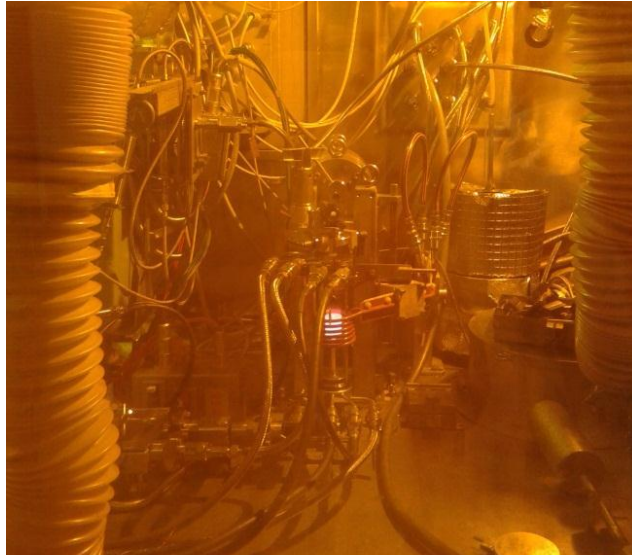


Figure 123: MERARG induction furnace

6.5.3. DURANCE

The DURANCE experimental loop is very similar to that the MERARG one, based on the same operating principle. The main component of the loop is an induction furnace which can be set into two different configurations. The first one is similar to that of MERARG (crucible placed at the centre of the induction spires) which allows an homogeneous heating of samples, and the second one in which a cooling circuit is added, allowing to generate a temperature gradient from the centre of the sample to the periphery. Tests have been performed using the "MERARG" configuration. A diagram describing the DURANCE experimental loop is presented in **Figure 124**.

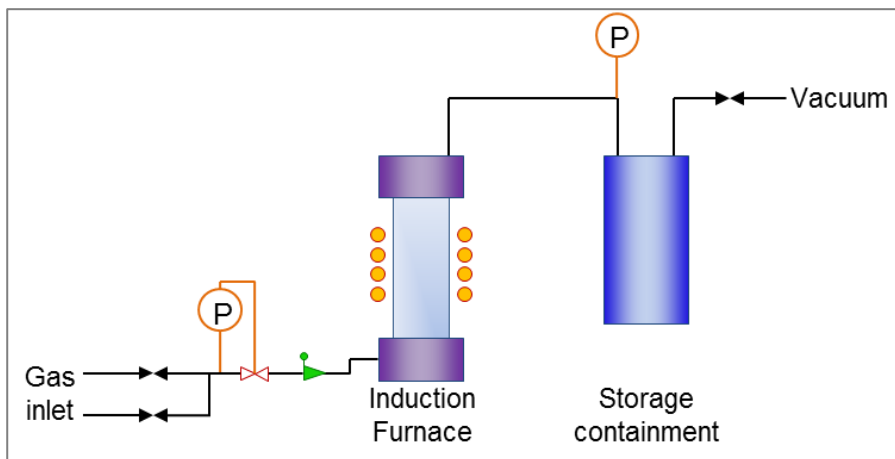


Figure 124: DURANCE experimental loop

6.5.4. Tests atmospheres

The irradiated fuel sample IF1500, and the SIMFUEL samples AT, R300, R1200, R1500 and R1700 (from sample sets I and II) were submitted to annealing tests under reducing atmosphere. This atmosphere consisted in Ar + 4%H₂ flowing at 60 cm³.min⁻¹.

Samples from set III (O300, O1200 and O1700) were submitted to annealing tests under oxidizing atmosphere, consisting in pure Ar flowing at 60 cm³.min⁻¹. The oxidizing character of this atmosphere lies in the presence of O₂ and other impurities. Argon characteristics are listed in **Table 54**.

Denomination	Argon N60
Provider	Air liquide
Pressure	200 bar
Global purity (%)	99.9999
Impurities (ppm)	H ₂ O<0.6
	O ₂ <0.1
	CO+CO ₂ <0.01
	C _n H _m <0.05
	N ₂ <0.3
	H ₂ <0.01

Table 54: Carrier gas (argon) characteristics, used in oxidizing tets

6.6. Appendix VI: Characterization methods

6.6.1. Optical Microscopy

Optical Microscopy was performed using a LEICA DM RXA2 device adapted for hot cell work. Image acquisition was done with a LEICA DFC 320 camera on the “SIS” acquisition system.

6.6.2. Scanning Electron Microscope

6.6.2.1. *SIMFUELS*

Scanning Electron Microscopy (SEM) was performed using a Philips XL30 FEG instrument, equipped with an EDAX-EDS system allowing us to determinate the distribution and content of FP using Energy Dispersive X-ray Spectroscopy (EDS) methods. Acceleration tension was set to 15 kV. The X-ray lines used to analyse the sample are the $L\alpha_1$ ones except to uranium and oxygen for which $M\alpha_1$ and $K\alpha_1$ have been respectively collected. Image analysis was performed using the analySIS pro 5.0 software, from Olympus Soft Imaging Solutions. This software allowed determining the ECD (Equivalent Circle Diameter) of precipitates as well as their area contribution (percentage of the total area that is occupied by precipitates).

6.6.2.2. *Irradiated Fuels:*

SEM observations on irradiated fuels samples were performed using a ‘Philips’ XL30 device on which the WDX ‘Microspec’ spectrometer has ‘home made’ shielding. Large field acquisitions were performed thanks to the ADDA ‘SIS’ system. The AnalySIS software was also used for the exploitation of these results.

6.6.3. Electron Probe Micro Analysis (EPMA)

EPMA analyses on irradiated fuel samples were performed using a shielded CAMECA SX100R device equipped with the ‘SAMx’ system for acquisition and exploitation of measurements. This device is also located at the LECA-STAR facility. Incident electron beam characteristics were set at 20 kV and 200 nA.

6.6.4. Secondary Ion Mass Spectroscopy (SIMS)

SIMS analyses both on irradiated fuel and SIMFUEL samples were performed at the SIMS device located at the LECA-STAR facility. A “CAMECA” IMS 6f secondary ion mass spectrometer, also installed inside a shielded glove-box cell was used. The key features of this device are presented in (Rasser et al., 2003). A diagram describing this device is presented in **Figure 125**. Regarding the experimental conditions, the beam acceleration tension was set to 10 keV with an intensity of 100 nA. Cs implantation profiles in SIMFUEL samples were obtained through the double crater method. This method consists in performing a scanning pulverisation with the probe in a fixed position, over a surface of 200 x 200 μm . Only ions coming from a 60 μm diameter circle centred in the scanned area are measured. The depth of the crater is then measured by SEM in order to determine the implantation depth.

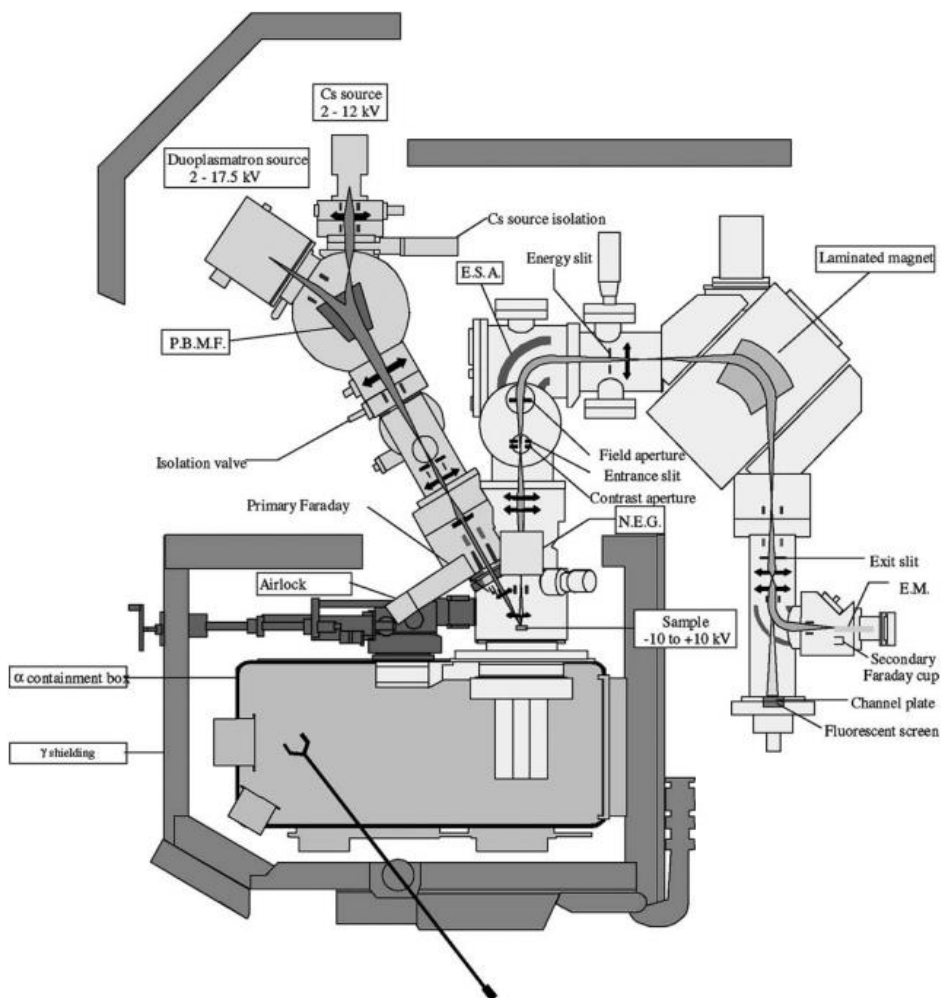


Figure 125: Diagram of the CAMECA IMS 6f

6.6.5. X-Ray Diffraction

XRD analyses on the VERDON 1 samples were performed at the LECA-SATR facility, using a special designed device. This equipment is located in a hot cell which allows the analysis of irradiated nuclear fuels. Besides, in order to avoid gamma radiation effects on X-ray detection, a point detector coupled to a graphite monochromator is used. The goniometer is a standard one (Type XRD 3001) from GE-Inspection Technologies Company. A specific focusing device has been designed (using K β mirrors), allowing a 100 μm diameter μ -X-ray beam. X-rays with two wavelengths (1.5406 and 1.5444 \AA) are produced by a conventional copper tube. A picture of the hot cell where the DRX device is placed is presented in **Figure 126**, along with a picture of the device itself.



Figure 126: Hot cell where the XRD equipment is placed (left) and the equipment itself (right)

6.6.6. X-ray Absorption Spectroscopy

Due to its ability to reveal information at the molecular level such as coordination geometry and oxidation states, X-ray Absorption Spectroscopy (XAS) experiments were performed on every FP of interest in this work: Mo, Cs, Ru, Ba and Zr. The measurements were carried out at the MARS beam-line, SOLEIL synchrotron radiation facility (France) (LLorenz et al., 2014). The main characteristics of a Synchrotron facility are described, followed by the particular of the MARS beam-line, where all XAS experiment of this work have been performed.

6.6.6.1. Synchrotron

XAS requires an intense and tuneable source of X-rays. Therefore, XAS analyses are performed exclusively in Synchrotron facilities. Synchrotron facilities are usually composed of accelerators aiming at producing electromagnetic radiation by accelerating particles (electrons in this case). A picture of SOLEIL synchrotron and its layout are presented in **Figure 127**.

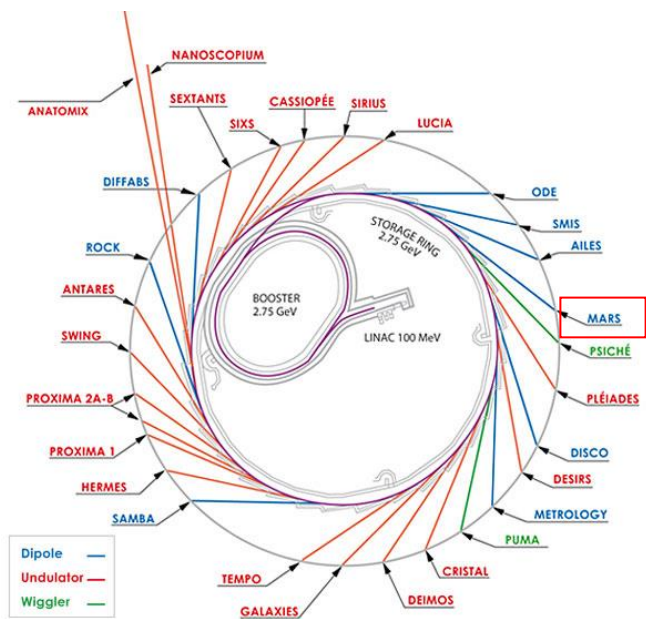


Figure 127: SOLEIL Synchrotron

6.6.6.2. *Beamlines*

A beamline is an experimental facility in which the light produced in the synchrotron is selected and focused in order to analyze the samples by means of monochromators, mirrors and optical devices. Each beamline has its own energy domain and enables using different techniques (XAS, XRD, etc.). All the XAS analyses of this work have been performed at the MARS beam of SOLEIL Synchrotron (LLorenz et al., 2014). This particular beamline allows performing XAS and High-resolution XRD on radioactive samples.

XAS analyses have been performed under top-up 4030 mA ring mode. The photon energy was scanned from 17.6 to 22.4 keV (Mo, Zr and Ru K-edges) and from 5.0 to 5.4 keV (Ba and Cs L₃-edges) using a Si(220) double-crystal monochromator (DCM) which allows a mean photon flux of about 2×10^{11} ph.s⁻¹ at 17.5 keV. Calibration was done using the K-edge excitation energies of Zr (17998 eV), Mo (20000 eV), Ru (22117 eV) and Ti (4966 eV) metallic foils.

The monochromatic beam was focused to 300 x 300 μm² for macro-beam experiments (Horizontal x Vertical Full Width at Half Maximum) and to 5 x 6 μm² for micro-beam ones. As FP are diluted elements in a heavy matrix, the fluorescence mode has been adopted. The XAS spectra have been collected with a Vortex-90-EX silicon drift detector.

6.6.6.3. *Samples preparation*

Radioactive samples may be analysed at the MARS beamline, but a double confinement is required. Particularly for the samples analysed in this work, this double confinement consisted in two kapton sheets. An image of a SIMFUEL sample with the first confinement is presented in **Figure 128**, along with an image of the samples holders. Once the sample is placed in the sample holder, a second kapton sheet is then placed.

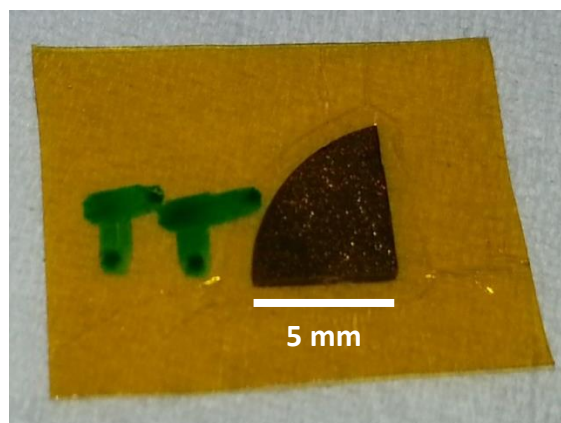


Figure 128: SIMFUEL sample in the first confinement barrier

6.6.6.4. *Results analysis*

The ATHENA software (Ravel and Newville, 2005) was used for normalizing XAS spectra oscillations from the raw absorption data and correcting the self-absorption phenomena. Pre-edge removal and normalization was achieved using linear functions. The post-edge line for XANES spectra was taken using the position 30 eV and 150 eV relatively to edge position E₀. The E₀ values and the white line maximum of each spectrum were taken as the first inflection point and the first zero-crossing of its first derivative.

The linear combinations fit for Mo were performed in the range (-20, 50) eV from the absorption edge position while those of Cs spectra were performed in the (-10, 30) eV. The self-absorption phenomena in Cs reference spectra was corrected considering an incident beam angle of 20° and exiting beam angle of 4°.

6.6.6.5. R-Factor

The R-factor calculated by the Athena software is a measure of the quality of the Linear Combination Fit. Its mathematical expression is:

$$R - Factor = \frac{\sum(data - fit)^2}{\sum(data)^2}$$

where the sums are over the data points in the fitting region. The lower the value of the R-factor is for a determined calculation, the better the results is.

6.7. Appendix VII: Résumé en Français

Etude du comportement des Produits de Fission (Ba, Cs, Mo et Ru) dans des combustibles nucléaires irradiés et leurs simulants en situations d'Accidents Graves par Spectroscopie d'Absorption des rayons X, SIMS, DRX et microsonde.

6.7.1. Contexte de l'étude

Malgré un niveau de sûreté élevé, des accidents peuvent se produire dans les réacteurs nucléaires à cause de dysfonctionnement des appareils, d'erreurs humaines ou de facteurs extérieurs tels que les catastrophes naturelles. Ces accidents peuvent avoir des conséquences différentes, mais quand une libération importante de produits de fission (PF) dans l'atmosphère est parmi eux, on parle d'accident grave. Des exemples de ces accidents sont l'accident de Tchernobyl en 1986, en Ukraine et l'accident de Fukushima Dai-Ichi en 2011, au Japon. La quantité totale et les caractéristiques des espèces radioactives relâchées dans l'atmosphère est appelé le terme source, qui est aujourd'hui estimé à l'aide des codes scénario. Afin d'améliorer ces estimations, le comportement des PF lors d'un accident grave doit être mieux compris. Bien que plusieurs programmes de recherche, tant analytiques qu'intégraux, aient été menés au niveau international afin d'étudier le comportement des PF dans ces conditions, de nombreuses incertitudes demeurent.

6.7.2. Objectif de la thèse et méthodologie

Un mécanisme de relâchement des PF hors le combustible nucléaire a été proposé par (Nicaise, 2004b) dans une tentative de décrire le comportement de Ba, Cs, Mo et Ru. Ce mécanisme propose un état initial et son évolution au cours d'un traitement thermique du type des essais VERCORS du CEA, qui reproduisent les conditions d'un accident nucléaire grave. Bien que basé principalement sur des estimations thermodynamiques et quelques résultats expérimentaux obtenus lors des différents programmes de recherche, notamment le programme VERCORS, la plupart des phases chimiques proposées dans le mécanisme restent hypothétiques. L'objectif de la thèse est, donc, de valider ou réfuter l'état initial et l'évolution proposés dans le mécanisme. Pour cela, deux axes de travail ont été mis en place dans lesquels des échantillons de combustibles irradiés à fort taux de combustion et des matériaux modèles sont soumis à des traitements thermiques sous atmosphère contrôlée et caractérisés avant et après chaque test. Les matériaux modèles, aussi appelés SIMFUELS, consistent en pastilles d' UO_2 naturel et non irradié, dopé avec 12 PF en concentrations représentatives à des combustibles nucléaires irradiés à 76 GWj.tn^{-1} . Le principal avantage de ces derniers est l'utilisation de méthodes de spéciation chimique comme la Spectroscopie d'Absorption des rayons X, qui permet de déterminer l'état d'oxydation d'un élément et sa chimie de coordination, mais qui n'est pas aujourd'hui encore disponible pour les combustibles irradiés.

6.7.3. Echantillons analysés

Trois échantillons de combustible irradiés et 11 échantillons SIMFUELS, décrits dans le **Tableau 55**, ont été étudiés lors des deux axes expérimentaux. Les 11 échantillons SIMFUELS ont été regroupés dans trois groupes, en fonctions des caractéristiques des échantillons et des traitements thermiques réalisés. Ainsi, le groupe I consiste en deux échantillons dopés avec 11 PF (Ba, Ce, La, Mo, Nd, Pd, Rh, Rh, Sr, Tc, Y et Zr, sans Cs), dont un a été soumis à un traitement thermique sous atmosphère réductrice ($Ar + 4\% H_2$); le groupe II consiste en cinq échantillons dopés avec 12 PF (les 11 PF mentionnés plus du Cs, implanté par la méthode d'implantation ionique) dont quatre ont aussi subi des traitements thermiques sous $Ar + 4\% H_2$ à des températures de 573, 1473, 1773 et 1973 K; et le dernier groupe, groupe III, consiste en quatre échantillons

similaires à ceux du groupe II mais qui ont subi des traitements thermiques sous des conditions oxydantes (Ar pur) jusqu'à 573, 1473 et 1973 K.

Axe de travail	Echantillon	Atmosphère	Température finale (K)	Temps à T max (min)	Caractérisations faites
Combustibles Irradiés	T ₀ -IF	-	-	-	MO, SIMS, μ sonde
	IF1500	Réductrice	1773	35	MEB, μ sonde
	VERDON 1	Oxydante, Réductrice	2873	0	MO, DRX, μ sonde
SIMFUELS	T ₀	-	-	-	MEB-EDS, SAX
	AT	Réductrice	1773	60	MEB-EDS, SAX
	T ₀ -R	-	-	-	MEB-EDS, SAX
	R300	Réductrice	573	180	MEB-EDS, SAX
	R1200	Réductrice	1473	30	MEB-EDS, SAX
	R1500	Réductrice	1773	15	MEB-EDS, SAX
	R1700	Réductrice	1973	10	MEB-EDS, SAX
	T ₀ -O	-	-	-	MEB-EDS, SAX
	O300	Oxydante	573	180	MEB-EDS, SAX
	O1200	Oxydante	1473	30	MEB-EDS, SAX
O1700	Oxydante	1973	10	MEB-EDS, SAX	

Table 55: Echantillons étudiés dans les deux axes expérimentaux

6.7.4. Résultats obtenus

Les résultats obtenus lors des deux axes expérimentaux ont permis de valider ou de réfuter la plupart des hypothèses faites dans le mécanisme proposé par (Nicaise, 2004b). Le mécanisme considère un état initial (avant que l'accident nucléaire ne commence) puis quatre étapes principales correspondant à 1300 K, entre 1400 et 1700 K, 2100 K et finalement 2600 K. Les hypothèses validées et réfutées sont indiquées en vert et rouge, respectivement, sur ce mécanisme présenté dans la **Figure 129**. Malgré les traitements thermiques et caractérisation réalisés, quelques hypothèses n'ont pas pu être vérifiées, notamment celles liées à la chimie du Cs et à l'état initial du Mo et du Ru. La principale raison à cela est que l'implantation des ions du Cs a créé des états chimiques métastables et que les techniques de caractérisations actuelles disponibles pour des combustibles irradiés permettent de déterminer la distribution des PF et leurs associations, mais pas leurs états chimiques. Particulièrement pour le Ba, il n'a pas été observé de précipités de ce PF n'existent pas dans un échantillon de combustible irradié dans des conditions normales de fonctionnement, même à très haut taux de combustion (150 GWd.t⁻¹). Au contraire, ce FP reste dissous dans la matrice de combustible et peut précipiter sous l'effet de la température, entre 1373 et 1773 K. Si le Ba est dissous dans la matrice, il est alors forcément sous une forme oxydée, tel que BaO.

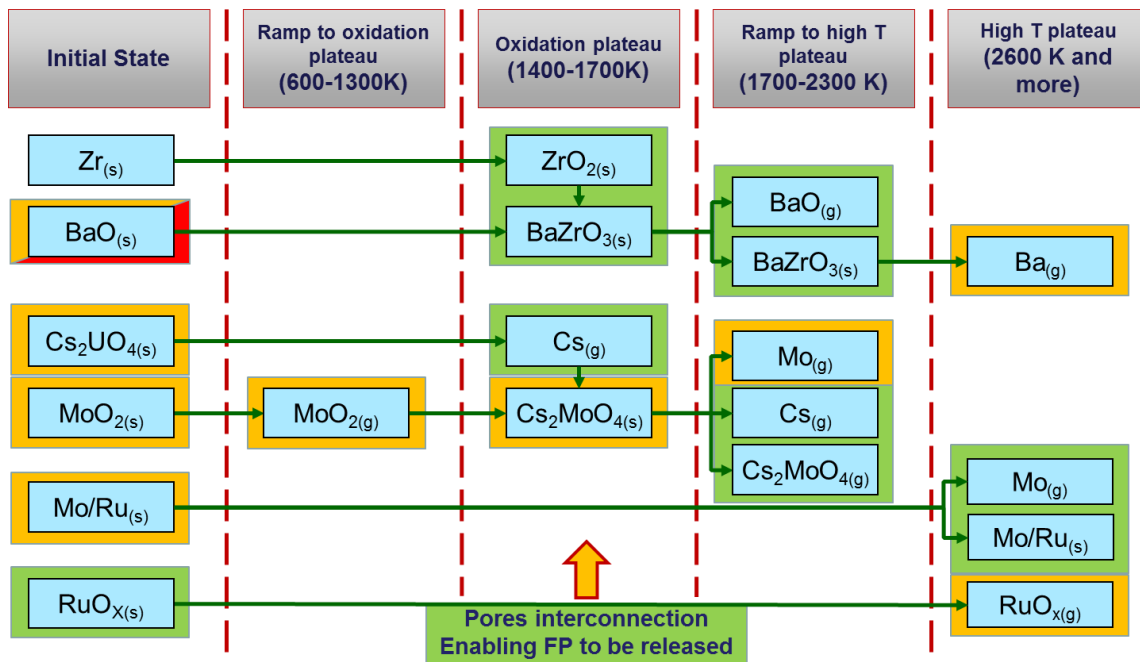


Figure 129: Hypothèses validées (vert), réfutées (rouge) et restantes (orange) du mécanisme proposé par Nicaise.

6.7.5. Nouveaux mécanismes

Le mécanisme original proposé par (Nicaise, 2004b) a été modifié à l'aide des résultats obtenus lors des deux axes expérimentaux mis en place dans cette thèse. Deux mécanismes ont été proposés dans ce travail, basés aussi sur un traitement thermique du type VERCORS (une étape initiale et quatre étapes intermédiaires). Le premier mécanisme, présenté dans la **Figure 130**, est principalement une modification du mécanisme original, qui prend en compte des résultats obtenus lors de l'axe des combustibles irradiés et des résultats obtenus à l'aide d'échantillons SIMFUELS, traités sous atmosphère réductrice. Les deux dernières étapes de ce premier mécanisme se déroulent sous atmosphère réductrice. Le deuxième mécanisme, présenté dans la **Figure 131**, considère que les deux dernières étapes (à 2100 et 2600 K) ont lieu sous atmosphère oxydante. Les phases hypothétiques qui n'ont pas pu être validées ou réfutées lors de cette thèse, tels que l'état initial du Cs et son évolution et la présence des oxydes du Mo et Ru à l'état initial, ont été reprises dans les deux mécanismes. L'état initial et les interactions qui ont lieu au cours des étapes intermédiaires sont décrites ci-dessous.

Etat initial

L'état initial considéré est similaire à celui du mécanisme proposé par (Nicaise, 2004b), à l'exception du baryum. En effet, les observations expérimentales ont démontré que le Ba peut rester dissous dans la matrice, même à des concentrations élevées. Donc, les précipités initiaux sont Cs_2UO_4 , MoO_2 , RuO_x et un alliage métallique composé de Mo, Ru, Pd, Rh et Tc, connu sous le nom des inclusions blanches.

1300 K

D'après le mécanisme initial, le MoO_2 devrait se volatiliser à 1300K. Néanmoins, le Mo n'est pas encore relâché car les pores ne sont pas interconnectés.

Plateau d'oxydation

Cette étape, comprise entre 1400 et 1800 K, se développe sous atmosphère oxydante. Comme observé lors des caractérisations faites sur les échantillons SIMFUELS soumis à des traitements thermiques en atmosphère oxydante, des précipités du Mo sous forme oxydée ont été formés à 1473 K. Ces précipités contenaient également du Ba, et en fonction des estimations thermodynamiques et des résultats de Spectroscopie d'Absorption des rayons X (SAX), la forme chimique serait BaMoO_4 . Des observations expérimentales ont démontré que Ba précipite également sous la forme BaZrO_3 , par interaction avec le Zr oxydé (Zr provenant de la gaine ainsi que produit de fission), entre 1373 et 1773 K. L'interconnexion partielle des pores a été observée dans l'échantillon d' UO_2 irradié traité à 1773 K sous atmosphère réductrice (échantillon IF1500). Cette interconnexion permettrait aux espèces gazeuses d'être relâchées hors le combustible. Le Mo présent dans les précipités métalliques serait oxydé et réagirait avec le BaZrO_3 pour former BaMoO_4 . Par rapport au Cs, il est considéré que la forme chimique initiale, Cs_2UO_4 , est partiellement détruite et le Cs commence à être relâché sous forme gazeuse. Néanmoins, la plupart du Cs réagirait avec le MoO_2 pour donner Cs_2MoO_4 , espèce moins volatile, en limitant le relâchement de du Cs.

Atmosphère Réductrice

2100 K

Dans ce cas, il est considéré que l'atmosphère devient réductrice après le plateau d'oxydation (néanmoins pas assez réductrice pour réduire le ZrO_2 de la gaine). Dans ce scénario, le MoO_2 existant serait réduit et réintégrerait les précipités métalliques. Le Cs_2MoO_4 formé lors du plateau d'oxydation serait partiellement détruit mais aussi volatilisé, conduisant à la libération du Cs et du Mo sous les formes Cs_{g} et $\text{Cs}_2\text{MoO}_{4\text{g}}$. Comme observé dans les traitements thermiques effectués sur des échantillons SIMFUEL sous atmosphère réductrice, le BaZrO_3 est partiellement détruit dans ces conditions et Ba est libérée sous la forme BaO_{g} .

2600 K

Lors du plateau à haute température (2600K et plus) sous atmosphère réductrice, la destruction de BaZrO_3 continuerait et Ba serait relâché sous la forme BaO_{g} . La plupart du ZrO_2 produit par la destruction du BaZrO_3 serait dissout dans la matrice d' UO_2 . Le Mo serait volatilisé sous la forme Mo_{g} et relâché, ainsi que les oxydes de Ru (RuO_{xg}).

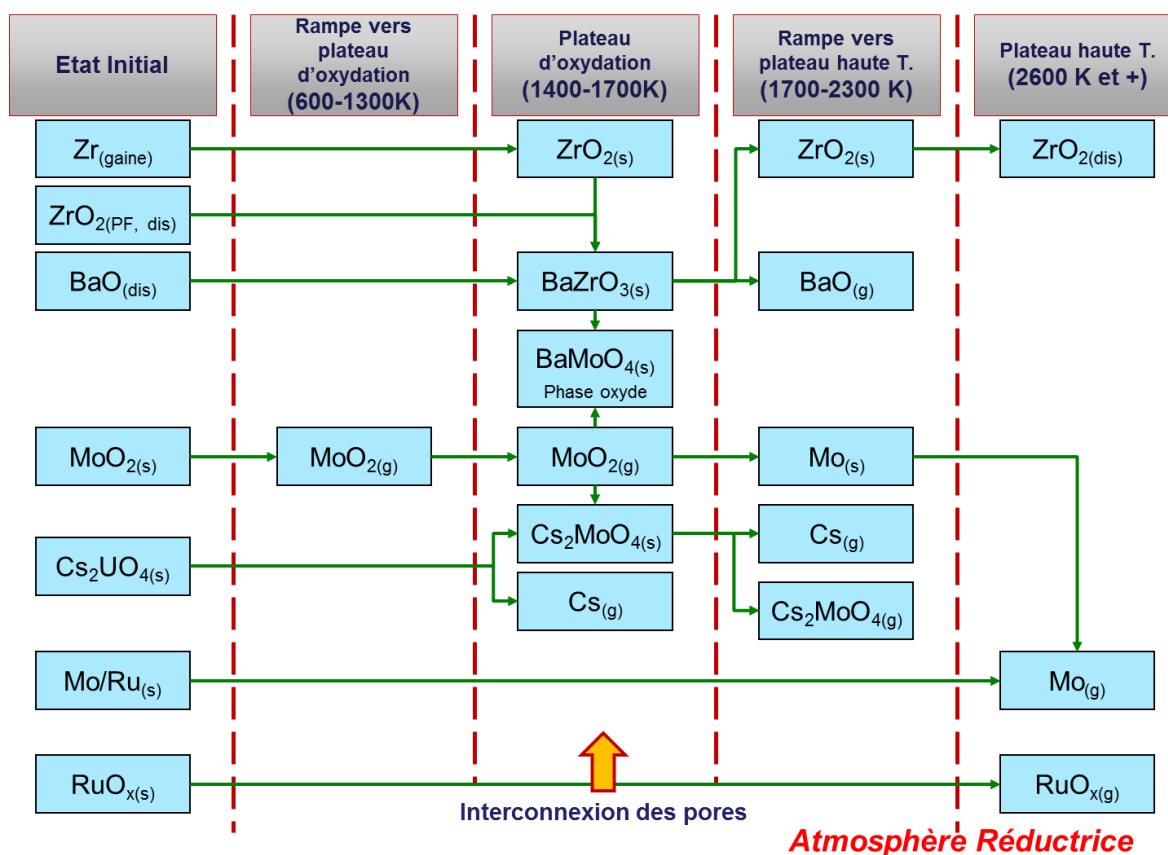


Figure 130: Nouveau mécanisme dont les deux dernières étapes se développent sous atmosphère réductrice

Atmosphère oxydante

2100 K

Au cours de cette rampe vers le plateau à haute température, sous atmosphère oxydante, le Mo présent dans les précipités métalliques continue à s'oxyder. Une fraction du Ru, aussi présent dans ces précipités serait également oxydée (en fonction du potentiel d'oxygène). Le Mo serait partiellement relâché sous forme MoO_2 mais serait également dissous dans la phase oxyde. Le Cs_2MoO_4 serait partiellement détruit mais aussi volatilisé, conduisant à la libération de Mo et Cs sous les formes Cs_g , $MoO_{2(g)}$ et $Cs_2MoO_{4(g)}$.

2600 K

Pendant le plateau à haute température, sous atmosphère oxydante, les précipités métalliques de Mo et Ru continueraient à être oxydés et relâchés. Le Ba présent dans la phase oxyde sous la forme $BaMoO_4$ serait relâché, sous les formes $BaMoO_{4(g)}$ ou BaO_g .

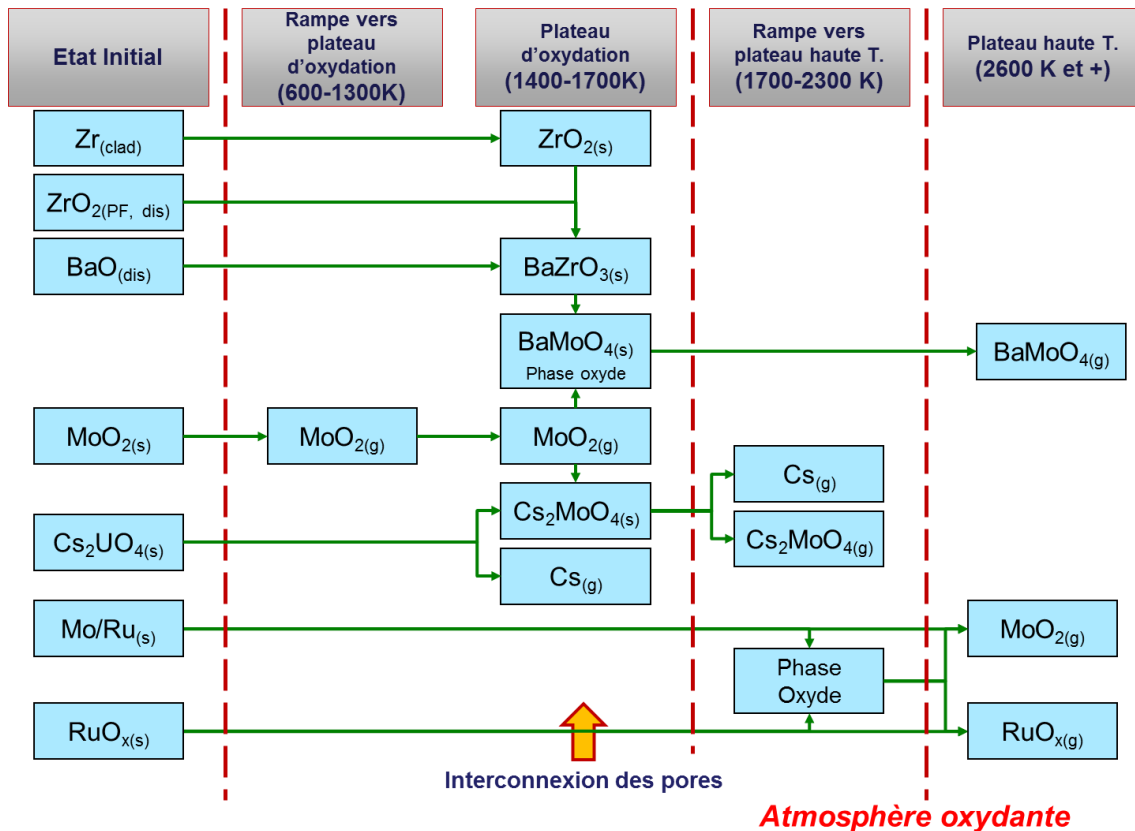


Figure 131: Nouveau mécanisme dont les deux dernières étapes se développent sous atmosphère oxydante.

6.7.6. Conclusions

Deux axes expérimentaux ont été mis en place avec l'objectif d'étudier le comportement du Ba, Cs, Mo et Ru lors d'un accident nucléaire grave. Des échantillons d' UO_2 irradié et des matériaux modèles ont été soumis à des conditions représentatives. Bien que ces matériaux modèles, connus sous le nom de SIMFUELS, présentent des limitations vis-à-vis de l'état initial d'un combustible irradié, ils permettent d'étudier le comportement des PF à haute température et sous différentes atmosphères. Les résultats expérimentaux obtenus dans ces deux axes ont été comparés à un mécanisme de relâchement proposé dans par (Nicaise, 2004b), dans le but de valider ou de réfuter les états chimiques initiaux proposés et leur évolution lors d'un essai du type VERCORS. Deux mécanismes ont été proposés, selon le type d'atmosphère lors des deux dernières étapes: réductrice dans un cas et oxydante dans l'autre. Néanmoins, des hypothèses sur certaines formes chimiques et leur évolutions tels que proposés dans le mécanisme original n'ont pas pu être validées. Des traitements thermiques sur des nouveaux types d'échantillons des matériaux modèles, qui permettraient d'étudier la chimie du Cs sont proposés, ainsi que des traitements thermiques sous des atmosphères plus oxydantes que celles étudiées dans cette thèse.

References

- AIEA, 2001. INES: Echelle Internationale des événements Nucléaires (Manuel de l'Utilisateur). AIEA, Vienna.
- Allen, M.D., Stockman, H.W., Reil, K.O., Grimley, A.J., Camp, W.J., 1988. Proceedings of the International Conference on Thermal Reactor Safety.
- André, B., Ducros, G., Leveque, J.P., Osborne, M.F., Lorenz, R.A., 1996. Fission product releases in severe light water reactor accident conditions: ORNL/CEA measurements versus calculations. *Nucl. Technol.* 114, 23–49.
- Baichi, M., 2001. Contribution à l'Etude du Corium d'un Réacteur Nucléaire accidenté: Aspects puissance résiduelle et thermodynamique des systèmes U-UO₂ et UO₂-ZrO₂ (PhD. Thesis). Institut National Polytechnique de Grenoble, Grenoble, France.
- Bair, W.J., 1970. Inhalation of radio nuclides and carcinogenesis. *Energy Cit. Database*.
- Baker, L., Fink, J.K., Simms, R., Schlenger, B.J., Herceg, J.E., 1988. Source Term Experiments Project (STEP): A Summary (NP-5753M). Electric Power Research Institute.
- Bale, C.W., Bélisle, E., Chartrand, P., Deckerov, S.A., Eriksson, G., Hack, K., Jung, I.-H., Kang, Y.-B., Melançon, J., Pelton, A.D., Robelin, C., Petersen, S., 2009. FactSage thermochemical software and databases — recent developments. *Calphad* 33, 295–311. doi:10.1016/j.calphad.2008.09.009
- Bernard, S., Gallais-During, A., 2013. International Source Term Program - VERDON-3 test: Fission Product Release from High Burn up MOX fuel in oxidizing conditions. CEA, CEA Cadarache.
- Bonnin, J., Berthet, B., Bayle, S., Hanniet, N., Jeury, F., Gaillot, S., Martin, C., Laurie, M., Siri, B., 1997. Phebus PF, FPT1 - Preliminary Report (IPSN/DRS/SEA/LERES/97/727, Note Technique LERES no. 24/97, Document Phebus PF IP/97/334).
- Broughton, J.M., Pui, K., Petti, D.A., Tolman, E.L., 1989. Scenario of the Three Mile Island Unit 2 accident Broughton. *Nucl. Technol.* 87, 34–53.
- Carboneau, M.L., Berta, V.T., Modro, M.S., 1989. Experiment Analysis and Summary Report for OECD LOFT Project Fission Product Experiment LP-FP-2 (No. OECD LOFT-T-3806). Organization for Economic Cooperation and Development.
- Chatelard, P., Reinke, N., Arndt, S., Belon, S., Cantrel, L., Carenini, L., Chevalier-Jabet, K., Cousin, F., Eckel, J., Jacq, F., Marchetto, C., Mun, C., Piar, L., 2006. ASTEC V2 severe accident integral code main features, current V2.0 modelling status, perspectives. *Nucl. Eng. Des.* doi:10.1016/j.nucengdes.2013.06.040
- Clément, B., Zeyen, R., 2013. The objectives of the Phébus FP experimental programme and main findings. *Ann. Nucl. Energy* 61, 4–10. doi:10.1016/j.anucene.2013.03.037
- Collins, J., Osborne, M.F., Lorenz, R.A., 1987. Fission Product Tellurium release behaviour under Severe Light Water Reactor Accident conditions. *Nucl. Technol.* 77, 18–31.
- Cox, D.S., Hunt, C.E.L., Barrand, R.D., O'Connor, R.F., Iglesias, F.C., 1991. American Nuclear Society International Topical Meeting on the Safety of Thermal Reactors.
- Cox, D.S., Hunt, C.E.L., O'Connor, R.F., Barrand, R.D., Iglesias, F.C., 1990. Proceedings of the International Symposium on High Temperature Oxidation and Sulphidation Process.
- Cox, D.S., Liu, Z., Dickson, R.S., Elder, P.H., 1992. Proceedings of the Third International Conference on CANDU Fuel.
- Cox, D.S., O'Connor, R.F., Smeltzer, W.W., 1992. Measurement of oxidation/reduction kinetics to 2100°C using non-contact solid-state electrolytes. *Solid State Ion.* 53–56, Part 1, 238–254. doi:10.1016/0167-2738(92)90387-5
- De Boer, R., Cordfunke, E.H.P., 1997. The chemical form of fission product tellurium during reactor accident conditions. *J. Nucl. Mater.* 240, 124–130. doi:10.1016/S0022-3115(96)00600-9
- De Boer, R., Cordfunke, E.H.P., 1995. Reaction of tellurium with Zircaloy-4. *J. Nucl. Mater.* 223, 103–108. doi:10.1016/0022-3115(95)00005-4

- Decanis, C., 2003. Résultats de perçages des crayons UO₂ ALIX 6 cycles FXOGAC N05, L01, E04 et Q02 réalisés dans le cadre du Projet Performances Burn-up (No. NT DEC/SA3C 03-056). CEA, Cadarache, France.
- DeVaal, J., Irish, J.D., Dickson, L., Craig, S.T., Jonckheere, M., Bourque, L.R., 1997. Proceedings of the Fifth International Conference on CANDU Fuel.
- DeVaal, J.W., Popov, N.K., MacDonald, R.D., Dickson, L.W., Cox, D.S., Jonckheere, M., Dutton, R.J., 1992. Proceedings of the Third International Conference on CANDU Fuel.
- Dickson, L., DeVaal, J., Irish, J.D., Elder, P., Jonckheere, M., Yamazaki, A.R., 1995a. Proceedings of the Fourth International Conference on CANDU Fuel.
- Dickson, L., Elder, P., DeVaal, J., Irish, J.D., Yamazaki, A.R., 1995b. Proceedings of the Canadian Nuclear Society 1995 Annual Conference.
- Dickson, R.S., Dickson, L.W., 1998. Third OECD Specialist Meeting on Nuclear Aerosols in Reactor Safety.
- Dubourg, R., Faure-Geors, H., Nicaise, G., Barrachin, M., 2005. Fission product release in the first two PHEBUS tests FPT0 and FPT1. Nucl. Eng. Des. 235, 2183–2208. doi:10.1016/j.nucengdes.2005.03.007
- Dubourg, R., Taylor, P., 2001. A qualitative comparison of barium behaviour in the PHEBUS FPT0 test and analytical tests. J. Nucl. Mater. 294, 32–38. doi:10.1016/S0022-3115(01)00471-8
- Ducros, G., 1996. Atmosphere dependence of fission products release: the VERCORS 4 and 5 experiments.
- Ducros, G., 1994a. Non-destructive location of Fission Products in a damaged fuel rod section using gamma-emission tomography.
- Ducros, G., 1994b. Non-destructive location of Fission Products in a damaged fuel rod section using gamma-emission tomography.
- Ducros, G., Bernard, S., Ferroud-Plattet, M.P., Ichim, O., 2009. Use of gamma spectrometry for measuring fission product releases during a simulated PWR severe accident: application to the VERDON experimental program. Presented at the Int. Conf. ANIMA 2009, Marseille, France.
- Ducros, G., Malgouyres, P., Kissane, M., Boulaud, D., Durin, M., 2001. Fission product release under severe accidental conditions: general presentation of the program and synthesis of VERCORS 1–6 results. Nucl. Eng. Des. 208, 191–203. doi:10.1016/S0029-5493(01)00376-4
- Ducros, G., Pontillon, Y., Malgouyres, P.P., 2013. Synthesis of the VERCORS experimental programme: Separate-effect experiments on Fission Product release, in support of the PHEBUS-FP programme. Ann. Nucl. Energy 61, 75–87. doi:10.1016/j.anucene.2013.02.033
- Duriez, C., Dupont, T., Schmet, B., Enoch, F., 2008. Zircaloy-4 and M5[®] high temperature oxidation and nitriding in air. J. Nucl. Mater. 380, 30–45. doi:10.1016/j.jnucmat.2008.07.002
- Elam, W.T., Ravel, B., Sieber, J.R., 2002. A new atomic database for X-ray spectroscopic calculations. Radiat. Phys. Chem. 63, 121–128.
- Ferroud-Plattet, M.P., Bonnin, J., Gallais-During, A., Bernard, S., Grandjean, J.P., Ducros, G., 2009. CEA VERDON laboratory at Cadarache: new hot cell facilities devoted to studying irradiated fuel behaviour and fission product releases under simulated accident conditions. Presented at the Int. Conf. HOTLAB 2009, Prague, Czech Republic.
- Gallais-During, A., Bonnin, J., Malgouyres, P.-P., Morin, S., Bernard, S., Gleizes, B., Pontillon, Y., Hanus, E., Ducros, G., 2014. Performance and first results of fission product release and transport provided by the VERDON facility. Nucl. Eng. Des. 277, 117–123. doi:10.1016/j.nucengdes.2014.05.045
- Giacchetti, G., Sari, C., 1976. Behavior of Molybdenum in Mixed-Oxide Fuel. Nucl. Technol. 31, 62–69.
- Giannici, F., Shirpour, M., Longo, A., Martorana, A., Merkle, R., Maier, J., 2011. Long-Range and Short-Range Structure of Proton-Conducting Y:BaZrO₃. Chem. Mater. 23, 2994–3002. doi:10.1021/cm200682d

- Gittus, J.H., Matthews, J.R., Potter, P.E., 1989. Safety aspects of fuel behaviour during faults and accidents in pressurised water reactors and in liquid sodium cooled fast breeder reactors. *J. Nucl. Mater.* 166, 132–159. doi:10.1016/0022-3115(89)90185-2
- Gleizes, B., Morin, S., 2012. International Source Term Program - VERDON-2 test: Fission Product Release and Transport from MOX fuel under air ingress conditions. CEA, CEA Cadarache.
- Grånäs, O., Korzhavyi, P.A., Kissavos, A.E., Abrikosov, I.A., 2008. Theoretical study of the Mo–Ru sigma phase. *Calphad* 32, 171–176. doi:10.1016/j.calphad.2007.06.001
- Gürler, R., 1999. Constitutional studies of molybdenum–ruthenium alloys using ultra-rapidly solidified samples. *J. Alloys Compd.* 285, 133–136. doi:10.1016/S0925-8388(98)00752-X
- Hanniet, N., Repetto, G., 1999. PHEBUS FPT0 Final Report, CD Version. Suntech 10/99.
- Herranz, L.E., Vela-García, M., Fontanet, J., Prá, C.L. del, 2007. Experimental interpretation and code validation based on the PHEBUS-FP programme: Lessons learnt from the analysis of the containment scenario of FPT1 and FPT2 tests. *Nucl. Eng. Des.* 237, 2210–2218. doi:10.1016/j.nucengdes.2007.03.022
- Hidaka, A., 2011. Outcome of VEGA Program on Radionuclide Release from Irradiated Fuel under Severe Accident Conditions. *J. Nucl. Sci. Technol.* 48, 85–102. doi:10.1080/18811248.2011.9711682
- Hidaka, A., Kudo, T., Nakamura, T., Uetsuka, H., 2002a. Enhancement of Cesium Release from Irradiated Fuel at Temperature above 2,800 K. *J. Nucl. Sci. Technol.* 39, 273–275. doi:10.1080/18811248.2002.9715185
- Hidaka, A., Kudo, T., Nakamura, T., Uetsuka, H., 2002b. Decrease of Cesium Release from Irradiated UO₂ Fuel in Helium Atmosphere under Elevated Pressure of 1.0 MPa at Temperature up to 2,773K. *J. Nucl. Sci. Technol.* 39, 759–770. doi:10.1080/18811248.2002.9715258
- Hobbins, R.R., Petti, D.A., Hargman, D.L., 1993. Fission product release from fuel under severe accident conditions. *Nucl. Technol.* 101, 270–281.
- Hofmann, P., 1999. Current knowledge on core degradation phenomena, a review. *J. Nucl. Mater.* 270, 194–211. doi:10.1016/S0022-3115(98)00899-X
- Hofmann, P., Hagen, S., Noak, V., Schanz, G., Sepold, L., 1997. Chemical-physical behavior of light water reactor core components tested under severe reactor accident conditions in the CORA facility. *Nucl. Technol.* 118, 200–224.
- Hunt, C.E.L., Iglesias, F.C., Cox, D.S., Keller, N., Barrand, R.D., Mitchell, R.F., O'Connor, R.F., 1986. Proceedings of the International Conference on CANDU Fuel.
- Iglesias, F.C., 1989. Ruthenium release kinetics from uranium oxides.
- Iglesias, F.C., Lewis, B.J., Reid, P.J., Elder, P., 1999. Fission product release mechanisms during reactor accident conditions. *J. Nucl. Mater.* 270, 21–38. doi:10.1016/S0022-3115(98)00738-7
- Irish, J.D., Craig, S.T., Bourque, L.R., Jonckheere, M., Kyle, G., Valliant, P.J., Dickson, L.W., Peplinskie, R.T., 1998. Proceedings of the 19th Annual Conference of the Canadian Nuclear Society.
- Irish, J.D., Craig, S.T., Valliant, P.J., 1999. Proceedings of the Sixth International Conference on CANDU Fuel.
- IRSN, n.d. Institute de Radioprotection et de Sûreté Nucléaire.
- Johnson, C.H., VanTassell, V.J., 1991. Acute barium poisoning with respiratory failure and rhabdomyolysis. *Ann. Emerg. Med.* 20, 1138–1142. doi:10.1016/S0196-0644(05)81393-9
- Johnson, I., Johnson, C.E., 1988. Mass spectrometry studies of fission product behavior: I. Fission products released from irradiated LWR fuel. *J. Nucl. Mater.* 154, 67–73. doi:10.1016/0022-3115(88)90120-1
- Kleykamp, H., 1993. The solubility of selected fission products in UO₂ and (U,Pu)O₂. *J. Nucl. Mater.* 206, 82–86.
- Kleykamp, H., 1989a. Constitution and thermodynamics of the Mo–Ru, Mo–Pd, Ru–Pd and Mo–Ru–Pd systems. *J. Nucl. Mater.* 167, 49–63. doi:10.1016/0022-3115(89)90424-8

- Kleykamp, H., 1989b. Constitution and thermodynamics of the Mo-Ru, Mo-Pd, Ru-Pd and Mo-Ru-Pd systems. *J. Nucl. Mater.* 167, 49–63. doi:10.1016/0022-3115(89)90424-8
- Kleykamp, H., 1988. The constitution of the Mo-Ru system. *J. Common Met.* 136, 271–275. doi:10.1016/0022-5088(88)90430-4
- Kleykamp, H., 1985. The Chemical State of Fission Products in Oxide Fuels. *J. Nucl. Mater.* 131, 221–246.
- Knipe, A.D., Ploger, S.A., Osetek, D., 1986. PBF Severe Fuel Damage Scoping Test – Test Results Report (No. NUREG/CR-4683). US Nuclear Regulatory Commission.
- Kudo, T., Hidaka, A., Nakamura, T., Uetsuka, H., 2001. Influence of Pressure on Cesium Release from Irradiated Fuel at Temperatures up to 2,773 K. *J. Nucl. Sci. Technol.* 38, 910–911. doi:10.1080/18811248.2001.9715115
- Kudo, T., Nakamura, T., Kida, M., Fuketa, T., 2006. Technical Meeting on Severe Accident and Accident Management.
- Lanning, D.D., Lombardo, N.J., Fitzsimmons, D.E., Hensley, W.K., Panisko, F.E., 1988a. Coolant Boilaway and Damage Progression Program Data Report: Full-Length High Temperature Experiment 4 (No. PNL-6368). Pacific Northwest Laboratories.
- Lanning, D.D., Lombardo, N.J., Fitzsimmons, D.E., Hensley, W.K., Panisko, F.E., 1988b. Coolant Boilaway and Damage Progression Program Data Report: Full-Length High Temperature Experiment 5 (No. PNL-6540). Pacific Northwest Laboratories.
- Leveque, J.P., Lhiaubet, G., Boulaud, D., 1991. Programme Expérimentale HEVA - Rapport Final.
- Lewis, B.J., Andre, B., Morel, B., Dehaut, P., Maro, D., Purdy, P.L., Cox, D.S., Iglesias, F.C., Osborne, M.F., Lorenz, R.A., 1995. Modelling the release behaviour of cesium during severe fuel degradation. *J. Nucl. Mater.* 227, 83–109. doi:10.1016/0022-3115(95)00130-1
- Lewis, B.J., Corse, B.J., Thompson, W.T., Kaye, M.H., Iglesias, F.C., Elder, P., Dickson, R., Liu, Z., 1998. Low volatile fission-product release and fuel volatilization during severe reactor accident conditions. *J. Nucl. Mater.* 252, 235–256. doi:10.1016/S0022-3115(97)00292-4
- Lewis, B.J., Dickson, R., Iglesias, F.C., Ducros, G., Kudo, T., 2008. Overview of experimental programs on core melt progression and fission product release behaviour. *J. Nucl. Mater.* 380, 126–143. doi:10.1016/j.jnucmat.2008.07.005
- Lewis, B.J., Thompson, W.T., Iglesias, F.C., 2012. 2.20 - Fission Product Chemistry in Oxide Fuels, in: Rudy J.M. Konings (Ed.), *Comprehensive Nuclear Materials*. Elsevier, Oxford, pp. 515–546.
- Liu, Z., Cox, D.S., Dickson, R.S., Elder, P.H., 1994. Proceedings of the 15th Annual Canadian Nuclear Society Conference.
- LLorenz, I., Solari, P.L., Sitaud, B., Bès, R., Camelli, S., Hermange, H., Othmane, G., Safi, S., Moisy, P., Wahu, S., Bresson, C., Schlegel, M.L., Menut, D., Bechade, J.L., Martin, P., Hazemann, J.L., Proux, O., Den Auwer, C., 2014. X-ray absorption spectroscopy investigations on radioactive matter using MARS beamline at SOLEIL synchrotron. *Radiochim Acta* 102, 957–972.
- Lombardo, N.J., Lanning, D.D., Panisko, F.E., 1988. Coolant Boilaway and Damage Progression Program Data Report: Full-Length High Temperature Experiment 2 (No. PNL-6551). Pacific Northwest Laboratories.
- Lorenz, R.A., Osborne, M.F., 1995. A summary of ORNL fission products release tests with recommended release rates and diffusion coefficients. NuregCR-6261.
- Lucuta, P.G., 1991a. Microstructural features of SIMFUEL - Simulated high-burnup UO₂-based nuclear fuel. *J. Nucl. Mater.* 178, 48–60.
- Lucuta, P.G., 1991b. Microstructural features of SIMFUEL - Simulated high-burnup UO₂-based nuclear fuel. *J. Nucl. Mater.* 178, 48–60.
- MacDonald, R.D., DeVaal, J., Cox, D.S., Dickson, L., Jonckheere, M., Ferris, C., Keller, N., Wadsworth, S.L., 1991. Proceedings of the Thermal Reactor Safety Meeting.
- March, P., Simondi-Teisseire, B., 2013. Overview of the facility and experiments performed in Phébus FP. *Ann. Nucl. Energy* 61, 11–22. doi:10.1016/j.anucene.2013.03.040

- Martella, T., Burle, M., Pras, M., 2002. ALIX PROGRAM - Non-destructive Examinations of E04 rod (FX0GAC), with M5 cladding, After six irradiation cycles in Gravelines 5 reactor (No. NT DEC/SA3C 02-102). CEA, Cadarache, France.
- Martin, P.M., Belin, R.C., Valenza, P.J., Scheinost, A.C., 2009. EXAFS study of the structural phase transition in the americium zirconate pyrochlore. *J. Nucl. Mater.*, Plutonium Futures - The Science 2008 Proceedings of a Topical Conference on Plutonium and Actinides: Plutonium Futures - The Science 2008 385, 126–130. doi:10.1016/j.jnucmat.2008.10.028
- Martinson, Z.R., Gasparini, M., Hobbins, R.R., Petti, D.A., Allison, C.M., Hohorst, J.K., Hargman, D.L., Vinjamuri, K., 1989. PBF Severe Fuel Damage Test 1-3 Test Results Report (No. NUREG/CR-5354, EGG-2565). US Nuclear Regulatory Commission.
- Martinson, Z.R., Petti, D.A., Cook, B.A., 1986. PBF Severe Fuel Damage Test 1-1 Test Results Report (No. NUREG/CR-4684, EGG-2463). US Nuclear Regulatory Commission.
- Mott, B.W., Williams, J., 1953. LXXXVIII. The thermal etching of uranium. *Lond. Edinb. Dublin Philos. Mag. J. Sci.* 44, 841–844. doi:10.1080/14786440808520349
- Newville, M., 2004. Fundamentals of XAFS.
- Nicaise, G., 2004a. Interprétation du relâchement de Cs, Mo, Ba, I, Ru dans les essais VERCORS, VERCORS HT et VERCORS RT. (Note technique DPAM/SEMIC No. 2004/37).
- Nicaise, G., 2004b. Interprétation du relâchement de Cs, Mo, Ba, I, Ru dans les essais VERCORS, VERCORS HT et VERCORS RT. (Technical Note DPAM/SEMIC No. 2004/37). IRSN.
- Nicaise, G., Ozrin, V.D., 2003. Analysis of accidental sequence tests and interpretation of Fission Product release: Interdependence of Cs, Mo and Ba release. 8th Int. Conf. CANDU Fuel.
- Nicoll, S., Matzke, H., Grimes, R.W., Catlow, C.R.A., 1997. The behaviour of single atoms of molybdenum in urania. *J. Nucl. Mater.* 240, 185–195. doi:10.1016/S0022-3115(96)00716-7
- Osborne, M.F., 1991. Data summary report for fission products release test VI-5. NuregCR-5668.
- Osborne, M.F., Lorenz, R.A., 1992. ORNL studies of fission product release under LWR severe accident conditions. *Nuclear Safety* 33, 344–365.
- Paschoal, J.O.A., Kleykamp, H., Thuemmler, F., 1987. Phase equilibria in the pseudoquaternary barium oxide-uranium dioxide-zirconium dioxide-molybdenum dioxide system. *J. Nucl. Mater.* 151, 10–21.
- Pena, J.J., Enciso, S., Reventos, F., 1992. Thermal-Hydraulic Post-Test Analysis of OECD LOFT LP-FP-2 Experiment (International Agreement Report No. NUREG/IA-0049/ICSP-LP-FP-2).
- Petti, D.A., Martinson, Z.R., Hobbins, R.R., Allison, C.M., Carlson, E.R., Hargman, D.L., Cheng, T.C., Hartwell, J.K., Vinjamuri, K., Seifken, L.J., 1989. Power Burst Facility (PBF) Severe Fuel Damage Test 1-4 Test Results Report (No. NUREG/CR-5163, EGG-2542). US Nuclear Regulatory Commission.
- Petti, D.A., Martinson, Z.R., Hobbins, R.R., Osetek, D., 1991. Results from the power burst facility severe fuel damage test 1-4. A simulated severe fuel damage accident with irradiated fuel rods and control rods. *Nucl. Technol.* 94, 313–335.
- Piluso, P., Trillon, G., Journeau, C., 2005. The UO₂-ZrO₂ system at high temperature (T > 2000 K): importance of the meta-stable phases under severe accident conditions. *J. Nucl. Mater.*, Proceedings of the 11th International Symposium on Thermodynamics of Nuclear Materials 344, 259–264. doi:10.1016/j.jnucmat.2005.04.052
- Pontillon, Y., Bonnin, J., Addes, E., Cochaud, J.J., Piquemal, J., Pontillon, M., Roure, C., Volle, G., 2005a. Fission gas release under normal and off-normal conditions: New analytical device implemented at the CEA-Cadarache.
- Pontillon, Y., Ducros, G., 2010a. Behaviour of fission products under severe PWR accident conditions. The VERCORS experimental programme—Part 3: Release of low-volatile fission products and actinides. *Nucl. Eng. Des.* 240, 1867–1881. doi:10.1016/j.nucengdes.2009.06.025

- Pontillon, Y., Ducros, G., 2010b. Behaviour of fission products under severe PWR accident conditions: The VERCORS experimental programme—Part 2: Release and transport of fission gases and volatile fission products. *Nucl. Eng. Des.* 240, 1853–1866. doi:10.1016/j.nucengdes.2009.06.024
- Pontillon, Y., Ducros, G., Malgouyres, P.P., 2010. Behaviour of fission products under severe PWR accident conditions VERCORS experimental programme—Part 1: General description of the programme. *Nucl. Eng. Des.* 240, 1843–1852. doi:10.1016/j.nucengdes.2009.06.028
- Pontillon, Y., Gallais-During, A., 2012. International Source Term Program - VERDON-1 test: Fission Product Release from High Burn up UO₂ Fuel In Severe Accident Conditions. CEA, CEA Cadarache.
- Pontillon, Y., Malgouyres, P.P., Ducros, G., Nicaise, G., Dubourg, R., Kissane, M., Baichi, M., 2005b. Lessons learnt from VERCORS tests.: Study of the active role played by UO₂–ZrO₂–FP interactions on irradiated fuel collapse temperature. *J. Nucl. Mater., Proceedings of the 11th International Symposium on Thermodynamics of Nuclear Materials 344*, 265–273. doi:10.1016/j.jnucmat.2005.04.053
- Pujol, X., Blay, T., Roure, I., Lamontagne, J., 2004. FXOGAC/E04/4034, analyse de la porosité à partir d'images acquises au MEB d'un combustible REP UO₂ Alix irradié 6 cycles dans Gravelines 5 (Technical Note No. NT DEC/SA3C/04-023).
- Rasser, B., Desgranges, L., Pasquet, B., 2003. A new shielded SIMS instrument for analysis of highly radioactive materials. *Appl. Surf. Sci., Secondary ion mass spectrometry SIMS XIII 203–204*, 673–678. doi:10.1016/S0169-4332(02)00789-4
- Rausch, W.N., Hesson, G.M., Pilger, J.P., King, L.L., Goodman, R.L., 1986. Coolant Boilaway and Damage Progression Program Data Report: Full-Length High Temperature Experiment 1 (No. PNL-5691). Pacific Northwest Laboratories.
- Ravel, B., Newville, M., 2005. ATHENA, ARTEMIS, HEPHAESTUS: Data analysis for X-ray absorption spectroscopy using IFEFFIT. *J. Synchrotron Radiat.* 12, 537–541. doi:10.1107/S0909049505012719
- Richard, A., 2012. Étude par diffraction des rayons X des déformations induites par irradiation/implantation d'ions dans le dioxyde d'uranium. Poitiers.
- Royl, P., Breitung, W., Fischer, E.A., Schumacher, G., Gauntt, R.O., Wright, S.A., 1987. Contributions from the ACRR in-pile experiments to the understanding of key phenomena influencing unprotected loss of flow accident simulations in LMFBRs. *Nucl. Eng. Des.* 100, 387–408. doi:10.1016/0029-5493(87)90088-4
- Schwarz, M., Hache, G., von der Hardt, P., 1999a. PHEBUS FP: a severe accident research programme for current and advanced light water reactors. *Nucl. Eng. Des.* 187, 47–69. doi:10.1016/S0029-5493(98)00257-X
- Sehgal, B.R. (Ed.), 2012a. Chapter 2 - In-Vessel Core Degradation, in: *Nuclear Safety in Light Water Reactors*. Academic Press, Boston, pp. 89–183.
- Sehgal, B.R. (Ed.), 2012b. Chapter 3 - Early Containment Failure, in: *Nuclear Safety in Light Water Reactors*. Academic Press, Boston, pp. 185–306.
- Sehgal, B.R. (Ed.), 2012c. Chapter 4 - Late Containment Failure, in: *Nuclear Safety in Light Water Reactors*. Academic Press, Boston, pp. 307–424.
- Stöcker, H., Zschornak, M., Richter, C., Hanzig, J., Hanzig, F., Hinze, A., Potzger, K., Gemming, S., Meyer, D.C., 2014. Surface-near modifications of SrTiO₃ local symmetry due to nitrogen implantation investigated by grazing incidence XANES. *Scr. Mater.* 86, 1–4. doi:10.1016/j.scriptamat.2014.02.014
- Thomas, L.E., Beyer, C.E., Chariot, L.A., 1992. Microstructural analysis of LWR spent fuels at high burnup. *J. Nucl. Mater.* 188, 80–89. doi:10.1016/0022-3115(92)90457-V
- Tourasse, M., Boidron, M., Pasquet, B., 1992. Fission product behaviour in phenix fuel pins at high burnup. *J. Nucl. Mater.* 188, 49–57. doi:10.1016/0022-3115(92)90453-R
- Ugajin, M., Nagasaki, T., Itoh, A., 1996. Contribution to the study of the U-Cs-Mo-I-O system. *J. Nucl. Mater.* 230, 195–207. doi:10.1016/0022-3115(96)80014-6
- Valliant, P.J., Irish, J.D., Craig, S.T., 1999. Proceedings of the Sixth International Conference on CANDU Fuel.

- Veshchunov, M.S., Dubourg, R., Ozrin, V.D., Shestak, V.E., Tarasov, V.I., 2007. Mechanistic modelling of uranium fuel evolution and fission product migration during irradiation and heating. *J. Nucl. Mater.*, E-MRS 2006: Symposium N 362, 327–335. doi:10.1016/j.jnucmat.2007.01.081
- Veshchunov, M.S., Ozrin, V.D., Shestak, V.E., Tarasov, V.I., Dubourg, R., Nicaise, G., 2006. Development of the mechanistic code MFPR for modelling fission-product release from irradiated UO₂ fuel. *Nucl. Eng. Des.* 236, 179–200. doi:10.1016/j.nucengdes.2005.08.006
- Von der Hardt, P., Tattgrain, A., 1992. The Phebus fission product project, in: Matzke, H. (Ed.), *Nuclear Materials for Fission Reactors*, European Materials Research Society Symposia Proceedings. Elsevier, Oxford, pp. 115–130.
- Walle, E., Perrot, P., Foct, J., Parise, M., 2005. Evaluation of the Cs–Mo–I–O and Cs–U–I–O diagrams and determination of iodine and oxygen partial pressure in spent nuclear fuel rods. *J. Phys. Chem. Solids*, Proceedings of the 11th International Conference on High Temperature Materials Chemistry (HTMC-XI) 66, 655–664. doi:10.1016/j.jpcs.2004.06.078
- Xiao, H.Y., Zhang, F.X., Gao, F., Lang, M., Ewing, R.C., Weber, W.J., 2010. Zirconate pyrochlores under high pressure. *Phys. Chem. Chem. Phys.* 12, 12472–12477. doi:10.1039/C0CP00278J
- Zhang, C., Gao, M.C., Yang, Y., Zhang, F., 2014. Thermodynamic modeling and first-principles calculations of the Mo–O system. *Calphad* 45, 178–187. doi:10.1016/j.calphad.2013.12.006
- Zhang, F.X., Lian, J., Becker, U., Wang, L.M., Hu, J., Saxena, S., Ewing, R.C., 2007. Structural distortions and phase transformations in Sm₂Zr₂O₇ pyrochlore at high pressures. *Chem. Phys. Lett.* 441, 216–220. doi:10.1016/j.cplett.2007.05.018
- Zhukovskii, V.M., Yanushkevich, T.M., Tel'nykh, T.F., 1972. Phase diagram of the molybdenum trioxide-strontium oxide system. *Zh Neorg Khim Russ J Inorg Chem Engl Transl* 17, 2827–2830.

Figures List

FIGURE 1: Γ -EMISSION TOMOGRAPHY OF THE FUEL ROD EXTRACTED FROM VERCORS 5	38
FIGURE 2: PROPOSED MECHANISM - INITIAL STATE	42
FIGURE 3: PROPOSED MECHANISM - STAGE 2: 1273 K.....	42
FIGURE 4: PROPOSED MECHANISM - STAGE 3: SECOND HALF OF TEMPERATURE RAMP, BEGINNING OF THE OXIDATION PLATEAU	43
FIGURE 5: PROPOSED MECHANISM - STAGE 4: RAMP TO HIGH TEMPERATURE PLATEAU.	43
FIGURE 6: PROPOSED MECHANISM - STAGE 5: AT THE HIGH TEMPERATURE PLATEAU.	44
FIGURE 7: SIMPLIFIED RELEASE MECHANISM FOR BA, CS, MO AND RU	44
FIGURE 8: VERCORS 4 RELEASED FRACTIONS	46
FIGURE 9: VERCORS 5 RELEASED FRACTIONS	47
FIGURE 10: REPRESENTATION OF WORK AXES.....	50
FIGURE 11: HYPOTHETICAL PHASES TO BE VERIFIED IN THIS AXIS.....	53
FIGURE 12: FRACTOGRAPHY OF THE E04 PERIPHERY	55
FIGURE 13: SEM-BSE IMAGE (LEFT) OF THE PERIPHERY OF A FX0GAC-E04 SAMPLE AND PU X-RAY MAP (RIGHT)	55
FIGURE 14: PU AND ND QUANTITATIVE PROFILES, SAMPLE FX0GAC-E04	56
FIGURE 15: T ₀ -IF SAMPLE SEM-SE IMAGE.....	56
FIGURE 16: ANNEALING SEQUENCE FOLLOWED BY THE IF1500 SAMPLE AND CS RELEASE.....	57
FIGURE 17: IF1500 SAMPLE OPTICAL MICROSCOPE IMAGE.....	57
FIGURE 18: VERDON 1 ORIGINAL SAMPLE	58
FIGURE 19: FP RELEASE KINETICS IN VERDON 1	59
FIGURE 20: SAMPLES A2 (LEFT) AND B (RIGHT), PREPARED FROM THE VERDON 1 SAMPLE AFTER TEST.....	60
FIGURE 21: SEM-BSE IMAGES OF THE PERIPHERY (LEFT) AND CENTRE (RIGHT) OF T ₀ -IF SAMPLE	60
FIGURE 22: BA AND ZR ION MAPS OBTAINED AT THE PERIPHERY, HALF RADIUS AND CENTRE OF THE SAMPLE	61
FIGURE 23: BA AND ZR CONCENTRATION PROFILES DETERMINED BY EPMA	61
FIGURE 24: T ₀ -IF SAMPLE FRACTOGRAPHY (LEFT) ALONG WITH CS (MIDDLE) AND O (RIGHT) X-RAY MAPS.....	62
FIGURE 25: ¹³⁷ CS SIMS ION MAPS FROM THE PERIPHERY, HALF RADIUS AND CENTRE OF T ₀ -IF SAMPLE	62
FIGURE 26: ⁹⁹ MO AND ¹⁰² RU ION MAPS FROM THE PERIPHERY, HALF RADIUS AND CENTRE OF T ₀ -IF SAMPLE.....	63
FIGURE 27: MO, RU AND PD CONCENTRATION PROFILES IN T ₀ -IF SAMPLE	63
FIGURE 28: SEM-BSE IMAGES FROM THE CENTRE (RIGHT) AND PERIPHERY (LEFT), IF1500 SAMPLE	64
FIGURE 29: BA (LEFT) AND BA/ZR (RIGHT, SUPERPOSED) X-RAY MAPS, IF1500 SAMPLE CENTRE.....	64
FIGURE 30: BA (LEFT) AND BA (GREEN) - ZR (RED), SUPERPOSED X-RAY MAPS, IF1500 SAMPLE PERIPHERY	65
FIGURE 31: CS AND XE X-RAY MAPS, CENTRE OF IF1500 SAMPLE	65
FIGURE 32: CS AND XE X-RAY MAPS, PERIPHERY OF IF1500 SAMPLE	66
FIGURE 33: MO (LEFT) AND MO/PD (RIGHT) SUPERPOSED X-RAY MAPS, IF1500 SAMPLE CENTRE	66
FIGURE 34: MO (LEFT) AND MO/PD (RIGHT) SUPERPOSED X-RAY MAPS, IF1500 SAMPLE PERIPHERY	67
FIGURE 35: SAMPLE B OM IMAGE. THE THREE ZONES ARE OBSERVED: A MODERATE POROSITY ZONE, (A), AN ELEVATED POROSITY ONE (B) AND A LOW POROSITY ONE (C).....	68
FIGURE 36: SEM-SE IMAGE AND MO, U AND ZR X-RAY MAPS, FISSURE CLOSE TO THE PERIPHERY, SAMPLE A2	69
FIGURE 37: O, U, ZR AND PU QUANTITATIVE ANALYSES COVERING THE THREE POROSITY REGIONS, FROM THE ELEVATED POROSITY ZONE TOWARDS THE LOW POROSITY ONE	70
FIGURE 38: SEM-SE IMAGE (LEFT) AND ZR X-RAY MAP (RIGHT), PERIPHERY OF SAMPLE B	71
FIGURE 39: U, ZR, O, PU AND ND CONCENTRATION PROFILES, PERIPHERY OF SAMPLE B	71
FIGURE 40: ZONES ANALYSED BY XRD, SAMPLE B.....	72
FIGURE 41: ZONE 1 DIFFRACTOGRAM, SAMPLE B.....	73
FIGURE 42: ZONE 2 DIFFRACTOGRAM, SAMPLE B.....	73
FIGURE 43: ZONE 3 DIFFRACTOGRAM, SAMPLE B.....	74

FIGURE 44: ZONES 1, 2 AND 3 DIFFRACTOGRAMS - MORU ₂ PD LINES	74
FIGURE 45: ZR AND BA X-RAY MAPS, ELEVATED POROSITY REGION, SAMPLE B	75
FIGURE 46: ZR AND BA X-RAY MAPS, MODERATE POROSITY REGION, SAMPLE B	76
FIGURE 47: ZR AND BA TRANSVERSAL QUANTITATIVE PROFILES, SAMPLE A2	76
FIGURE 48: SEM-SE IMAGE AND CS X-RAY MAP, MODERATE POROSITY REGION, SAMPLE B	77
FIGURE 49: XE AND CS TRANSVERSAL QUANTITATIVE PROFILES, SAMPLE A2	77
FIGURE 50: ZONE 2 SEM-SE IMAGES, SAMPLE A2	78
FIGURE 51: SEM-SE IMAGE AND MO X-RAY MAP, LOW POROSITY REGION, SAMPLE A2	78
FIGURE 52: QUANTITATIVE PROFILES IN LARGE METALLIC PRECIPITATES LOCATED NEAR THE PERIPHERY (LEFT) AND CENTRE (RIGHT) OF SAMPLE A2.....	79
FIGURE 53: SEM-SE AND MO-PD SUPERPOSED X-RAY MAPS, MODERATE POROSITY REGION, SAMPLE A2	79
FIGURE 54: UO ₂ -ZRO ₂ PSEUDO BINARY PHASE DIAGRAM FROM (PILUSO ET AL., 2005)	81
FIGURE 55: ZR/(ZR+U) RATIO EVOLUTION FROM THE ELEVATED POROSITY ZONE TOWARDS THE LOW POROSITY ONE	81
FIGURE 56: UO ₂ -BAO PSEUDO BINARY PHASE DIAGRAM EXTRACTED FROM (PASCHOAL ET AL., 1987)	82
FIGURE 57: ELLINGHAM DIAGRAM EXTRACTED FROM (KLEYKAMP, 1985)	83
FIGURE 58: HYPOTHETICAL INTERACTIONS AND PHASES TO BE VERIFIED IN THIS AXIS	90
FIGURE 59: METALLIC MO K-EDGE ABSORPTION SPECTRUM	91
FIGURE 60: ANNEALING TESTS PERFORMED WITH SAMPLES SETS II AND III	94
FIGURE 61: PREDOMINANCE DIAGRAM FOR THE MO-CS-BA-ZR-U SYSTEM	95
FIGURE 62: SEM IMAGES OF THE SAMPLES BEFORE (T ₀ , LEFT) AND AFTER (AT, RIGHT) ANNEALING TEST.....	96
FIGURE 63: BA (LEFT) AND ZR (RIGHT) X-RAYS MAPS COLLECTED IN SAMPLES T ₀ (TOP) AND AT (BOTTOM) FROM SET I.....	97
FIGURE 64: BA L ₃ -EDGE (LEFT) HERDF-XANES AND ZR K-EDGE (RIGHT) XANES SPECTRA MEASURED ON SIMFUEL SAMPLES AND REFERENCES.....	98
FIGURE 65: MO (LEFT) AND RU (RIGHT) X-RAY MAPS, SAMPLES T ₀ AND AT.....	100
FIGURE 66: MO (LEFT) AND RU (RIGHT) K-EDGE XANES SPECTRA COLLECTED ON SET I SAMPLES AND REFERENCES.	101
FIGURE 67: SEM-BSE IMAGES OF SAMPLES R300, R1200, R1500 AND R1700, FROM SET II	102
FIGURE 68: SR, ZR, CS, CE AND ND CONCENTRATION EVOLUTION IN SET II SAMPLES MATRIX	103
FIGURE 69: BARIUM (LEFT) AND ZIRCONIUM (RIGHT) X-RAY MAPS OF SAMPLES SET II.....	104
FIGURE 70: SR, ZR, BA AND U CONCENTRATION EVOLUTION IN OXIDE PRECIPITATES OF SET II SAMPLES	105
FIGURE 71: BA/(ZR+BA) RATIO EVOLUTION IN OXIDE PRECIPITATES OF SET II SAMPLES	105
FIGURE 72: MO (LEFT) AND RU (RIGHT) X-RAY MAPS, SAMPLE SET II	107
FIGURE 73: QUANTITATIVE ANALYSES PERFORMED ON SAMPLES SET II METALLIC PRECIPITATES, REPRESENTED IN THE MO - RU BINARY PHASE DIAGRAM EXTRACTED FROM (KLEYKAMP, 1989A).....	108
FIGURE 74: XANES SPECTRA COLLECTED ON SAMPLE T ₀ -R MATRIX AND PRECIPITATES.....	109
FIGURE 75: MO - O PHASE DIAGRAM. ACCORDING TO THIS DIAGRAM, MOO ₃ CANNOT EXIST IN EQUILIBRIUM WITH METALLIC MO (ZHANG ET AL., 2014)	110
FIGURE 76: MO XANES SPECTRA, SAMPLE SET II.....	112
FIGURE 77: SAMPLES R1500, R1700 AND MO REFERENCE SUPERPOSED SPECTRA, HIGHLIGHTING THE MODIFICATION OF MO LOCAL ENVIRONMENT AT 1973 K.	113
FIGURE 78: ¹³³ CS ION IMAGES AT THE SURFACE AND BOTTOM OF THE CRATER, T ₀ -R SAMPLE.....	114
FIGURE 79: SEM-BSE IMAGES AND CORRESPONDING CS X-RAY MAPS, SAMPLES SET II.....	115
FIGURE 80: CS XANES SPECTRA, SAMPLE SET II	115
FIGURE 81: SAMPLE R300 AND CS ₂ MOO ₄ SUPERPOSED L3 XANES SPECTRA, SAMPLES SET II.....	116
FIGURE 82: SEM-BSE IMAGE OF SAMPLE O300, SAMPLE SET III	118
FIGURE 83: SEM-BSE (LEFT) AND SEM-SE (RIGHT) IMAGE OF SAMPLE O1200, SAMPLE SET III	118
FIGURE 84: SEM-BSE (LEFT) AND SEM-SE (RIGHT) IMAGE OF OXIDE PRECIPITATES PRESENT IN SAMPLE O1200, SAMPLE SET III.....	119

FIGURE 85: SEM-BSE (LEFT) AND SEM-SE (RIGHT) IMAGE OF METALLIC INCLUSIONS PRESENT IN SAMPLE O1200, SAMPLE SET III.....	119
FIGURE 86: SEM-BSE (LEFT) AND SEM-SE (RIGHT) IMAGES OF SAMPLE O1700, SAMPLES SET III.....	119
FIGURE 87: EVOLUTION OF FP CONCENTRATION IN SET III SAMPLES MATRIX	120
FIGURE 88: CS X-RAY MAPS ACQUIRED ON SAMPLES FROM SET III	121
FIGURE 89: CS XANES SPECTRA COLLECTED ON SAMPLES FROM SET III	122
FIGURE 90: BA (LEFT) AND ZR (RIGHT) X-RAY MAPS, SAMPLE SET III.....	123
FIGURE 91: MO (LEFT) AND RU (RIGHT) X-RAY MAPS COLLECTED ON SAMPLES FROM SET III	125
FIGURE 92: QUANTITATIVE ANALYSES PERFORMED ON SAMPLES SET III METALLIC PRECIPITATES, REPRESENTED IN THE MO - RU BINARY PHASE DIAGRAM EXTRACTED FROM (KLEYKAMP, 1989A).....	127
FIGURE 93: MO XANES SPECTRA, SAMPLES SET III	128
FIGURE 94: MOO ₃ -SRO PSEUDO BINARY PHASE DIAGRAM EXTRACTED FROM (ZHUKOVSKII ET AL., 1972)	134
FIGURE 95: HYPOTHETICAL PHASES INITIALLY PRESENT IN AN IRRADIATED FUEL AND THEIR EVOLUTION DURING A NUCLEAR SEVERE ACCIDENT.....	141
FIGURE 96: RELEASE MECHANISM INDICATING THE VALIDATED (GREEN), REFUTED (RED) AND UNANSWERED HYPOTHESES (ORANGE)	149
FIGURE 97: REPRESENTATION OF THE INITIAL STATE, NEW RELEASE MECHANISM.....	150
FIGURE 98: REPRESENTATION OF THE STAGE AT 1300K, NEW RELEASE MECHANISM.....	151
FIGURE 99: REPRESENTATION OF THE OXIDATION PLATEAU, FROM 1400 TO 1800 K, NEW RELEASE MECHANISM	152
FIGURE 100: REPRESENTATION OF THE RAMP TO HIGH TEMPERATURE PLATEAU UNDER REDUCING ATMOSPHERE, NEW RELEASE MECHANISM	153
FIGURE 101: REPRESENTATION OF THE RAMP TO HIGH TEMPERATURE PLATEAU UNDER OXIDIZING ATMOSPHERE, NEW RELEASE MECHANISM	154
FIGURE 102: REPRESENTATION OF THE HIGH TEMPERATURE PLATEAU UNDER REDUCING ATMOSPHERE, NEW RELEASE MECHANISM	155
FIGURE 103: REPRESENTATION OF THE HIGH TEMPERATURE PLATEAU UNDER OXIDIZING ATMOSPHERE, NEW RELEASE MECHANISM	156
FIGURE 104: NEW RELEASE MECHANISM PROPOSED, LAST TWO STAGES UNDER REDUCING ATMOSPHERE.....	157
FIGURE 105: NEW RELEASE MECHANISM PROPOSED, LAST TWO STAGES UNDER OXIDIZING ATMOSPHERE.....	158
FIGURE 106: INES SCALE	167
FIGURE 107: SAMPLE EMPLOYED ON THE VI SERIES.	169
FIGURE 108: FURNACE OF THE VI SERIES.	170
FIGURE 109: VI CONFIGURATION EXPERIMENTAL LOOP.	171
FIGURE 110: EXPERIMENTAL LOOP OF THE CRL SERIES.	172
FIGURE 111: VEGA EXPERIMENTAL LOOP	173
FIGURE 112: TEMPERATURE EVOLUTION ON VEGA-1 TEST.....	174
FIGURE 113: SAMPLE USED IN VERCORS RT7 TEST.....	175
FIGURE 114: VERDON 2 SAMPLE RADIOGRAPHY	175
FIGURE 115: VERCORS 1-6 EXPERIMENTAL LOOP.....	176
FIGURE 116: HORIZONTAL SECTION OF THE PHEBUS PF EXPERIMENTAL DEVICE.	179
FIGURE 117: PHEBUS PF EXPERIMENTAL FACILITY	180
FIGURE 118: ¹³³ CS IMPLANTATION PROFILES	181
FIGURE 119: ESTIMATED IMPLANTATION CS IMPLANTATION PROFILE AND DPA	182
FIGURE 120: VERDON 1 EXPERIMENTAL LOOP.....	184
FIGURE 121: VERDON 1 INDUCTION FURNACE	185
FIGURE 122: MERARG EXPERIMENTAL LOOP	186
FIGURE 123: MERARG INDUCTION FURNACE.....	187
FIGURE 124: DURANCE EXPERIMENTAL LOOP	187
FIGURE 125: DIAGRAM OF THE CAMECA IMS 6F.....	190
FIGURE 126: HOT CELL WHERE THE XRD EQUIPMENT IS PLACED (LEFT) AND THE EQUIPMENT ITSELF (RIGHT).....	191

FIGURE 127: SOLEIL SYNCHROTRON	191
FIGURE 128: SIMFUEL SAMPLE IN THE FIRST CONFINEMENT BARRIER.....	192
FIGURE 129: HYPOTHESES VALIDEES (VERT), REFUTEES (ROUGE) ET RESTANTES (ORANGE) DU MECANISME PROPOSE PAR NICAISE.	197
FIGURE 130: NOUVEAU MECANISME DONT LES DEUX DERNIERES ETAPES SE DEVELOPPENT SOUS ATMOSPHERE REDUCTRICE	199
FIGURE 131: NOUVEAU MECANISME DONT LES DEUX DERNIERES ETAPES SE DEVELOPPENT SOUS ATMOSPHERE OXYDANTE.	200

Tables List

TABLE 1: MAIN CHARACTERISTICS OF INTEGRAL AND ANALYTICAL TESTS AND THE TMI-2 ACCIDENT	19
TABLE 2: PHEBUS PROGRAM TEST GRID.	23
TABLE 3: HI SERIES TEST GRID	25
TABLE 4: VI SERIES TEST GRID	26
TABLE 5: HEVA TEST GRID	29
TABLE 6: VERCORS TEST GRID	30
TABLE 7: VERCORS RT TEST GRID	31
TABLE 8: VERCORS HT TEST GRID	32
TABLE 9: VEGA PROGRAM TEST GRID AND RESULTS	33
TABLE 10: CONDITIONS AND RESULTS OF SOME CRL TESTS	35
TABLE 11: REPRESENTATIVE RESULTS FROM PBF, PHEBUS FP, ORNL AND VERCORS TESTS AND TMI-2 ACCIDENT	36
TABLE 12: VERCORS 4 AND 5 TESTS CONDITIONS AND RESULTS	46
TABLE 13: SUMMARY OF SAMPLES STUDIED IN THE IRRADIATED FUELS WORK AXIS	54
TABLE 14: VERDON 1 FATHER ROD CHARACTERISTICS	54
TABLE 15: VERDON 1 TEST CONDITIONS	58
TABLE 16: FP GLOBAL RELEASED FRACTIONS DURING VERDON 1 TEST. ^A KR, XE.....	59
TABLE 17: THEORETICAL AND ESTIMATED LATTICE PARAMETERS (Å) OF THE PHASES IDENTIFIED BY XRD, SAMPLE B	75
TABLE 18: FP CONCENTRATIONS IN SAMPLE SET I	92
TABLE 19: FP CONCENTRATION IN SAMPLES SETS II AND III.....	93
TABLE 20: CALCULATED OXYGEN POTENTIALS FOR EACH ANNEALING TEST	94
TABLE 21: CHEMICAL SPECIES IN EQUILIBRIUM FOR EACH ZONE	95
TABLE 22: MAIN FP DISSOLVED IN SET I SAMPLES UO ₂ MATRIX.....	96
TABLE 23: OXIDE PRECIPITATES QUANTITATIVE ANALYSIS	98
TABLE 24: CHARACTERISTICS OF OXIDE PRECIPITATES CONTAINING BA AND ZR IN SAMPLES T ₀ AND AT	98
TABLE 25: E ₀ AND WHITE LINE POSITIONS OF SAMPLES AND REFERENCES SPECTRA COLLECTED AT THE BA L ₃ -EDGE AND ZR K-EDGE. INCERTITUDE: ± 0.5 FOR BA SPECTRA, ± 0.8 FOR ZR ONES	99
TABLE 26: METALLIC PRECIPITATES CHEMICAL COMPOSITION	100
TABLE 27: CHARACTERISTICS OF METALLIC PRECIPITATES, BEFORE AND AFTER TEST	100
TABLE 28: ABSORPTION EDGE (E ₀) AND WHITE LINE POSITION OF SAMPLES AND REFERENCES SPECTRA COLLECTED AT THE MO AND RU K-EDGES. EXPERIMENTAL INCERTITUDE: ± 0.8	101
TABLE 29: FP CONCENTRATION IN SET II SAMPLES FUEL UO ₂ MATRIX	103
TABLE 30: FP CONCENTRATION IN OXIDE PRECIPITATES FROM SET II SAMPLES	105
TABLE 31: OXIDE PRECIPITATES CHARACTERISTICS IN SAMPLES FROM SET II	105
TABLE 32: FP CONCENTRATION IN METALLIC PRECIPITATES OF SAMPLES FROM SET II.....	106
TABLE 33: METALLIC PRECIPITATES CHARACTERISTICS, SAMPLE SET II	106
TABLE 34: E ₀ AND WHITE LINE POSITIONS OF SAMPLE T ₀ -R MATRIX AND PRECIPITATES XANES SPECTRA. INCERTITUDE: ± 0.8 EV	109
TABLE 35: LINEAR COMBINATION FIT RESULTS FOR SAMPLE T ₀ -R PRECIPITATES	110
TABLE 36: LINEAR COMBINATION FIT RESULTS FOR SAMPLE T ₀ -R USING PRECIPITATES XANES SPECTRA. INCERTITUDE: 2%	111
TABLE 37: E ₀ AND WHITE LINE POSITIONS OF MO SPECTRA COLLECTED ON SET II SAMPLES AND REFERENCES. INCERTITUDE: ± 0.8 EV	112
TABLE 38: MO SPECTRA LINEAR COMBINATION FIT RESULTS OF SAMPLES FROM SET II. INCERTITUDE: 2%	114
TABLE 39: CS ABSORPTION EDGE POSITION AND WHITE LINE POSITION, SAMPLE SET II. INCERTITUDE: ± 0.5 EV	115
TABLE 40: LINEAR COMBINATION FIT OF CS SPECTRA, SAMPLE SET II. INCERTITUDE: 2%	116

TABLE 41: MAIN FP CONCENTRATION IN SET III SAMPLES MATRIX.....	120
TABLE 42: CS SPECTRA E_0 AND WHITE LINE POSITIONS, SAMPLES FROM SET III. INCERTITUDE: ± 0.5 EV	122
TABLE 43: FP CONCENTRATION IN OXIDE PRECIPITATES, SAMPLE SET III.....	124
TABLE 44: OXIDE PRECIPITATES CHARACTERISTICS, SAMPLE SET III	124
TABLE 45: FP CONCENTRATION IN METALLIC PRECIPITATES OF SAMPLES FROM SET III.....	126
TABLE 46: CHARACTERISTICS OF THE METALLIC PRECIPITATES ON SAMPLES FROM SET III	126
TABLE 47: MO XANES SPECTRA E_0 AND WHITE LINE POSITIONS, SET III SAMPLES. INCERTITUDE: ± 0.8 EV.....	128
TABLE 48: SAMPLES FROM SET III MO XANES SPECTRA FIT RESULTS. INCERTITUDE: 2%	129
TABLE 49: SUMMARY OF SAMPLES STUDIED IN THIS WORK.....	142
TABLE 50: DESCRIPTION OF EACH LEVEL DEFINED IN THE INES SCALE.....	168
TABLE 51: SIMFUEL SAMPLES COMPOSITION	181
TABLE 52: MAXIMAL ^{133}CS IMPLANTATION VALUES.....	181
TABLE 53: FP CONCENTRATION IN SAMPLES FROM SETS II AND III	182
TABLE 54: CARRIER GAS (ARGON) CHARACTERISTICS, USED IN OXIDIZING TETS.....	188
TABLE 55: ECHANTILLONS ETUDIES DANS LES DEUX AXES EXPERIMENTAUX	196

Titre : Etude du comportement des Produits de Fission (Ba, Cs, Mo et Ru) dans des combustibles nucléaires irradiés et leurs simulants en situations d'Accidents Graves par Spectroscopie d'Absorption des rayons X, SIMS et μ sonde.

Mots clés : UO_2 , matériaux modèles, accident nucléaire, relâchement de produits de fission, SAX

Résumé : L'identification des mécanismes de relâchement des Produits de Fission (PF) hors de combustible nucléaire irradié lors d'un accident grave est primordiale pour le développement de codes capables d'estimer précisément le terme source (nature et quantité des radionucléides émis dans l'environnement). Parmi les différents PF, les Ba, Cs, Mo et le Ru sont particulièrement intéressants, car ils peuvent interagir entre eux ou avec d'autres éléments et donc affecter leur relâchement. Dans le cadre de cette thèse, deux axes de travail ont été mis en place avec l'objectif d'identifier les phases chimiques présentes avant l'accident et leur évolution au cours de l'accident lui-même. L'approche expérimentale a consisté à reproduire les conditions d'un accident nucléaire à l'échelle du laboratoire, en utilisant des échantillons de combustibles irradiés et des matériaux modèles (UO_2 vierge dopés en 12 PF).

Le principal avantage de ces derniers est l'utilisation de méthodes de spéciation chimique comme la Spectroscopie d'Absorption des rayons X, qui n'est pas aujourd'hui encore disponible pour les combustibles irradiés. Trois échantillons de combustible irradié ont été étudiés, représentatifs de l'état initial (i.e. avant l'accident), d'une étape intermédiaire en température (1773 K) et d'un état avancé d'accident nucléaire (2873 K). Pour les matériaux modèles, plusieurs séquences accidentelles (de 573 K à 1973 K) ont été réalisées. Les résultats expérimentaux ont permis d'établir un nouveau mécanisme de relâchement des PF en fonction des conditions oxydantes et réductrices du scénario accidentel. Ces résultats ont démontré aussi l'importance des matériaux modèles pour l'étude des accidents nucléaires graves, en complémentarité aux combustibles irradiés.

Title: Study of Fission Products (Ba, Cs, Mo and Ru) behaviour in irradiated and simulated Nuclear Fuels during Severe Accidents using X-ray Absorption Spectroscopy, SIMS and EPMA

Keywords: UO_2 , model materials, nuclear accidents, fission products release, XAS

Abstract: The identification of Fission Products (FP) release mechanism from irradiated nuclear fuels during a severe accident is of main importance for the development of codes for the estimation of the source-term (nature and quantity of radionuclides released into the environment). Among the many FP Ba, Cs, Mo and Ru present a particular interest, since they may interact with each other or other elements and thus affect their release. In the framework of this thesis, two work axes have been set up in order to identify, firstly, the chemical phases initially present before the accident and, secondly, their evolution during the accident itself. The experimental approach consisted in reproducing nuclear severe accidents conditions at laboratory scale using both irradiated fuels and model materials (natural UO_2 doped with 12 FP).

The advantage of these latter is the possibility of using characterization methods, such as X-ray Absorption Spectroscopy, which are not yet available for irradiated fuels. Three irradiated fuel samples have been studied, representative to an initial state (before the accident), to an intermediate stage (1773 K) and to an advanced stage (2873 K) of a nuclear severe accident. Regarding model materials, many accident sequences have been carried out, from 573 to 1973 K. Experimental results have allowed establishing a new release mechanism, considering both reducing and oxidizing conditions during an accident. These results have also demonstrated the importance of model materials as a complement to irradiated nuclear fuels in the study of nuclear severe accidents.

